

DESIGN OF AIRCRAFT WHEELS AND BRAKE SYSTEMS

I. I. Zverev and S. S. Kokonin

(NASA-TT-F-15764) DESIGN OF AIRCRAFT WHEELS  
AND BRAKE SYSTEMS (Scientific Translation  
Service) 260 p HC \$8.50 CSCL 01C

N75-25918

Unclas

63/05 27327

Translation of "Proyektirovaniye aviat-  
sionnykh koles i tormoznykh sistem", Moscow,  
Mashinostroyeniye Press, 1973, 224 pp.



1. Report No. NASA TT F 15,764		2. Government Accession No.		3. Recipient's Catalog No.	
4. Title and Subtitle DESIGN OF AIRCRAFT WHEELS AND BRAKE SYSTEMS				5. Report Date June, 1975	
				6. Performing Organization Code	
7. Author(s) I. I. Zverev and S. S. Kokonin				8. Performing Organization Report No.	
				10. Work Unit No.	
9. Performing Organization Name and Address SCITRAN Box 5456 Santa Barbara, CA 93108				11. Contract or Grant No. NASW-2483	
				13. Type of Report and Period Covered Translation	
12. Sponsoring Agency Name and Address National Aeronautics and Space Administration Washington, D.C. 20546				14. Sponsoring Agency Code	
15. Supplementary Notes  Translation of: "Proyektirovaniye aviatsionnykh koles i tormoznykh sistem," Mashinostroyeniye Press, Moscow, 1973, 224 pp.					
16. Abstract An attempt is made in this book to summarize the experience in the design and analysis of aircraft wheels and brakes, brake systems, brake control systems, and antiskid systems. We examine some questions of the static and fatigue strength of aircraft wheels, calculation of brake service life, brake dynamics, techniques for increasing brake energy absorption capacity, and design of the basic antiskid system elements. The book is intended for personnel in the aircraft industry and organizations operating aircraft.					
17. Key Words (Selected by Author(s))				18. Distribution Statement  Unclassified - Unlimited	
19. Security Classif. (of this report) Unclassified		20. Security Classif. (of this page) Unclassified		21. No. of Pages 260	22. Price

## TABLE OF CONTENTS

	Page
FOREWORD	iv
CHAPTER 1. AIRCRAFT LANDING GEARS	1
1. Landing Gear Geometries	2
2. Basic Geometric Parameters of Tricycle Gear and Its Arrangement on the Airplane	9
3. Landing Gear Shock Absorber System	14
CHAPTER 2. LOADS ACTING ON WHEELS AND BRAKES	21
1. General Requirements on Wheels and Brakes	21
2. Moment of Wheel-to-Runway-Surface Traction Force	22
3. Forces Acting on Wheel during Airplane Motion	28
4. Determination of the Kinetic Energy Transformed by the Brakes into Heat during Airplane Braking	33
CHAPTER 3. FUNDAMENTALS OF WHEEL AND BRAKE STRENGTH ANALYSIS	38
1. Analysis of Wheel Subject to Tire Air Pressure	38
2. Determination of Stresses in a Rolling Wheel	44
3. Wheel Bearing Analysis	48
4. Calculation of Wheel Brake Basic Characteristics and Strength	53

5.	Calculation of Brake System Energy Capacity	61
6.	Strength Analysis of Brake Details	63
7.	Brake Strength Analysis with Side Loads Acting on the Wheel	66
CHAPTER 4.	BRAKED AIRCRAFT WHEEL CONSTRUCTION	71
1.	Wheels with Disc Brakes	71
2.	Wheels with Expander Tube Brakes	74
3.	Wheels with Shoe Brakes	77
4.	Special Wheels	79
5.	Basic Wheel and Brake Component Construction	80
CHAPTER 5.	AIRCRAFT TIRES	86
1.	Basic Characteristics of Tires	86
2.	Aircraft Tire Construction	93
CHAPTER 6.	FRICITION AND CONSTRUCTION MATERIALS FOR BRAKES AND WHEELS	101
1.	Materials for Brake Friction Pairs	101
2.	Wheel Structural Materials	110
CHAPTER 7.	BASES FOR THE SELECTION OF TIRES, WHEELS, AND BRAKES IN AIRPLANE DESIGN	112
1.	Tire Selection	113
2.	Wheel Size Determination	115
3.	Wheel Weight Determination	116
CHAPTER 8.	AIRPLANE BRAKE SYSTEMS	123
1.	Basic Brake System Requirements	123
2.	Direct Control Brake Systems	125
3.	Remote Control Brake Systems	126
4.	Pneumatic Brake System Analysis	131
5.	Hydraulic Brake System Analysis	137
CHAPTER 9.	AUTOMATION OF THE BRAKING PROCESS	145
1.	Wheel Skid Onset Conditions	145
2.	Construction and Operating Principle of the Electroinertial Controller and the Direct Acting Automatic Controller	147
3.	Brake Systems and Antiskid Systems	156

CHAPTER 10.	BRAKE SYSTEM COMPONENT DESIGN	172
	1. Pneumatic Brake System Components	172
	2. Hydraulic Brake System Components	180
	3. Remote Control Brake System Components	196
CHAPTER 11.	AIRCRAFT BRAKE COOLING AND TIRE PRESSURE REGULATION SYSTEMS	200
	1. Brake and Wheel Cooling Techniques	200
	2. Tire Pressure Regulation Systems	206
	3. Liquid Cooling and Tire Pressure Regulation System Components	210
CHAPTER 12.	STAND TESTS OF AIRPLANE LANDING GEAR AND BRAKE SYSTEMS	214
	1. Landing Gear Shock Absorber Tests	214
	2. Basic Wheel Tests	216
	3. Brake Tests	219
	4. Wheel and Brake Test Equipment	219
	5. Stand Check of Inertial Sensors and Antiskid Controllers	222
	6. Brake and Antiskid System Stand Tests	224
CHAPTER 13.	WHEEL AND BRAKE SYSTEM FLIGHT TESTS	228
	1. General Information	228
	2. Ground Tests	230
	3. Flight Tests	231
CHAPTER 14.	BASIC RULES FOR TECHNICAL OPERATION OF BRAKES, WHEELS, AND TIRES	234
	1. Rules for Brake, Wheel, and Tire Use	234
	2. Installation of Assembled Wheel on Airplane Landing Gear	237
	3. Inspections	240
	4. Tire Installation and Removal	242
REFERENCES		250

## ANNOTATION

An attempt is made in this book to summarize the experience in the design and analysis of aircraft wheels and brakes, brake systems, brake control systems, and antiskid systems. We examine some questions of the static and fatigue strength of aircraft wheels, calculation of brake service life, brake dynamics, techniques for increasing brake energy absorption capacity, and design of the basic antiskid system elements. The book is intended for personnel in the aircraft industry and organizations operating aircraft.

## FOREWORD

The weight increase and also the increased takeoff and landing 13  
speeds of passenger and cargo aircraft have led to increased  
complication of aircraft wheel construction.

The mechanical and thermal loads on the wheels and brake  
systems have increased markedly. We need only note that the wheel  
brakes of the Il-62 passenger airplane must absorb an energy of  
about  $18 \cdot 10^6$  in a single braking after landing which, when  
transformed into heat, raises the temperatures of the individual  
brake elements to  $500^\circ \text{C}$ . The temperature at the friction surface  
of the friction elements in this case may reach  $1000 - 1100^\circ \text{C}$ .

Along with the development and perfection of aircraft wheel  
construction, the brake control systems have also become more  
complicated and advanced. For example, more than 100 different  
hydraulic and electrical components are used in the Il-62 braking  
system.

Intorduction of an automatic antiskid controller into the brake  
control system has been necessary in order to improve braking  
effectiveness and reduce tread wear. Special liquid or air cooling  
systems are used to reduce brake temperatures, and tire pressure  
regulation systems are used to improve wheel flotation on various  
soils.

Thus, the range of questions associated with the design of aircraft wheels and brake systems has broadened considerably.

The basic questions covered in the book include determination of brake energy absorption capacity, calculation of airplane landing distance, analysis of the magnitude of the coefficient of traction of the tire with the airdrome runway surface, and the methods for thermal and strength analysis of the basic wheel and brake components.

We examine some questions of the design and analysis of the brake system, antiskid control system, cooling system, tire pressure regulation system, and also certain questions of the design and analysis of the components of these systems. The final sections of the book cover questions associated with wheel and brake testing and the equipment necessary for these tests.

The authors wish to thank Cand. of Tech. Sci. I. I. Khazanov and V. N. Parfenov for their advice and comments on individual sections and Ye. S. Yudayev, M. S. Zukher, M. V. Malyutin, A. A. Matveyev, Yu. P. Bazhanov, and A. V. Reut for their assistance in preparing the manuscript.

All comments should be addressed to: Moscow, B-78, 1<sup>st</sup> Basmannyi Lane, 3, Mashinostroyeniye Press.

## CHAPTER 1

### AIRCRAFT LANDING GEARS

The static and dynamic loads experienced by an airplane when parked, while taxiing about the airdrome, and using braking are first transmitted to the landing gear structural elements (struts, braces, shocks, and wheels) and then to the airplane structural elements.

/5\*

The action of the vertical dynamic loads depends to a considerable degree on the characteristics of the landing gear shock struts and the magnitude of the internal air pressure in the tires. The loads in the brake system structural elements (levers and rods) are determined by the magnitude of the braking moment developed by the wheel brakes.

The strength and dynamic characteristics of the brake and landing gear are interrelated. For example, instability of brake or brake system operation may lead to torsional oscillations of the strut around the vertical axis, and insufficient wheel axle stiffness may lead to premature failure of both the wheel and the brake.

---

\*Numbers in the margin indicate the pagination of the original foreign text.

Experience has shown that a useful operational reliability criterion is the ratio of the landing gear structure weight to the airplane weight and the ratio of the wheel and tire assembly weight to the landing gear weight. From statistical data for previously constructed airplanes with takeoff weight from 45 to 190 metric tons:

— the weight of the main gear with completely outfitted wheels (with tires) is 3.5 — 4.3% of the airplane takeoff weight  $G_{to}$ , and the weight of the nose gear with completely outfitted wheels is 0.3 — 0.64%;

— the main gear wheel-tire assembly weight is 43 — 59% of the total gear weight and the nose gear wheel-tire assembly weight is 18 — 29%.

For preliminary calculations, we can take the completely outfitted main gear weight to be

$$G_{mg} \approx 3.85 \cdot 10^{-2} G_{to},$$

and the completely outfitted nose gear weight

/6

$$G_{ng} \approx 0.47 \cdot 10^{-2} G_{to}.$$

The weight of the outfitted main gear wheels can be taken as about 50% and the weight of the outfitted nose wheels — 20% of the total gear weight.

### 1. Landing Gear Geometries

The following landing gear geometries are used on airplanes (Figure 1.1):

— three-support gear with pivoting aft (tail) wheel, in which the primary load is on the two main wheels located ahead of the airplane center of gravity (CG);

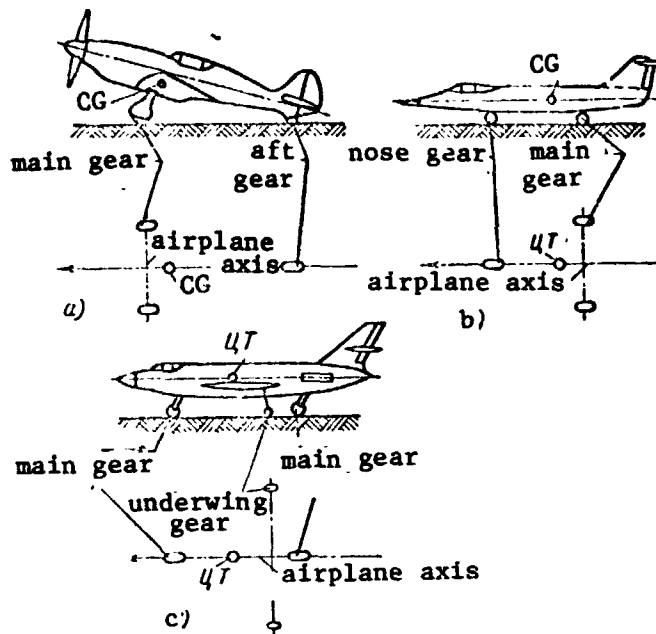


Figure 1.1. Basic landing gear geometries.

a- three-support with pivoting tail wheel; b- tricycle with controllable nose wheel; c- bicycle.

— three-support gear with pivoting forward (nose) wheel, in which the primary load is on the two main wheels located behind the airplane CG;

— bicycle or two-support gear with two auxiliary outrigger wheels under the wings. In this scheme, all the load is on the wheels located under the fuselage behind and ahead of the airplane CG. In this gear, the outriggers support the wing as the airplane banks while parked or taxiing.

At the present time, the three-support gear with tail wheel (Figure 1.2) is found only on relatively light airplanes. In this gear, only the main wheels are braked. The primary drawbacks of the tail wheel gear are inadequate airplane maneuverability because of the absence of a steerable nosewheel and the possibility of noseover in case of excessively heavy braking. In this case (Figure 1.3), the inertial force  $P_1$  which arises during braking creates an overturning moment about the point Q whose magnitude is greater than

/7

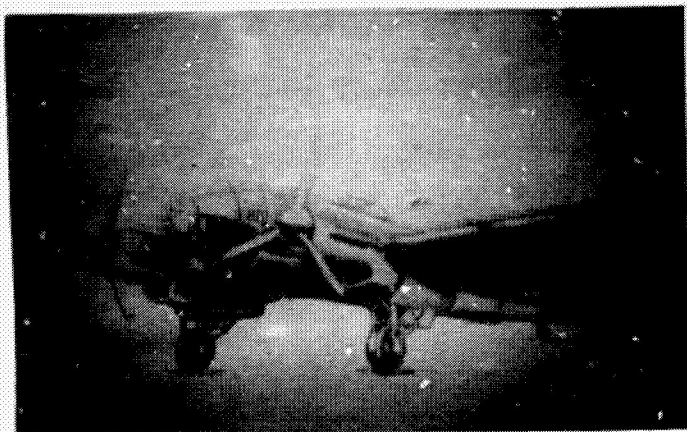


Figure 1.2. Three-support gear with tail wheel.

the stabilizing moment from the airplane landing weight ( $G_a$ ), and

the resultant  $R$  of these forces passes ahead of the point  $O$ .

We see from examination of the acting forces that

$$\varphi = \text{arctg} \frac{P_1}{G_a},$$

where  $P_1 = ma_d$ ;  $a_d = \mu g$ ;  $G_a = mg$ , where  $m$  is the airplane mass,  $a_d$  is the airplane deceleration during braking;  $g$  is the free-fall acceleration;  $\mu$  is the coefficient of traction of the wheel with the airdrome surface.

Considering these equations, we obtain

$$\varphi = \text{arctg} \frac{a_d}{g} = \text{arctg} \mu,$$

or

$$\mu = \text{tg} \varphi.$$

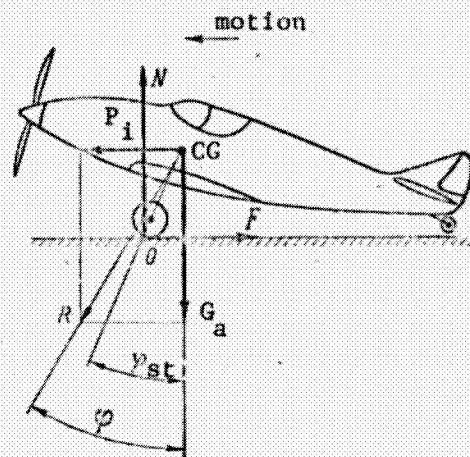


Figure 1.3. Diagram of forces acting on airplane with three-support gear and tail wheel during braking.



To prevent noseover, it is necessary that

$$\mu \leq \operatorname{tg} \varphi_{st}$$

Thus, the value of the realizable coefficient of the wheel traction with the airdrome surface determines the main landing gear wheel stagger angle  $\varphi_{st}$ . It is

Figure 1.4. Tricycle gear with steerable nose wheel.

obvious that the stagger angle magnitude can be varied in order to reduce the danger of airplane noseover during braking; however, this hazard cannot be entirely eliminated in the tail wheel configuration. It is also obvious that braking intensity is limited in this gear configuration.

We also note that "ballooning" is characteristic of airplanes with this gear geometry in case of hard wheel impact on the ground at the moment of touchdown, because of the appearance of a couple (from the landing weight  $G_a$  and the wheel reaction  $N$ ) which increases the angle of attack and, therefore, the wing lift force. Flight experience has shown that, for the airplane with a tail wheel three-support gear, the only possible normal landing is a three-point landing.

The drawbacks characteristic for the tail wheel gear are absent in the tricycle configuration with nose gear, which is most widely used (Figure 1.4). In this scheme, the two main wheels must be equipped with brakes, while the nose wheel may be either braked or unbraked.

/9

The tricycle gear with two multiwheel bogies (left and right) and dual-wheel nose gear is widely used for intermediate and heavy aircraft. Such a gear of the Boeing KC-135 is shown in Figure 1.5. The nose gear is steerable and rotates about the vertical axis. The rotation angle is controlled by the pilot. The nose wheels are not braked.

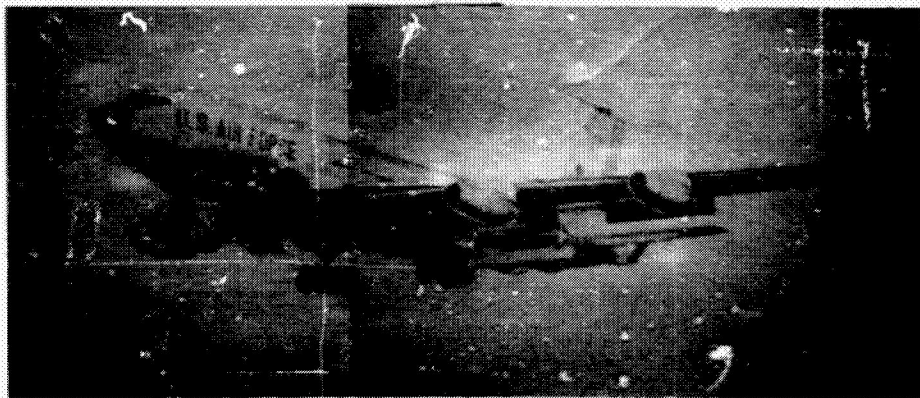


Figure 1.5. Multiwheel tricycle gear with steerable nose wheel on Boeing KC-135.

The tricycle gear with multiwheel bogies on each strut has several advantages, the primary being:

- high flotation and comparatively small volume occupied by the structure;
- high operational reliability;
- possibility of landing simultaneously on all three points (wheels) at a small angle of attack and on the main wheels at large angles of attack;
- possibility of increasing braking intensity and shortening landing rollout by installing braked wheels on the nose strut;
- horizontal fuselage attitude when parked and taxiing;
- directional stability of the airplane when taxiing and during takeoff run and landing rollout.

Let us see how directional stability of the airplane on the three-support gear with nose wheel and tail wheel is provided if airplane drift at the angle  $\beta_a$  occurs for one reason or another (Figure 1.6). The reason for the drift may be inequality of the main wheel braking forces, impact of the rolling wheel on some obstacle, inequality of the engine thrust forces, etc. Let us assume that the nose wheel and tail wheel are swiveling and do not create lateral reaction forces from the ground surface during drift.

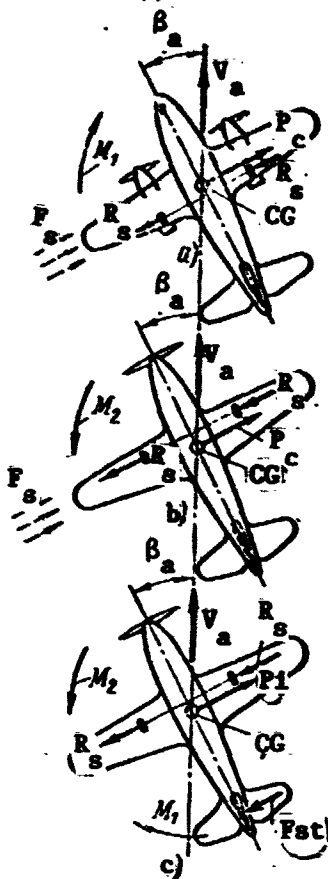


Figure 1.6. Diagrams illustrating airplane directional stability with different landing gear configurations.

a- gear with swiveling nose wheel; b- gear with swiveling tail wheel; c- gear with locked tail wheel.

tional stability. When the tail wheel is locked, a side force  $F_{st}$  arises on the wheel and the moment of this force about the airplane CG is stabilizing, i.e., it reduces the drift angle  $\beta_a$ .

In addition to directional stability, the so-called airplane weathercock stability, which shows up in a crosswind and airplane landing with drift, is also important. We noted above that a couple (side force  $F_s$  on the main wheels and centrifugal force  $P_c$  applied at the CG) is created at the instant of contact with the ground. The moment of this couple in the case of a tricycle gear

We see from the diagram of the forces applied to the airplane having the nosewheel gear that the centrifugal  $P_c$  and side  $R_s$  reaction forces (from the wheel side friction force) will create a moment which eliminates the initial yaw and returns the airplane to the original trajectory. Therefore, the nose wheel gear facilitates significantly the pilot's control of a multiengine airplane during takeoff in case of engine failure. Experience shows that airplanes with nosewheels are capable of automatically maintaining rectilinear takeoff run in case of engine failure.

In the tailwheel gear airplane case, the forces which arise during drift will tend to turn the airplane still further; therefore, the tail wheel is locked, i.e., fixed in the neutral position, during the takeoff run in order to improve the direc-

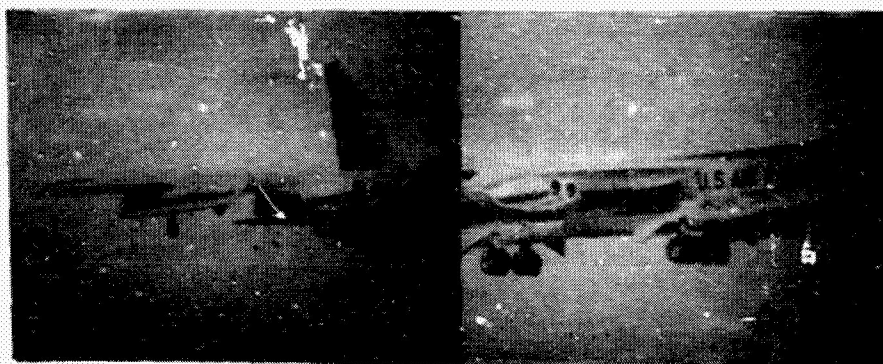


Figure 1.7. Boeing B-52 bicycle landing gear.

and airplane CG ahead of the main gear leg will turn the airplane into the wind in the direction of action of the resultant moment  $M_1$ . In the case of an aft CG and tail wheel gear, the moment from this couple turns the airplane against the wind in the direction of the resultant moment  $M_2$ . In the latter case, the airplane will not have weathercock stability and has a tendency toward overturning about the outer (relative to the center of rotation) wing. This tendency is explained by the lift force increase on the inner wing and the moment of the force  $P_c$  on an arm equal to the airplane CG distance from the ground. /11

The bicycle type landing gear is usually used with a relatively thin wing profile, when wheel stowage in the wings is either impossible or degrades the airplane aerodynamics. Figure 1.7 shows such a landing gear on the Boeing B-52. It consists of forward and aft bogies with four braked wheels on each, left and right outriggers with unbraked wheels. In the bicycle gear, a definite relationship is used between the braking forces on the wheels of the forward and aft bogies in order to maintain airplane directional stability during landing rollout braking. The braking force on the forward bogie wheels usually does not exceed 70 — 75% of the maximal possible force for the aft bogie wheels.

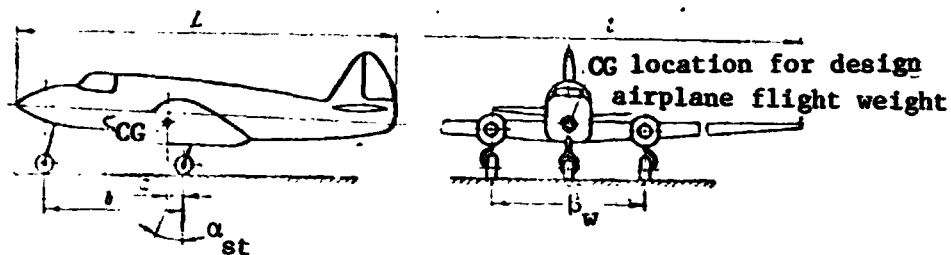


Figure 1.8. Basic geometric parameters of nosewheel landing gear.

## 2. Basic Geometric Parameters of Tricycle Gear and Its Arrangement on the Airplane

Locating the tricycle gear on the airplane reduces to determining the optimal wheelbase and track dimensions and also selecting a rational location of the main wheels relative to the airplane CG. /12

The minimal acceptable distance  $a$  from the airplane CG to the main wheel axle is determined by the following condition: the projection of the CG on the horizontal plane with any airplane position relative to the airdrome surface must always remain ahead of the vertical plane drawn through the line of contact of the main wheels with the ground (Figure 1.8). If this condition is not met, the airplane tail section may strike the airdrome surface during landing and taxiing.

In existing designs, the ratio of the parameter  $a$  to the wheelbase  $b$  varies in the range  $0.1 - 0.15$ . The slope  $\alpha_{st}$  of the shock strut axis to the vertical is considered positive if the strut is swept forward and negative if the strut is swept aft, or zero if the strut is vertical. Usually, the positive and negative angles vary in the range  $\pm(10 - 12^\circ)$ , and we consider that a negative angle creates greater stability during airplane rollout with braking.

The wheelbase  $b$  is the distance from the main wheel axle to the nose wheel axle. It is advisable to make the wheelbase as large as possible, since this reduces the vertical loads on the nose wheel from the airplane weight. In spite of the fact that forward shift

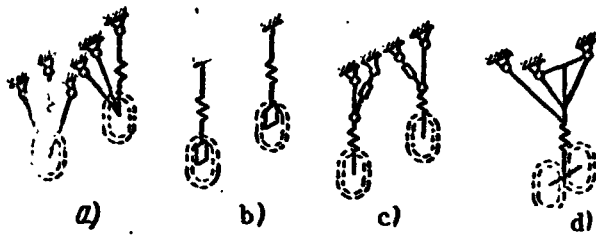


Figure 1.9. Landing gear strut configurations.

a- truss; b- cantilever beam;  
c- braced beam; d- beam truss.

of the nose wheel increases the length of the nose part of the fuselage which experiences the load from the nose wheel, the longer wheelbase is sometimes structurally advantageous. The ratio of the wheelbase  $b$  to airplane length  $L$  varies in the range 0.25 — 0.35.

The landing gear track  $B_w$  is

determined from the condition that

the wingtips not contact the runway when the airplane lands with bank angles up to  $10^\circ$ . A wide track makes it possible to control the airplane more effectively with the brakes when moving over the ground. However, an excessively wide track increases airplane sensitivity to inadvertent turns as a result of any wheel impacts on airdrome irregularities. Usually the track is 20 — 30% of the wing span.

/13

The gear struts vary in configuration as shown in Figure 1.9.

With regard to shock absorber location, we differentiate telescopic struts which are integrated with the shock absorber and struts with external shock absorber. With regard to structural configurations, we differentiate gears of truss construction (see Figure 1.9a), cantilever beam gear (see Figure 1.9b), braced beam gear (see Figure 1.9c), and the beam truss gear (see Figure 1.9d).

The truss gear construction is bulky, creates high drag during takeoff, and also leads to retraction difficulties. It is used primarily on airplanes with low takeoff and landing speeds.

The cantilever beam gear without bracing (see Figure 1.9b) is structurally the simplest and is convenient for folding during retraction into the corresponding fuselage or wing bays.

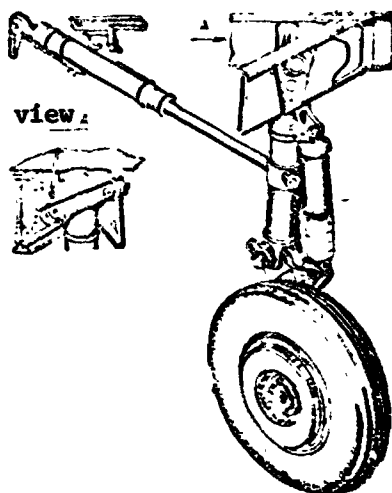


Figure 1.10. Beam type main gear leg construction with retracting brace.

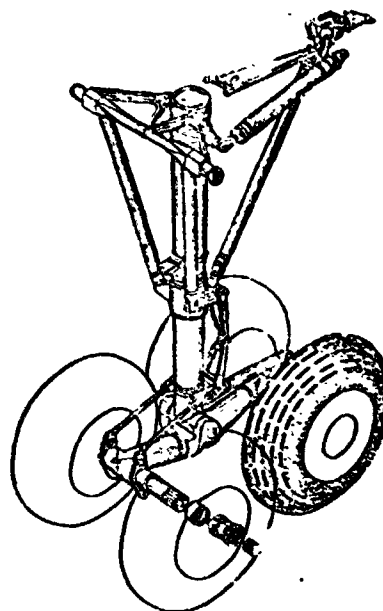


Figure 1.11. Beam truss main gear strut construction.

The beam type braced gear is most widely used. The main structural feature of this gear is that the upper end of the strut is rigidly attached to the wing, but is hinged in the plane perpendicular to the strut. The lower end of the strut is extended into place by a brace. Figure 1.10 shows a beam main gear leg construction with side brace for retracting and extending the gear leg.

The beam truss type landing gear consists of a strut reinforced by a system of braces and rods which reduce the bending moments acting on the strut and increase its stiffness. A typical main gear leg of the beam truss strut construction with bogie is shown in Figure 1.11.

Most modern airplanes with takeoff weight of 40 metric tons or more have multiwheel bogies. On such bogies, it is necessary that the braking moments of the front and rear bogie wheels be completely utilized in order to achieve maximal braking effect. This is achieved with the aid of a system of tie rods and braces comprising a compensation mechanism.

/14

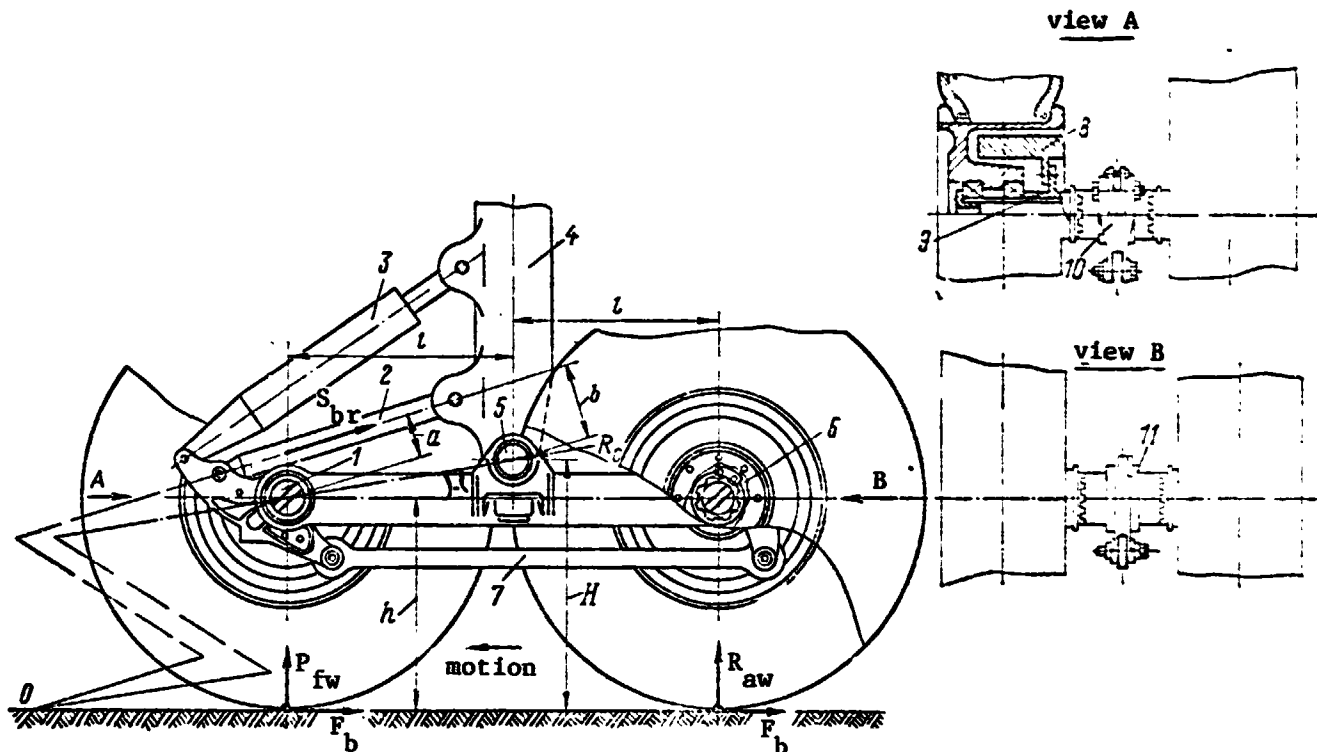


Figure 1.12. Multiwheel main gear leg bogie.

1, 6- wheel axles; 2- brace; 3- shock absorber; 4- strut; 5- bogie axle; 7- tie rod; 8- brake; 9- flange; 10, 11- levers.

Figure 1.12 shows a bogie having such a mechanism. The bogie is equipped with four wheels mounted in pairs on the axles 1 and 6. The axles are rigidly mounted in the fork of a welded framework which is hinged to the strut 4. The brake housing 8 is bolted to the flange 9 and the flange 9 is connected with the lever 10 or 11 by splines and can rotate through some angle relative to the axles 1 and 6. The levers 10 and 11 are connected with one another by the tie rod 7. The front lever 10 is also connected with the shock absorber 3 and the brace 2. The braking moment from the rear wheel is taken by the lever 11 and from the front wheels by the lever 10. The braking moment from the rear wheels is transformed into a force which is transmitted by the rod 7 to the lever 10. The overall load from the action of the front and rear wheel braking moments is taken through the brace 2 by the strut 4. Here rotation of the bogie relative to the axle 5 in the direction of action of the moments and redistribution of the loads between the wheels does not take

place if the bogie is in equilibrium under the action of the braking force  $F_b$ , the overall force  $S_{br}$  in the brace, and the reaction  $R_0$  in the axle 5, which must pass through the front wheel axle 1, as follows from equilibrium of the forces on the axle 1. Since the forces  $R_0$ ,  $S_{br}$ , and  $F_b$  must intersect at the single point 0 for equilibrium, if we know the location of point 0, it is easy to determine the required direction of the brace 2. /16

The condition of equilibrium of the forces applied to the bogie can be represented in the form of equality of the moments of these forces relative to the axle 5, i.e..

$$\Sigma M_5 = 2R_{fw}l - 2R_{aw}l - 4F_b h + S_{br}b = 0,$$

where  $R_{fw}$  is the reaction force on the front wheels;  $R_{aw}$  is the reaction force on the aft wheels;  $l$  is the distance between the front wheel axle and the strut axle;  $b$  is the distance between the strut axle 5 and the axis of the brace 2;  $H$  is the strut axle height.

If redistribution of the loads between the wheels does not take place, the following equality is satisfied:

$$R_{fw} = R_{aw}.$$

Then, obviously,

$$S_{br}b - 4F_b H = 0.$$

By analogy, the sum of the moments relative to the front wheel axle 1

$$\Sigma M_1 = S_{br}a - 4F_b h = 0,$$

where  $a$  is the distance between the brace and the front wheel axle;  $h$  is the wheel axle height.

Since  $\Sigma M_1 = \Sigma M_5$ , then  $b/a = H/h$ .

This relation makes it possible to determine the direction of the brace 2.

### 3. Landing Gear Shock Absorber System

The landing gear shock absorber system reduces the loads from the impacts and shocks experienced by the wheels during airplane landing and taxi. This system includes the gear shock absorbers and the tires. The work which the shock absorber system performs is usually termed the normed work, since it is specified by the norms and, in general form, is determined from the formula:

$$A_n = m_{\text{red}} \frac{V_y^2}{2}, \quad (1.1)$$

where  $A_n$  is the normed work;  $m_{\text{red}}$  is the reduced airplane mass (airplane mass per landing gear leg); and  $V_y$  is the airplane vertical /17 velocity at the instant the wheels contact the runway.

The normed work is split between the gear shock absorber and the tire. However, the shock absorber work must be calculated so that the force arising at the end of the absorber travel will not exceed the allowable load on the wheel. Otherwise, overloading of the tire is inevitable and may lead to failure of both the tire and wheel.

The shock absorbers transform the airplane impact energy at the instant of touchdown or when the wheels encounter obstacles into the heat of friction force work and working fluid deformation. The absorbers may be liquid gas, rubber, or spring types.

At the present time, the liquid gas shock absorbers are most widely used, since they provide most complete impact energy transformation and are compact and operationally reliable.

On the basis of many years of operating experience, the following basic requirements are imposed on landing gear shock absorbers, regardless of their type:

1. transformation of the impact energy into heat of friction force work during the forward (working) stroke in order to reduce the load on the airplane structural components to the design value;
2. uniform and smooth increase of the load to the maximal value at the end of the forward stroke;
3. short shock absorber reverse travel time.

It should be noted that, if the energy absorbed by the shock absorber is stored in the form of energy of the compressed working fluid, then, after removal of the load, the shock absorber will extend with high velocity. In this case, the landing gear elements experience an additional shock load which affects the airplane structure. Therefore, a large part of the energy absorbed by the shock absorber must be transformed into heat and dissipated in order to reduce such loads.

The difference between the energies absorbed by and returned by the shock absorber, transformed into heat, is called the hysteresis work. It is obvious that the magnitude of this work should be as large as possible for the shock absorber.

Let us examine the configuration of the liquid gas shock absorber and analyze the principle of its operation (Figure 1.13).

The shock absorber consists of the cylinder 1 and the piston rod 8 which travels in the cylinder. The cylinder is usually attached to the landing gear strut or the fuselage and the piston rod — to either the wheel axle or the bogie axle. The rod has two supports in the cylinder: the upper bushing 3 and the lower support 7. The sleeve 2, mounted rigidly in the cylinder, can be profiled along the outer contour or have a constant annular section. The

/18

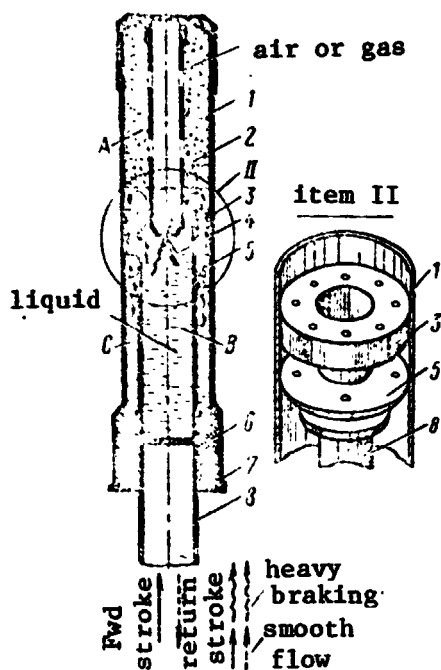


Figure 1.13. Cutaway of liquid gas shock absorber.

1- cylinder; 2- sleeve; 3- upper bushing; 4- restrictor orifice; 5- reverse travel restrictor valve; 6- seal; 7- lower bushing; 8- piston rod.

the shock absorber piston to the original position after removal of the load on the wheel.

During the working stroke, the fluid is forced from chamber B into the cylindrical chamber A through the annular clearance between the rod and the sleeve 2 and through the restricting orifice 4. Part of the work performed during landing is expended in forcing the fluid from chamber B into chamber A and is transformed into thermal energy and dissipated into the surrounding medium. Simultaneously with upward movement of the rod, the fluid from the chamber A through the ports in the rod opens the annular valve 5 and enters chamber C. Fluid flow from chamber A into chamber C takes place with small pressure losses. During the reverse stroke, the piston rod, subject to the pressure of the gas in the upper part of chamber A, begins to travel downward. At this time, under the fluid pressure, the

restrictor orifice 4 is located in the bottom of the sleeve. The annular reverse travel restrictor valve 5 is seated on the piston rod. The shock absorber chamber A is filled with compressed nitrogen at an absolute pressure of 30 — 60 kgf/cm<sup>2</sup>, while chambers B and C are filled with the working fluid (AMG-10 oil or a glycerine mixture in a ratio of 70% glycerine and 30% alcohol). An annular clearance is provided between the rod 8 and the sleeve 2 for working fluid flow. The seal 6 is provided where the rod leaves the cylinder in order to eliminate fluid leakage. During the forward (working) stroke, the rod 8 travels upward. At this time, the gas in chamber A is compressed and thus provides for subsequent return of

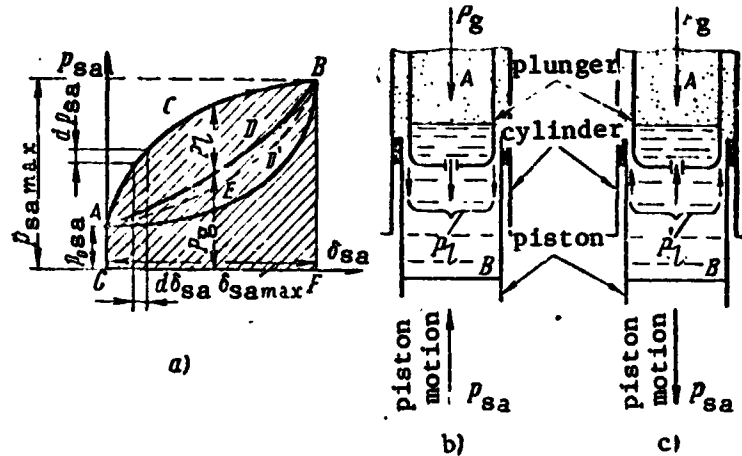


Figure 1.14. Diagram illustrating shock absorber operating principle.  
 a- shock absorber work diagram; b- schematic clarifying shock absorber operation during rod forward stroke; c- diagram illustrating shock absorber operation during piston reverse stroke.

valve 5 closes the large ports in the rod and the fluid flows from chamber C into chamber A only through the small openings in valve 5 itself. Fluid flow through these orifices provides comparatively slow shock absorber return to the original position and softens the impact force in the reverse stroke. The fluid flows from chamber A into chamber B through the annular slot between the sleeve 2 and piston rod 8, and through the orifice 4.

/19

The operation of the liquid gas shock absorber is characterized by the diagram expressing the force  $P_{sa}$  acting on the piston versus rod travel  $\delta_{sa}$  (Figure 1.14a). For simplicity of the analysis, we examine the shock absorber without reverse travel restrictor valve, whose schematic for forward and reverse piston rod strokes is shown in Figures 1.14b and c. If we ignore the inertia force of the moving rod, we can consider that the external force  $P_{sa}$  and the retarding forces  $P_g$  and  $P_l$ , directed opposite the rod motion, are equal. In this case, we have, for the forward stroke:

$$P_{sa} = P_g + P_l, \quad (1.2)$$

where  $P_{sa}$  is the external force acting on the shock absorber piston rod;  $P_g$  is the force of compressed gas pressure on the rod; and  $P_l$  is the resisting force of the working fluid as it flows through the calibrated orifices.

The force  $P_g$  will vary in accordance with the following law during the forward stroke:

$$P_g V^n = \text{const}, \quad (1.3)$$

where  $n$  is the polytropic exponent ( $n \approx 1.3$ );  $V$  is the compressible gas volume.

In the coordinates  $P_{sa}$  and  $\delta_{sa}$ , the Equation (1.3) is represented by the curve ADB. The initial ordinate  $P_{0sa}$  of this curve depends on the magnitude of the initial pressure  $P_0$  in the shock absorber (charging pressure).

The resisting force from fluid flow through the calibrated orifices is

/20

$$P_l = kV_l^2, \quad (1.4)$$

where  $k$  is a coefficient of proportionality accounting for the specific fluid weight, viscosity, and other parameters; and  $V_l$  is the fluid velocity.

The piston rod velocity at the initial and final positions and, consequently, the fluid flow velocity are equal to zero. Therefore, the force  $P_l$  is also equal to zero. If we plot the magnitudes of the forces arising with fluid motion on the hysteresis diagram from the curve ADB rather than from the abscissa axis, then the curve ACB will characterize the magnitude of the overall force  $P_{sa}$ . It is obvious that, in this case, all the work performed by the shock absorber during the piston rod forward stroke will be:

$$A_{sa} = \int_0^{\delta_{sa \max}} P_{sa} d\delta_{sa} \quad (1.5)$$

and will be determined by the area ACBFGA on the hysteresis diagram. It is obvious that this work will be equal to the normed work for the landing rear strut minus the work  $A_t$  performed by the wheel tires, i.e.,

$$A_{sa} = A_n - A_t. \quad (1.6)$$

During the piston rod reverse stroke, the fluid resistance as it flows from chamber A into chamber B will be

$$P'_l = k(V'_l)^2, \quad (1.7)$$

where  $V'_l$  is the velocity of the fluid flowing through the calibrated orifice.

It is obvious that, for the reverse stroke,

$$P_{sa} = P_g - P'_l. \quad (1.8)$$

In Figure 1.14 the difference of the forces  $P_g - P'_l$  is represented by the curve AEB. Consequently, the work of the resistance forces

$$A_{rev} = \int_{\delta_{sa \max}}^0 P_{sa} d\delta_{sa} \quad (1.9)$$

and corresponds to the area BEAGFB on the hysteresis diagram. The work performed by the shock absorber in its entire working cycle during the forward and reverse rod strokes, i.e., the work corresponding to the hysteresis loop area (ACBEA in Figure 1.14)

$$A_{hyst} = A_{sa \text{ fwd}} - A_{sa \text{ rev}}. \quad (1.10)$$

The piston rod annular clearance flow section area has a very large influence on the shape of the curve ACB, characterizing the variation of the force  $P_{sa}$  along the piston rod travel. For most modern shock absorbers, this area amounts to 2 — 5% of the rod area. If this area is less than the lower limit, the fluid flow velocity and its resistance increase. In this case, the force on the shock absorber piston rod increases during the forward stroke and decreases during the reverse stroke. As a result, the hysteresis loop area and, consequently, the shock absorber work increase. In this case, the shock absorber becomes stiff, i.e., the force increases more rapidly as a function of rod travel. This means that, in case of a hard landing, the forces experienced by the airplane increase markedly. With increase of the annular clearance flow section, the shock absorber becomes soft but the area of the hysteresis loop and, consequently, its work, decrease.

In order to obtain a sufficiently elastic shock absorber which is capable of performing the specified normed work, we introduce into its construction a restrictor valve which operates during reverse travel of the piston rod. In this case, the deflection during piston rod forward travel will again take place along the curve ACB, but during the reverse travel, it will follow the curve BDA (see Figure 1.14). In such shock absorbers, the forces increase more smoothly during the piston rod forward stroke and the hysteresis loop area decreases very little.

In the liquid gas shock absorbers, the flow section area may be either constant or variable along the piston rod length.

## CHAPTER 2

### LOADS ACTING ON WHEELS AND BRAKES

#### 1. General Requirements on Wheels and Brakes

/22

Aircraft wheels and airplane brake systems must satisfy the requirements established in the airplane airworthiness standards.

Such standards exist in various countries with certain differences. We shall present the basic assumptions and requirements on wheels, brakes, and tires from these standards.

The main landing gear wheels must be equipped with brakes and be designed for the loads at the maximal allowable airplane takeoff and landing weights. In the rejected takeoff case, at maximal airplane takeoff weight, the wheels and tires must not catch fire or burst when heavy braking is used. One mandatory requirement is for numerous sequential airplane takeoffs and landings, the number and intervals between which depend on the airplane mission. The wheel mounting on the landing gear must permit inspection of the condition of the primary wheel attachment components and the brake system.

The wheel brakes must be designed for braking throughout the entire range of airplane landing speeds with account for the possibility of their heating. High wheel reliability under the specified airplane operating conditions is mandatory. The brake effectiveness must correspond to the normed braking force work in the course of the entire operating service life established for the airplane.

The guaranteed braking moment must provide airplane deceleration equal to  $\sim 0.2$  g for all allowable airplane weights and center of gravity locations. The guaranteed braking moment must hold the airplane with maximal takeoff weight when parked on a 1:10 slope. Moreover, the brakes must provide parking braking for 24 — 48 hours, operate until the friction material is completely worn out, and provide effective braking during operation. The possibility of replacing damaged friction elements without preliminary run-in of the new elements should be provided in the brake design. /23

In order to determine the loads acting on the wheel and brake, we must have certain information on the airplane for which the wheel is designed, namely: landing gear configuration and type, takeoff and landing weights, specified landing rollout distance with the use of brakes, landing and takeoff speeds, airdrome class on which the airplane will be used, etc. These data make it possible to determine the basic wheel and brake design parameters.

We shall examine the primary factors determining the loading of the braked wheel.

## 2. Moment of Wheel-to-Runway-Surface Traction Force

The incompletely braked wheel, while rolling (Figure 2.1), is subjected to radial load ( $P_r$ ), traction moment ( $M_{tr}$ ), and braking moment ( $M_b$ ). The traction force moment\* depends on several factors and can be expressed by the formula known from mechanics:

---

\*It would be more correct to call this moment the moment of the friction forces between the tire tread and the runway surface, but considering that the term "traction force moment" has become established in the specialized literature, we shall retain it unchanged in the following discussion.

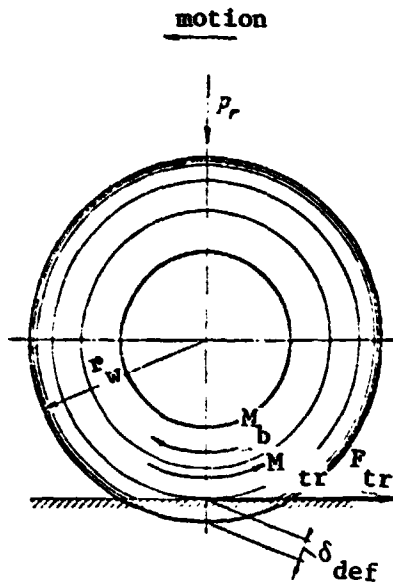


Figure 2.1. Forces and moments acting on wheel during braking.

$$M_{tr} = \mu P_r (r_w - \delta_{def}) = F_{tr} r_d, \quad (2.1)$$

where  $\mu$  is the coefficient of traction between the tire and the runway surface ( $\mu = F_{tr}/P_r$ );  $r_w$  is the wheel geometric radius;  $\delta_{def}$  is the tire deflection under the radial load;  $r_d$  is the wheel dynamic rolling radius ( $r_d \approx r_w - \delta_{def}$ ); and  $F_{tr}$  is the traction force between the tire and the runway surface.

The traction coefficient  $\mu$  is a variable quantity. While varying over quite wide limits, it can, in each specific wheel loading case, reach a definite limiting value

$$\mu_{lim} = F_{tr \max} / P_{r \max}. \quad (2.2)$$

Experimental studies have established the dependence of the traction coefficient  $\mu$  on the wheel rolling velocity, tire pressure, tire type, tire tread condition, and runway surface condition. In the skidding case, the braked wheel will slide without rolling over the runway surface; in this case, the traction coefficient will be equal to the sliding friction coefficient, which is the ratio of the traction force ( $F'_{tr}$ ) of the completely braked wheel to its radial load, i.e.,

$$\mu = \mu_{sl} = F'_{tr} / P_r.$$

Numerous studies have shown that the limiting traction coefficient  $\mu_{lim}$  always remains larger than the sliding coefficient  $\mu_{sl}$ . The results shown in Figures 2.2 and 2.3 of studies of aircraft tire traction coefficient dependence on several factors make it possible to draw the following conclusions:

/25

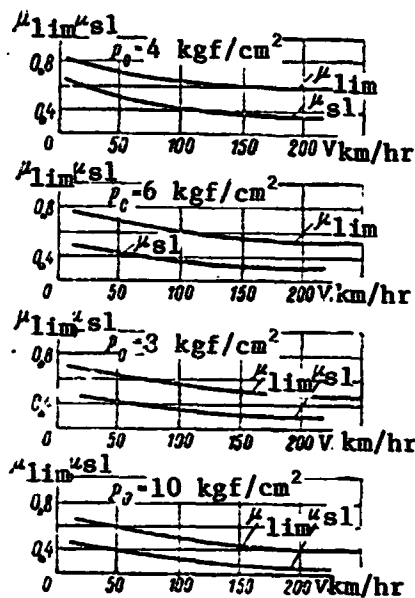


Figure 2.2. Wheel traction coefficients  $\mu_{lim}$  and  $\mu_{sl}$  (for dry concrete runway) as functions of translational velocity  $V$  and tire air pressure  $p_0$ .

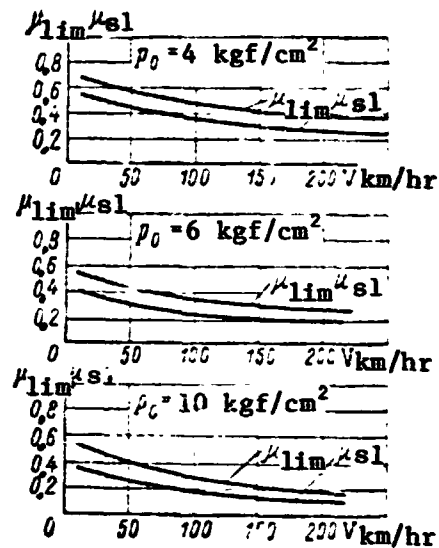


Figure 2.3. Wheel traction coefficients  $\mu_{lim}$  and  $\mu_{sl}$  (for wet concrete runway) as functions of translational velocity  $V$  and tire air pressure  $p_0$ .

— the limiting traction coefficient decreases with increase of the velocity  $V$  (for  $V = 0$   $\mu_{lim} = 0.8$ , while for  $V = 250$  km/hr,  $\mu_{lim} = 0.6$ );

— with increase of the tire pressure ( $P_0$ ), the coefficient  $\mu_{lim}$  decreases because of reduction of the area of tire contact with the runway surface.

On a wet (after rain or snow) concrete runway,  $\mu_{lim}$  decreases still more, since, in this case, only the middle part of the track obtained from tread contact with the runway as the wheel rolls remains dry. A special tread pattern may improve the conditions of its traction with the wet runway surface.

To clarify the influence of the tread pattern on  $\mu_{lim}$ , we can use the experimental data for automobile tires shown in Figure 2.4. We see from the curves in this figure that intermediate values of

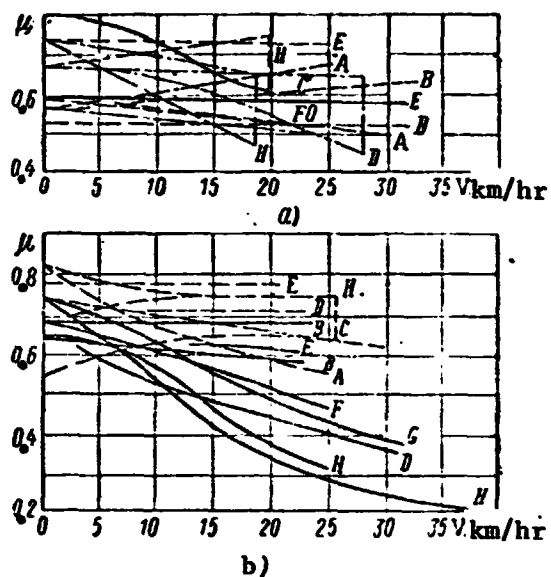


Figure 2.4. Traction coefficient  $\mu$  of an automobile tire with various tread patterns versus speed for various runways (dashed line indicates dry pavement, solid line indicates wet pavement).

a- road with concrete pavement;  
b- road with asphalt pavement.

the traction coefficient for both dry and wet pavement are obtained for the tread with longitudinal grooves (type A). The tire with tread type E showed good results in the tests.

The  $\mu(V)$  curves obtained for treads with different patterns (C, D, E, and others) showed that the tread should not be continuous; it is better if the tread is comprised of individual segments (blocks). The poorest results were obtained on tire H with worn tread. We note that the results shown in Figure 2.4 cannot be applied to aircraft tires without account for the influence of airplane speed on the sliding coefficient.

The tire-to-runway-surface traction conditions depend considerably on the degree of smoothness of the runway surface itself. For example, it has been found that, during rain, a coarse concrete runway surface (with greater roughness) may be more favorable, since the surface roughness may destroy the liquid film under the tread and thereby improve wheel traction with the runway during braking.

However, if the runway is covered with a sufficiently thick water layer, the phenomenon of tire hydroplaning on the runway is possible. In this case, wheel separation from the runway surface is even possible at some definite speed under the influence of the hydrodynamic forces. The speed at which the wheel separates from the runway is called the hydroplaning initiation speed  $V_{hp}$ .

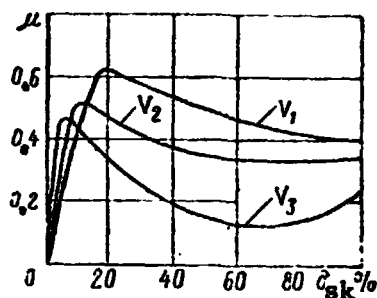


Figure 2.5. Traction coefficient  $\mu$  versus relative wheel skidding  $\delta_{sk}$  for various translational velocities  $V_1, V_2, V_3$  during braking ( $V_1 < V_2 < V_3$ ).

$$V_{hp} = 16.7\sqrt{14.2p_0}, \quad (2.3)$$

where  $p_0$  is the tire inflation pressure.

As a braked wheel rotates, there is always some wheel skidding, i.e., the braked wheel rotation speed is always less than the free (unbraked) wheel rotation speed. The degree of wheel skidding  $\delta_{sk}$  in percent can be found from the formula:

$$\delta_{sk} = \frac{n_0 - n}{n_0} \cdot 100 = \frac{\omega_0 - \omega}{\omega_0} \cdot 100,$$

where  $n_0, \omega_0$  are the rpm and angular velocity of the free wheel (rolling without braking); and  $n, \omega$  are the braked wheel rpm and angular velocity.

Curves of  $\mu(\delta_{sk})$  for various translational velocities and constant tire pressure  $p_0 = 6 \text{ kgf/cm}^2$  are shown in Figure 2.5. We note that, although the values of the coefficients  $\mu_{sk}$  are different /27 for each tire type, the nature of the  $\mu(\delta_{sk})$  curves is the same for all tires. We see from these curves that, with increase of the airplane translational speed, the coefficient  $\mu$  maximum shifts in the direction of smaller  $\delta_{sk}$  values. The peak lies essentially in the range 10 — 20%.

Therefore, in determining the traction force moment, we can take, for a dry concrete runway,  $\mu = 0.6 \div 0.7$  for  $V = 0$  and  $\mu = 1/2 (\mu_{sk} + \mu_{sl})$  for  $V = 0$ .

In the latter expression,  $\mu_{sk}$  and  $\mu_{sl}$  are taken from curves analogous to those shown in Figures 2.2 and 2.3, but relating to the specific aircraft tire types. For preliminary calculations, we can take  $\mu = 0.35$  for  $V \neq 0$ . Depending on the relationship between the magnitudes of the moments  $M_{tr}$  and  $M_b$ , the following three braked wheel motion cases are possible.

1.  $M_{tr} > M_b$ . In this case, we have rolling of the wheel with skidding and a definite angular deceleration, whose magnitude is determined by the ratio of the airplane linear deceleration ( $a_d$ ) to the tire dynamic rolling radius ( $r_d$ ), i.e.,  $d\omega/d\tau = a_d/r_d$ . If  $d\omega/d\tau = \text{const}$ , the wheel angular velocity and rpm decrease linearly.

2.  $M_{tr} = M_b$ . In this case, we again have rolling of the wheel along with definite skidding. However, in this regime, reduction for some external reason of the traction force moment  $M_{tr}$  or increase of the braking moment  $M_b$  leads to marked change of the wheel motion nature. Therefore, this regime can be considered an unstable motion regime.

3.  $M_{tr} < M_b$ . In this case, the wheel locks up (does not roll) and skids. When the wheel locks up, its equation of motion takes the form

$$J_w \frac{d\omega}{d\tau} = M_{tr} - M_b = -\Delta M.$$

The expression  $d\omega/d\tau$  is the magnitude of the wheel angular deceleration.

We see from these wheel motion cases that, in order to obtain minimal airplane landing rollout braking distance, it is necessary that

/28

$$M_{b \max} = M_{tr \ sk} = \mu_{sk} P_r (r_w - \delta_{def}).$$

The ratio

$$M_{tr \ sk} / M_{b \max} = k_{eff}$$

can be considered the braking system effectiveness coefficient, which, in the ideal case, is equal to one.

### 3. Forces Acting on Wheel During Airplane Motion

We see from Figure 2.6 that, during motion over the runway, the airplane is subject to the lift force  $Y$ , drag force  $Q$ , engine thrust  $T$ , airplane weight  $G_a$ , runway reaction forces on the main  $N_{mw}$  and nose  $N_{nw}$  wheels, friction forces on the main  $F_{mw}$  and nose  $F_{nw}$  wheels.

It is obvious that

$$F_{mw} = \mu_{mw} N_{mw}; \quad F_{nw} = \mu_{nw} N_{nw},$$

where  $\mu_{mw}$  and  $\mu_{nw}$  are the traction coefficients, respectively, of the main and nose wheels with the runway. The variation of the lift force  $Y$  and radial load  $P_r$  on the wheel during landing rollout is shown in Figure 2.7.

The airplane motion along the runway can be described by the system of equations:

$$\frac{G_a}{g} \cdot \frac{dV}{dt} = T - Q - (F_{mw} + F_{nw});$$

$$Y + (N_{mw} + N_{nw}) - G_a = 0; \quad (2.4) \quad \underline{/29}$$

$$(N_{nw}a - N_{mw}b) - (F_{nw} = F_{mw})h = 0.$$

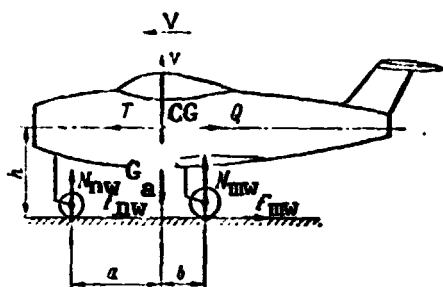


Figure 2.6. Forces acting on wheels of tricycle gear with braked nose wheel during airplane landing rollout braking.

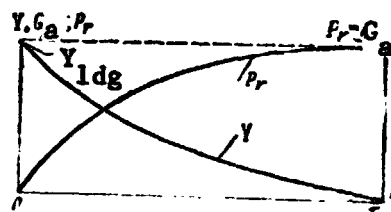


Figure 2.7. Lift force  $Y$  and radial load ( $P_r = G_a - Y$ ) on wheels as a function of landing rollout distance  $L$  and braking time  $t$ .

Replacing the friction forces by the ground reaction forces on the wheels and solving the second and third equations of this system for these forces, we obtain:

$$\begin{aligned} N_{mw} &= \frac{(G_a - Y)(a - \mu_{nw}h)}{a + b + (\mu_{mw} - \mu_{nw})h}; \\ N_{nw} &= \frac{(G_a - Y)(b + \mu_{mw}h)}{a + b + (\mu_{mw} - \mu_{nw})h}. \end{aligned} \quad (2.5)$$

Then we transform the expression  $G_a - Y = G_a(1 - [Y/G_a])$ , using the known relation

$$\frac{Y}{G_a} = \frac{\frac{1}{2} c_y \rho S V^2}{\frac{1}{2} c_{y \text{ ldg}} \rho S V_{\text{ldg}}^2} = \frac{c_y}{c_{y \text{ ldg}}} \cdot \frac{V^2}{V_{\text{ldg}}^2} = \frac{1}{k} \cdot \frac{V^2}{V_{\text{ldg}}^2},$$

to the form

$$G_a - Y = G_a \left(1 - \frac{1}{k} \frac{V^2}{V_{\text{ldg}}^2}\right).$$

Denoting the fraction of the airplane weight on the main wheels by

$$x = \frac{a - \mu_{nw}h}{a + b + (\mu_{mw} - \mu_{nw})h}$$

we can finally write (2.5) in the form

$$\begin{aligned} N_{mw} &= \kappa G_a \left(1 - \frac{1}{k} \frac{V^2}{V_{ldg}^2}\right); \\ N_{nw} &= (1 - \kappa) G_a \left(1 - \frac{1}{k} \frac{V^2}{V_{ldg}^2}\right). \end{aligned} \quad (2.6)$$

If the wheel traction coefficients  $\mu_{mw}$  and  $\mu_{nw}$  are constant throughout the landing rollout, the friction forces

$$\begin{aligned} F_{mw} &= \mu_{mw} \kappa G_a \left(1 - \frac{1}{k} \frac{V^2}{V_{ldg}^2}\right); \\ F_{nw} &= \mu_{nw} (1 - \kappa) G_a \left(1 - \frac{1}{k} \frac{V^2}{V_{ldg}^2}\right) \end{aligned} \quad (2.7)$$

Finally, the overall wheel braking force

/30

$$\begin{aligned} F_{mw} + F_{nw} &= [\kappa \mu_{mw} + (1 - \kappa) \mu_{nw}] G_a \left(1 - \frac{1}{k} \frac{V^2}{V_{ldg}^2}\right) = \\ &= \mu_{av} G_a \left(1 - \frac{1}{k} \frac{V^2}{V_{ldg}^2}\right), \end{aligned}$$

where  $\mu_{av}$  is the average coefficient of main and nose wheel friction during braking,  $\mu_{av} = \kappa \mu_{mw} + (1 - \kappa) \mu_{nw}$ . During airplane rollout without braking, the overall wheel friction force is

$$F = \mu_0 G_a \left(1 - \frac{1}{k} \frac{V^2}{V_{ldg}^2}\right)$$

where  $\mu_0$  is the coefficient of wheel rolling friction.

If, in (2.5) and (2.6), we take  $V = 0$ ,  $\mu_{mw} = \mu_{nw} = 0$ , the reactions (loads) on the wheels with the airplane parked are:

$$N_{mw} = \frac{a}{a+b} G_a \text{ and } N_{nw} = \frac{b}{a+b} G_a. \quad (2.8)$$

In order to hold the airplane parked with the engines running with the aid of the brakes, it is necessary that  $F_{mw} + F_{nw} = T$ .

Then, obviously, the loads on the wheels are

$$N_{mw} = \frac{a}{a+b} G_a - \frac{h}{a+b} T \quad \text{and} \quad N_{nw} = \frac{b}{a+b} G_a + \frac{h}{a+b} T. \quad (2.9)$$

The airplane kinetic energy which is transformed by the brakes into heat during rollout can be calculated for the tricycle gear with unbraked nose wheel under the following assumptions:

— constant magnitude of the wheel-to-runway traction coefficient throughout the rollout;

— absence of wheel lockup (skidding).

The friction forces in (2.4) can be expressed as:

$$F_{mw} = \mu_{mw} \kappa (G_a - Y) \text{ and } F_{nw} = \mu_0 (1 - \kappa) (G_a - Y),$$

where  $\mu_{mw}$  is the overall coefficient of main wheel traction with the runway surface during rollout with braking ( $\mu_{mw} = \mu_b + \mu_0$ ); and  $\mu_{nw} = \mu_0$  is the nose wheel rolling friction coefficient.

We use these expressions to transform (2.4) to the form:

$$m \frac{dV}{d\tau} + \mu_{mw} \kappa (G_a - Y) + \mu_0 (1 - \kappa) (G_a - Y) + Q - T = 0$$

/31

and after dividing by  $G_a$ , obtain

$$\begin{aligned} \frac{1}{g} \frac{dV}{d\tau} + \mu_{mw} \kappa \left(1 - \frac{y}{G_a}\right) + \mu_0 (1 + \kappa) \times \\ \times \left(1 - \frac{y}{G_a}\right) + \frac{Q}{G_a} - \frac{T}{G_a} = 0. \end{aligned} \quad (2.10)$$

Using the formulas known from aerodynamics, we find

$$\frac{Q}{G_a} = \frac{c_x S \frac{V^2}{2}}{c_y \text{ldg} \rho S \frac{V_{\text{ldg}}^2}{2}} = \frac{\frac{c_x}{c_y} V^2}{\frac{c_y \text{ldg}}{c_y} V_{\text{ldg}}^2} = \frac{\epsilon}{k} \frac{V^2}{V_{\text{ldg}}^2},$$

where  $\epsilon = c_x/c_y$  is the reciprocal airplane L/D during rollout;  $k$  is the effective airplane L/D during rollout ( $k = [c_y \text{ldg}/c_y]$ ).

Substituting these expressions into (2.10) and making some transformations, we obtain:

$$\begin{aligned} \frac{1}{g} \frac{dV}{d\tau} + \frac{V^2}{V_{\text{ldg}}^2} \frac{\epsilon}{k} - \frac{\mu_{\text{mw}} \kappa - \mu_0(1 - \kappa)}{k} + \\ + \mu_{\text{mw}} \kappa + \mu_0(1 - \kappa) - \varphi = 0, \end{aligned} \quad (2.11)$$

where  $\varphi = T/G_a$ .

Introducing the notations  $c = [\epsilon - \mu_{\text{mw}} \kappa - \mu_0(1 - \kappa)]/k$  and  $a = \mu_{\text{mw}} \kappa + \mu_0(1 - \kappa) - \varphi$ , we reduce (2.11) to the form

$$\frac{1}{g} \frac{dV}{d\tau} + c \frac{V^2}{V_{\text{ldg}}^2} + a = 0.$$

Introducing the new variable  $z^2 = V^2/V_{\text{ldg}}^2$ , we obtain

$$\frac{V_{\text{ldg}}^2}{g} \frac{z dz}{dL} + cz^2 + a = 0, \quad (2.12)$$

where  $dL$  is the differential braking distance ( $dL = V d\tau$ ).

#### 4. Determination of the Kinetic Energy Transformed by the Brakes into Heat during Airplane Braking

/32

With the aid of (2.12), we can determine not only the rollout distance  $L$  and the braking time  $\tau$ , but also that part of the airplane kinetic energy which is transformed into thermal energy by the brakes and wheels.

The work performed by a single braked main wheel is

$$A_b = \int_L F_{mw} dL = \frac{1}{n} \int_L \mu_{mw} \kappa (G_a - Y) dL = \quad (2.13)$$

$$\frac{1}{n} \mu_{mw} \kappa G_a \int_L \left(1 - \frac{Y}{G_a}\right) dL,$$

where  $n$  is the number of airplane landing gear braked main wheels.

Considering (2.7) and (2.12), we transform (2.13) to the form

$$A_b = -\frac{1}{n} \mu_{mw} \kappa G_a \frac{V^2}{g} \int \left(1 - \frac{1}{k} z^2\right) \frac{z dz}{cz^2 + a}. \quad (2.14)$$

Integrating (2.14), we obtain

$$A_{bz} = -\frac{\mu_{mw} \kappa G_a V^2}{ng} \left[ \frac{1}{2c} \left(1 + \frac{a}{ck}\right) \ln(cz^2 + a) - \frac{z^2}{2ck} \right] + B. \quad (2.15)$$

For  $z = 1$  and  $A_{bz} = 0$ , the constant of integration

$$B = \frac{\mu_{mw} \kappa G_a V^2}{ng} \left[ \frac{1}{2c} \left(1 + \frac{a}{ck}\right) \ln(c + a) - \frac{1}{ck} \right].$$

Substituting this value of  $B$  into (2.15), we have

$$A_{bz} = \frac{\mu_{mw} \kappa G_a V^2}{2ghc} \left[ \left(1 + \frac{a}{ck}\right) \ln \frac{cz^2 + a}{c + a} + \frac{1}{k} (z^2 - 1) \right] \quad (2.16)$$

or, in dimensionless form:

$$a_{bz} = \frac{A_{bz}}{G_a V_{ldg}^2 / 2gn} = \quad (2.17)$$

$$\frac{\mu_{mw}^K}{c} \left[ \left(1 + \frac{a}{ck}\right) \ln \frac{c+a}{cz^2+a} + \frac{1}{k} (z^2 - 1) \right].$$

From (2.17) for  $z = 0$ , we find the fraction of the airplane kinetic energy which is transformed by the brake and wheel into heat during rollout, i.e., /33

$$a_{b0} = \frac{\mu_{mw}^K}{c} \left[ \left(1 + \frac{a}{ck}\right) \ln \left(1 + \frac{c}{a}\right) - \frac{1}{k} \right].$$

It is better to plot the relation  $a_b = f(z)$  as a function of the difference of the values

$$\bar{a}_{bz} = a_{b0} - a_{bz} = \frac{\mu_{mw}^K}{c} \left[ \left(1 + \frac{a}{ck}\right) \ln \left(1 + \frac{c}{a} z^2\right) - \frac{z^2}{k} \right].$$

Then the ordinate of the  $\bar{a}_{bz}$  curve will show the fraction of the energy which will be transformed into thermal energy by the brake and wheel by the time the airplane comes to a complete stop (Figure 2.8). The total energy which will be absorbed by the brake and wheel beginning from any velocity at the instant of braking initiation is calculated from the formula:

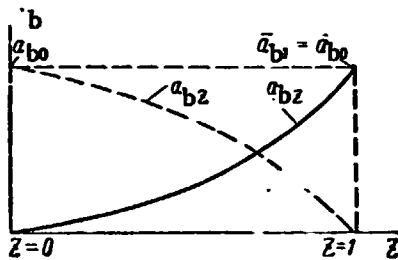


Figure 2.8. Plot of the function  $a_b = f(z)$

$$\bar{A}_b = \frac{G_a V_{ldg}^2}{2gn} \bar{a}_{bz}.$$

If  $c = 0$ ,

$$\bar{a}_{bz} = \frac{\mu_{mw}^K}{2ka} z^2 (2k - z^2),$$

and for  $z = 1$ ,

$$\bar{a}_{bz} = \frac{\mu_{mw}^K}{2ka} (2k - 1).$$

The rollout distance found from (2.12) is

$$L = - \frac{v^2}{2gc} \ln(cz^2 + a) + B_1. \quad (2.18)$$

For  $z = 1$  and  $L = 0$ ,

$$B_1 = \frac{v^2}{2gc} \ln(c + a) \quad (2.19)$$

and

$$L = \frac{v^2}{2gc} \ln \frac{c + a}{cz^2 + a}.$$

For  $c = 0$ ,

$$L = \frac{v^2}{2g} \frac{1 - z^2}{a}.$$

For  $z = 0$ ,

$$L = \frac{v^2}{2ga}.$$

In practice, the airplane piloting process during landing provides for two characteristic stages.

*The first stage* (immediately after airplane touchdown) is motion on the two main wheels with the nose wheel off the runway and the brakes not in use. In this stage, only part of the airplane kinetic energy is transformed into work of the force of resistance to its motion.

*The second stage* (from the moment the nose wheel is lowered and contacts the runway surface) is motion on all the wheels with immediate use of the brakes.

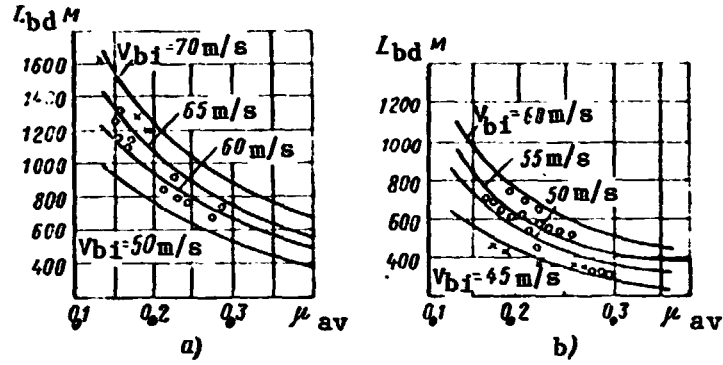


Figure 2.9. Braking distance  $L_{bd}$  versus traction coefficient  $\mu_{Av}$  and braking initiation speed  $V_{bi}$ .  
a- Tu-104; b- Tu-124.

Considering these stages, we obtain:

a. for the first stage (subscript 1), we have  $c = c_1$ ,  $a = a_1$ , and  $z = z_1$ , which corresponds to the velocity at the initiation of the braked rollout. Then, from (2.19),

$$L_1 = \frac{V_1^2}{2gc} \ln \frac{c_1 + a_1}{c_1 z_1^2 + a_1};$$

b. for the second stage (subscript 2), we have  $c = c_2$  and  $a = a_2$ . Taking in (2.18)  $z = z_1$  and  $L = 0$ , we obtain

$$B_1 = \frac{V_1^2}{2gc_2} \ln(c_2 z_1^2 + a_2).$$

Hence, (2.19) will have the form

$$L = \frac{V^2}{2gc_2} \ln \frac{c_2 z_1^2 + a_2}{c_2 z^2 + a_2}.$$

Setting  $z = 0$ , we obtain

$$L_2 = \frac{V^2}{2gc_2} \ln \left( 1 + \frac{c_2}{a_2} z_1^2 \right).$$

The overall airplane rollout distance  $L = L_1 + L_2$ .

If all the wheels are equipped with brakes, the braking distance calculation is made similarly to the above procedure.

Airplane flight tests have confirmed agreement of the measured braked rollout distances with the calculated values.

Figure 2.9 shows braking distance as a function of traction coefficient  $\mu_{av}$  and braking initiation speed for the Soviet Tu-104 and Tu-124 passenger airplanes.

## CHAPTER 3

### FUNDAMENTALS OF WHEEL AND BRAKE STRENGTH ANALYSIS

The following forces act on the wheel during airplane motion (Figure 3.1): the vertical airplane weight force  $P_y$ , the tangential force  $P_x$  from tire traction with the runway surface, and the side force  $P_z$ , which arises as the airplane travels along a curvilinear trajectory, during landing with drift, or when taxiing in a cross wind. In addition, the wheel flange and rim are loaded by forces from the air pressure in the tire. With account for the well-known force independence principle, we shall examine the stress-strain state of a drum subject to air pressure in the tire (Figure 3.2). /36

#### 1. Analysis of Wheel Subject to Tire Air Pressure

The tire air pressure exerts very high loads on the drum flanges, transmitting to the flanges the axial forces  $Q_1$  and  $Q_2$ .

The overall axial loads  $Q_1$  and  $Q_2$  acting on the flanges for circular cross section tires can, with adequate degree of accuracy, be determined from the formulas: /37

$$\begin{aligned} Q_1 &= p_0 \pi [(R + r)^2 - R_t^2]; \\ Q_2 &= p_0 \pi [(R - r)^2 - R_w^2] \end{aligned} \quad (3.1)$$

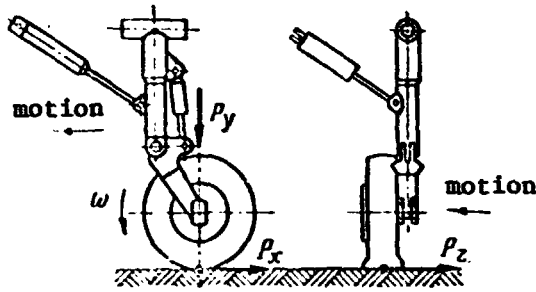


Figure 3.1. Forces acting on wheel as airplane moves.

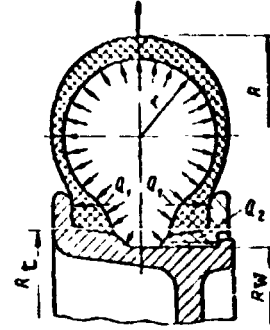


Figure 3.2. Forces acting on wheel drum flange.

where  $p_0$  is the air pressure in the tire;  $R$ ,  $r$ , and  $R_t$  are the tire dimensions, and  $R_w$  is the wheel flange seating diameter.

The Expressions (3.1) were obtained from examination of the stress state of the tire as it interacts with the drum elements.

The drum analysis diagram shown in Figure 3.3 reduces to examination of the working conditions of a thin wall cylindrical shell (rim) together with the elastic annular flange.

The following internal loads, uniformly distributed around a circle of radius  $R_{av}$ , act in the section where the flange and rim join:  $F_0$  is the normal force,  $Q_0$  is the transverse force, and  $M_0$  is the bending moment.

From the equilibrium condition follows

$$F_0 = \frac{Q_1}{2\pi R_{av}}.$$

The moment  $M_0$  and force  $Q_0$  are found from the flange and rim deformation compatibility condition, i.e., equality of the section displacements  $W$  and rotation angles  $\varphi$

$$\begin{aligned} W_{ben} + W_{tr} + W_{pr} &= W_{fl}; \\ \varphi_{ben r} + \varphi_{tr r} + \varphi_{pr r} &= \varphi_{fl}, \end{aligned} \quad (3.2)$$

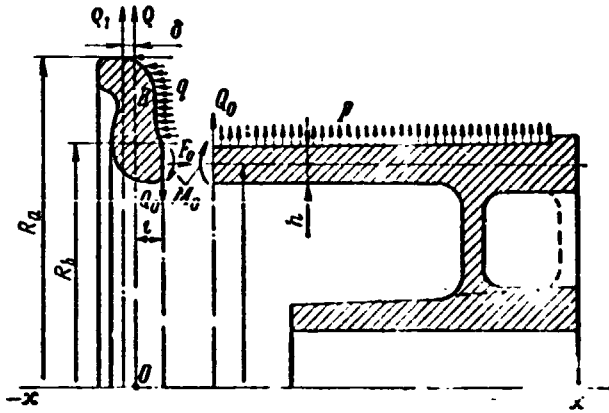


Figure 3.3. Wheel drum analysis diagram.

where  $W_{ben}$ ,  $W_{tr}$ , and  $W_{pr}$  are the rim radial deformations from the moment  $M_0$ , force  $Q_0$ , and pressure  $p_0$ , respectively;  $\varphi_{benr}$ ,  $\varphi_{trr}$ , and  $\varphi_{pr r}$  are the rim angular deformations from the moment  $M_0$ , force  $Q_0$ , and pressure  $p_0$ , respectively;  $\varphi_{fl}$  is the overall flange rotation angle.

To determine the rim deformations, we use the known thin wall cylindrical shell equation

$$\frac{d^4 W}{dx^4} + 4k^2 W = \frac{P_0}{D}, \quad (3.3)$$

where

$$k = \sqrt{\frac{3(1-\nu^2)}{R_{av}^2 h^3}}; \quad D = \frac{Eh^3}{12(1-\nu^2)};$$

$x$  is the section coordinate ( $x$  axis is directed along the wheel axis);  $W$  is the radial displacement;  $R_{av}$  is the average rim radius;  $h$  is the rim wall thickness; and  $E$  and  $\nu$  are, respectively, the elastic modulus and Poisson ratio of the drum material.

The general solution of (3.3) can be written as:

$$W = e^{-kx}(C_1 \sin kx + C_2 \cos kx) + W_0, \quad (3.4)$$

where  $W_0$  is the particular solution of (3.3); and  $C_1$  and  $C_2$  are arbitrary constants.

The particular solution of (3.4) will be

$$W_0 = \frac{p_0}{4k^4 D} = \frac{p_0 R_{av}^2}{Eh} \quad (3.5)$$

Locating the coordinate origin at the junction of the flange and rim and also considering the known expressions for the bending moment and shearing force, we obtain the following boundary conditions:

$$M_{x=0} = D \left( \frac{d^2 W}{dx^2} \right)_{x=0} = M_0; \quad (3.6)$$

$$Q_{x=0} = D \left( \frac{d^3 W}{dx^3} \right)_{x=0} = Q_0. \quad (3.7)$$

We differentiate (3.4) three times with respect to  $x$

$$\begin{aligned} \frac{dW}{dx} &= ke^{-kx} [-(C_1 + C_2) \sin kx + (C_1 - C_2) \cos kx]; \\ \frac{d^2 W}{dx^2} &= 2k^2 e^{-kx} (C_2 \sin kx - C_1 \cos kx); \\ \frac{d^3 W}{dx^3} &= 2k^3 e^{-kx} [(C_1 - C_2) \sin kx + (C_1 + C_2) \cos kx]. \end{aligned} \quad (3.8) \quad \underline{139}$$

Substituting these derivatives into (3.6) and (3.7), we find the constants of integration and then the expression for the rim section radial displacement

$$W = \frac{e^{-kx}}{2k^3 D} [kM_0(\sin kx - \cos kx) + Q_0 \cos kx] - \frac{p_0 R_{av}^2}{Eh}. \quad (3.9)$$

Taking  $x = 0$  in (3.9), we obtain the rim edge radial displacements:

$$W_{M_0} = \frac{M_0}{2k^3 D}; \quad W_{Q_0} = \frac{Q_0}{2k^3 D}; \quad W_{p_0} = - \frac{p_0 R_{av}^2}{Eh}. \quad (3.10)$$

Considering that the section rotation angle

$$\varphi = \frac{dW}{dx},$$

we obtain for  $x = 0$ , the expression for the rim deformation:

$$\varphi_{\text{ben } r} = \frac{M_0}{kD}; \quad \varphi_{\text{tr } r} = \frac{Q_0}{2k^2D}; \quad \varphi_{\text{pr } r} = 0. \quad (3.11)$$

On the basis of wheel operating conditions, the flanges must be sufficiently rigid to exclude the possibility of the tire coming off the drum. Flange stiffness is achieved by giving the flange a contoured cross section shape and also by the use of structural stiffeners (ribs, beads, etc.).

To determine the flange rotation angle, we use the theory of axisymmetric ring deformation, based on the assumption of cross section shape invariability.

The wheel flange is loaded by the transverse force  $Q_0$ , normal force  $F_0$ , moment  $M_0$ , and pressure  $q$  (Figure 3.3).

The pressure is distributed along the annular flange surface, bounded by the radii  $R_a$  and  $R_b$ , and can be found from the formula

$$q = \frac{Q_1}{\pi(R_a^2 - R_b^2)}$$

Let us examine flange deformation under the action of the applied loads. We align the  $x$  axis with the wheel axle and direct the  $\rho_0$  axis along the flange neutral line. /40

During rotation of the section through the small angle  $\varphi$ , an arbitrary point B with the coordinates  $\rho$  and  $x_0$  acquires a radial displacement defined by the equality

$$\Delta\rho \cong \varphi x_0.$$

The relative elongation of the annular fiber B is then

$$\varepsilon = \frac{\Delta\rho}{\rho} = \frac{\varphi}{\rho} x_0. \quad (3.12)$$

Hence, the corresponding tangential stress

$$\sigma_t = \frac{Ex_0}{\rho} \varphi. \quad (3.13)$$

The internal force factors at any flange cross section reduce to the normal force  $N$  and bending moment  $M$ .

They are associated with the tangential stress  $\sigma_t$  by the simple relations

$$M = \int_F \sigma_t x dF \quad \text{and} \quad N = \int_F \sigma_t dF. \quad (3.14)$$

Substituting (3.13) into (3.14), we obtain

$$\varphi = \frac{M}{E \int_F \frac{x^2 dF}{\rho}}. \quad (3.15)$$

For our case

$$M = \frac{1}{2} \left[ \int_0^\pi q \rho^2 \sin \alpha d\alpha d\tau - \int_0^\pi F_0 R_{av} \sin \alpha d\alpha - \right. \\ \left. - \int_0^\pi M_0 R_{av} \sin \alpha d\alpha - \int_0^\pi Q_0 l R_{av} \sin \alpha d\alpha \right],$$

where  $l$  is the distance between the flange neutral axis and the point of application of the force  $Q_0$ .

After integrating, we obtain

$$M = \frac{q}{3} (R_a^3 - R_b^3) - F_0 R_{av}^2 - M_0 R_{av} - l Q_0 R_{av}. \quad (3.16)$$

Substituting the values of  $q$  and  $F_0$  into (3.16), we have

/41

$$M = p_0 [(R - r)^2 - R_b^2] \left[ \frac{R_a^3 - R_b^3}{3(R_a^2 - R_b^2)} - \frac{R_{av}}{2} \right] - R_{av} (M_0 + l Q_0). \quad (3.17)$$

Then we find the normal force N from (3.14)

$$N = -\frac{1}{2} \int_0^\pi Q_0 k_{av} \sin \alpha d\alpha = -R_{av} Q_0. \quad (3.18)$$

Substituting the flange and rim deformations found above into (3.2), we obtain

$$\left. \begin{aligned} \frac{1}{2k^3 D} (Q_0 - kM_0) - \frac{p_0}{4k^4 D} &= 0; \\ -\frac{1}{2k^3 D} (Q_0 - 2kM_0) &= \varphi; \end{aligned} \right\} \quad (3.19)$$

$$M_0 = p_0 \left\{ \frac{[(R-r)^2 - R_b^2] \left[ \frac{(R_a^3 - R_b^3)}{3(R_a^2 - R_b^2)} - \frac{R_{av}}{2} \right] - \frac{2R_{av}}{2k} + \frac{6(1-\nu^2)J}{2k^3 h^3}}{R_{av}(1+l) + \frac{6(1-\nu^2)J}{kh^3}} \right\}; \quad (3.20)$$

$$\begin{aligned} Q_0 = p_0 \left\{ \frac{[(R-r)^2 - R_b^2] \left[ \frac{R_a^3 - R_b^3}{3(R_a^2 - R_b^2)} - \frac{R_{av}}{2} \right] - \dots}{R_{av}(1+l) + \frac{6(1-\nu^2)J}{kh^3}} \dots \right. \\ \left. \dots - \frac{2R_{av}}{2k} + \frac{6(1-\nu^2)J}{2k^3 h^3} \right. \\ \left. \dots \rightarrow \frac{\dots}{R_{av}(1+l) + \frac{6(1-\nu^2)J}{kh^3}} + \frac{1}{k^2} \right\}. \end{aligned} \quad (3.21)$$

With account for (3.20) and (3.21), the maximal meridional stresses at any rim cross section are found from the formula

$$\sigma = \frac{6}{h^2} e^{-kx} \left[ M_0 \cos kx + \left( M_0 - \frac{Q_0}{k} \right) \sin kx \right] + 2\pi R_{av} h \quad (3.22)$$

## 2. Determination of Stresses in a Rolling Wheel

The load on the wheel flange from the internal tire pressure can be considered a static load, since the air pressure in the tire changes very little as the tire deflects. However, as the wheel rolls under load, cyclic stresses whose magnitudes change with wheel

/42

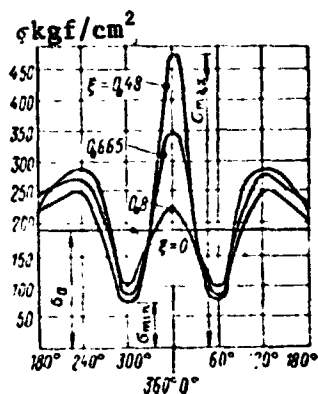


Figure 3.4. Typical meridional stress variation curves for rolling of a 660 x 200 mm wheel with different tire deflections.

meridional stress variation curves for different tire deflections for a 660 x 200 mm wheel.

The constant stresses  $\sigma_a$  from internal pressure for the undeflected tire are shown by the straight line parallel to the abscissa axis, while the curves of meridional stress variation for the wheel rolling under load have three peaks with the stress maximum located at the midpoint of the area of wheel contact with the supporting surface. The meridional stress curve also has two minima, located symmetrically relative to the line of vertical force action. The stress variation cycle in the rolling wheel is characterized by /43 the maximal and minimal stresses.

To determine these stresses, we introduce the following ratio

$$k_s = \frac{\sigma}{\sigma_p}, \quad (3.23)$$

where  $k_s$  is the flange secondary load coefficient, accounting for the stress increase with deflection of the tire by the radial load in comparison with the stress for the undeflected tire;  $\sigma$  is the meridional stress in the given section from the tire air pressure, determined from (3.22); and  $\sigma_p$  is the maximal stress at the given section due to additional flange spreading as the tire deflects.

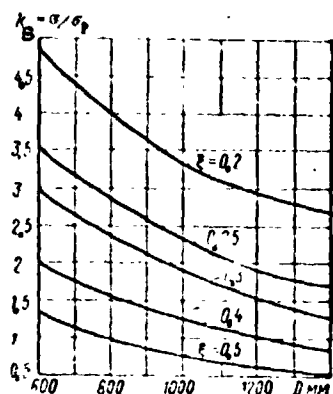


Figure 3.5. Experimental variation of flange secondary load coefficient  $k_s$  versus tire diameter  $D$  for various deflection ratios  $\xi$ .

Figure 3.5 shows the experimental dependence of the coefficient  $k_s$  on tire diameter for various degrees of tire deflection. By degree of tire deflection, we mean the quantity:

$$\xi = \frac{\delta_{\text{def}}}{\delta'_{\text{def}}}$$

where  $\delta_{\text{def}}$  is the tire deformation (deflection) for the given load and  $\delta'_{\text{def}}$  is the maximal possible tire deformation.

The flange secondary loading coefficient  $k_s$  can be either more or less than one. If  $k_s < 1$ , this means that the maximal stress in the flange cross section from the vertical load exceeds the stress from the tire pressure.

#### Influence of Wheel Flange and Rim Geometric Parameters on Magnitude of the Edge Forces and Stresses

Let us find how the various wheel geometric factors affect the conditions of occurrence and nature of manifestation of the edge effect at the wheel flange and rim junction, i.e., on the quantities  $M_0$  and  $Q_0$ .

The overall maximal stress at any flange section will be

$$\sigma_{\text{max}} = \sigma \left( 1 + \frac{1}{k} \right). \quad (3.24)$$

It has been established experimentally that the coefficient  $k_s$  is independent of tire pressure and will be constant, regardless of the particular combination of loading and tire pressure for which the given deflection is obtained. Figure

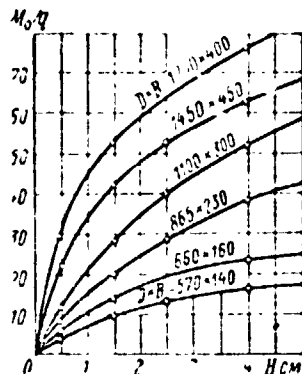


Figure 3.6. Relative edge moment  $M_0/q$  versus flange height  $H$  for different size wheels ( $D$  is the tire diameter,  $B$  is the tire width)

From examination of (3.20) and (3.21), we can draw the following conclusions: the moment  $M_0$  and force  $Q_0$  and, along with them, the stresses in the wheel flanges and rim depend linearly on the tire air pressure. /44

The moment  $M_0$  and force  $Q_0$  have a complex functional dependence on the flange height and its moment of inertia  $I$ , the average rim radius, and the rim wall thickness.

For any values of the parameters, the edge force and edge moment can take only positive values.

In the following, when analyzing (3.20) and (3.21), we shall take only one of the variables as an argument and assign it definite numerical values. We shall specify its range of variation so that it will lie in narrow limits which are of practical importance for wheel design.

First of all, the relative edge bending moment  $M_0/q$  for wheels of different dimensions, other parameters remaining the same, increases with increase of the flange height  $H$  (Figure 3.6).

Figure 3.7 shows the relative edge moment  $M_0/q$  and edge force  $Q_0/q$  versus rim wall thickness  $h$  for different size wheels. We see from Figure 3.7 that there is some increase of the edge moment  $M_0/q$  with increased rim wall thickness near the junction with the flange, and this increase is most significant for small and medium size wheels. Therefore, the meridional stress reduction at these sections will not be proportional to the square of the wall thickness change. For example, calculations show that increase of the rim wall /45

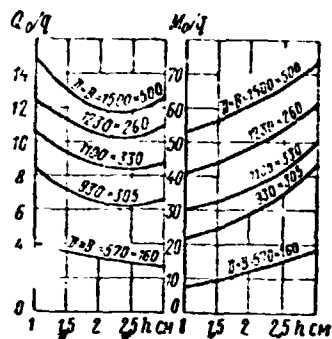


Figure 3.7. Relative edge force  $Q_0/q$  and moment  $M_0/q$  versus rim wall thickness  $h$  for different size wheels.

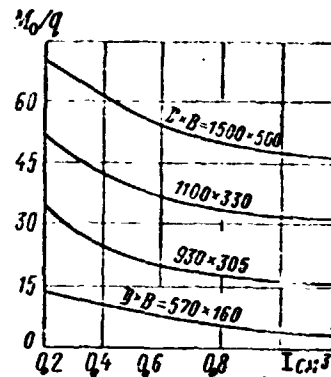


Figure 3.8. Relative edge moment  $M_0/q$  versus flange moment of inertia  $I$  for different size wheels.

Thickness from one to three centimeters in a 1500 x 500 mm wheel increases the moment  $M_0$  by 1.38 times and reduces the stress in the wall by 6.5 times, while for the 570 x 160 mm wheel, the factors are 2.2 and 4, respectively.

Thus, increase of the rim wall thickness as a technique for reducing the rim stresses is most effective for large wheels.

Figures 3.7 and 3.8 show the relative edge force and edge moment as functions of rim wall thickness and wheel flange moment of inertia. Reduction of the edge force is observed up to a definite wall thickness, equal to approximately 2 cm, and then the force increases. In many cases, rim wall thickness increase is not possible for constructional reasons. In this case, stress reduction is achieved by increasing the flange radial moment of inertia.

### 3. Wheel Bearing Analysis

Aircraft wheels utilize conical roller bearings, whose loading conditions differ significantly from those for conventional bearings used in general machine construction. Aircraft wheel bearings experience particularly large radial and side loads during airplane takeoff and landing. In addition, they operate at wheel rotational

speeds which vary over a very large range (from zero to maximum during takeoff and from maximum to zero during landing).

For the analysis, we use three bearing operating regimes, corresponding to airplane takeoff, landing, and taxiing. For the takeoff regime, we specify the maximal bearing rpm  $n_1$ , operational radial load  $P_{r1}$ , operational axial load  $P_{ax1}$ , and the takeoff ground run  $L_1$ ; for the landing regime, we take, correspondingly,  $n_2$ ,  $P_{r2}$ ,  $P_{ax2}$ , and  $L_2$ ; for the taxi regime, we take  $n_3$ ,  $P_{r3}$ , and  $L_3$ .

In the analysis, we must also consider the allowable bearing operating temperature  $t^\circ \text{C}$ , the magnitudes of the possible short term radial  $P_{r \text{ max}}$  and axial  $P_{ax \text{ max}}$  impact overloads, wheel radius  $R_w$ , and the number of bearing operating cycles  $n_b$  (one cycle includes takeoff, landing, and taxi). /46

First, using the work capacity coefficient required by the operating conditions, we select from the catalog a suitable bearing, determine its possible service life, and the number of cycles  $n_b$  which the bearing can withstand in accordance with its load capacity rating.

The bearing work capacity coefficient is calculated from the known formula:

$$k_b = P_{r \text{ eqv}} k_d k_r k_t \left[ \frac{n_b (L_1 + L_2 + L_3)}{377 R_r} \right]^{0.3}, \quad (3.25)$$

where  $k_d$  is a dynamic coefficient (usually  $k_d = 1.8 \div 2.5$  for aircraft wheels);  $k_r$  is a coefficient accounting for which bearing race rotates (with inner race rotation,  $k_r = 1$ , with outer race rotation,  $k_r = 1.35$ );  $k_t$  is a coefficient accounting for the influence of bearing temperature regime on service life.

Its values are given in the table:

t in ° C	125	150	175	200	225	250
k <sub>t</sub>	1.05	1.10	1.15	1.25	1.35	1.40

$P_{r \text{ eqv}}$  is the equivalent radial load on the bearing, found from the formula

$$P_{r \text{ eqv}} = \sqrt[3.33]{a_1^3 Q_1^{3.33} + a_2^3 Q_2^{3.33} + a_3^3 Q_3^{3.33}}. \quad (3.26)$$

Here

$$a_1 = \tau_1/T, \quad a_2 = \tau_2/T, \quad \text{and} \quad a_3 = \tau_3/T;$$

$\tau_1$  is the operating time during takeoff [ $\tau_1 = (L_1 \cdot 1000)/(2\pi R_r n'_1)$ ];  
 $\tau_2$  is the operating time during landing [ $\tau_2 = (L_2 \cdot 1000)/(2\pi R_r n'_2)$ ];  
 $\tau_3$  is the operating time during taxi [ $\tau_3 = (L_3 \cdot 1000)/(2\pi R_r n'_3)$ ];  
 $T$  is the complete cycle operating time ( $T = \tau_1 + \tau_2 + \tau_3$ );  $\beta_1, \beta_2,$  /47  
and  $\beta_3$  are the ratios of the average number of bearing revolutions in the corresponding regime to the equivalent number of revolutions per cycle. Thus,  $\beta_1 = n'_1/n_{\text{eqv}}$ ;  $\beta_2 = n'_2/n_{\text{eqv}}$ ; and  $\beta_3 = n'_3/n_{\text{eqv}}$ , where  $n'_1, n'_2,$  and  $n'_3$  are the average bearing rpms in the corresponding regimes ( $n'_1 = n_{1 \text{ max}}/2$ ;  $n'_2 = n_{2 \text{ max}}/2$ ; and  $n'_3 = n_{3 \text{ max}}/2$ );  $n_{\text{eqv}} = (n'_1 \tau_1 + n'_2 \tau_2 + n'_3 \tau_3)/T$  is the equivalent number of bearing revolutions;  $Q_1, Q_2,$  and  $Q_3$  are the reduced axial loads in the corresponding regimes:

$$Q_1 = R'_1 + mA_1; \quad Q_2 = R'_2 + mA_2; \quad Q_3 = R'_3 + mA_3,$$

(here  $R'_1 = \frac{2}{3} R_1, R'_2 = \frac{2}{3} R_2$  and  $R'_3 = R_3$ ) ; and  $m$  is the coefficient of axial load reduction to an equivalent radial load, defined as

$$m = \frac{1}{2.6 \lg \beta},$$

where  $\beta$  is the contact angle between the roller and the retainer.

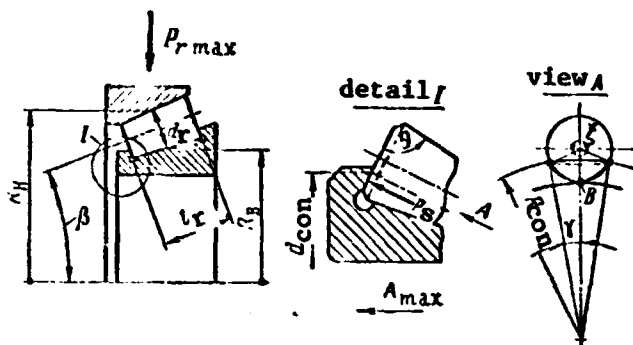


Figure 3.9. Wheel bearing analysis diagram.

After selecting the bearing, we determine its service life  $h$  in hours from the relation (the coefficient  $C$  is taken from the handbook)

$$C = Q_{eqv} k_{fl} k_r k_t (n_{eqv} h)^{0.3}.$$

The number  $n_b$  of bearing operating cycles is found from the formula

$$n_b = 60h/T.$$

Then we make a check calculation of the selected bearing in the following sequence: we determine the maximal allowable contact pressure on the bearing inner race; the allowable overload with account for short term action of the maximal side and maximal radial loads; the allowable specific pressure on the inner race thrust collar based on absence of lubricant and carbon deposit formation.

The wheel bearing analysis diagram is shown in Figure 3.9.

The maximal contact stress on the bearing inner race is found from the formula

$$\sigma_{max} = 613 \sqrt{\frac{P}{l_r} \left( \frac{Z}{d_r} + \frac{1}{R_B} \right)}. \quad (3.27)$$

where  $P$  is the radial load on the most highly loaded roller  $P = \frac{4.6 P_{r \max}}{Z \cdot \cos \beta}$  (here  $P_{r \max}$  is the maximal radial load);  $Z$  is the number of rollers;  $\beta$  is the contact angle;  $l_r$  is the roller length;  $d_r$  is the average roller diameter;  $R_B$  is the rolling radius at the average roller diameter.

To ensure reliable bearing operation, the maximal contact pressure should not exceed  $50,000 \text{ kgf/cm}^2$ .

We calculate the specific pressure on the inner race thrust collar surface with the maximal axial force  $A_{\max}$  acting on this collar. We first determine the area of roller contact with the race thrust collar:

$$S_{\text{con}} = \left( \frac{\pi}{180} 2\xi - \sin 2\xi \right) \frac{r_{\min}^2}{2} + \left( \frac{\pi}{180} 2\gamma - \sin 2\gamma \right) \frac{R_{\text{con min}}^2}{2},$$

where  $\xi$  is the angle of roller contact with the inner race thrust collar;  $r_{\min}$  is the minimal dimension of roller contact with the thrust collar;  $\gamma$  is the angle between the point of roller contact with the inner race and the thrust collar; and  $R_{\text{con min}}$  is the minimal radius of roller contact with the thrust collar.

The maximal side force  $P_s$  acting on the bearing collar is

$$P_s = \frac{4.6R_{\max}}{Z} \frac{\sin \varphi}{\cos \beta \sin \theta} + \frac{A_{\max}}{Z} \frac{\sin \varphi}{\sin \beta \sin \theta}.$$

where  $\varphi$  is the angle between the roller generators;  $\theta$  is the angle between the roller generator and end face. /49

From the maximal load  $P_s$  and the contact area, we find the specific pressure on the bearing collar

$$p_{\text{sp}} = P_s / S_{\text{con}}.$$

The allowable value of  $p_{\text{sp}}$  for a bearing should not exceed 3 — 4 kgf/mm<sup>2</sup>.

It is necessary that the bearing withstand, without failure, short term overloads  $Q_{\text{dyn}}/Q_{\text{st}} \leq 5$ , where  $Q_{\text{dyn}}$  is the variable short term load, equal to  $R_{\max} + mA_{\max}$  (here  $m$  is the axial load reduction coefficient);  $Q_{\text{st}}$  is the allowable static load, determined from the catalog.

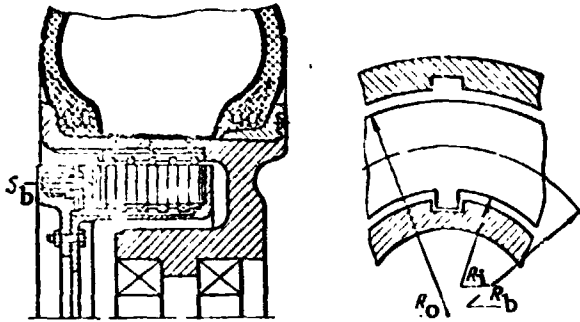


Figure 3.10. Schematic of disc wheel brake.

For conical roller bearings of the ultralight and light duty series,  $m = 1.5$ , for bearings of the intermediate series,  $m = 1.8$ .

#### 4. Calculation of Wheel Brake Basic Characteristics and Strength

Wheel brake analysis involves determining the braking moment, friction element service life, brake energy absorption capacity, and also calculation of the strength of the basic constructional element details.

*Braking moment calculation.* For effective wheel braking, it is necessary that

$$M_{tr} = M_b.$$

The wheel brake braking moment depends on several factors. For example, for the disc brake shown schematically in Figure 3.10, the braking moment is

$$M_b = f_b S_b R_b n,$$

where  $f_b$  is the friction coefficient of the brake friction pair;  $S_b$  is the axial brake disc compressive force;  $R_b$  is the effective friction radius; and  $n$  is the number of friction surface pairs.

The magnitude of the effective friction radius  $R_b$  depends on the contacting surface shape and specific pressure distribution over the friction area. For the disc brake shown in Figure 3.10

$$R_b \approx \frac{R_o + R_1}{2},$$

where  $R_o$  is the disc outer radius and  $R_1$  is the disc inner radius.

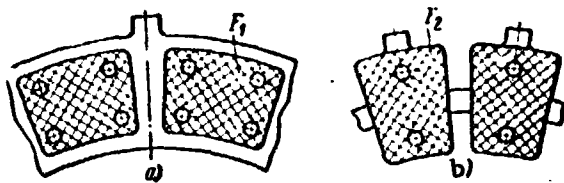


Figure 3.11. Brake disc construction.  
a- cermet; b- bimetallic.

Knowing the required braking moment and the number  $n$  of friction surface pairs, we can find the brake disc compressive force  $S_b$  from the formula

$$S_b = \frac{M_b}{f_b R_b n} \quad (3.28)$$

From the force  $S_b$ , we calculate the working pressure in the brake actuating cylinders

$$p_b = 1.2 S_b / F_p,$$

where 1.2 is a coefficient accounting for the pressure losses in overcoming the spring elastic force and the friction force;  $F_p$  is the total area of all the cylinder block pistons.

The brake friction discs are the primary structural element and determine, to a considerable degree, brake performance. Improperly selected friction material characteristics or improperly selected disc geometry can cause brake vibration, friction pair material galling, or large braking moment overshoots. Brake friction element design reduces primarily to determining the geometric (theoretical) friction area, the mutual overlap coefficient, and the geometric friction area variation coefficient. The geometric (theoretical) friction area of the friction discs is the ideal, with respect to contact conditions, area on which the friction forces are created. This area depends on the disc dimensions and construction.

51

Figure 3.11 shows the structural elements of cermet (a) and bimetallic (b) discs with the geometric friction areas  $F_1$  and  $F_2$ .

The contact area on the brake discs does not cover the entire disc area, but rather only a part, reaching in certain cases only 10% of the geometric area.

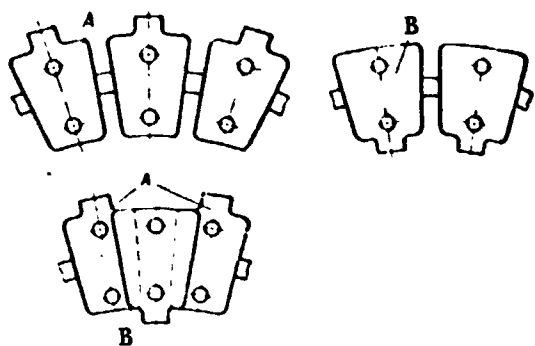


Figure 3.12. Illustration of brake friction disc operation with improperly selected disc sectors.

As a rule, small discs consisting of individual sectors or segments have better contacting capability than continuous discs. In calculations of the friction characteristics of a brake with such discs, it is necessary to know the disc mutual overlap coefficient

$$k_{\text{mut}} = F_c F_b / F_e^2, \quad (3.29)$$

where  $F_c$  and  $F_b$  are the geometric (theoretical) friction area of one side of the first (cermet) and second (bimetallic) friction elements; and  $F_e$  is the effective friction area, obtained with rotation of the friction pair elements about the center of revolution.

The mutual overlap coefficient was introduced into the calculations by A. V. Chichinadze. The magnitude of the coefficient  $k_{\text{mut}}$  influences the nature of the temperature distribution in the brake discs and, to a considerable degree, determines the average surface and in-depth temperatures, on which depend in turn the friction coefficient and friction pair surface wear. In modern disc brakes, the mutual overlap coefficient varies in the range 0.6 — 0.8. In disc brakes with exposed friction surface  $k_{\text{mut}} = 0.2 \div 0.3$ .

The geometric friction area variation which can take place with improperly selected friction disc parameters has a significant influence on brake dynamic performance. In order to clarify this influence, we shall examine how the friction discs shown in Figure 3.12 operate. These discs have the same number of sectors which are identical in size and shape. It is quite obvious that the geometric friction area will vary as the cermet disc A slides over the bimetallic disc B. The friction area will be maximal when sector B lies on sector A and minimal when sector B simultaneously overlaps two adjacent sectors A. Thus, the friction area will change as the wheel turns. This variation is shown in Figure 3.13a for a brake /52

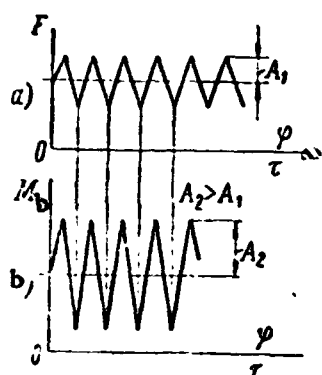


Figure 3.13. Geometric friction area  $F$  (a) and braking moment  $M_b$  (b) for disc brake (with improperly selected discs) as functions of wheel rotation angle  $\varphi$  and braking time  $\tau$ .

having the described discs. The coefficient accounting for geometric friction area variation is:

$$\gamma_F = \frac{F_{\max} - F_{\min}}{F_{\max} + F_{\min}} 100\% \quad (3.30)$$

For wheel braking to be smooth, the coefficient  $\gamma_F$  should not exceed 5%. When it exceeds this value, the amplitude of the braking moment oscillation may increase.

The occurrence of resonant strut vibrations is possible for a certain combination of disc and brake housing stiffness, friction material quality, and landing gear element stiffness. Excessively large variation of the geometric friction area also has an unfavorable influence on the brake pair load capacity and the magnitude of the working surface wear. Knowing the theoretical friction area and the kinetic energy which is transformed by the brake into heat energy, we can determine the specific braking work and the average specific friction power. The specific braking work /53

$$A_{sp \ f} = \frac{A_b}{nF_g} = \frac{M_b \varphi}{nF_g}, \quad (3.31)$$

where  $A_b$  is the kinetic energy transformed into heat by the brake;  $n$  is the number of friction surface pairs;  $F_g$  is the geometric (theoretical) area of one friction surface;  $M_b$  is the braking moment; and  $\varphi$  is the braking distance, expressed in radians.

The average specific friction power

$$(N_{sp \ f})_{av} = \frac{A_{sp \ f}}{\tau} \approx \frac{M_b \omega_{b1}}{2nF_g} \quad (3.32)$$

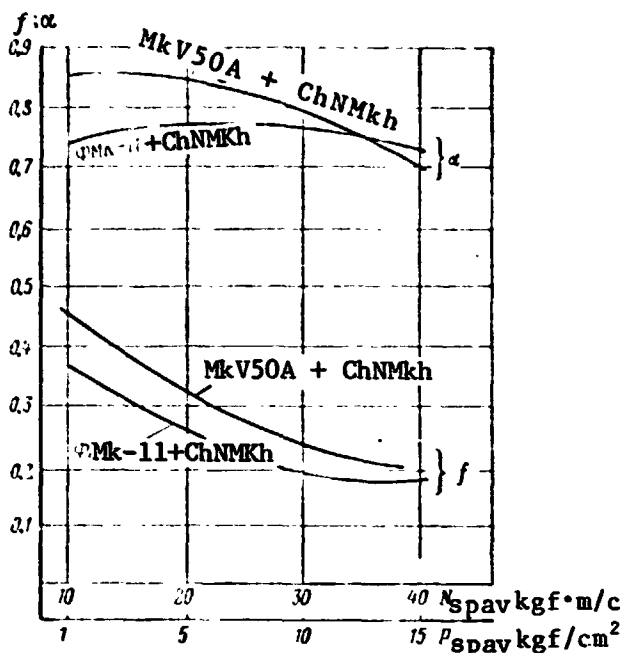


Figure 3.14. Friction coefficient  $f$  as a function of the average specific pressure  $p_{spav}$ , and stability coefficient  $\alpha_{st}$  as a function of the average specific braking power  $(N_{sp f})_{av}$ .

rate of transformation of mechanical energy into the thermal energy.

Studies have shown that, for aircraft disc brakes, the friction coefficient and its stability depend both on the initial sliding velocity  $V_{sl i}$ , specific braking work  $A_{sp f}$ , and mass average temperature  $\theta_v$ , and on the quantity  $(N_{sp f})_{av}$ . Figure 3.14 shows the friction coefficient  $f$  versus average specific pressure for multi-disc aircraft wheel brakes (friction pair: cermet MKV-50A and iron ChNMkh). This dependence is generalized for initial sliding velocities  $V_{sl i} = 18 \div 30$  m/sec, specific braking work  $A_{sp f} = 200 \div 500$  kgf/cm<sup>2</sup>, and mass average brake disc packet temperatures  $\theta_v = 350 \div 600^\circ$  C. Possible combinations of  $V_{sl i}$ ,  $A_{sp f}$ , and  $\theta_v$  in the indicated variation ranges can yield deviations in the magnitude of the friction coefficient of order  $\pm 10\%$ . This same figure shows

where  $\tau$  is the braking time; and  $\omega_{b1}$  is the wheel angular velocity at the moment of braking initiation.

The specific braking work, the average specific friction power, and also the speed at which sliding of the friction elements begins are the basic parameters determining the brake operating regime. The specific braking work  $A_{sp f}$  is equivalent to the heat energy generated in the braking process per unit friction element contact area.

The quantity  $(N_{sp f})_{av}$  is the average power per unit contact area. It expresses the

the stability coefficient  $\alpha_{st}$  versus average specific braking pressure. The stability coefficient is the ratio

$$\alpha_{st} = \frac{M_{b\ st}}{M_{b\ max}}$$

/54

where  $M_{b\ av}$  is the average braking moment during the braking time; and  $M_{b\ max}$  is the maximal braking moment for the given braking operation.

We see from the figure that, for  $(N_{sp\ f})_{av} = 30\ \text{kgf/m/(cm}^2/\text{sec)}$ , the stability coefficient  $\alpha_{st}$  does not exceed 0.57, which is its maximal allowable normed value. Consequently, use of the given friction pair cannot be recommended for  $(N_{sp\ f})_{av} \geq 30\ \text{kgf/m/(cm}^2/\text{sec)}$ .

The cermet wear rate depends on  $(N_{sp\ f})_{av}$  and  $A_{sp\ f}$ . Figure 3.15 shows this dependence for several values of  $(N_{sp\ f})_{av}$ , generalized for  $V_{sl\ i} = 10 : 30\ \text{m/sec}$  and  $\theta_v = 350 : 600^\circ\ \text{C}$ . Different combinations of  $v_{sl\ i}$  and  $\theta_v$  may yield deviations of  $I_h$  from the values shown in the figure by 30%. The wear rate of ChNMKh iron is less than the wear rate of MKV-50A cermet by a factor of three to four.

It is more convenient to examine the brake friction element wear rate  $I_h$  calculation for a specific example with the following basic data:

Kinetic energy absorbed by the brake in a single actuation $A_b$	$6.6 \cdot 10^5\ \text{kgf/m}$
Braking moment $M_b$	$330\ \text{kgf/m}$
Angular friction element sliding velocity at braking initiation $\omega_{bi}$	$200\ \text{sec}^{-1}$
Brake disc outer diameter $D_o$	$245\ \text{mm}$

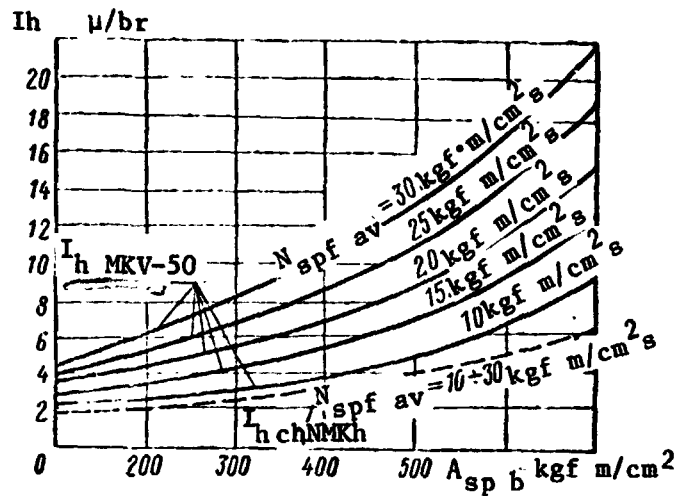


Figure 3.15. Wear rate  $I_h$  of MKV-50A cermet versus specific braking work  $A_{sp}$  for various average specific powers,

Brake disc inner diameter $D_1$	140 mm
Average friction area radius $R_b$	96 mm
Theoretical friction area of one side of cermet disc $F_c$	276 cm <sup>2</sup>
Theoretical friction area of one side of bimetallic disc $F_b$	280 cm <sup>2</sup>
Effective friction area for one side of disc $F_e$	317 cm <sup>2</sup>
Number of brake surface pairs $n'$	8

The calculation begins with determining the mutual overlap coefficient from (3.29)

$$k_{mut} = \frac{F_c \cdot F_b}{F_e^2} = 0.77.$$

Then we determine the theoretical friction area for one side of the friction disc

$$F_f = F_e \cdot k_{mut} = 244 \text{ cm}^2.$$

After finding  $F_f$ , we determine the average specific friction power (under the condition  $M_b \approx \text{const}$ ) for the paired (cermet and bimetallic) friction surfaces

/56

$$(N_{sp f})_{av} = \frac{M_b \omega_{b1}}{2F_f \cdot n'} = 17 \text{ kgf/m/(cm}^2/\text{sec)}$$

and the specific braking work

$$A_{sp f} = \frac{A_b}{F_f \cdot n'} = 340 \text{ kgf/m/cm}^2.$$

The values of the friction coefficient and the stability coefficient, determined from the curves of  $f(N_{sp f})_{av}$  and  $\alpha_{st}(N_{sp f})_{av}$  in Figure 3.14, are

$$f \approx 0.3 \pm 10\% \quad \text{and} \quad \alpha_{st} \geq 0.7.$$

The values of the cermet (MKV-50A) and iron (ChNMKh) wear for a single braking, determined from the  $I_h(A_{sp f})$  curves in Figure 3.15, are

$$(I_h)_{MKV} \leq 6 \cdot 10^{-6} \text{ mm}, \quad (I_h)_{ChNMKh} \leq 3 \cdot 10^{-6} \text{ mm}.$$

The overall friction pair wear is

$$\Sigma I_h = (I_h)_{MKV} + (I_h)_{ChNMKh} \leq 9 \cdot 10^{-6} \text{ mm}.$$

The brake disc service life is found from this overall wear and the allowable friction layer thickness.

The required disc clamping force, found from (3.28) is

$$S_b = \frac{M_b}{f R_b n'} \approx 1400 \text{ kgf}.$$

The average specific pressure on the friction elements is

$$P_{sp} = \frac{S_b}{F_f} \approx 5.75 \text{ kgf/cm}^2.$$

For an overall cylinder block piston area  $F_p$  equal to  $18 \text{ cm}^2$ , the brake system working pressure is

$$p_b = \frac{1.2 S_b}{F_p} \approx 95 \text{ kgf/cm}^2.$$

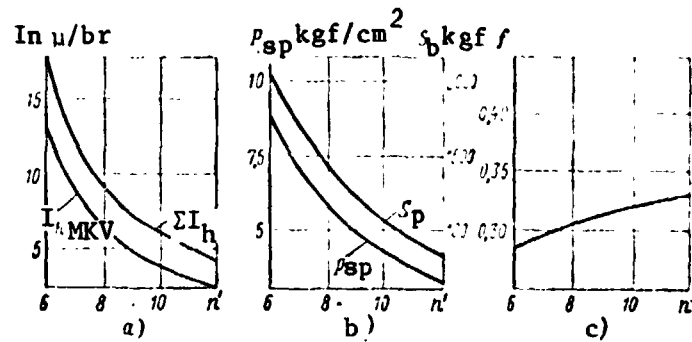


Figure 3.16. Friction pair wear rate  $I_h$  (a), specific pressure  $p_{sp}$ , and clamping force  $S_b$  (b), and friction coefficient  $f$  (c) versus number  $n'$  of brake discs.

The results of such a calculation for different number of friction surface pairs are shown in Figure 3.16. We see from the analysis of these curves that reduction of the number of friction surface pairs (number of discs), while retaining the braking moment constant, leads to increase of the spreading force, increase of the specific pressure on the friction elements, and, therefore, to sharp increase of the wear rate  $I_h$  and decrease of the friction coefficient  $f$ . Therefore, increase of the number ( $n'$ ) of friction surfaces is sometimes used in order to increase friction element service life. /57

## 5. Calculation of Brake System Energy Capacity

The friction pair is the most highly loaded component with regard to thermal loading. The thermal effect shows up most markedly on the brake and wheel components: cylinder block, where there are rubber details, wheel hub with the bearings, and the tire. For these components, there is some maximal temperature rise, exceeding which may lead to shortening the component service life or component failure.

The amount of heat absorbed by the brake system is proportional to its mass, the heat capacity of the materials used in the system, and the allowable mass average friction pair temperature

$$Q = k_d \left( \sum_{i=1}^n G_i c_{pi} \right) (\theta_v - \theta_0), \quad (3.29)$$

where

$$G_i c_{pi} = G_1 c_{p1} + \dots + G_n c_{pn}.$$

Here  $G_1$  is the weight of the disc structural elements;  $n$  is the number of discs;  $c_{pi}$  is the specific heat capacity of the structural element;  $k_d$  is a coefficient accounting for heat dissipation during braking and in the temperature equalization process ( $k_d \approx 0.85$ );  $\theta_v$  is the allowable mass average temperature rise of the brake packet structural elements;  $\theta_0$  is the initial temperature of the brake structural elements. /58

The brake system energy absorption capacity is

$$A_b = \frac{k_d}{\frac{1}{427}} (\theta_v - \theta_0) \sum_{i=1}^n G_i c_{pi}, \quad (3.30)$$

where  $A_b$  is the allowable kinetic energy which the brake is capable of transforming;  $1/427$  is the heat equivalent of work.

As a rule, the maximal allowable brake packet temperature rise should not exceed  $400 - 500^\circ \text{C}$ .

Calculation of the brake energy absorption capacity involves determining the mass average packet temperature for the given kinetic energy and packet mass. We shall illustrate the procedure for calculating the brake energy absorption capacity using an example with the following initial values:

Kinetic energy to be absorbed by brake  
in one application

$$A_b = 800,000 \text{ kgf/m}$$

Overall weight of brake packet steel  
components (steel housings, cermet  
discs, etc.)

$$G_{st} = 14.6 \text{ kgf}$$

Total weight of cermet in braking	$G_c = 4.42 \text{ kgf}$
Overall brake disc iron sector weight	$G_c = 18.5 \text{ kgf}$
Heat capacity:	
steel	$c_{p \text{ st}} = 0.12 \text{ kcal/(kgf/°C)}$
cermet	$c_{p \text{ c}} = 0.17 \text{ kcal/(kgf/°C)}$
iron	$c_{p \text{ i}} = 0.15 \text{ kcal/(kgf/°C)}$

If we take  $\theta_0 = 20^\circ \text{ C}$  as the initial brake temperature, the mass average brake disc packet temperature, found from (3.30), will be

$$\theta_0 = \frac{A_b}{k_d \Sigma G_i c_{pi}} \frac{1}{427} = 400^\circ \text{ C};$$

$$\Sigma G_i c_{pi} = c_{p \text{ st}} G_{\text{st}} + c_{p \text{ c}} G_{\text{c}} + c_{p \text{ i}} G_{\text{i}} = 5.41 \text{ kcal/°C}.$$

Thus, the mass average packet temperature does not exceed the allowable value ( $400^\circ \text{ C}$ ) and this is a guarantee that the temperature of the other structural elements also will not exceed the allowable value.

## 6. Strengtn Analysis of Brake Details

The primary disc brake friction elements which must be analyzed for strength include the tenon-type friction element joints, the riveted sector joints, the cylinder blocks. etc.

*Analysis of brake disc tenon joints.* In brake element strength 59 analysis, the theoretical ultimate braking moment  $M_{bth}$  must be greater than the operating moment.

The force  $P_{\text{ten}}$  acting on the rotating disc tenon (Figure 3.17) is found from the formula

$$P_{\text{ten}} = \frac{8M_{bth}}{k_n n_{\text{ten}} (D_1 + D_2) n_c}$$

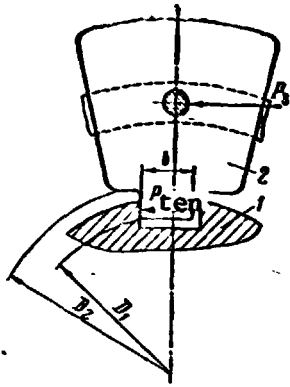


Figure 3.17. Diagram of forces acting on disc tenon during braking.

where  $n_{ten}$  is the number of disc tenons;  $n'$  is the total number of brake friction surfaces;  $M_{bth}$  is the theoretical ultimate braking moment;  $k_n$  is a coefficient accounting for tenon load nonuniformity [its value depends on assembly accuracy (usually  $k_n = 0.75$ )];  $D_1$  is the tenon circle outer diameter; and  $D_2$  is the tenon circle inner diameter.

The tenon joint (tenon on the disc and groove in the drum) is analyzed in bending, shearing, and bearing:

a. bending stress in tenon

$$\sigma_{ben\ ten} = \frac{3P_{ten}(D_1 - D_2)}{2 \cdot b_{ten} \delta_{ten}} \left( \frac{1}{b} + \frac{f_{ten}}{\delta_{ten}} \right), \quad (3.31)$$

where  $b_{ten}$  is the tenon width;  $\delta_{ten}$  is the tenon thickness;  $f_{ten}$  is the coefficient of friction between the tenon and the groove (usually  $f_{ten} = 0.1 \div 0.15$ );

b. shearing and bearing stresses in tenon

$$\tau_{sh} = \frac{3P_{ten}}{2b\delta_{ten}}, \quad (3.32)$$

$$\sigma_{be} = \frac{P_{ten}}{\delta_{ten} h_{be}} \quad (3.33)$$

where  $h_{be}$  is the bearing area height.

In all the above calculations, the strength safety factor is determined from the relations:

$$\eta = \frac{\sigma_u}{\sigma} - 1 \geq 0, \quad \text{or} \quad \eta = \frac{\tau'_{sh}}{\tau_{sh}} - 1 \geq 0,$$

where  $\delta'_1 \tau_{sh}$  is the component material ultimate strength with account for heating (in bending and shear).

*Analysis of riveted joint.* Rivets are used to attach the cermet or iron sectors to the steel load-carrying structure. The force applied to the rivet is found from the formula (see Figure 3.17)

$$P_{riv} = \frac{4M_{b\ th}}{k_n(D_3 + D_2)n_s n_f n_{riv}}, \quad (3.34) \quad /60$$

where  $M_{b\ th}$  is the theoretical ultimate braking moment;  $D_3$  is the sector outer diameter;  $D_2$  is the sector inner diameter;  $n_s$  is the number of disc sectors;  $n_f$  is the number of brake friction surfaces; and  $n_{riv}$  is the number of rivets per sector.

*Verification of brake cylinder block strength* is made on the basis of the theoretical ultimate pressure in the brake system

$$P_{b\ th} = k_s \frac{1.2S_f}{F_p} \quad (3.35)$$

where  $k_s$  is the safety factor;  $F_p$  is the overall piston area;  $S_f$  is the brake spreading force.

In the strength calculation, the bottom of the cylindrical part of the cylinder block is considered a circular plate, clamped along the outer edge and loaded by the uniformly distributed pressure  $p_{b\ th}$  (Figure 3.18). The maximal stress at the outer edge

$$\sigma_{max} = \frac{3}{4} \frac{p_{b\ th} R^2}{\delta_1^2} \quad (3.36)$$

where  $R$  is the cylindrical part bottom radius; and  $\delta_1$  is the cylinder block bottom wall thickness.

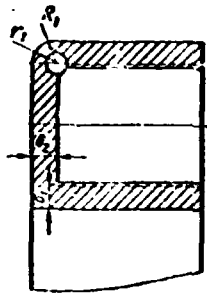


Figure 3.18. Schematic for brake cylinder block cylindrical segment analysis.

The stress at the center of the cylinder block bottom

$$\sigma = \frac{3R^2 p_b}{8\delta_1^2} \frac{th(1+\nu)}{th}, \quad (3.37)$$

where  $\nu$  is the Poisson ratio of the cylinder block material.

The cylinder block strength is verified for constant wall

thickness  $\delta_1$  and uniform loading by the internal pressure ( $p_b th$ ) on the basis of the stress

$$\sigma = \frac{p_b th R_{sh}}{\delta_1}, \quad (3.38)$$

where  $R_{sh}$  is the average cylinder block radius.

The stresses in the block channel walls are found from the known Lamé formula

$$\sigma = p_b th \frac{R_1^2 + r_1^2}{R_1^2 - r_1^2}, \quad (3.39)$$

where  $R_1$  is the channel outer radius;  $r_2$  is the channel inner radius. /61

The strength condition for all these calculations is

$$\eta = \frac{\sigma_u}{\sigma} - 1 \geq 0,$$

where  $\sigma_u$  is the cylinder block material ultimate strength.

## 7. Brake Strength Analysis with Side Loads Acting on the Wheel

During airplane taxi, takeoff run, or postlanding rollout, lateral oscillations of both the wheel axle and the brake which is rigidly mounted on the landing gear may arise because of runway surface irregularities. These vibrations are transmitted from the brake housing to the brake disc packet. Since the brake discs can

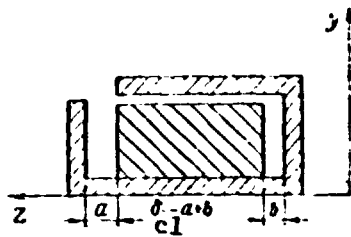


Figure 3.19. Schematic for analyzing brake under the action of side loads.

appearance of large axial loads on the brake details and peak braking moment values.

move freely in the housing slots and are not rigidly coupled with the housing, this leads to the appearance of a difference between the brake housing linear velocity and the brake packet velocity. As a result, the brake packet may contact the brake housing, which leads to the

26

The peak braking moments can be reduced by installing in the brake packet elastic damping elements which are capable of reducing the packet impact energy. The basic parameters of such damping elements are determined as follows (Figure 3.19).

The basic data for the calculation are:

- brake disc packet weight  $G_b$
- maximal clearance between the disc packet and the brake housing support flange  $\delta_{cl} = (a + b)$ ;
- brake axial oscillation frequency  $f'$ ;
- maximal load factor  $n'_{ax}$  in the axial direction for a particular oscillation frequency.

We assume that the wheel oscillations  $Z$  in the axial direction are harmonic and follow a sinusoidal law, i.e.,

$$Z = A' \sin \omega \tau, \quad (3.40)$$

where  $Z$  is the instantaneous brake housing vibration amplitude;  $A'$  is the maximal vibration amplitude;  $\omega$  is the vibration angular frequency; and  $\tau$  is the vibration time.

In accordance with (3.40), the maximal wheel and brake housing acceleration is

$$Z = A'\omega^2.$$

Considering that  $Z = n_{ax}'g$  and  $\omega = 2\pi f'$ , we obtain the vibration amplitude

$$A' = \frac{\ddot{Z}}{\omega^2} = \frac{n_{ax}'g}{\omega^2}$$

The brake packet maximal velocity is found from the relation

$$V_{max} = A'\omega. \quad (3.41)$$

The packet relative velocity (relative to the housing) at the instant of impact is

$$V_{imp} = V_{max} - \dot{Z} = V_{max} - A'\omega \cos \omega\tau_0,$$

where  $\dot{Z}$  is the brake housing velocity in the axial direction;  $\tau_0$  is the time of disc packet movement from the instant of reaching the velocity  $V_{max}$  until contact with the brake housing, found from the equation

$$\delta_{cl} = \int_0^{\tau_0} V_{imp} d\tau = \int_0^{\tau_0} (V_{max} - A'\omega \cos \omega \cdot \tau) d\tau, \quad (3.42)$$

$$\delta_{cl} = V_{max}\tau_0 - A \sin \omega\tau_0.$$

/63

From the values of the velocity  $V_{imp}$  and the disc packet weight, we find the packet kinetic energy at the instant of contact with the brake housing

$$U_{imp} = \frac{G_b \cdot V_{imp}^2}{g \cdot 2}$$

The force arising on the brake housing support flange at the instant of impact can be found from the formula

$$P_{dyn} = k_{dyn} \cdot G_b, \quad (3.43)$$

where

$$k_{\text{dyn}} = 1 + \sqrt{1 + \frac{U_{\text{imp}}}{U_{\text{pot}}}};$$

$$U_{\text{pot}} = \frac{1}{2}G_b \delta_{\text{st}};$$

$\delta_{\text{st}}$  is the support flange deformation with static application of a load equal to  $G_b$ .

For ratio  $U_{\text{imp}}/U_{\text{pot}} \geq 110$  and taking  $G_b = c\delta_{\text{st}}$ , we obtain from (3.43)

$$P_{\text{dyn}} = c \sqrt{\frac{mV_{\text{imp}}^2}{c}} = \sqrt{mV_{\text{imp}}^2} c,$$

where  $m$  is the brake disc packet mass and  $c$  is the brake housing support flange stiffness.

This force exceeds the brake disc clamping force  $S_b$  in certain cases by a factor of 3 — 4, which is the reason for the appearance of the braking moment peak overshoots.

The braking moment overshoot peaks can be reduced by installing in the brake packet elastic damping elements which are capable of reducing the impact force. The basic parameter (stiffness) of such a damping element can be found as follows. Assuming that the force  $P_{\text{dyn}}$  must not exceed the clamping force  $S_b$ , we obtain

$$P_{\text{dyn}} = S_b = \sqrt{mV_{\text{imp}}^2} c,$$

hence,

$$c_{\text{el}} = \frac{S_b^2}{mV_{\text{imp}}^2}.$$

In this case, the brake packet kinetic energy at the moment of impact with the brake housing support flange is equal to the elastic damping element deformation energy, i.e.,

$$\frac{G_b v_{imp}^2}{g \cdot 2} = \frac{1}{2} c_{el} \delta_{el}^2,$$

where  $\delta_{el}$  is the elastic element deformation with application of the load  $P_{dyn} = S_b$ .

## CHAPTER 4

### BRAKED AIRCRAFT WHEEL CONSTRUCTION

#### 1. Wheels with Disc Brakes

/65

The braked wheel with a disc brake has a complex construction with a large number of components and detail parts (Figure 4.1). The wheel itself is a cast or stamped drum 2 with two outer flanges which restrain the tire securely. One of the flanges is integral and is fabricated as one with the wheel. The other removable flange is formed from two removable half-flanges 5 mounted on the drum (Figure 4.2). The half-flanges 8 are located on the drum by the stationary keys 7 and are connected with one another by the joining plate 9 and bolts 10. The axial force from the tire acting on the half-flanges is taken by a special thrust ring. Two radial thrust roller bearings 17, between the inner races of which there is a spacer sleeve 16 to prevent overtightening of the bearings, are pressed into the drum hub. The outer grease seals 12 are installed to seal the drum inner cavity between the bearings and prevent lubricant leakage from the cavity. The protective cover 11 protects the outer grease seal and axle details from any possible damage. Steel guides 5 which are attached to the drum by the rivets 6 are pressed into slots on the wheel drum. The tenons of the rotating brake discs extend into the guides.

/67

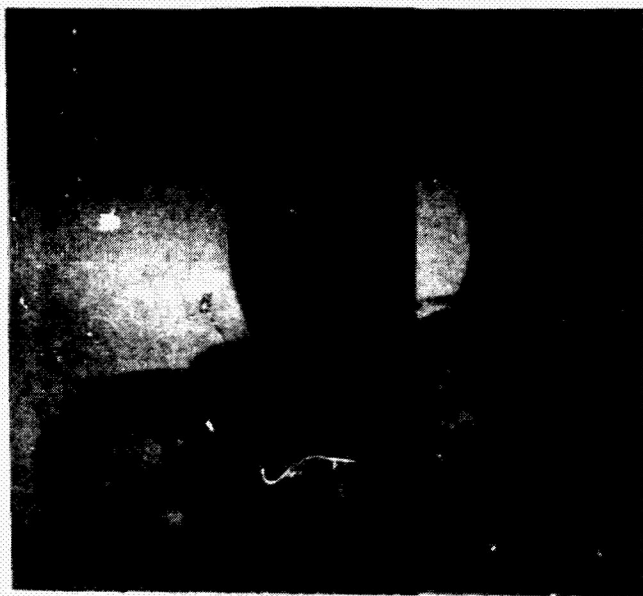


Figure 4.1. General view of wheel with disc brake.

1- tire; 2- drum; 3- radial thrust bearings; 4- protective covers; 5- removable half-flanges; 6- brake.

The basic brake components are: housing 18, cylinder block 19, nonrotating bimetallic discs 3, rotating cermet discs 4, clamping disc 2, and brake release units 15. On one side of the brake housing, usually fabricated from alloy steel, there is a support flange with bimetallic sectors riveted to it, and on the other side, there is a flange for mounting the brake on the landing gear. The brake housing has longitudinal slots, into which the bimetallic disc tenons extend. The bimetallic and cermet discs consist of a set of sectors riveted on a

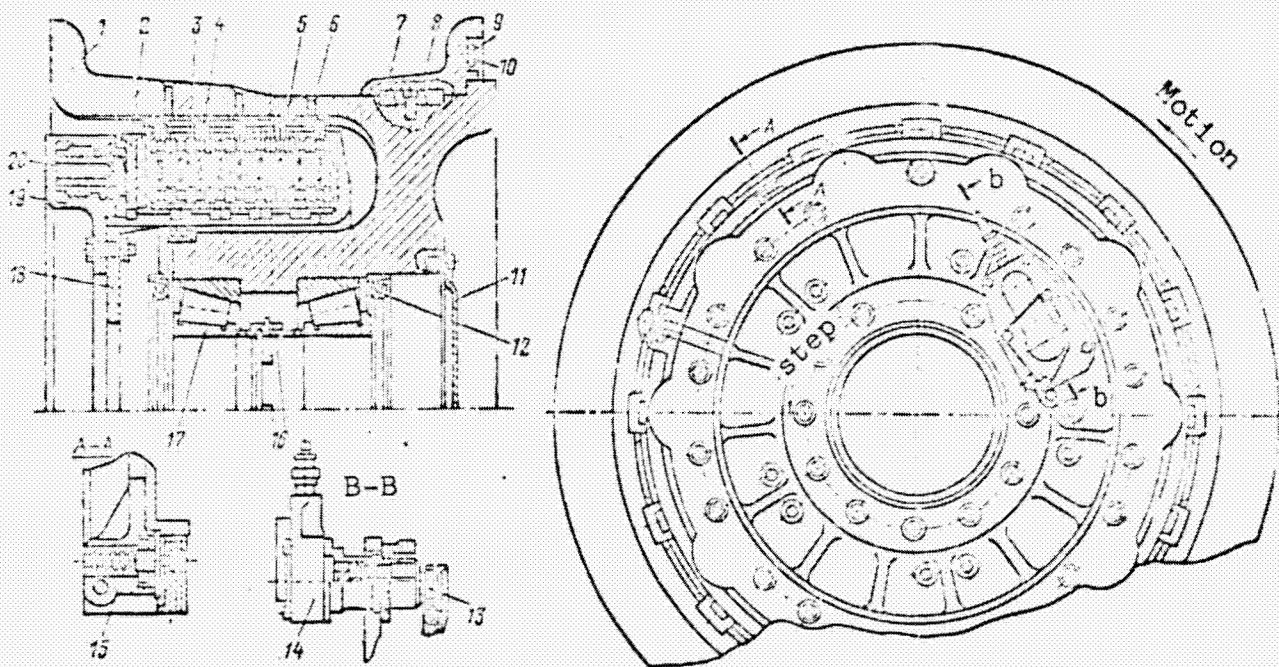


Figure 4.2. Construction of wheel with disc brake.

1- wheel drum; 2- clamping disc; 3- nonrotating disc; 4- rotating disc; 5- guide; 6- rivet; 7- key; 8- half-flange; 9- joining plate; 10- bolt; 11- protective cover; 12- grease seals; 13- geared drive; 14- electrical sensor of antiskid system control; 15- brake release unit; 16- sleeve; 17- roller bearing; 18- brake housing; 19- cylinder block; 20- cylinder block piston.

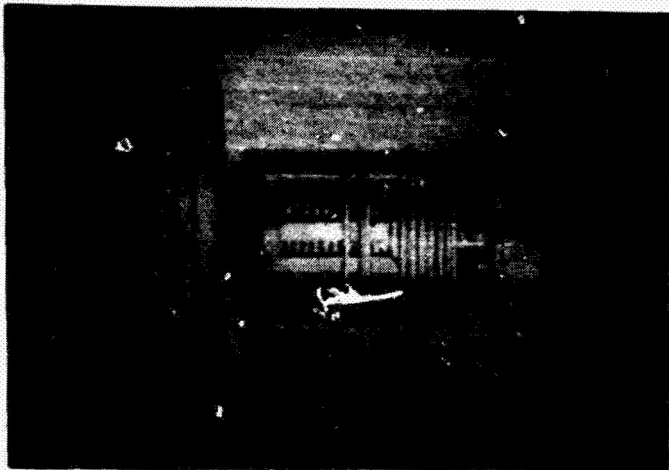


Figure 4.3. XB-70 brake.

ring. For smoothness of braking, the number of bimetallic and cermet sections on the discs should be different. Wide use has recently been made of a different cermet disc construction, consisting of steel bodies with special radial slots to compensate for the temperature deformations and cermet sectors riveted on both sides of the discs.

During braking, the working fluid or air, entering the cylinder block under pressure, displaces the pistons 20 and creates an axial force (see Figure 4.2). This force displaces the clamping disc 2, which forces together the bimetallic and cermet discs.

As a rule, an antiskid controller or the electrical sensor 14 of an antiskid system controller is mounted on all braked wheels. The sensor is mounted on a special bracket on the brake housing and is driven by the geared drive 13.

An important drawback of disc brakes is the slow cooling rate. Therefore, forced cooling with the aid of special cooling systems is often required for such brakes.

Another braked wheel variant with disc brakes, used on the XB-70 Valkyrie, is shown in Figure 4.3. In this construction, the braking element is located in the bogie itself. In this configuration, the wheel drum is isolated from the brake and, consequently, tire overheating is eliminated. In addition, according to the manufacturer, the bogie constructional volume makes it possible to obtain a braking moment on the order of  $3 \cdot 10^6$  kgf/m with comparatively small tire diameter (1050 mm).

/68

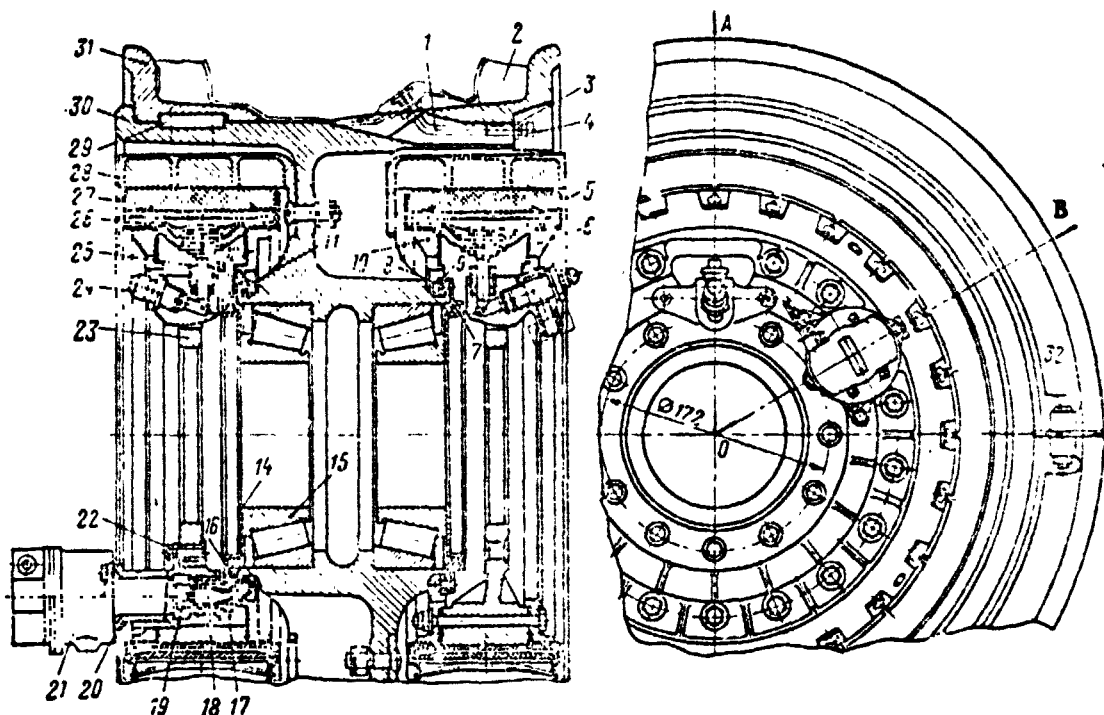


Figure 4.4. Aircraft wheel with expander tube brake.

1- valve; 2- tire; 3- nut; 4- cap; 5- cup; 6, 10- flanges; 7- felt ring; 8- bolt; 9- grease seal body; 11- self-locking nut; 12- flange with grease seal seat; 13- grease seal; 14- cap; 15- roller bearing; 16, 17- driving and driven gears; 18, 19- splined sleeves; 20- sensor bracket; 21- sensor; 22- bolt; 23- brake housing; 24- fitting; 25- valve; 26- brake expander tube; 27- shoe; 28- lining; 29- key; 30- drum; 31- half-flange; 32- bolt.

## 2. Wheels with Expander Tube Brakes

Expander tube brakes are very simple in construction, however, they have quite good operational characteristics. Figure 4.4 shows a wheel with two expander tube brakes. The wheel drum is cast. At one end of the drum there is a thrust collar, on which the removable half flanges 31 are mounted and are held in place by the key 29 and tie bolts 22. The bimetallic braking linings 28, which are steel rings with special iron sintered to them, are attached to the drum disc by special screws.

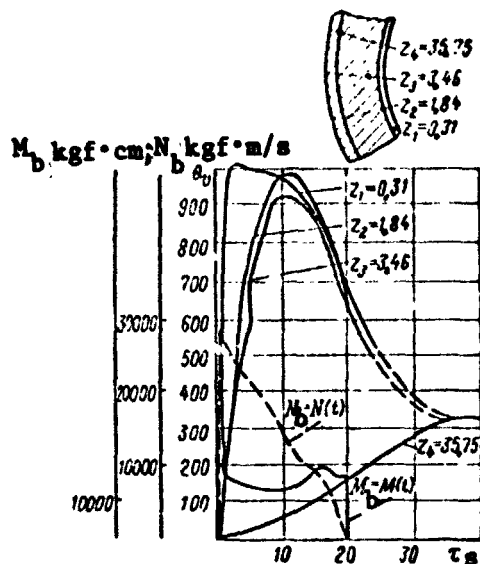


Figure 4.5. Variation of bulk temperature  $\theta$ , braking moment  $M_b$ , and power  $N_b$  in expander tube brake during braking.

special bracket 20. The sensor is rotated by a drive consisting of the gears 17 and 16 and the splined sleeves 19 and 18.

The brake works as follows. Upon actuation of the brake, the brake expander tube under the pressure of the entering air (or liquid) forces the brake shoes against the lining. The resulting friction force creates the braking moment. In the wheels with expander tube brakes, the heat created during braking is absorbed by the brake lining, whose temperature may reach  $300^\circ\text{C}$ . At the same time, the temperature at the brake lining friction surface may reach  $1000^\circ\text{C}$  during the braking process.

Figure 4.5 shows typical curves of mass average temperature  $\theta_v$ , braking moment  $M_b$ , and brake power  $N_b$  during the braking process. The maximal temperature differential through the lining thickness (from the contact surface to the periphery) is observed at braking initiation and reaches approximately  $1000^\circ\text{C}$ . This temperature differential may lead, in the course of time, to the appearance of cracks and separation of the iron from the steel ring.

The wheel brake consists of the housing 23, mounted on the landing gear flange, the cups 5 and flanges 6, forming a cavity for the brake expander tubes 26, on which there are mounted the brake shoes 27 (rectangular plastic blocks reinforced by a steel carcass). The pressure is supplied to the brake expander tube through the fitting 24 and tube valve 25. The tire is inflated with air through the valve 1. The wheel is equipped with the antiskid system controller electromechanical sensor 21, mounted on the

The temperature of the other brake and wheel elements is usually considerably lower than that of the brake lining. For example, the temperature of the drum under the tire bead is usually  $1/4 - 1/5$  of the lining temperature and the temperature in the bearing area is about  $1/8 - 1/10$  of the lining temperature. The wheel drum temperature rise depends to a considerable degree on the size of the air gap between the brake lining and the drum inner surface.

The wheel braking moment can be found from the formula

$$M_b = f_{bs} p_{fr} F_e r, \quad (4.1)$$

where  $f_{bs}$  is the coefficient of friction between the brake shoes and lining,  $f = 0.4$ , depending on the friction pair material;  $p_{fr}$  is the specific pressure on the friction surface;  $F_e$  is the effective friction area; and  $r$  is the brake lining inner surface radius.

The magnitude of the specific pressure  $p_{fr} = p_c - p_{bp}$ , where  $p_c$  is the pressure in the brake tube and  $p_{bp}$  is the backpressure, whose /71 magnitude depends on the elasticity of the brake tube and the return springs.

The effective friction area

$$F_e = k_{mu} a 2\pi r, \quad (4.3)$$

where  $k_{mu}$  is the coefficient of mutual overlap, accounting for the brake construction ( $k_{mu} = 0.8 \div 0.9$ );  $a$  is the brake shoe width; and  $r$  is the brake lining inner surface radius.

The braking moment formula (4.1) can be transformed to the form

$$M_b = C_2 f_{bs} p_{fr}, \quad (4.4)$$

where  $C_c$  is a constructional constant ( $C_c = F_e r$ ).

Along with the advantage of constructional simplicity, the expander tube brakes have significant drawbacks. These are, first of all, the possibility of brake tube failure as a consequence of overheating and the resulting possibility of fire as the brake fluid contacts the hot lining. Another drawback of the brake is the absence in its construction of a brake shoe wear compensator. As the brake shoes wear, the clearance between them and the lining increases and, therefore, the amount of liquid (for hydraulic brakes) or air (for pneumatic brakes) required to force the shoes against the lining increases, as a result of which the brake application time increases and the brake system dynamics deteriorate.

### 3. Wheels with Shoe Brakes

At the present time, wheels with shoe type brakes are used on comparatively small airplanes.

A typical construction of a wheel with shoe brakes is shown in Figure 4.6. The brake has two independent rigid cast shoes 3 with brake linings. Each shoe is hinged to an anchor shaft 10, which is mounted rigidly in ears of the brake housing 14.

Two cylinders 7 are mounted on the brake housing and their working chambers are interconnected by tubing. The cylinders have an external fitting 16 for connection to the airplane brake line. The cylinder pistons 5 have circular sealing rings and protective rubber sleeves 8 to seal the cylinder working chambers.

Expansion of the shoes is accomplished with the aid of the unequal arm lever 9, which is hinged on the shoe anchor shaft. The short lever arm, having at the end the regulating screw 1 with the nut 2, rests on the free end of the shoe, while the rod 6 at the end of the long lever arm rests on the piston. When fluid is supplied under pressure to the cylinders, the shoes are forced against the

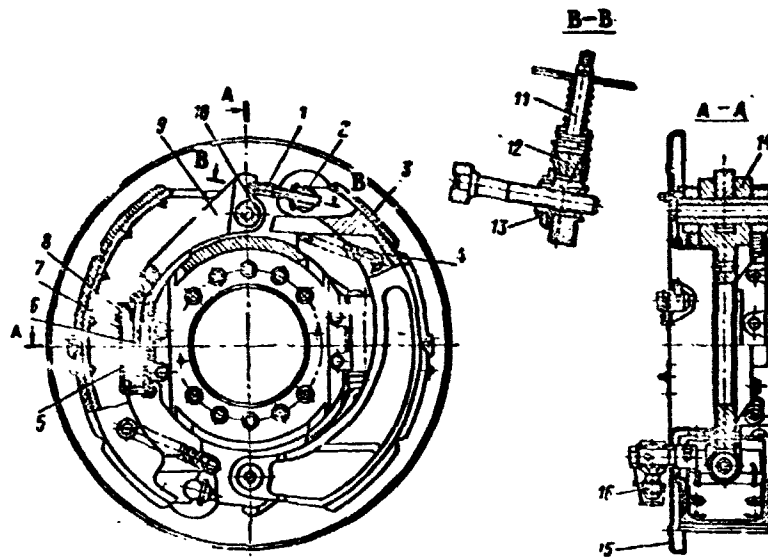


Figure 4.6. Shoe type brake construction.

1- regulating screw; 2- nut; 3- cast shoes; 4- return spring; 5- piston; 6- rod; 7- cylinder; 8- protective sleeve; 9- unequal arm lever; 10- anchor shaft; 11- regulating screw; 12- bevel gear; 13- bevel gear; 14- brake housing; 15- cover plate; 16- external fitting.

wheel brake linings and retard the wheel. The higher the fluid pressure, the larger the braking moment developed by the brake. The moment is transmitted through the anchor shafts to the brake housing, which is bolted to the landing gear flange.

The central hole in the brake housing is used to center the housing relative to the wheel axle. When the pressure in the cylinders is released, the return springs 4 pull the shoes away from the lining to the initial position and unbrake the wheel. In the unbraked state, a clearance equal to 0.3 — 0.4 mm is provided between the brake lining and the shoes, and this clearance is established and regulated by the regulating screw 11, which is rotated by the bevel gears 12 and 13. The protective cover 15 protects the brake against dirt.



Figure 4.7. Mirage airplane wheel and brake manufactured by Hispano-Suiza.

#### 4. Special Wheels

These wheels include the hermetically sealed wheels used for amphibian airplanes, wheels with variable tire pressure, and wheels with fan cooling of the brakes. Their structural elements are fabricated just as in the cases examined above, except for the materials of the individual detail parts.

173

In order to ensure smoothness of the braking process and eliminate braking moment overshoots in the various regimes, use is made of a special disc brake construction. Smoothness of the operation of this brake is achieved by introducing on the support flange side of an annular lyre-shaped spring which plays the role of a pretensioned spring damper.

Figure 4.7 shows the wheel and brake manufactured by Hispano-Suiza for the Mirage airplane [35]. The wheel is split and consists of two halves which are bolted together; a disc type brake is used.

Lightweight disc brakes with exposed friction surface are sometimes used for the wheels of light airplanes or helicopters. Figure 4.8 shows disc brakes with exposed friction surface manufactured by Messier.



Figure 4.8. Disc brakes with exposed friction surface manufactured by Messier.

#### 5. Basic Wheel and Brake Component Construction

/74

Standardized elements and components are used in the construction of various braked wheels: pistons and cylinders; brake discs, clearance regulators, etc. For example, these components include the standard hydraulic brake piston unit consisting of the sleeve 2, which is threaded into the block 1, and the piston 3 which displaces under the action of the pressure force or the return spring elastic force (Figure 4.9). The sleeve 2 is sealed by the O ring 6, which is compressed by 20 — 25% of its volume as the sleeve is installed in the block, while sealing of the moving piston is accomplished by the rubber O ring 5, installed in the forward part of the sleeve and which is compressed by 15 — 20%.

The teflon washer 4 is installed ahead of the O ring 5 to protect the latter against dirt. The location of the piston O ring 5 in the forward part of the sleeve ensures good lubrication of the piston pair by the working fluid. In addition, when using a hollow piston, the working fluid will cool the sliding rubber seal.

A typical pneumatic brake piston unit is shown in Figure 4.10. Its construction is more complex than that of the hydraulic brake piston unit because of the necessity for a high degree of hermeticity and provision for effective lubrication of the unit. In this element, sealing of the stationary sleeve is accomplished by the rubber ring 1, while sealing of the piston is accomplished by the ring 2, located

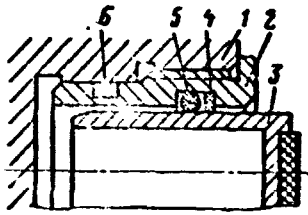


Figure 4.9. Hydraulic brake piston element.

1- block; 2- sleeve; 3- piston; 4- washer; 5, 6- O rings.

in the forward part of the sleeve.

Lubricant is supplied into the

zone between rings 2 and 4 from chamber A by the piston 3 when the working pressure is applied to the block chamber B and the cylinder chamber.

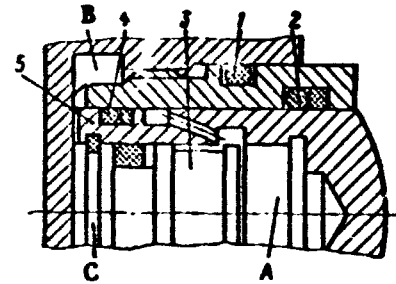


Figure 4.10. Pneumatic brake piston element.

1- sleeve O ring; 2- piston O ring; 3- piston; 4- O ring; 5- actuating piston.

Figure 4.11 shows a typical wheel brake release unit which does not have automatic regulation of the clearance between the pressure disc and the brake packet. The unit consists of the spring 2, one end of which rests on the end plate 1 and the other end of the plate of rod 3. The rod is connected with the pressure disc by either a threaded connection or a Tee-type connection.

/75

A typical collet type wheel brake release unit with automatic regulation of the clearance between the pressure disc and brake packet is shown in Figure 4.12. Such units are used with strictly limited clearance between the pressure disc and the brake packet, since with excessively large clearance formed because of friction disc wear, the fluid volume necessary for wheel brake application increases, and, in addition, disc centering deteriorates.

In this unit, the profiled rod 5 is connected with the pressure disc 6. The sleeve 3 on the end of which the spring 4 bears is rigidly attached to the rod 5 itself. The rod 5 is partially centered in the threaded insert 7, which is screwed into the collet 2. The teeth of the lobes C of the collet 2 enter the

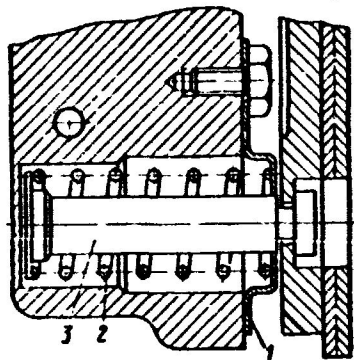


Figure 4.11. Brake release unit.  
1- end plate; 2- spring; 3- rod.

grooves of the rod 5, whose profile permits the rod 5 to displace

only in one direction. During brake application, the pressure disc 6, displacing through the distance A, compresses the brake packet. The rod 5 and the attached sleeve 3, which compresses the spring 4, displace together with the pressure disc. The collet 2 also displaces along with the rod until its shoulder contacts the body of the block 1. If the clearance  $A < B$ , the unit cannot automatically regulate the clearance between the pressure disc and the brake packet.

Automatic regulation of the clearance between the disc and the packet takes place as follows.

As the brake packet wears, the clearance A increases and, during braking, the shoulder of the collet 2 contacts the body of the block 1 before the pressure disc contacts the brake packet. With further movement of the pressure disc 6, the rod 5 begins to displace relative to the collet 2, thereby compensating for brake packet wear. When the packet wear reaches a magnitude equal to the rod profile tooth pitch S, the collet lobes spread and the rod advances one tooth, by the magnitude of the wear S. After brake release, the spring 4 returns the sleeve 3, rod 5, collet 2, and disc 6 to the initial position. In this case, the clearance A again becomes equal to its initial value, while the spring is further compressed by the

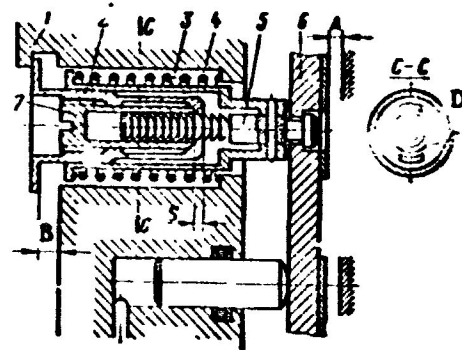


Figure 4.12. Collet type brake release unit with automatic regulation.

1- block; 2- collet; 3- sleeve; 4- spring; 5- rod; 6- pressure disc; 7- threaded insert.

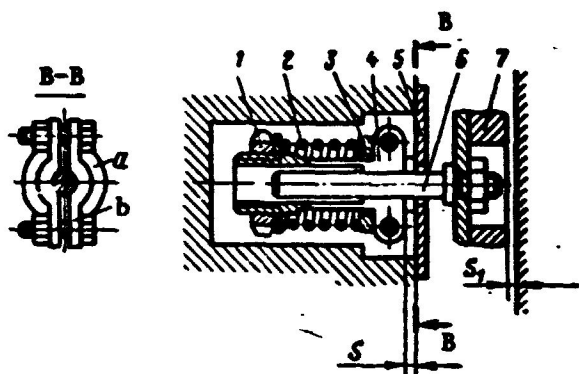


Figure 4.13. Friction type brake release unit with automatic regulation.

1- thrust nut; 2- spring; 3- ring; 4- clamp; 5- cover; 6- rod; 7- pressure disc.

split collar 4 with the thrust nut 1. Between the ring 3 and the nut 1, there is the precompressed spring 2; the lobes b of the collar 4 are drawn together by two bolts, as a result of which the rod 6 can extend only with application to it of a definite force. The entire unit is mounted in the brake cylinder block and enclosed by the protective cover 5. During piston movement, the pressure disc 7 and the rod 6, held by the clamp 4, displace together. In this case, the ring 3 remains stationary while the spring 2 is compressed by the displacement of the pressure disc 7. As the pressure on the piston decreases, the spring 2 displaces the clamp 4 and the rod 6 coupled with it (to the left in the figure). When the brake disc wear becomes such that the pressure disc must displace by a magnitude  $S_1 > S$ , in order to bring the discs together, the clamp 4 contacts the cover 5 and the rod 6, overcoming the friction force, displaces by some distance relative to the clamp 4. We note that the friction force, which holds the rod relative to the clamp 4, must naturally be greater than the compression force of the spring 2 and must not change during operation. Reduction of the friction force leads to maladjustment of the brake release unit, while excessive increase of the friction force leads to reduction of the braking moment as the brake discs wear.

magnitude  $S$ . Thus, the unit makes it possible to alter automatically the clearance between the pressure disc and the brake packet in the limits from  $A$  to  $A + S$ .

Figure 4.13 shows a friction type brake release unit with automatic regulator of the clearance between the disc and the packet. In this unit, the rod 6, one end of which is connected with the pressure disc 7, is located inside the

/77

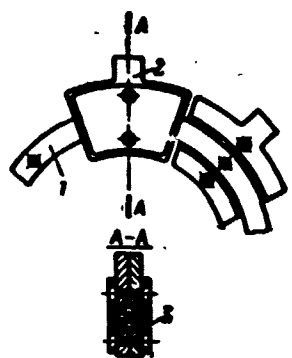


Figure 4.14. Sectional cermet disc on ring.

1- ring; 2- sector; 3- steel plate.

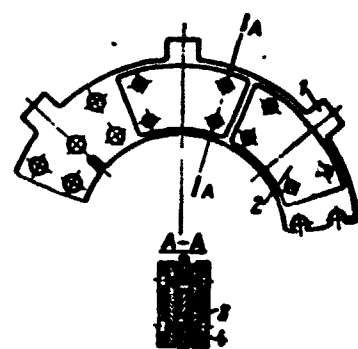


Figure 4.15. Sectional cermet disc on carcass.

1- carcass; 2- sector; 3- bushing; 4- rivet.

Cermet and bimetallic discs are used as the friction elements in wheel brakes. In construction, they may be either monolithic or built up from individual sections. The choice of the particular construction depends primarily on brake operating conditions and required brake service life.

Sectional construction of the discs on either a ring or carcass permits the brakes to function with very high specific energy loadings. The high disc temperatures, reaching  $500^{\circ}\text{C}$  during braking, cause high temperature stresses in the discs and, as a consequence, deformations in the individual elements. In this regard, sectional discs are better than continuous cermet and bimetallic types. The built-up section cermet disc and ring construction usually consists of a continuous ring 1 with a set of sectors 2 riveted on both sides (Figure 4.14). Each half of the sector 2 is a steel plate 3 of the required configuration, to which a cermet layer is sintered. Each sector (or every other sector) is coupled with the ring by a steel shaft which also takes part of the load acting on the sector during braking.

178

The carcass type disc construction consists of the steel carcass 1, having radial slots, and the bushings 3 (Figure 4.15). The cermet sectors 2 (steel plates with cermet sintered to their surface) are

attached in pairs on the carcass by the rivets 4. After assembly on the carcass, each cermet sector must have some free displacement (free play) in the friction plane relative to the steel carcass.

Usually high alloy or high temperature steel is used for the cermet disc carcasses. Continuous discs with cermet sintered on them are used in certain brake designs.

## CHAPTER 5

### AIRCRAFT TIRES

/79

#### 1. Basic Characteristics of Tires

The shock absorbing and load carrying capacity of tires depends on their geometric dimensions, internal pressure, and structural stiffness. These properties are characterized by the curves of radial load  $P_r$  on the wheel versus tire deflection  $\delta_{def}$ . Typical deflection curves for different tire pressures are shown in Figure 5.1. There are several characteristic points on the deflection curve:  $\delta_{st def}$  is the tire deflection corresponding to the static radial load  $P_{st}$  on the wheel with the airplane parked and is usually equal to 30 — 35% of the total deflection;  $\delta_{tot def}$  is the total deflection (see Figure 5.3) corresponding to the total radial load  $P_{tot}$ ;  $\delta_{a def}$  is the maximal allowable deflection corresponding to the maximal allowable radial load  $P_a$  and usually equal to 95% of the total deflection;  $\delta_{bur def}$  is the deflection corresponding to the bursting load  $P_{bur}$  at which the tire may burst.

For nose wheels, in addition to the static load  $P_{st}$  acting on them, we also specify the airplane dynamic load  $P_{dyn}$  acting during braking. In this case, the tire deflection should be:

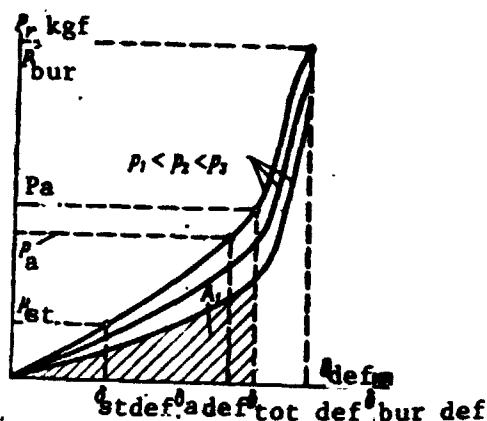


Figure 5.1. Tire deflection diagram.

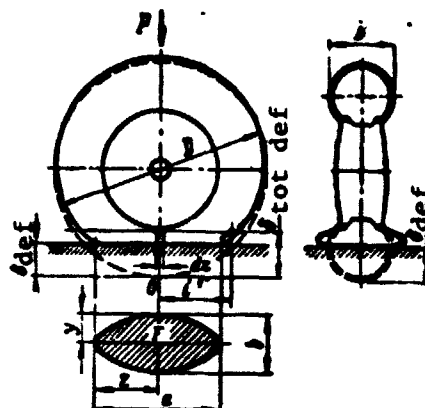


Figure 5.2. Illustration for determining contact area for tire of circular profile.

$$\delta_{a \text{ def}} \approx 0.5 \delta_{\text{tot def}}$$

The basic tire characteristics are: supporting surface area  $F$ , /80 radial load  $P_r$ , and magnitude of the work  $A$  during deflection.

As a rule, these characteristics are determined experimentally by static or dynamic deflection of the tire on a press or impact tester. However, in wheel or tire design, the necessity for determining these tire characteristics by calculation arises in certain cases.

#### Determination of Tire Supporting Surface Area

We can consider with accuracy adequate for practical purposes that, for a tire of circular cross section, the supporting surface is an ellipse with semiaxes  $y$  and  $z$  (Figure 5.2). The magnitudes of the semiaxes  $y$  and  $z$  depend on the tire degree of deflection  $\delta_{r \text{ def}}$  under radial load. The theoretical tire supporting surface area is

$$F_{th} = \pi y z, \quad (5.1)$$

TABLE 5.1\*

Tire size (DxB)	Tire pressure kgf/cm <sup>2</sup>	Actual area F <sub>ac</sub>	Print length and width (axb)	Theoretical area F <sub>t</sub>	Correction factor k
600×200	10	320	28,6 × 13	296	1,08
800×200	12	390	32,5 × 14,5	365	1,07
880×230	13	525	36 × 17,6	494	1,06
930×305	9	788	42 × 21	694	1,09
1100×330	9	924	45 × 23,5	832	1,11

\*Commas in numbers indicate decimal points.

where  $k$  is a correction factor which is the ratio of the actual contact area  $F_{ac}$  to the theoretical area  $F_{th}$ , calculated for an ellipse with the same axes.

According to the experimental data, for tires of circular (or nearly so) profile, the factor  $k$  varies from 1.03 to 1.14 (1.08 can be taken as the average value of  $k$ ).

Table 5.1 presents the actual and theoretical contact areas for Soviet tires for  $\delta_{st \text{ def}}$ .

The values of  $y$  and  $z$  are found from the empirical formulas

$$y = (B_1 + \xi) \sqrt{\frac{\delta_r \text{ def}}{\delta_{tot \text{ def}}}} \quad z = r' \sqrt{\frac{\delta_r \text{ def}}{\delta_{tot \text{ def}}}},$$

where  $r' = 0.94 \sqrt{D \delta_{tot \text{ def}} - \delta_{tot \text{ def}}^2}$  is the semi-major axis of the supporting contact area ellipse with complete tire deflection;  $\xi$  is the linear dimension between the rim flange and the point bounding the axial transverse dimension of the contact area with complete deflection (Figure 5.3), which depends on the tire sidewall stiffness and its geometrical dimensions

$$\xi = 0.45 \delta_{tot \text{ def}}^{1/2} e^{1/2} d.$$

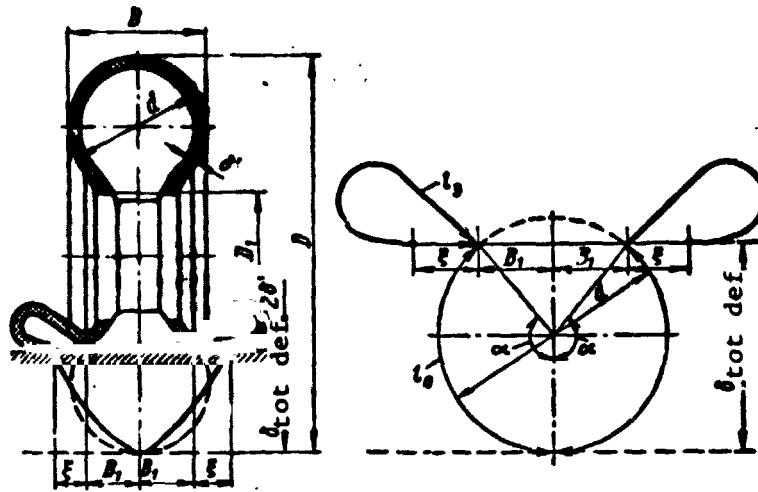


Figure 5.3. Schematic of tire deformation during deflection.

Here  $l_e = l_0 - B_1$  is the length of a closed tire element of width  $dz$  cut out in the vertical direction (see Figure 5.2) and  $l_0 = (d/2)\alpha$ , and the angle  $\alpha$  (in radians) is found from the equation

$$\cos \alpha = 1 - \frac{2\delta_{\text{tot def}}}{d}.$$

With account for the formulas for  $y$  and  $z$ , the theoretical tire /82  
contact area will be

$$F_{\text{th}} = 3.4r'(B_1 + \xi) \frac{\delta_{\text{def}}}{\delta_{\text{tot def}}}. \quad (5.2)$$

#### Determination of Allowable Radial Load on Tire

The radial load experienced by a tire is

$$P_r = c_{\text{stit}} F_{\text{th}} P_{\text{ex}} \quad (5.3)$$

where  $p_{\text{ex}}$  is the excess pressure in the tire;  $c_{\text{stit}}$  is the tire stiffness coefficient. (It has been found experimentally that, on the average,  $c_{\text{stit}} = 1.12$ , i.e., the stiffness is about 12% of the radial load on the tire).

The excess pressure in the tire

$$p_{ex} = p' - 1 = \frac{2V_0 p_0}{2V_0 - r' \delta_{tot \text{ def}} (B_1 + \xi) r} - 1,$$

where

$$r = \frac{\pi \delta_{def}}{\delta_{tot \text{ def}}} - \sin \left( \frac{\pi \delta_{def}}{\delta_{tot \text{ def}}} \right);$$

$p'$  is the absolute tire pressure referred to atmospheric pressure;  $p_0$  is the absolute initial tire pressure; and  $V_0$  is the initial tire air volume

$$V_0 = \frac{\pi^2 d_1^2}{4} (D_1 + 0.9d),$$

here  $D_1$  is the wheel rim diameter,  $d_1$  is the average tire cross section diameter based on the average tire wall thickness ( $d_1 = d - 2\delta'$ ).

Approximately, the initial tire volume

$$V_0 = 1.84d^2(D - d),$$

where  $D$  is the tire outer diameter.

Substituting the expressions found for  $F_{th}$  and  $p_{ex}$  into (5.3), we obtain

$$P_r = 3.8r'(B_1 + \xi) \left[ \frac{2V_0 p_0}{2V_0 - r' \delta_{tot \text{ def}} (B_1 + \xi) r} - 1 \right] \frac{\delta_{def}}{\delta_{tot \text{ def}}} \quad (5.4)$$

For small changes of the tire air volume and comparatively high initial pressures (more than  $3 \text{ kgf/cm}^2$ ), taking  $p'_0 \approx p_0$  and  $p' \approx p$ , we obtain

$$P_r = \frac{7.6r'(B_1 + \xi) p_0 V_0}{2V_0 - r' \delta_{tot \text{ def}} (B_1 + \xi) r} \cdot \frac{\delta_{def}}{\delta_{tot \text{ def}}} \quad (5.5) \quad \underline{183}$$

where  $p_0$  is the internal tire pressure.

The radial load for complete deflection, i.e., for  $\delta = \delta_{\text{tot def}}$

$$(P_r)_{\text{tot def}} = \frac{7.5'(B_1 + B)P_0V_0}{2V_0 - \pi' \delta_{\text{tot def}}(B_1 + B)} \quad (5.6)$$

#### Determination of Pressure Force Work During Tire Deflection

The pressure force work during tire deflection is found by planimetry of the shaded area bounded by the deflection curve  $P_r(\delta_{\text{def}})$ , constructed experimentally or from (5.8), and the abscissa axis, as shown in Figure 5.1.

The shaded area is the work  $A$  for internal tire pressure  $p_0$  and complete tire deflection  $\delta_{\text{tot def}}$ .

Analytically, this work can be determined approximately from the formula

$$A = \frac{1}{2} \pi p_0 \delta_{\text{tot def}}^2 \sqrt{DB},$$

where  $D$  and  $B$  are the tire dimensions (diameter and width).

#### Influence of Nature of Action of Load Applied to Tire on Deflection Work

In the case of static tire deflection with the airplane parked, the air in the tire is compressed isothermally, while during airplane landing, when complete deflection takes place in 0.1 — 0.3 seconds, the air is compressed adiabatically.

We assume the change of the theoretical contact area  $F_{\text{th}}$  as a function of deflection magnitude to be the same for static and dynamic action of the load on the tire. Then, neglecting the action of the tire inertia forces for the dynamic ( $P_{\text{dyn}}$ ) and static ( $P_{\text{st}}$ ) loads, we obtain:

$$P_{\text{dyn}} = c_s F_{\text{th}} P_{\text{ad}};$$

$$P_{\text{st}} = c_s F_{\text{th}} P_{\text{ex}};$$

$$k_1 = \frac{P_{\text{ad}}}{P_{\text{ex}}}$$

$$k_1 = k_1' + \frac{k_1' - 1}{P_0'^n - 1}.$$

/84

Taking  $k_1' = n^{0.41}$ , where  $n = V_0/V$  is the degree of air compression in the tire, we obtain

$$P_{\text{dyn}} = k_1 P_{\text{st}} = \left( k_1' + \frac{k_1' - 1}{P_0'^n - 1} \right) P_{\text{st}}.$$

The compression work for a dynamic load

$$A_{\text{dyn}} = k_2 A_{\text{st}},$$

where

$$k_2 = k_2' + \frac{k_2' - 1}{P_0' k_2'' - 1}; \quad k_2' = 2.46 \frac{n^{0.41} - 1}{\ln n};$$

$$k_2'' = \frac{n \ln n}{n - 1}.$$

Considering that the degree of air compression in tires  $n$  can vary from 1 to 2, with adequate degree of accuracy we obtain

$$k_1 = 0.35n + 0.65; \quad k_2 = 0.16n + 0.84; \quad k_2' = 0.41n + 0.59$$

for  $n = 1; k_1' = k_2' = k_2'' = 1$ .

Studies and calculations have shown that influence of the dynamic nature of the load action is not very great and the increment of the force  $P_r$  does not exceed 10 — 15%. However, in particularly unfavorable cases, for example, during hard airplane landing, this force along with the pressure in the tire may increase by 25 — 30%.

## 2. Aircraft Tire Construction

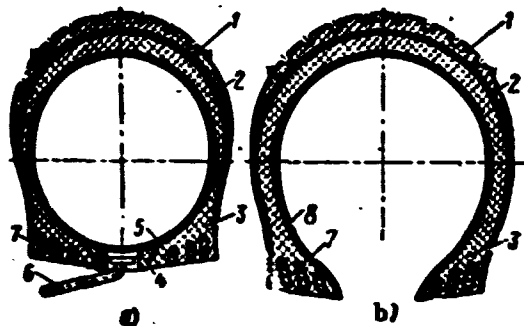


Figure 5.4. Construction of tube type (a) and tubeless (b) tires.

1- tread; 2- breaker; 3- body;  
4- chafing strip; 5- innertube;  
6- valve; 7- stiffening ring;  
8- rubber layer.

At the present time, both tube type and tubeless tires are used on airplanes (Figure 5.4).

The tubeless tire consists of the body 3, stiffening rings 7, breaker 2, and tread 1. The tube tire has, in addition, the innertube 5 with valve 6 and chafing strip 4.

For complete hermeticity, the tubeless tire has an additional rubber sealing layer 8.

The multilayer tire body is fabricated from cotton or kapron cord. Stiffening rings made from special wire are built into the bead in order to increase the stiffness. The body is reinforced by the breaker — a rubber layer over which the tread 1 is laid.

Various materials are used for the tire body, depending on the operating conditions. In those cases when the operating temperature range is  $\pm 55^{\circ}\text{C}$  and the tire temperature rise after braking does not exceed  $+100^{\circ}\text{C}$  at the point of tire contact with the wheel drum, cotton cord and conventional non-heat-resisting rubber are generally used for the body. Kapron cord and heat-resistant rubbers are used to increase the tire heat resistance.

/85

In tire design, we must consider that, in the event of excessive heating, the excessive pressure in the tire must sometimes be relieved through special safety valves in order to avoid tire bursting.

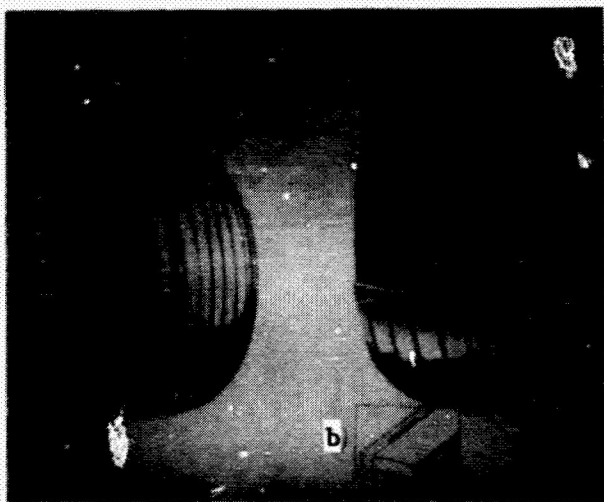


Figure 5.5. Construction of tires with protective layer.  
a- tire with steel wire belt;  
b- tire with dual undertread wire layer.

Some foreign firms produce tires with a protective layer in order to increase tire reliability and protect the tire against mechanical damage. For example, the tires made by Goodrich have a steel wire belt between the tread and the cord layers, and the Thompson tire has a dual undertread wire layer (Figure 5.5).

Tires with metal studs are sometimes used to improve tire traction with the ground during the winter period.

Under particularly severe operating conditions, it is possible to use wheels with metal tires in brush form, which is a construction consisting of a large number of radially positioned steel wires of definite length. A tire of this type made by Goodyear is shown in Figure 5.6.

Tires can be arbitrarily divided into the following groups on the basis of the internal pressure: group I are the ultra-low pressure tires (to  $3.5 \text{ kg/cm}^2$ ); group II are the low pressure tires ( $3.5 - 6.5 \text{ kg/cm}^2$ ); group III are the high pressure tires ( $6.5 - 10 \text{ kg/cm}^2$ ); group IV are the super-high pressure tires ( $10 - 13.5 \text{ kg/cm}^2$ ).

/86

It is well known that the tire pressure determines, to a considerable degree, airplane flotation on various soils and the stresses which develop in the soil. The higher the internal pressure, the poorer the tire flotation and the higher the soil stresses. Moreover, with pressure increase, tire service life decreases, since the tire loses elasticity at high pressure and any small mechanical

/87

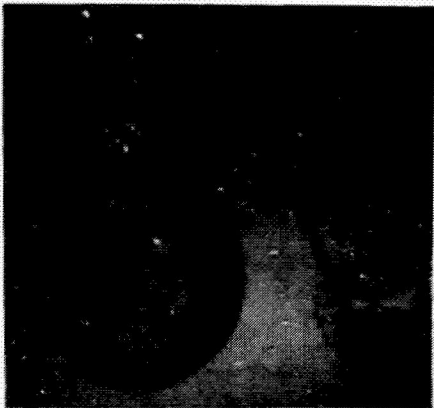


Figure 5.6. Airplane wheel with metal tire for particularly severe operating conditions.

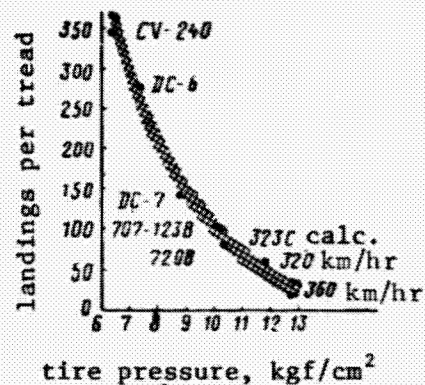


Figure 5.7. Influence of tire pressure on service life.

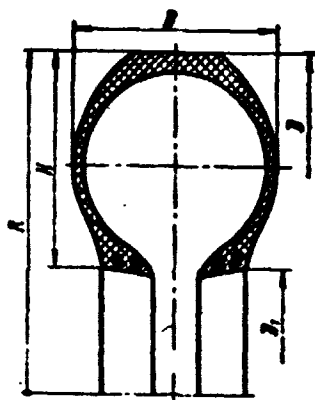
irregularities (stones, etc.) on the runway are not circumvented but rather embed into the tire and gradually destroy the tire.

Figure 5.7 shows the experimental dependence of tire service life on the magnitude of the internal pressure [28]. We note that, on the DC-6, DC-7, and 707-123B airplanes, the tire pressure is different for the same tire size. The tire manufacturer states that, with pressure increase from 7.4 kg/cm<sup>2</sup> (DC-6) to 8.8 kg/cm<sup>2</sup> (DC-7), the tire service life decreased from 272 to 145 landings. The tire service life on the 707 is only 95 landings. Cases have been reported by the American aircraft industry in which tire service life decreased to 30 — 50 landings with tire pressure increase to 12 — 14 kg/cm<sup>2</sup>. Usually tire pressures higher than 10 kg/cm<sup>2</sup> are not used in order to ensure reasonable service life.

The tire construction type is determined by the magnitude of the internal pressure and is characterized by definite relationships between the tire profile parameters.

We shall characterize the ratio of tire profile width  $B$  to height  $H$  or the degree of profile circularity (Figure 5.8) by the coefficient

$$K_1 = B/H.$$



The ratio of profile height  $H$  to radius  $R$  is characterized by the profile relative height coefficient  $K_2 = H/R$ , and the ratio of width  $B$  to outer diameter  $D$  is characterized by the profile relative width coefficient

$$K_3 = B/D.$$

Figure 5.8. Basic tire geometric dimensions.

Table 5.2 presents the average profile parameter

coefficients  $K_1$ ,  $K_2$ , and  $K_3$  for several Soviet tire types in a given range of airplane takeoff and landing speeds.

TABLE 5.2

Group No.	Tire group classification	Operating pressure range in $\text{kg/cm}^2$	Profile parameter coefficients			Airplane takeoff and landing speed in km/hour
			$K_1 = \frac{B}{H}$	$K_2 = \frac{H}{R}$	$K_3 = \frac{B}{D_1}$	
I	Superlow pressure	2 — 3.5	1.18	0.63	0.36	No more than 200
II	Low pressure	3.5 — 6.5	1.44	0.5	0.36	No more than 250
III	High pressure	6.5 — 10	1.13	0.55	0.32	Over 250
IV	Superhigh pressure	10 — 13.5	1.09	0.47	0.26	Over 300

According to the data of Table 5.2, airplane speed is no more than 200 km/hr for ultra-low pressure tires and no more than 250 km/hr for low pressure tires. High pressure or ultra-high pressure tires are used when the airplane speed exceeds 250 km/hr. This is explained by the fact that, with increase of the airplane speed, the centrifugal forces in the tire structural elements increase. The effect of these forces can be compensated by increase of the

TABLE 5.3\*

Tire size in inches	Tire size in mm	$p_0$ in kG/cm <sup>2</sup>	$D_1$ in mm	H in mm	$K_1 =$ B/H	$K_2 =$ H/R	$K_3 =$ B/ $D_1$	V in km/hr
32×11,5	810×290	8,5	380	230	1,25	0,57	0,36	to 250
41×15	1040×380	11	458	291	1,31	0,56	0,365	to 250
50×20	1270×510	9,5	508	381	1,33	0,61	0,4	to 250

\*Commas in numbers indicate decimal points.

tire internal pressure, reducing the number of layers in the tire body, reducing tread thickness, and also by changing the tire profile geometry.

With regard to construction, the tires of group I in the table are of the balloon or semi-balloon type, the tires of group II are of the arched type. The third and fourth groups are the tires of circular profile, having the highest "circularity."

We see from the data of Table 5.2 that, with internal pressure increase, the tire cross section becomes more nearly circular ( $K_1$ ) with simultaneous decrease of the profile relative height ( $K_2$ ) and relative width ( $K_3$ ). Exceptions are the low pressure tires of the arched type, for which the average value of  $K_1$  is 1.44.

In recent times, wide profile tires with high pressure, for which the ratio  $K_1 > 1.25$ , have begun to be used in connection with the requirements for increasing airplane flotation on the ground.

Table 5.3 presents the basic geometric and speed parameters of American tires.

During the last decade tire development has been characterized by increase of the loads acting on the tires and reduction of the tire dimensions (Table 5.4).

TABLE 5.4

Airplane data and tire characteristics	Airplane		
	Douglas DC-3	Douglas DC-6	Boeing 707
Maximum takeoff speed in km/hr	145	193	362
Maximum tire load in tons	7.26	13.56	17.37
Tire designation	17.00 - 16	15.5 - 20	46 - 16
Air pressure in kG/cm <sup>2</sup>	4.2	9.4	12.9
Contact ellipse area in cm <sup>2</sup>	1632	1393	1342
Footprint pressure in kG/cm <sup>2</sup>	4.4	9.7	12.9

TABLE 5.5

Airplane data and tire characteristics	Airplane		
	Convair 340 & 440	Trident 1C	NAA F-86
Maximum takeoff speed in km/hr	193	312	322
Tire designation	12.50 — 16	34 x 9.50 — 18	29 x 7.7
Maximum tire load in tons	5.810	5.990	6.260
Air pressure in kG/cm <sup>2</sup>	5.2	9.4	16.1
Contact ellipse area in cm <sup>2</sup>	1013	613	413
Footprint pressure in kG/cm <sup>2</sup>	5.7	9.8	15.1

The data of Table 5.4 show that, with increase of the tire load capacity and airplane takeoff speed, the air pressure in the tires increases. Since the contact ellipse area is approximately the same for all the tires compared, it is obvious that the specific pressure on the tire tread increases at the same time. In this regard, the tires designed for approximately the same maximal loading of 6000 kG are characteristic (Table 5.5). /89

We see from the table that each succeeding tire differs from the preceding tire, not only in increase of the takeoff speed and internal pressure, but also in considerable reduction of the profile and outer diameter. Reduction of the overall tire dimensions has had a marked influence on the contact ellipse area and, consequently, on the tread specific pressure. Bearing in mind that, with reduction of the tire dimensions, the tread length and volume decrease, the /90

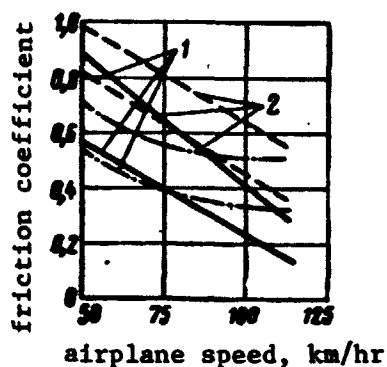


Figure 5.9. Friction coefficient for various tires.

1- made from standard rubber;  
2- made from "High  $\mu$ " rubber.

reduction of the  $29 \times 7.7$  tire service life, in comparison with the  $12.50 - 16$  and  $34 \times 9.50 - 18$  tires, becomes quite understandable.

Reduction of tire service life not only complicates operations, but also leads to high costs. Thus, according to the foreign press, American Airlines spends more than one million dollars a year for 707/720

airplane tires, 600,000 dollars for its Convair 990 airplanes, and about 150,000 dollars for piston engine airplanes. The total expenses associated with tires amounts to 1,750,000 dollars. The costs per landing for the CV 240 are one dollar, for the Convair 990 — 17 dollars, and for the 707-3230 cargo airplane — 25 dollars.

The requirements with regard to safety and braking effectiveness increase with increase of the airplane takeoff and landing speeds. Since braking effectiveness depends on the magnitude of the coefficient of tire traction with the airdrome surface, this parameter receives particular attention in tire design.

Numerous studies have shown that wheel motion stability and tire traction depend on the tread pattern.

We noted in Chapter 2 that, for aircraft tires, the pattern in the form of broad longitudinal ridges alternating with narrow grooves is most widely used, and with increase of the ridge width, the groove depth increases.

New rubber types are being used to increase the tire traction coefficient. Thus, in the synthetic foreign rubber of the "High  $\mu$ " type, the traction (friction) coefficient exceeds the friction coefficient of the standard types of rubber. The dependence of this coefficient on speed is shown in Figure 5.9. /91

The basic Soviet tire characteristics necessary for tire calculations and selection are presented in Table 5.6.

TABLE 5.6\*

Tire size	$p_Q$ in kG/cm <sup>2</sup>	$\delta$ mm	$\delta_{ma}$ mm	$P_{st}$ kG	$P_{ma}$ kG	$A_{ma}$ kG/m	$V$ km/hr	$G$ kG
Semi-balloon tires								
200×80	3,5	11,5	32	165	465	6	160	1,5
300×125	3,5	18,5	65	370	1340	36	200	3,5
400×150	4	30	99	925	3000	130	200	5
470×210	3,5	29	115	1150	4500	200	185	9
500×125	3,5	20	64	575	1800	50	165	6
500×150	2,5	23	88	480	1800	60	120	7
595×185	2,5	26	106	630	2550	140	105	10
600×180	4,5	20	104	810	4500	200	200	10
600×250	2,5	46	159	1300	4470	315	125	16
800×260	4,5	52	165	2800	8900	670	160	25
900×300	4,5	58	187	3830	12300	1050	160	36
1200×450	3,8	78	270	6000	20800	2600	125	80
Arch-shaped tires								
500×180	6	25	77	1300	4050	126	250	7,5
700×250	4,5	50	127	3150	7500	410	100	16,5
840×300	5,2	48	140	3800	11000	680	140	28
950×350	5,2	58	186	4800	15300	1200	160	37
1100×400	6,5	58	180	7900	24400	1840	230	62
1450×520	5,5	100	276	14300	38800	4500	220	130
High pressure tires (circular profile)								
570×140	7	20	85	1200	5250	190	240	9
660×200	9	42	107	3600	9300	430	315	15
800×225	9	39	132	4200	14200	800	300	22
930×305	8,5	69	176	7720	24000	1740	260	35
1100×330	9,5	58	197	9500	32000	2680	300	67
1500×500	9,5	80	305	20000	68000	8900	300	180
Superhigh pressure tires (circular profile)								
570×140	10,5	36	86	2600	7650	290	290	9
600×155	10,5	31	97	2300	9100	387	300	9,3
660×200	12	47	112	4500	13200	749	340	15,3
800×200	12	44	122	5400	18900	1010	385	23,5
880×230	13,5	49,5	111	7600	20800	1000	420	27,8
1160×290	13,5	67,5	159	110000	33600	2270	430	71,5

\*Commas in the numbers indicate decimal points.

## CHAPTER 6

### FRICITION AND CONSTRUCTION MATERIALS FOR BRAKES AND WHEELS

/92

#### 1. Materials for Brake Friction Pairs

The specific brake operating conditions have required the use for friction elements of special materials having special friction characteristics. Actually, during wheel braking, the brake elements are subjected to heating similar to thermal shock. The high sliding velocities (up to 30 m/sec) and the high specific pressures (up to 10 kG/cm<sup>2</sup> for multidisc brakes and up to 30 kG/cm<sup>2</sup> for single disc brakes) on the friction surfaces of the friction pairs and the high specific braking work values complicate both the selection of friction materials from the available types and the search for new and improved materials. At the same time, the friction materials must ensure stability of the basic characteristics (friction coefficient, wear resistance, frictional thermal stability, and mechanical strength) throughout the braking process.

The friction material characteristics depend on a whole series of factors. For example, the friction coefficient depends on the physical and chemical properties of the brake friction pair materials, temperature of the rubbing surfaces, relative sliding velocity of the friction pair, and the magnitude of the specific pressure on this pair, and the presence of lubricant on the rubbing surfaces.

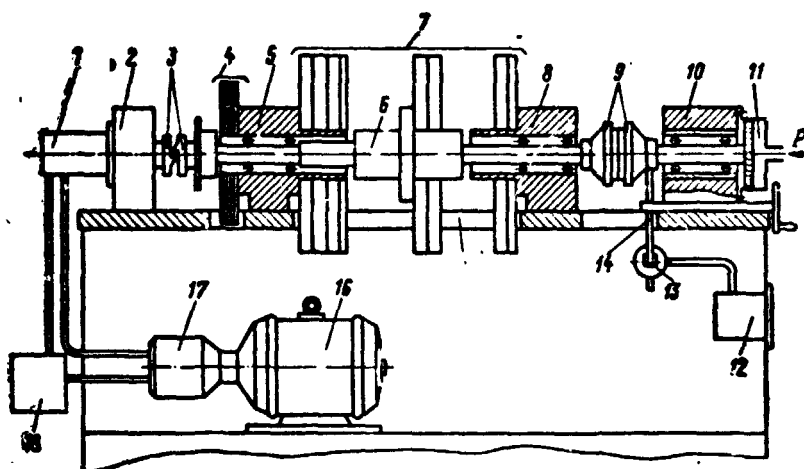


Figure 6.1. Schematic of facility for studying friction material properties.

1- hydraulic motor; 2- mechanical speed reducer; 3- clutch; 4- small flywheels; 5- aft support; 6- shaft; 7- large flywheels; 8- forward support; 9- test material specimen holder; 10- adjustable mandrel; 11- pressure cylinder; 12- brake moment recorder; 13- hydraulic dynamometer; 14- lever; 15- frame; 16- electric motor; 17- hydraulic pump; 18- hydraulic fluid tank.

The physical and mechanical properties of the friction materials and their characteristics are studied on special facilities. One such facility is the M-58 friction machine shown in Figure 6.1, which simulates actual brake operating conditions in regard to sliding velocity, specific pressure on the contact surfaces, and braking time.

The test material specimens of special form are mounted in the holders 9. Depending on the test regime, the flywheels 4 or 7, with moments of inertia of a definite magnitude, are selected.

The speed of the shaft 6 required to ensure the desired sliding velocity  $V_{sl}$  is established by the speed reducer 2 and the variable output hydraulic pump. After acceleration, the clutches 3 release the flywheels and they rotate by inertia. At the same time the clutches are released, pressure is supplied to the pressure cylinder 11, which provides the required specific pressure. The braking moment which develops on the friction surfaces during braking is transmitted by the lever 14 to the hydraulic dynamometer 13 and is recorded by the recorder 12.

The magnitude of the average friction coefficient obtained during braking on this facility is determined as follows. The kinetic rotating flywheel energy  $A_k$ , which is transformed into heat by the friction elements, is

$$A_k = \frac{I\omega_{bi}^2}{2} = M_{fr\ av} \varphi_b, \quad (6.1)$$

where  $I$  is the rotating flywheel moment of inertia;  $\omega_{bi}$  is the angular velocity at which braking begins;  $M_{fr\ av}$  is the average braking moment created by the friction elements;  $\varphi_b$  is the braking distance in radians.

The average braking moment

/94

$$M_{fr\ av} = f_{av} p_{sp} F_t \frac{D_{av}}{2}, \quad (6.2)$$

where  $f_{av}$  is the average friction coefficient;  $p_{sp}$  is the theoretical specific pressure on the friction elements;  $F_t$  is the theoretical friction element contact area; and  $D_{av}$  is the average diameter of the annular test material specimen.

The braking distance

$$\varphi_b = \omega_{av} \tau_b = \frac{\omega_{bi}}{2} \tau_b \quad (6.3)$$

where  $\tau_b$  is the braking time.

Substituting the expressions found from  $M_{fr\ av}$  from (6.1) and for  $\varphi_b$  from (6.3), we obtain

$$f_{av} = \frac{4k_1 A_k}{p_{sp} F_t D_{av} \omega_{bi} \tau_b}$$

where  $k_1$  is a coefficient accounting for the bearing friction losses.

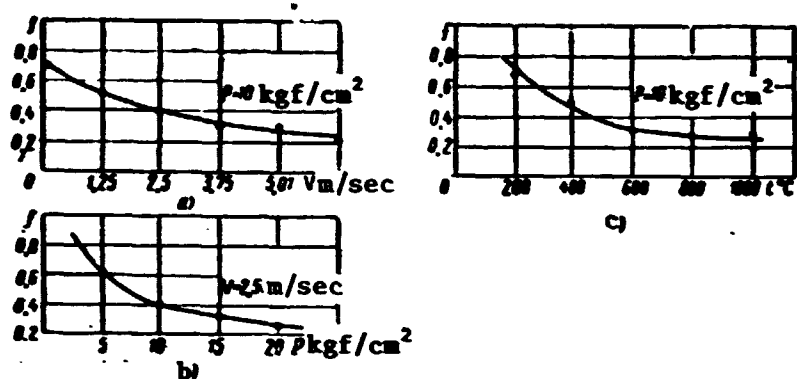


Figure 6.2. Experimental curves of friction coefficient  $f$  versus friction pair sliding velocity (a), contact surface specific pressure (b), and temperature (c).

From the  $M_b(\tau_b)$  curve recorded on the test facility, we determine the friction coefficient stability  $\alpha_{st}$ , which is the ratio of the average braking moment to the maximal value

$$\alpha_{st} = \frac{M_{fr \text{ av}}}{M_{fr \text{ max}}}.$$

The average linear specimen wear during a single braking is found from the difference of the specimen linear dimension measurements before and after the tests

$$J_h = \frac{\Sigma J_h}{n},$$

where  $n$  is the number of braking cycles performed; and  $\Sigma J_h$  is the specimen wear in  $n$  braking cycles.

The experimental data on the friction coefficient dependence on sliding velocity, temperature rise during braking, and specific pressure on the friction element surfaces are shown in Figure 6.2. The friction coefficient is different for the different friction materials and may vary from 0.18 to 0.45.

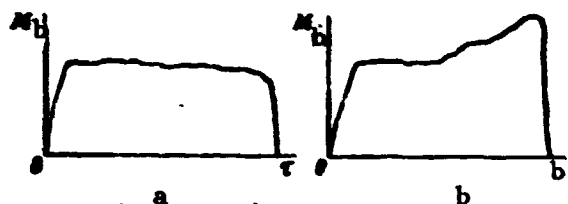


Figure 6.3. Braking moment as function of braking time for two wheel brake friction pair materials.

a- iron with plastic; b- iron with cermet.

The difference in the brake element material properties with respect to friction coefficient and its stability leads to different nature of the braking moment variation as a function of braking time.

Figure 6.3. shows curves of /95  
braking moment versus braking time for friction pairs with

plastic and cermet working with iron. Characteristic for the friction pair with cermet is increase of the braking moment toward the end of the braking period, while the plastic tends toward reduction of the braking moment. In both cases, the theoretical friction surface specific pressure was kept the same. The braking moment reduction for the friction pairs with plastic is explained by the marked friction coefficient reduction with increase of the friction element temperature, which cannot be compensated by reducing the sliding velocity. For the friction pairs with cermet, the braking moment increases as a result of marked friction coefficient increase with reduction of the sliding velocity, which exceeds considerably the friction coefficient reduction with friction element temperature increase because of heating. Variation of the braking moment during braking is an undesirable phenomenon, since braking effectiveness /96  
decreases with reduction of the braking moment while overloading of the brake system takes place with braking moment increase.

Plastics and cermets are the primary materials used at the present time for friction pairs. Plastics are used when the friction element temperature does not exceed 350° C, and the cermets are used at temperatures of 500 — 600° C. The cermets are composition materials fabricated by powder metallurgy methods. The cermet charge is a mechanical mixture of several components. The charge chemical composition (in percent by weight) of one cermet version is

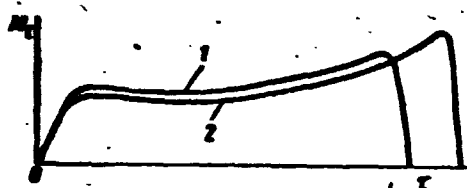


Figure 6.4. Variation of braking moment  $M_b$  with braking time  $\tau$  for cermet friction elements with different carbon content

1- normal carbon content; 2- reduced carbon content.

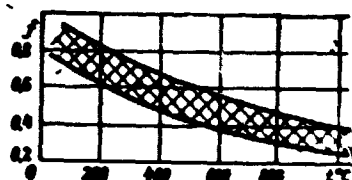


Figure 6.5. Region of variation of the friction coefficient  $f$  as function of sliding velocity  $V$  and friction contact surface temperature rise  $t$  °C.

Copper	Sand	Asbestos	Barite	Graphite	Iron
14 — 16	2 — 4	2 — 4	4 — 6	7.5 — 8.5	Rest

After thorough mixing, the charge is pressed into sector blanks which are sintered at high temperatures with a steel carcass.

Since the basic cermet component is iron, its friction properties depend to a considerable degree on the percentage carbon content. With reduction of the carbon content, the friction coefficient decreases and its stability deteriorates. Figure 6.4 shows the variation of  $M_b$  during braking for the same brake with cermet lining with different cermet carbon content.

Figure 6.5 shows the region of limiting cermet friction coefficient values as a function of sliding velocity and friction pair friction surface temperature. The widely used friction cermet operates satisfactorily with sliding velocity no higher than 30 m/sec, theoretical specific pressure on the material no more than  $12 \text{ kg/cm}^2$ , and mass average friction element temperature up to  $450 - 500^\circ \text{C}$ .

Plastics of the FK-16L type and cermets can operate in brakes together with iron of chemical composition (in percent by weight)\*

C	Mn	Si	Ni	Mo	Cr	S	P	Fe
3,2—3,8	0,6—1,0	1,6—2,3	0,3—1,4	0,2—0,5	0,15—0,45	0,1	0,3	Rest

\*Commas in numbers indicate decimal points.

Because of its brittleness, iron cannot be used directly in the friction elements; therefore, it is bonded to steel plates which are then shaped to the desired contour.

In addition to iron, in many cases, wide use is made of special friction steels with high chromium content (in percent by weight):\*

C	Si	Mn	Cr	P	S	Fe
0.13— 0.34	<0,6	<0,6	12—14	<0,030	<0,025	Rest

An important friction material characteristic is its hardness. Brake operating experience has shown that cermet hardness should be in the limits HRF 60 — 95, iron HRF 160 — 220, and steel HRF 200 — 220. Simple carbon steel may be used together with plastic as the friction material in certain brake designs. The basic characteristics of some foreign friction plastics operating together with iron or steel are presented in Table 6.1.

The characteristics of certain foreign cermet friction materials operating together with steel and iron are given in Table 6.2.

We noted above that the parameters which determine brake energy capacity include: specific heat capacity of the housing, disc, and friction element materials, maximal allowable friction element temperature rise during braking, and disc weight. The specific heat capacity of the housing material used and friction elements varies from 0.12 to 0.17 kcal/kg/°C. The allowable mass average temperature rise of modern friction pair materials with significant friction pair service life (about 500 brake applications), usually varies in the range 400 — 450° C. Search for new materials with high specific /98 (weight) heat capacity is one technique for increasing aircraft wheel brake specific energy capacity.

Increasing attention has been devoted in recent years to this question abroad. Use of beryllium in brake systems has been initiated recently in the USA and use of the low melting metals (lithium, potassium, sodium) has been reported. For example, Douglas Aircraft has proposed the use of beryllium sectors attached directly to the brake discs in brake construction. According to Douglas, brake discs with such sectors under normal operating conditions have an energy capacity on the order of 40,000 kG/m/kg. The allowable

\*Commas in numbers indicate decimal points.

TABLE 6.1

Friction pair materials	Specific pressure kg/cm <sup>2</sup>	Friction coefficient f	Friction coefficient stability $\alpha_{st}$	Material wear per brake application $I_h$ in mm	
				Plastics	Steel (iron)
Dunlop plastic — Dunlop steel	18	0.35	0.78	190	3
Dunlop plastic-iron	18	0.38	0.72	200	5
Ferodo plastic-iron	24	0.29	0.84	225	8.7
Plastic X-iron	18	0.43	0.76	132	8

TABLE 6.2

Friction pair materials	Specific pressure kg/cm <sup>2</sup>	Friction coefficient f	Friction coefficient stability $\alpha_{st}$	Material wear per brake application in mm	
				Cermet	Steel (iron)
Cermet No. 1 - steel	18 - 20	0.18	0.43	4.3	2
Cermet No. 2 - iron	18 - 20	0.35	0.9	43 — 80	1
Cermet No. 3 - steel	18 - 20	0.38	0.8	25 — 50	2

maximal mass average temperature in discs with such loading is 700° C. Provision is made in the brake design (with the brake disassembled) for washing off the toxic beryllium oxide which forms on the contacting surfaces during braking. In another brake design, beryllium is used as a filler in a thin-wall shell having frictional properties (Figure 6.6). Such a shell will also prevent beryllium oxidation and toxic oxide formation during operation. Some detail brake and wheel parts, in addition to the brake disc sectors, can also be fabricated from beryllium.

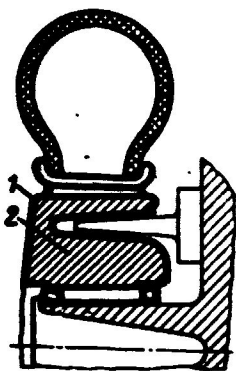


Figure 6.6. Construction of brake with beryllium heat sink sectors designed by Douglas Aircraft.

1- shell; 2- beryllium.

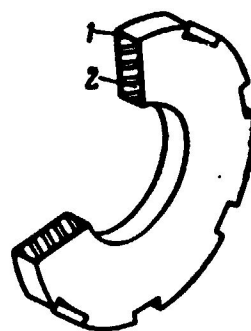


Figure 6.7. Construction of brake disc filled with sodium or lithium fusible heat sink.

1- shell; 2- heat sink.

Increase of brake energy capacity can be achieved by using fusible heat sinks, for example, lithium, sodium, and potassium. Figure 6.7 shows a brake disc with sodium or lithium fusible heat sink enclosed in a shell. During braking, the heat sink is raised to a high temperature and melts.

Use of the heat absorbing materials listed above (beryllium, sodium, etc.) leads to increase of the wheel brake structural volume because of the very low specific weight of these materials. Therefore, for example, when using lithium, a brake with structural volume about 1.5 times greater than that of the brake with iron heat sink is required for the same energy capacity. In this case, the brake must extend beyond the wheel structure (Figure 6.8). Usually, such designs are difficult to realize for the aircraft wheels used /100 on modern airplanes. Therefore, materials with high specific heat capacity (per unit volume) and low specific weight are necessary for high energy capacity brakes.

The prospects for the use of such materials in brake construction can be evaluated from the data presented in Figure 6.9. We see from analysis of these data that, for the same energy absorbed by the brake and the same temperature rise  $500^{\circ}\text{C}$ , the beryllium or lithium brake discs (in a shell) will occupy in comparison with steel about

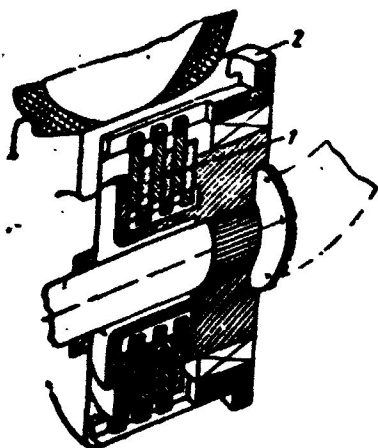


Figure 6.8. Brake design with beryllium heat sink.

1- brake disc; 2- external heat accumulator.

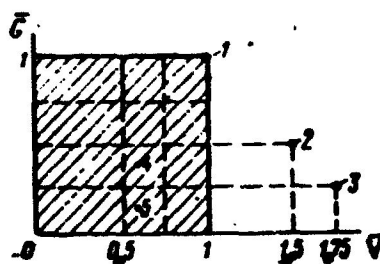


Figure 6.9. Relative weight ( $\bar{G}$ ) and relative volume ( $\bar{V}$ ) of brake packet with constant energy capacity for several materials.

1- iron; 2- beryllium; 3- lithium; 4- chromium carbide; 5- zirconium carbide.

1.5 — 1.75 times more structural volume. The materials yielding

improvement in both weight and volume lie in the shaded zone. Such materials include the carbides of certain metals.

## 2. Wheel Structural Materials

Aircraft wheels are usually fabricated from magnesium or aluminum alloys by casting or forging with subsequent machining. The wide use of magnesium and aluminum alloys for wheels is due to their low specific weight and comparatively high mechanical properties. For example, magnesium casting alloys for wheel drums have strength up to  $25 \text{ kg/mm}^2$  and the wrought alloys have strength up to  $38 \text{ kg/mm}^2$ .

In selecting braked wheel drum material, it is necessary to consider that the drum must operate under conditions of periodic heating during braking to  $100 - 120^\circ \text{C}$  with subsequent cooling to normal temperature.

/101

High strength magnesium casting alloys based on magnesium-zinc-zirconium, for example, the English alloy Z5Z, have been used recently in several countries for wheels. A characteristic feature of the magnesium-zirconium based alloys is a higher yield limit and good plasticity, which makes it possible to use them for detail

parts operating under reversing load conditions. The mechanical properties of the new magnesium casting alloys depend, to a considerable degree, on the zinc and zirconium content in the alloys. The highest strength of the Z5Z alloy is obtained with 4 — 5% zinc and 0.6 — 1.1% zirconium. According to the foreign press, the Z5Z alloy is recommended for detail parts operating at temperatures up to +150° C. The alloy is subjected to surface hardening to increase the service life of parts fabricated from it and has satisfactory corrosion resistance. The wrought magnesium alloys are used in place of the casting alloys if it is necessary to increase the strength. The mechanical properties of one such foreign alloy are presented in the following table:

$E$ kG/mm <sup>2</sup>	$G$ kG/mm <sup>2</sup>	$\delta_u$ kG/mm <sup>2</sup>	$\delta_{0.2}$ kG/mm <sup>2</sup>	$\tau_{av}$ kG/mm <sup>2</sup>	HB kG/mm <sup>2</sup>	$\delta$ in %
4300	1600	32	26	20	60	8

Among the aluminum wrought alloys widely used for wheel drums, we can cite, for example, the 2014 alloy, whose properties are presented in the following table:

$E$ kG/mm <sup>2</sup>	$G$ kG/mm <sup>2</sup>	$\delta_u$ kG/mm <sup>2</sup>	$\delta_{0.2}$ kG/mm <sup>2</sup>	$\tau_{av}$ kG/mm <sup>2</sup>	HB kG/mm <sup>2</sup>	$\delta$ in %
7200	2700	40	30	30	130	8

In addition to the wrought aluminum alloys, wide use is made of the casting alloys with strength to 26 kG/cm<sup>2</sup>. Data on the use of titanium in wheel construction has appeared recently in the foreign press. In addition to the magnesium and aluminum alloys, various alloyed and simple carbon steels are used in wheel and brake construction.

## CHAPTER 7

### BASES FOR THE SELECTION OF TIRES, WHEELS, AND BRAKES IN AIRPLANE DESIGN

Experience in airplane design and operation shows that wheel, /102  
tire, and brake parameters determine, to a considerable degree, the  
airplane takeoff and landing characteristics, the possibility of  
airplane operation on airdromes with various surfacing, and the  
service life and reliability of both the entire landing gear and  
the individual gear elements.

The primary parameters necessary for wheel selection  
are:

- tire pressure, which determines airplane flotation on various  
soils;
- airplane takeoff and landing speeds, which determine the  
tire speed characteristics;
- static and dynamic wheel loads, which determine the tire  
dimensions;
- airplane kinetic energy during landing rollout, which is  
transformed by the brakes into heat and determines brake size,  
weight, and construction.

## 1. Tire Selection

Wheel selection usually begins with tire selection. We mentioned in Chapter 5 that the existing tire types are arbitrarily broken down into four groups on the basis of nominal tire operating pressure. Therefore, we first determine the appropriate group on the basis of the flotation requirements with account for the airplane takeoff and landing speeds. After determining the tire group and construction type, we use the formulas presented in Chapter 5 to determine the tire dimensions (diameter and width in mm) on the basis of the specified load on the wheel or its load capacity. In addition to these formulas, we can use the following empirical formula, which expresses the load on the wheel as a function of tire dimensions and tire working pressure. This relation was derived on the basis of analysis and statistical reduction of a large amount of data on braked and unbraked wheels /103

$$P_{st\ to} = kDB(p_0 + 1), \quad (7.1)$$

where  $P_{st\ to}$  is the allowable static takeoff load (load capacity per wheel in kG);  $D$  is the tire diameter in mm;  $B$  is the tire width in mm;  $p_0$  is the tire pressure in  $\text{kG/cm}^2$ ; and  $k$  is a coefficient of proportionality (for tires of diameter to 1100 mm,  $k = 0.25$ ; for tires of diameter more than 1100 mm,  $k = 0.23$ ).

In the final tire size determination, we should restrict ourselves to the following standard or frequently used sizes:

Tire diameter in mm	660	680	910	1050	1100	1280	1450	1600	1750
Tire width in mm	200	230	305	300	330	390	450	550	750

Figure 7.1 shows calculated load capacity curves of all four tire groups as functions of tire pressure and tire size, plotted using (7.1). We can determine the tire diameter and width from these curves on the basis of the specified static takeoff load per wheel and tire pressure. The static takeoff load per wheel and tire

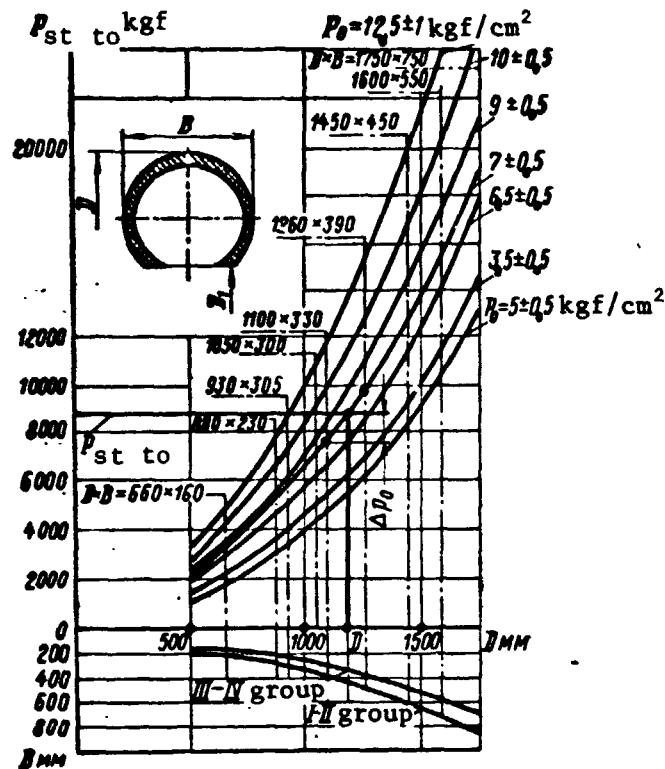


Figure 7.1. Calculated curves of tire load capacity versus tire size ( $D \times B$ ) and tire pressure  $p_0$ .

pressure are considered the most important criteria for determining the size of the tire.

If, on the basis of the specified load  $P_{st} \text{ to}$ , the tire dimensions ( $D \times B$ ) are found to be nonstandard, they should be modified on the basis of the following considerations.

If we take a smaller standard size (for  $D \times B$ ), we can compensate for the resulting deficiency with respect to tire load capacity by increasing the tire pressure by  $\Delta p_0$ , but  $\Delta p_0$  should not exceed 5 — 10% of the nominal pressure. We must bear in mind that the tire may not have the required strength margin in this case.

If we take a larger standard size, the tire will have a margin with respect to both load capacity and pressure, which is particularly favorable for newly designed airplanes.

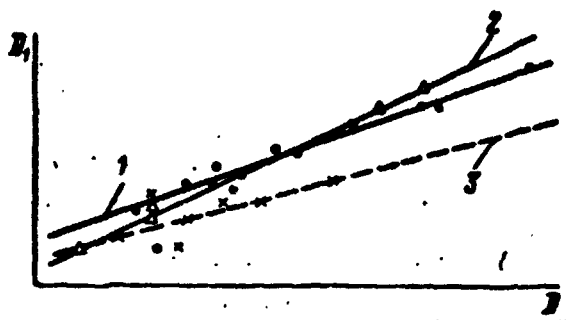


Figure 7.2. Averaged wheel drum seating diameter ( $D_1$ ) versus tire outer diameter ( $D$ ).  
 1- circular profile tires ( $p_0 \geq 6.5 \text{ kG/cm}^2$ ); 2- arch-shaped tires ( $p_0 = 3.5 - 3.6 \text{ kG/cm}^2$ ); 3- semi-balloon tires ( $p_0 = 3.5 \text{ kG/cm}^2$ ).

it is necessary to either increase the tire pressure or select a larger tire. In addition to the static load, the selected tire size must correspond to the normed landing gear shock absorber work with this tire.

After determining the tire size, we check its shock absorbing characteristics on the deflection curve.

It is considered acceptable if the tire deflection under the action of the static takeoff load does not exceed on the average, 30 — 35% the total deflection, since excessive deflection leads to marked tire service life reduction. If, for the tire with the specified load, the deflection is more than 35%,

/106

## 2. Wheel Size Determination

The selected tire dimensions (diameter and width) also determine the wheel dimensions, and the drum outer diameter is defined by the tire seating diameter.

Figure 7.2 shows the averaged wheel drum seating diameter ( $D_1$ ) dependence on tire outer diameter ( $D$ ) for various tire pressures, and Table 7.1 shows the actual dimensions of some tires used in the USSR.

The tire size and pressure determine, in the final analysis, the brake structure volume  $V_b$ , in which we consider the space for the brake with the limiting brake energy capacity and service life (Figure 7.3). The quantity  $b$  usually varies in the limits of  $(0.05 - 0.1)E$ .

/106

TABLE 7.1

Outer Diameter D mm	Group I		Groups I and II		Groups III and IV	
	Width B mm	Seating diameter D <sub>1</sub> mm	B mm	D <sub>1</sub> mm	B mm	D <sub>1</sub> mm
500	180	250	—	—	—	—
600	—	—	180	280	—	—
650	—	—	250	150	—	—
660	—	—	—	—	160	355
700	200	335	150	400	—	—
700	250	356	—	—	—	—
720	310	247	—	—	—	—
770	—	—	330	250	—	—
800	—	—	260	330	200	416
840	300	419	—	—	—	—
865	280	430	—	—	—	—
880	—	—	—	—	230	468
900	—	—	300	370	—	—
930	—	—	—	—	305	406
950	350	451	—	—	—	—
1000	—	—	350	370	—	—
1050	—	—	—	—	300	508
1100	—	—	—	—	330	508
1260	—	—	450	430	390	590
1325	480	635	—	—	—	—
1450	520	685	—	—	450	630
1500	—	—	—	—	500	630
1600	—	—	—	—	550	680
1750	—	—	—	—	550	725

### 3. Wheel Weight Determination

After determining the tire and wheel dimensions and limit allowable brake energy capacity, we find the first estimate of the weight of the wheel, together with the brake, from the formula:

$$G_{w \text{ ass}} = G_{wd} + G_b + G_t,$$

where  $G_{wd}$  is the weight of the wheel drum with bearings;  $G_b$  is the brake weight; and  $G_t$  is the tire weight.

The wheel drum weight can be determined approximately from the allowable drum specific output  $q_{wd}$ , which is the ratio of the static takeoff load to drum weight and depends on the drum material, required service life, temperature regime, and wheel size. Figure 7.4 shows the curve of allowable specific output of a drum fabricated

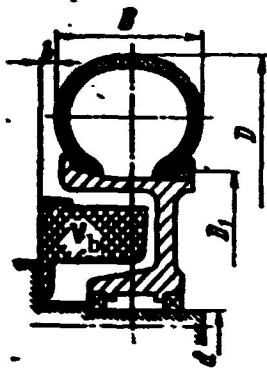


Figure 7.3. Wheel construction.

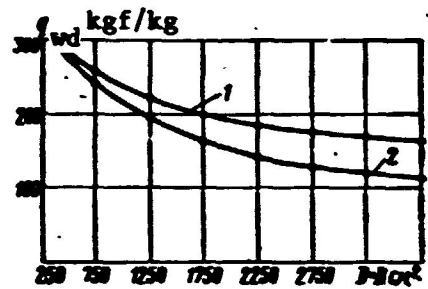


Figure 7.4. Allowable wheel drum specific output  $q_{wd}$  versus tire size  $D \times B$ .

1- forged; 2- cast.

from magnesium alloys (cast and forged) versus tire size. Using this relation, for known geometric tire dimensions  $D$  and  $B$ , we determine the limiting value of  $q_{wd}$  and the wheel drum weight:

$$G_{wd} = P_{st} / q_{wd}.$$

However, the brake assembly weight can be determined approximately from the brake energy capacity ( $A_b$ ) using the curve in Figure 7.5, plotted from calculation of the energy absorbed by the brake per landing with heavy braking.

The tire weight and specific output can be found from a curve analogous to that shown in Figure 7.6.

Of interest is the graphical method (Figure 7.7) which has been proposed by Messier for selecting the disc brake on the basis of energy capacity and weight. The figure is plotted from calculation of the transformation of work equal to 750,000 kG/m into heat in the nominal braking regime. The emergency regime is determined on the basis of obtaining a mass average heat sink temperature on the order of 800 — 1000° C. The ordinate axis is the tire seating diameter in inches and millimeters, the left abscissa axis is the brake weight and the right abscissa axis is the kinetic energy transformed by the brake into heat during emergency normal braking. This method is used to expand the range of applications, depending on the heat sink (brake disc) material.

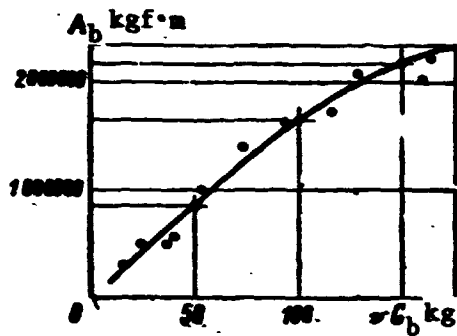


Figure 7.5. Brake energy capacity  $A_b$  versus brake weight  $G_b$ .

The first version is with steel heat-absorbing brake discs (rotating and stationary). One of the discs has cermet bonded to it.

In the second version, the heat sink is a packet of steel and reinforced beryllium discs. The rotating discs are steel and the nonrotating discs are beryllium reinforced with steel. The steel is coated with friction material.

In the third version, the heat sink consists of beryllium discs reinforced by steel with friction material bonded to the surface.

In the fourth version, the heat sink consists of copper discs operating together with a plastic disc. This version is usually used for single disc brakes with exposed friction surface.

Messier states that the second and third version brakes have not yet found operational application because of several technological difficulties in fabricating the discs. However, the firm believes that these versions are very promising.

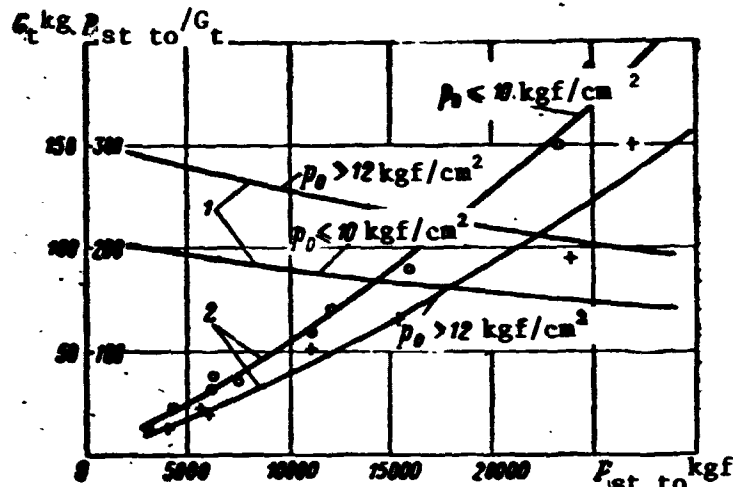


Figure 7.6. Tire weight  $G_t$  and specific output  $P_{st\ to} / G_t$  versus static load and internal pressure  $p_0$ .

1- specific output; 2- tire weight.

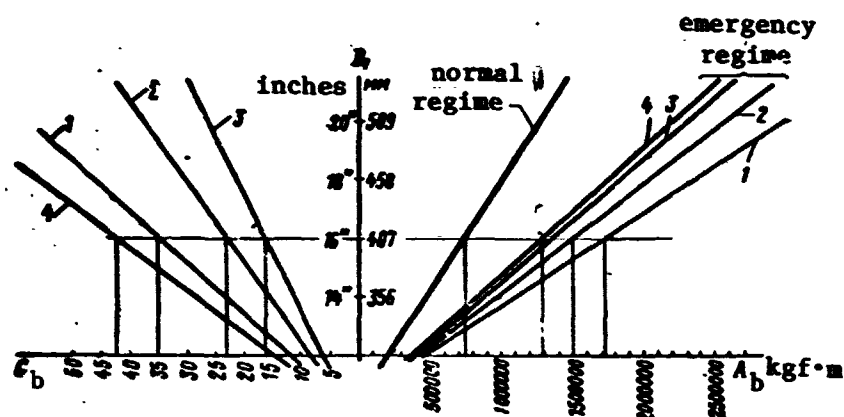


Figure 7.7. Graph for selecting wheel disc brakes using the Messier method.

1, 2, 3, 4- first and subsequent versions.

The figure is used as follows for disc brake selection. After /108  
determining the wheel and tire sizes, we find the tire seating  
diameter  $D_1$  (in inches or millimeters).

Then, for this diameter  $D_1$ , we find as a function of the heat  
sink material properties the brake weight and energy capacity,  
i.e., the amount of energy which it is capable of absorbing during /109  
normal or emergency braking.

We shall illustrate the use of the figure by the following  
example. For example, let the selected wheel have seating diameter  
 $D_1$  equal to 16" (or 407 mm), then the brake weight for the first  
version is about 35 kG, for the second version — about 23 kG, for  
the third version — about 16 kG, and for the fourth version —  
about 42.5 kG.

In the emergency braking regime, the brake energy capacity now  
depends on the properties of the heat sink material and amounts to:  
for the heat sink using the first version — 1,700,000 kG/m; for  
the second version — 1,500,000 kG/m; for the third version —  
1,350,000 kG/m; and for the fourth version — 1,300,000 kG/m.

TABLE 7.4

Heat sink material	Brake specific energy capacity in kg/m	
	Normal regime	Emergency regime
Steel	21 500	48 500
Steel + reinforced beryllium	32 500	65 000
Reinforced beryllium	47 000	85 000
Copper	17 500	30 500

The brake specific energy capacity as a function of the material and braking regime is shown in Table 7.4.

Tables 7.5, 7.6, and 7.7 present the characteristics of some operational Soviet and foreign wheels, brakes, and tires.

TABLE 7.5\*  
BASIC CHARACTERISTICS OF SOVIET WHEELS AND TIRES

Wheel size D x B	Tire pressure kg/cm <sup>2</sup>	Static load, kg		Braking moment in kg/m	Brake energy capacity kg/m	Takeoff speed in km/hr	Landing speed in km/hr	Weight in kg			
		Landing	Take-off					Wheel assem- bly (with tire)	Drum assem- bly	Brake assem- bly	Tire
500x150	7	1 150	1 350	11 600	216 000	250	200	29,5	16	6,25	7,25
600x180	10	1 245	2 350	18 000	260 000	60	35	28,0	12,5	4,2	11,3
600x250	2,5	—	1 300	—	—	110	110	19,15	6,65	—	12,5
700x150	3,5	—	925	—	—	150	150	19,5	9,5	—	10
700x200	10,5	1 500	3 300	18 700	286 000	370	250	54	14	21	19
700x250	6,5	—	2 000	—	—	250	220	29,8	13,4	—	16,4
720x310	4,6	—	3 750	—	—	—	210	37,5	15	—	22,5
770x330	4	—	3 500	—	—	180	180	36,4	14,7	—	21,7
800x260	4,5	—	2 800	32 200	135 000	150	150	36,4	21	5,6	23
840x300	5,2	3 800	3 800	51 400	272 000	140	140	77,3	41,2	9,6	26,5
865x280	6,5	3 950	4 300	55 300	650 000	250	240	116	32	58	26
900x300	5	2 650	2 700	—	—	220	205	50	20	—	30
950x350	5,2	4 700	4 800	—	—	—	—	113	51,0	23,40	38,6
1000x350	4,7	5 180	5 180	58 000	260 000	160	160	86,8	36,7	7,6	42,5
1200x450	3,8	6 000	6 000	121 000	248 800	160	140	116,3	37	9,3	70
1325x480	7,0	15 000	16 850	125 000	1 040 000	60	80-100	208,84	101,34	21	86,5
1450x520	7,0	12 905	14 820	260 000	1 250 000	215	195	421	188	130	108

\*Commas in the numbers indicate decimal points.

TABLE 7.6\*

BASIC CHARACTERISTICS OF FOREIGN WHEELS AND TIRES WITH  
PRESSURE FROM 7.5 TO 10.5 kg/cm<sup>2</sup>

Wheel size D x B	Airplane type	Static load in kg		Landing speed in km/hr	Tire pressure kg/cm <sup>2</sup>	Brake energy capacity, kg/m	Weight in kg			Tire
		Land- ing	Take- off				Wheel assembly (with tire)	drum assembly	Brake assembly	
139x139	Boeing KC-135	1940	2880	—	9,6	—	22	8	—	14
660x197	Vampire	—	3200	—	8,0	187 000	—	—	—	13
660x197	Breguet 1150	—	3200	255	8,0	—	21	8	—	13
737x194	Avro 100	—	3750	—	9,0	123 000	—	—	—	—
737x194	Gloster Meteor	—	4500	—	10,0	—	32	12	—	20
774x219	Canadair 44D	3940	5070	240	9,5	—	32	12	—	20
836x251	Belfast	3780	6350	270	9,8	—	—	—	—	27
836x251	Lockheed	5000	6350	—	9,8	—	43	16	—	27
889x229	Comet	—	6000	200	8,5	587 000	48	—	—	29
889x229	Caravelle	5700	6000	237	8,5	950 000	48	—	—	29
889x229	Comet-4	5330	7200	203	10,5	962 000	—	—	—	30
905x260	Boeing 377	6000	6800	—	8,3	—	47	17	—	30
905x270	Viscount	—	6850	—	8,3	—	—	—	—	35
965x314	Vickers VC-10	4950	7000	248	7,0	—	78	29	—	49
965x314	Boeing 707	4950	7800	260	10,3	—	55	18	—	37
965x314	Breguet 1150	—	10250	255	10,5	600 000	122	27	45	50
1100x297	Gloster Javelin	7950	9100	—	10,2	—	—	—	—	—
1020x300	Bristol Britannia	6750	14290	—	9,7	825 000	—	—	—	—
1225x428	Lockheed 1049	11300	15650	—	8,4	1 270 000	—	—	—	90
1225x428	Boeing 707	9900	15650	260	9,1	2 460 000	258	80	95	83
1225x428	Boeing 727	10400	13800	223	9,1	2 460 000	258	80	95	83
1423x496	Boeing 377	12200	—	—	8,4	1 220 000	266	97	76	93

\*Commas in the numbers indicate decimal points.

TABLE 7.7\*  
BASIC CHARACTERISTICS OF FOREIGN WHEELS AND TIRES WITH  
PRESSURE MORE THAN 10.5 kg/cm<sup>2</sup>

Wheel size D x B	Airplane type	Static load in kg		Landing speed in km/hr	Tire pressure in kg/cm <sup>2</sup>	Brake energy capacity in kg/m	Weight in kg			
		Land- ing	Take- off				Wheel assembly (with tire)	Drum assembly	Brake assembly	Tire
644x165	Sabre 86	—	3930	240	12	—	—	—	—	—
644x165	Boeing B-47	4200	4600	—	13	—	25	9	—	—
774x219	Bristol Brittonia	5050	6800	—	12.7	—	32	12	—	—
803x160	Republic 84	—	6125	240	18	895 000	90.5	27.5	43	—
838x278	Douglas DC-8	6100	8300	240	11.6	—	54.5	20.5	—	—
889x229	Caravelle	—	8000	320	12	—	—	—	—	—
914x278	NAA	—	8600	—	11	910 000	—	—	—	—
1000x346	Lockheed L-188	9570	12500	—	11	93500	158	44	54	—
1000x346	Douglas DC-9	11900	12560	215	11.2	—	—	—	—	—
1020x305	Canadair 44D	8400	10800	240	11.6	—	—	—	—	—
1020x445	Boeing B-70	11300	20800	320	11.2	—	—	—	—	—
1086x394	Douglas DC-8	12850	17420	240	13	—	—	—	—	—
1110x330	Douglas DC-8	—	19800	280	12.7	2100 000	—	—	—	—
1423x496	Boeing B-47	18200	20000	—	12.5	1340 000	290	88	92	—

\*Commas in the numbers indicate decimal points.

## CHAPTER 8

### AIRPLANE BRAKE SYSTEMS

#### 1. Basic Brake System Requirements

/113

The airplane brake system is used to control the wheel brakes by varying the braking moment and also for automatic elimination of wheel lockup (skidding). Brake systems in which the magnitude of the braking moment is established automatically in order to realize the limiting traction coefficient  $\mu_{lim}$  have recently come into use.

The modern airplane brake system is an assemblage of various functional devices (hydraulic, pneumatic, electrical, and mechanical) interconnected by the required couplings (hydraulic lines, electrical wiring, mechanical linkages). The total number of such devices in the brake system may be very large. For example, the brake system of the Il-62 airplane has more than 100 components.

Definite requirements are imposed on the brake systems during design and operation. First of all, the systems must be operationally reliable, simple, and easy to control. The braking moment must be proportional to the controlling signal magnitude. The brake system must have adequate response speed, which is characterized by the time from the instant of application of a step function maximal input signal until the creation of the maximal braking moment. For the brake systems of modern airplanes, this time is one to 1.5 seconds.

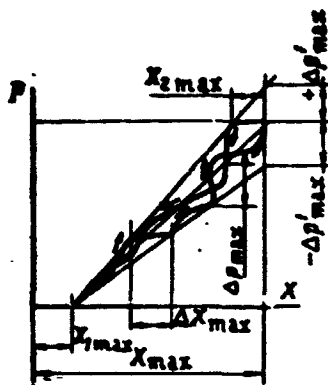


Figure 8.1. Airplane brake system pressure versus input signal or controller travel.

Since the braking moment  $M_b$  is determined by the brake pressure  $p_b$ , one of the important indices of efficiency of the brake system and its individual components are the errors of the static characteristic  $p_b(X)$ , where  $X$  is the magnitude of the input signal or controlling element travel. Usually, the static characteristic errors (Figure

8.1) are established by the specifications as follows: maximal controlling element dead zone  $X_{1 \max} \leq 0.25 X_{\max}$ , maximal allowable travel insensitivity  $\Delta X_{\max} \leq 0.1 X_{\max}$ , maximal allowable brake pressure overshoot  $\Delta p_{\max} \leq 0.15 p_{\max}$ , maximal allowable final pressure deviation  $\pm \Delta p'_{\max} \leq 0.1 p_{\max}$ , and maximal travel hysteresis  $X_{2 \max} \leq 0.15 X_{\max}$ . /114

These deviations characterize the quality of the brake system as a whole and the technical efficiency of its individual components.

At the present time, pneumatic, hydraulic, and combined (pneuhydraulic) brake systems are used on airplanes. The pneumatic systems are used on light airplanes and the hydraulic — on heavy airplanes, since the latter have powerful hydraulic systems servicing various users.

The combined brake systems, in which the hydraulic part is the main system and the pneumatic part is the emergency system, are used comparatively rarely.

With regard to operating principle, the brake systems can be divided into those with direct and remote control.

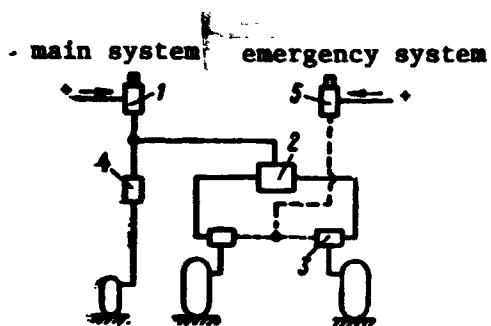


Figure 8.2. Pneumatic brake system with direct control for tricycle gear airplane with braked nose wheel.

1, 5- reduction valves; 2- differential; 3- shuttle valve; 4- nosewheel brake shutoff valve.

## 2. Direct Control Brake Systems

In the direct control brake systems, the pressure in the brakes is created by a special reducing valve as the pilot actuates it either directly or through a system of levers and links. A schematic of a pneumatic brake system with direct control for a tricycle gear airplane with braked nosewheel is shown in Figure 8.2. This system has main and emergency (standby)

systems. The pressure in the brakes is created by the reducing valve 1 with direct input from the pilot. The air in the primary subsystem is fed to the main wheel brakes through the differential 2 and shuttle valve 3. Air enters the nosewheel brake from the valve 1, bypassing the differential. When using the emergency system, the air from the valve 5 goes directly to the main wheel brakes only. The differential in the brake system serves for separate application of right and left main wheel braking, while the shuttle valve isolates the emergency system from the main system.

The hydraulic brake system with direct control for a heavy airplane having multiwheel bogies is shown in Figure 8.3. With input to the reduction valve 1, the working fluid is supplied to the wheel brakes through the shuttle valves 2, electromagnetic valve 3, and hydraulic fuse 4. Fluid is supplied to the wheel brakes of the left bogie from the left reduction valve and to the wheel brakes of the right bogie from the right reduction valve (first or second pilot). In this way, individual braking of the left and right bogie wheels is provided in order to improve maneuverability during airplane taxiing. If wheel lockup (skidding) occurs, the valve 3 isolates the wheel brakes from the supply line and connects them to the return line. When emergency braking is necessary, the valve 5 is actuated and the working fluid enters the wheel brakes through

/115

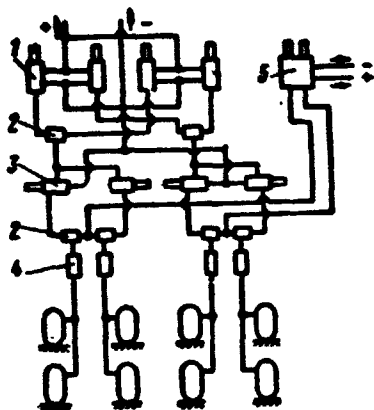


Figure 8.3. Hydraulic brake system of heavy airplane with multiwheel landing gear and direct control.

1- reduction valve; 2- shuttle valve; 3- electromagnetic valve; 4- hydraulic fuse; 5- reduction valve.

the shuttle valves 2 and the hydraulic fuses 4. The hydraulic fuses 4 block the supply line automatically if there is damage to any system line located downstream of them.

Differential braking of the right and left wheels is not required in the brake system of the airplane with bicycle landing gear, since the gear track is very narrow. During taxiing, airplane control is accomplished by turning the front strut and differential engine power. Operational

experience has shown that the maximal braking moment on the front wheels should be 25 — 30% less than on the rear wheels in order to ensure airplane stability during landing rollout. The direct control brake systems are constructionally simpler than the remote /116 control systems and more reliable in operation. However, the requirements for response speed in the case of considerable hydraulic system line length, for example on heavy airplanes, are satisfied better by the remote control systems.

### 3. Remote Control Brake Systems

In the remote control systems, the brake pressure is created by an executive unit (specifically, by a reduction valve) which is remotely controlled. In these systems, the controlling input is converted by a special controller into an electrical, hydraulic, or pneumatic signal, which is then transformed into the brake pressure. The electrohydraulic remote control braking systems have been most widely used. In the remote control brake systems, the cockpit and passenger cabin are not encumbered by plumbing lines, the brake

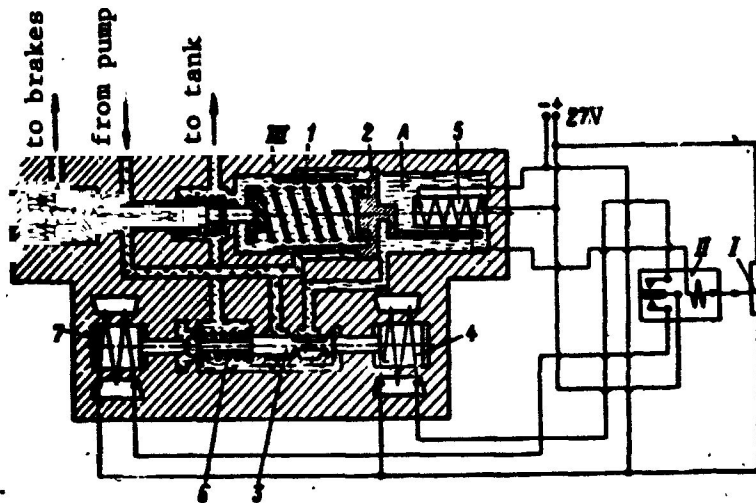


Figure 8.4. Remotely controlled electrohydraulic system.

I- control potentiometer; II- polarized relay; III- electrohydraulic reduction valve; 1- reduction spring; 2- differential cylinder piston; 3- slide valve; 4, 7- magnets; 5- feedback potentiometer; 6- centering spring.

system response speed is faster, the system configuration on the airplane is better, the system weight is reduced, and it becomes possible to automate the airplane braking process during landing to a considerable degree.

A schematic of a remote control electrohydraulic system is shown in Figure 8.4. The system consists of the control potentiometer I, polarized relay II, and electrohydraulic reduction valve III. The electrical bridge circuit of the system is shown in Figure 8.5. The bridge resistances are the control 1 and feedback 2 potentiometers. The polarized relay 3 winding is connected into the bridge diagonal. During braking, the pilot displaces the control potentiometer 1. Since the feedback potentiometer 2 in the reduction valve is stationary at the first instant, because of the control potentiometer displacement, an error voltage is created between points a and b. As soon as the error magnitude reaches a definite value, the polarized relay actuates and applies voltage to the reduction valve electromagnet 4. /117

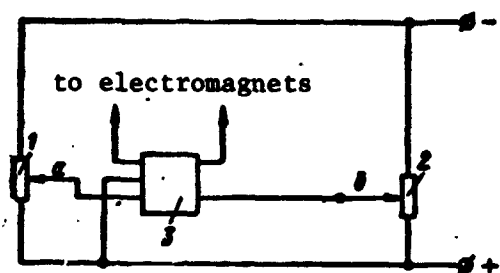


Figure 8.5. Electrical circuit of electrical remote control system.

1- control potentiometer; 2- feedback potentiometer; 3- polarized relay.

Reduction of the pressure is accomplished by compression of the reduction spring 1 (see Figure 8.4) by the differential cylinder piston 2. The piston 2 displaces the feedback potentiometer slider, thereby eliminating the error between points a and b. Control of the differential cylinder piston is accomplished by supplying pressure to chamber A from the slide valve 3. During brake applica-

tion, when because of the error the relay II activates the magnet 4, the latter displaces the slide valve 3 to the left. As soon as the feedback potentiometer 5 eliminates the error, the relay de-energizes the magnet 4 and the centering spring 6 establishes the slide valve 3 in the neutral position and cuts off pressure supply to chamber A. Chamber A is blocked, the piston 2 is stationary, and the reduced pressure is constant.

During brake release, the pilot displaces the control potentiometer in the reverse direction and creates an error of the opposite sign. In this case, the polarized relay energizes the magnet 7 which displaces the slide valve 3 to the right. The chamber A is open to the return line and the piston 2 moves to the right as a result of the pressure acting on the annular section of the piston 2. As the piston moves to the right, it reduces the compressive force of the spring 1 and thereby lowers the reduced pressure.

/118

The described system makes it possible to vary the reduced pressure as a function of control potentiometer displacement following a nearly linear law. In addition, the operation of this circuit is not disrupted with supply voltage oscillations over quite wide limits, since the electromagnets 4 and 7 are designed for the minimal voltage.

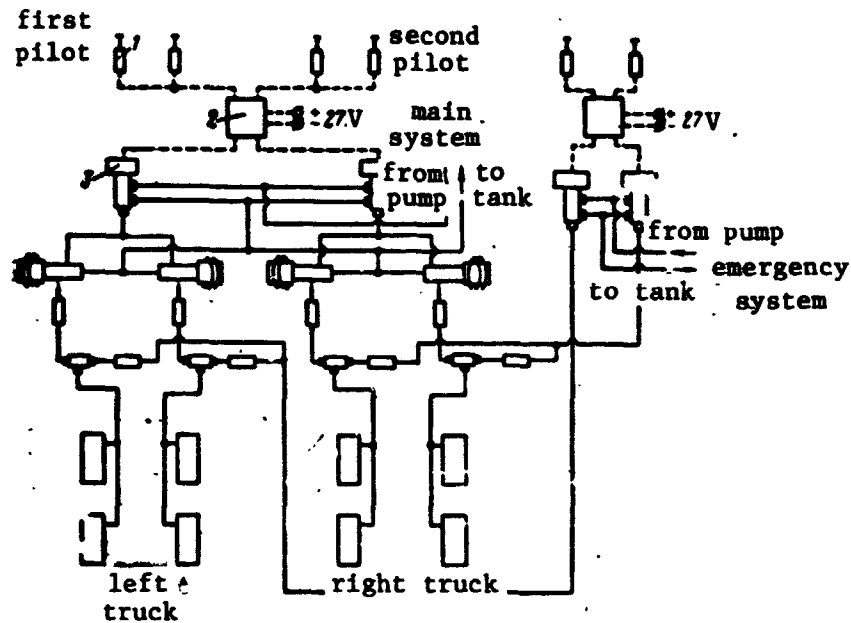


Figure 8.6. Brake system with electrohydraulic reduction valves. 1- potentiometer; 2- distribution box; 3- electrohydraulic valve.

A schematic of a brake system with electrohydraulic reduction valves is shown in Figure 8.6. In this system, each pilot controls, through his rudder pedals, the two potentiometers 1, the signals from which travel to the distribution box 2 and from there to the valves 3.

The left potentiometer (of the first and second pilots) controls the left reduction valve and, therefore, the brakes of the left bogie. The right potentiometer (of the first and second pilots) controls the right reduction valve and the brakes of the right bogie. If the left and right potentiometers are actuated at the same time, the signal goes simultaneously to both reduction valves. If the first and second pilots attempt to control the brakes simultaneously, the distribution box cuts off the signals from the potentiometers of the second pilot and makes it possible for the first pilot to control the braking.

/119

The emergency system is analogous to the main system and consists of the same units. The control potentiometers are located only in the first pilot's control circuit.

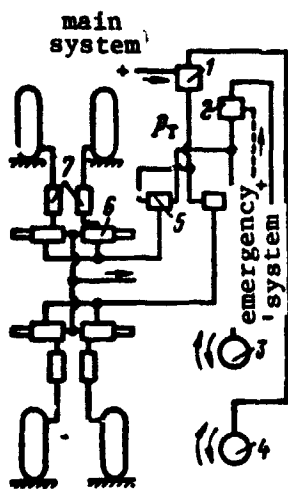


Figure 8.7. Remote electrically controlled hydraulic braking system of airplane with bicycle landing gear.

1, 2- reduction valves; 3, 4- emergency and main system controls; 5- shuttle valve; 6- electromagnetic valve; 7- hydraulic fuses.

shown in Figure 8.7. The pilot actuates, through the electrical main 4 or emergency 3 system controls, located right in the cockpit, with the aid of an electrical signal, the electrohydraulic reduction valves 1 and 2, located in the immediate vicinity of the airplane landing gear. Depending on the electrical signal, the reduction valve creates more or less braking pressure  $p_b$ . The fluid under pressure travels to the wheel brakes through the shuttle valve 5, electromagnetic valve 6, and hydraulic fuses 7.

The circuit of a pneumatic remote control brake system is shown in Figure 8.8. The controlling reduction valve 1 creates the controlling pressure  $p_y$ , which — after passing through the differential 2 — is transformed in the reducer 3 to the pressure  $p_b$  entering the wheel brakes. For emergency braking, the pilot activates the switch T and sends pressure directly to the brakes, blocking off the main system by the shuttle valves 4.

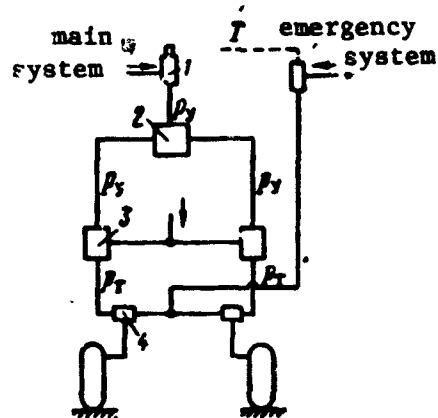


Figure 8.8. Remote control pneumatic braking system.

1- reduction valve; 2- differential; 3- remote pressure reducer; 4- shuttle valve.

The circuit of an electrically controlled remote hydraulic braking system of an airplane with bicycle landing gear is

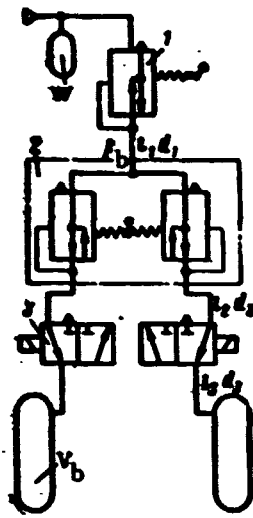


Figure 8.9. Pneumatic brake system.

1- reduction valve; 2- differential; 3- electromagnetic valve.

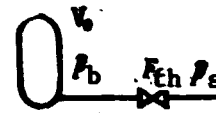


Figure 8.10. Simplified idealization of pneumatic brake system.

#### 4. Pneumatic Brake System Analysis

We shall examine a simplified method for calculating the brake application and brake release times of a pneumatic brake system, which is confirmed by the experimental data.

The pneumatic braking system schematic is shown in Figure 8.9, where  $W$  is the air accumulator volume;  $V_b$  is the wheel brake expander tube or brake cylinder volume;  $l$  is the plumbing line length;  $d$  is the line inside diameter;  $p_s$  is the system pressure;  $p_b$  is the brake pressure.

Assuming that the flow sections of the differential 2 and electromagnetic valve 3 are equal to the line section, the computational scheme of this system can be simplified (Figure 8.10).

In this system,  $V_0$  is the overall volume,  $V_b$  is the brake volume,  $V_l$  is the line volume;  $F_{th}$  is the flow section area of the reduction valve 1;

$$V_0 = V_b + V_l; V_l = \sum_{i=1}^n \frac{\pi d_i^2}{4} l_i.$$

*Brake application time.* Determination of the brake system application time reduces to determining the time for filling of the volume  $V_0$  to the pressure  $p_b$  through the throttle of constant section  $F_{th}$  with constant pressure  $p_s$  in the system.

We know from gasdynamics that filling of the volume may take place in the subcritical or supercritical regimes.

The critical regime under conditions of continuously varying pressure  $p_b$  is a transient regime. /121

The critical pressure ratio

$$\epsilon_{cr} = \frac{p_{cr}}{p_s} \quad (8.1)$$

for a polytropic process is defined by the formula

$$\epsilon_{cr} = \left( \frac{2}{n+1} \right)^{\frac{n}{n-1}}. \quad (8.2)$$

where  $n$  is the polytropic exponent.

Considering that there is no marked heat transfer at the throttle during filling of the brake system volume, we can take  $n = 1.4$ . In this case,  $\epsilon_{cr} = 0.528$ .

The filling regime will be characterized by the ratio

$$\epsilon = \frac{p_b}{p_s} \quad (8.3)$$

where  $\epsilon > \epsilon_{cr}$  for the subcritical regime and  $\epsilon < \epsilon_{cr}$  for the supercritical regime.

In the vast majority of brake systems, filling takes place in the supercritical regime.

The air flowrate in the throttle when filling in the supercritical regime will be constant and equal to:

$$G_{a \text{ cr}} = a F_{th} \frac{p_d}{RT} \sqrt{g n RT} \cdot \sqrt{\left(\frac{2}{n+1}\right)^{\frac{n+1}{n-1}}}, \quad (8.4)$$

where  $\sqrt{g n RT} = V$  is the speed of sound in air;

$$\sqrt{\left(\frac{2}{n+1}\right)^{\frac{n+1}{n-1}}} \approx 0.57 \text{ for } n = 1.4;$$

T is the temperature in K; R is the gas constant;  $p_s$  is the supply system pressure; a is the flow coefficient, equal to 0.4 — 0.6; and  $F_{th}$  is the throttle flow section area.

To determine the filling time for the volume  $V_0$ , we use the gas equation of state:

$$p V_0 = RT Q_a. \quad (8.5)$$

The system volume filling equation can be obtained by assuming that the specific heat of the gas varies little during the filling process and the process polytropic exponent can be assumed constant ( $n = \text{const}$ ). /122

We write the characteristic air flowrate equation in differential form:

$$V_0 dp = RT dQ_a, \quad (8.6)$$

where  $dp$  is the pressure increment in the system; and  $dQ_a$  is the incremental air weight in the system.

We divide the left and right sides of (8.6) by the infinitesimal time increment  $d\tau$

$$\frac{dp}{d\tau} = \frac{RT}{V_0} \cdot \frac{dQ_a}{d\tau}. \quad (8.7)$$

Considering that

$$\frac{dQ_a}{d\tau} = G_a, \quad (8.8)$$

we obtain

$$\frac{dp}{d\tau} = \frac{RT}{V_0} G_a \quad (8.9)$$

Since the filling process takes place in the supercritical regime, we obtain

$$\begin{aligned} G_a &= G_{a \text{ cr}}; \\ \frac{dp}{d\tau} &= \frac{RT}{V_0} G_{a \text{ cr}}. \end{aligned} \quad (8.10)$$

Solving (8.10) for  $d\tau$  and integrating it in the limits from  $p_1$  to  $p_{cr}$ , we obtain the filling time for the isothermal process

$$\tau_1 = \frac{V_0(p_{cr} - p_1)}{RTG_{a \text{ cr}}}. \quad (8.12)$$

As we noted above, in brake systems  $p_{b \text{ max}} < p_{cr}$ , then

$$\tau_a = \frac{V_0 p_b}{RTG_{cr}}, \quad (8.13)$$

where  $\tau_a$  is the time to fill the volume to the pressure  $p_b$  (brake application time).

*Brake release time.* In order to determine the brake system release time, we use the equations of gasdynamics. Since the air discharges into the atmosphere and  $\epsilon_{cr} = 0.528 - 0.607$ , we have

$$p_{cr} = \frac{p_1}{\epsilon_{cr}} = 1.65 - 1.9 \text{ kg/cm}^2. \quad (8.14)$$

Thus, release system pressure to  $p_{cr}$  takes place in the supercritical regime and further brake release takes place in the subcritical regime. In practice, in actual brake systems, the segment with subcritical discharge regime can be neglected.

Thus, by analogy with (8.10), we can write (taking the flow-rate to be negative)

$$\frac{dp}{d\tau} = -\frac{RT}{V_0} G_a, \quad (8.15)$$

and

$$G_a = G_{a\ cr} = aF_{th} p_c,$$

where

$$c = \frac{V_0 a RT}{RT} \cdot \sqrt{\left(\frac{2}{n+1}\right)^{\frac{n+1}{n-1}}}.$$

Then

$$\frac{dp}{p} = -\frac{RT}{V_0} aF_{th} c d\tau. \quad (8.16)$$

After integrating in the limits from  $p_{b\ max}$  to  $p_b$  ( $p_b$  will be not less than  $p_{cr}$ ), we have

$$\ln \frac{p_b}{p_{b\ max}} = -\frac{RTaF_{th} c \tau}{V_0}; \quad (8.17)$$

$$\tau = \ln \frac{p_{b\ max}}{p_b} \frac{V_0}{RTaF_{th} c} = B \ln \frac{p_{b\ max}}{p_b}, \quad (8.18)$$

where

$$B = \frac{V_0}{RTaF_{th} c} = \text{const.}$$

Since  $B$  depends only on the valve geometric parameters and the initial process conditions, (8.18) can be written in the form

$$\frac{\tau}{B} = \ln \frac{p_{b \max}}{p_b}. \quad (8.19)$$

The dependence of  $p_b/p_{b \max}$  on  $\tau/B$  can be represented in the form of curves (Figure 8.11) for the isothermal process  $n = 1$  and for the adiabatic process  $n = k = 1.4$ .

To find the pressure  $p_b$  corresponding to the given time  $\tau$ , we must calculate the constant  $B$  and find the ratio  $\tau/B$ , then we find, from the graph, the corresponding value of  $p_b/p_{b \max}$ .

Knowing the initial pressure in the brake chamber  $p_{b \max}$ , we /124  
obtain the corresponding pressure  $p_b$ . The problem of determining the time  $\tau$  from a given pressure  $p_b$  is solved similarly.

The graph shows that the difference in the pressures for the isothermal and adiabatic processes is small. This situation makes it possible to calculate the system brake release time on the basis of the isothermal process, obtaining in so doing results which are quite close to the actual values.

The considerable length of the brake system lines also aids in equalizing the temperatures during brake release and brings this process closer to the isothermal process.

This computation method does not consider the inertia of the moving masses of the pneumatic rubber expander tubes and the brake cylinder pistons, since experience shows that their influence can be neglected.

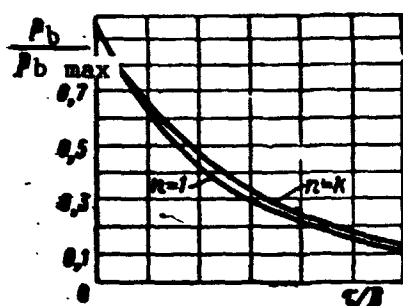


Figure 8.11. Dependence of  $p_b/p_b \max$  on  $\tau/B$  for pneumatic brake system.

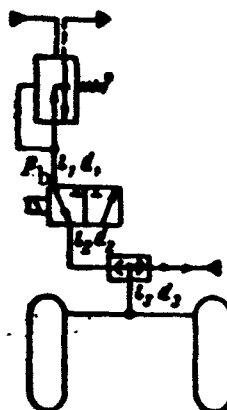


Figure 8.12. Idealization of hydraulic brake system.

## 5. Hydraulic Brake System Analysis

Analysis of hydraulic brake systems, just as that of pneumatic systems, reduces to determining the system response speed: its brake application and brake release times. For the calculation, we must know the following system parameters: brake system schematic, line lengths and diameters, volume of the system and brakes, working pressure in the system, and working pressure in the brakes.

Figure 8.12 shows a segment of the hydraulic brake system. We take the following notations for the calculation:  $p_s$  is the system pressure;  $p_b$  is the brake pressure;  $l_1$  is the line length;  $d_1$  is the line diameter;  $V_1$  is the initial geometric volume (prior to the instant of braking initiation);  $V_{inc}$  is the increase of the initial geometric volume (in the brake application process).

The initial volume  $V_1$  of the brake and system is the volume when all the moving brake elements are in the initial position and the excess pressure in the system is equal to zero. This volume is always filled with liquid. The increase of the initial geometric volume is equal to the volume of liquid entering the brake through the reduction valve and providing displacement of the brake moving parts prior to the instant the friction surfaces come into contact.

/125

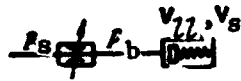


Figure 8.13. Simplified schematic of hydraulic brake system.

In the system analysis, we take the reduction valve flow section to be constant and equal to  $F_{th}$ . The flow sections of all the other units are assumed to be no smaller than the flow section of the line coming from the reducer.

The system analysis is made using the simplified schematic (Figure 8.13) and includes determining the time for filling the volume  $V_{inc}$  to the pressure  $p'_b$  necessary for displacement of the brake moving parts until full contact of the brake friction surfaces, and determination of the time for the pressure to increase from  $p'_b$  to  $p_{b \max}$ , when the friction surfaces are clamped together with the design force.

The increase of the geometric volume with pressure increase because of deformation of the brake elements (with increase of the pressure from  $p'_b$  to  $p_{b \max}$ ) is not considered.

Let us examine the first calculation stage — determining the time for filling of the volume  $V_{inc}$  to the pressure  $p'_b$ .

The liquid flowrate through the constant section throttle is found from the formula:

$$Q_L = A_{th} \cdot F_{th} \sqrt{\Delta p}, \quad (8.20)$$

where  $Q_L$  is the liquid flowrate;  $F_{th}$  is the throttle flow section area;  $\Delta p$  is the pressure differential;  $A_{th} = k_f \sqrt{\frac{2g}{\gamma}}$  is the reduced flowrate coefficient (here  $k_f = 0.6$  is the flowrate coefficient,  $g = 9.81 \text{ cm/sec}^2$ ).

In the brake system, the reduction valve is the throttle. Let us examine the brake application process with fully open reduction valve. In this case, the average pressure differential across the throttle

$$\Delta p = p_s - (p_{ll} + \frac{p'_b}{2}), \quad (8.21)$$

where  $p_{ll}$  are the pressure losses in the equivalent line from the valve to the brake. /126

The pressure variation as the moving elements displace follows a linear law.

For the laminar fluid flow case, the magnitude of the pressure losses in the line is found from the formula:

$$p_{ll} = \lambda \frac{8\gamma}{g} \cdot \frac{1}{\pi^2} \frac{l}{d^5} Q_L^2, \quad (8.22)$$

where  $l$  is the line length; and  $d$  is the line diameter;

$$\lambda \approx \frac{75}{Re}. \quad (8.23)$$

Here  $Re = vd/\nu = 4Q_L/\nu\pi d$  is the Reynolds number (8.24)

where  $v$  is the fluid flow velocity in the line; and  $\nu$  is the kinematic viscosity.

After making the corresponding transformations, we obtain:

$$p_{ll} = 48 \frac{\gamma}{g} \frac{l}{d^5} Q_L^2. \quad (8.25)$$

If the system consists of several lines with different lengths and diameters, the pressure losses can be found from the equation:

$$p_{ll} = 48 \frac{\gamma}{g} \left( \frac{l_1}{d_1^5} + \frac{l_2}{d_2^5} + \dots + \frac{l_n}{d_n^5} \right) Q_L^2. \quad (8.26)$$

Thus, (8.20), with account for the losses in the system lines and the average backpressure in the cylinders, will have the form:

$$Q_{L1} = A_{th} F_{th} \sqrt{p_s - p_{L1} - \frac{p'_b}{2}} \quad (8.27)$$

or

$$Q_{L1} = A_{th} F_{th} \sqrt{p_s - D Q_{L1} - \frac{p'_b}{2}}, \quad (8.28)$$

where

$$D = 48 \frac{\nu \gamma}{g} \sum_{i=1}^n \frac{L_i}{d_i^5}$$

Solving (8.28), we obtain

$$\begin{aligned} Q_{L1}^2 &= (A_{th} F_{th})^2 p_s - (A_{th} F_{th})^2 D Q_{L1} - (A_{th} F_{th})^2 \frac{p'_b}{2}; \\ Q_{L1}^2 + (A_{th} F_{th})^2 D Q_{L1} - (A_{th} F_{th})^2 (p_s - \frac{p'_b}{2}) &= 0, \end{aligned} \quad /127$$

hence,

$$\begin{aligned} Q_{L1} &= -\frac{A_{th}^2 F_{th}^2 D}{2} \pm \\ &\pm \sqrt{\left(\frac{A_{th}^2 F_{th}^2 D}{2}\right)^2 + A_{th}^2 F_{th}^2 (p_s - \frac{p'_b}{2})}. \end{aligned}$$

The real solution will be

$$Q_{L1} = \sqrt{\left(\frac{A_{th}^2 F_{th}^2 D}{2}\right)^2 + A_{th}^2 F_{th}^2 (p_s - \frac{p'_b}{2})} - \frac{A_{th}^2 F_{th}^2 D}{2}. \quad (8.29)$$

Knowing the initial volume increase  $V_{inc}$  and the average flow-rate in this segment, we obtain the volume filling time

$$\tau_1 = \frac{V_{inc}}{Q_{L1}}. \quad (8.30)$$

After filling of the volume  $V_{inc}$ , the variation of the pressure  $p_b$  with time is defined by the relation:

$$K_0 \frac{dp_b}{d\tau} = Q_{L \text{ av}}, \quad (8.31)$$

where  $Q_{L \text{ av}}$  is the average flowrate during the entire process;  
 $K_0$  is the system elasticity,

$$K_0 = F_l l \left( \frac{d}{\delta_l E} + \frac{1}{E_1} \right) + \frac{V_s}{E_1}, \quad (8.32)$$

where  $F_l$  is the line flow section area;  $l$  is the line length;  
 $d$  is the line diameter;  $\delta_l$  is the line wall thickness;  $E$  is the line material elastic modulus;  $E_1$  is the working fluid elastic modulus; and  $V_s$  is the overall system volume  $V_s = V_1 + V_{inc}$ .

If the system consists of lines of different lengths and diameters, then  $l$  and  $d$  are taken to be the equivalent values, i.e., such that for the flowrate  $Q_L$ , they create the same resistance as

$$\sum_{i=1}^n \frac{l_i}{d_i^5}$$

For linear variation of the pressure from  $p_b'$  to  $p_b''$ ,

$$Q_{L2} = \left( \frac{A_{th}^2 F_{th}^2 D}{2} \right)^2 + A_{th}^2 F_{th}^2 \left[ p_s - \left( \frac{p_b' + p_b''}{2} \right) \right] - \quad (8.33) \quad \underline{/128}$$

$$\frac{A_{th}^2 F_{th}^2 D}{2} = K_0 \frac{dp_b}{d\tau},$$

hence

$$\frac{dp_b}{d\tau} = \frac{Q_{L2}}{K_0}, \quad (8.34)$$

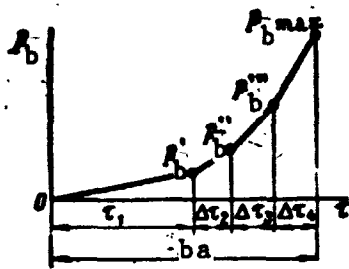


Figure 8.14. Brake pressure variation during brake application.

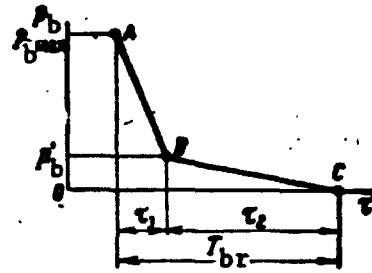


Figure 8.15. Brake pressure variation during brake release.

where  $dp_b/d\tau$  is the rate of pressure change in the system.

The time for pressure rise from  $p_b'$  to  $p_b''$  is

$$\Delta\tau_2 = \frac{p_b'' - p_b'}{\frac{dp}{d\tau}} \quad (8.35)$$

The times  $\Delta\tau_3$  and  $\Delta\tau_4$  for the remaining system segments are determined similarly.

The brake pressure variation with time during brake application is shown in Figure 8.14.

Obviously, the total brake application time is found as:

$$T_{ba} = \tau_1 + \Delta\tau_2 + \dots + \Delta\tau_n. \quad (8.36)$$

The values of  $p_b''$  and  $p_b'''$  are, by convention, taken equal to  $1/3$  and  $2/3$  of  $p_{b \max}$ , respectively, where  $p_{b \max}$  is the maximal regulated pressure in the brake system.

In order to determine the brake system release time, we find the amount of fluid entering the system with increase of the pressure from  $p_b'$  to  $p_{b \max}$ . This amount is found as the sum of the volumes calculated for each segment separately. Then

$$\Delta V = \Delta V_1 + \Delta V_2 + \Delta V_3 + \dots + \Delta V_i, \quad (8.37)$$

where

$$\Delta V_i = Q_{L1} \Delta \tau_i. \quad (8.38)$$

After determining  $\Delta V$  and knowing the system elasticity, we find /129 the fluid flowrate through the valve 1 (see Figure 8.12), whose flow section area for return flow is  $F'_{th}$ . Consequently,

$$Q_L = A_{th} F'_{th} \sqrt{\Delta p_{av}}, \quad (8.39)$$

where

$$\Delta p_{av} = \frac{p_{b \max} - p'_b}{2}.$$

During brake release, the pressure drop curve has the form shown in Figure 8.15. In segment AB, the volume  $\Delta V$  is displaced from the system and in segment BC, the volume  $V_{inc}$  is discharged. In segment AB, the system elasticity  $K_0 = \text{const.}$  We can consider that the discharge process that takes place at a constant pressure differential equal to the average differential  $\Delta p_{av}$  (we neglect the return line resistance). Then

$$Q_L = A_{th} F'_{th} \sqrt{\frac{p_{b \max} - p'_b}{2}}. \quad (8.40)$$

The time for emptying the volume  $\Delta V$

$$A_{th} F'_{th} \sqrt{\frac{p_{b \max} - p'_b}{2}}. \quad (8.41)$$

For the segment BC we obtain

$$A_{L2} = F_{th} F'_{th} \sqrt{\frac{p'_b}{2}}, \quad (8.42)$$

hence

$$v = \frac{V_{inc}}{A_{th} F_{th} \sqrt{p_u/2}} . \quad (8.43)$$

The total brake release time

$$T_{br} = v + a$$

## CHAPTER 9

### AUTOMATION OF THE BRAKING PROCESS

/130

#### 1. Wheel Skid Onset Conditions

##### Automatic Antiskid Control System

We noted previously that braking effectiveness is determined by the magnitude of the traction coefficient realized. Braking is most effective when the limiting coefficient of tire traction with the runway ( $\mu_{lim}$ ) is realized. In this case, the wheel rolls with relative sliding equal to  $\delta_{lim}$ . Increase of the braking moment (for any reason) leads to increase of the relative sliding above  $\delta_{lim}$  and marked reduction of the traction coefficient. The larger, in absolute magnitude difference, of the moments  $\Delta M = M_{tr} - M_b$  which arises as a result of this leads to complete wheel lockup. A similar phenomenon also takes place in the case of marked reduction of the traction moment because of reduction of either the traction coefficient or the radial load on the wheel with constant braking moment. This situation is possible, for example, when the wheel encounters a wet or icy spot on the runway. In either case, complete wheel lockup causes either local elliptical-shaped abrading of the tire tread or complete tire failure.

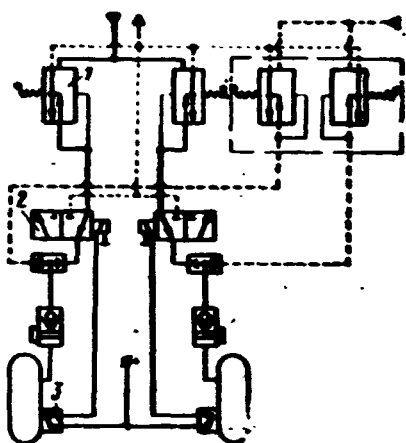


Figure 9.1. Airplane braking system with electroinertial sensors.

1- reduction valve; 2- electromagnetic valve; 3- electroinertial controller.

For the most effective nonskid braking, it is necessary to regulate the braking moment so that rolling of the braked wheel takes place with relative sliding corresponding to the limiting coefficient of tire traction with the runway at the given instant. The pilot cannot accomplish such braking because of the large number of factors determining these conditions. Therefore, most modern airplanes have special automatic antiskid systems to ensure nonskid braking and obtain acceptable braking effectiveness.

At the present time, two automatic antiskid systems have found wide application: remote acting systems with electroinertial or electrical controllers and systems with direct acting automatic controllers.

/131

In the remote acting systems, the electroinertial or electrical controller is mounted rigidly on the brake and its sensitive element (flyweight in the electroinertial sensor or generator armature in the electrical sensor) is coupled with the wheel through gearing. The system shown in Figure 9.1 is an example of a very simple system with electroinertial controller. In this system, during braking, the pressure from the reduction valve 1 enters the brake through the electromagnetic valve 2. If the wheel starts skidding during the braking process, there is marked change of the wheel rpm and the relative sliding. The sensitive element of the controller 3 reacts to the resulting rpm change and sends a signal in the form of an electrical pulse to the valve 2, which releases the wheel brake. The system with direct acting automatic control does not have a separate valve 2, since the automatic control itself is mounted on the brake and includes both a sensitive element and valve unit.

Systems which automatically ensure the most effective nonskid braking have been developed and put into use only very recently.

## 2. Construction and Operating Principle of the Electroinertial Controller and the Direct Acting Automatic Controller

One of the widely used electroinertial controller designs is shown in Figure 9.2 and operates as follows. During airplane landing rollout, wheel rotation is transmitted through gearing to the spider 3 and then to the shaft 4. The shaft 4 transmits the rotation through the plunger 8 to the sleeve 5, which is coupled through the spring loaded clutch 7 with the

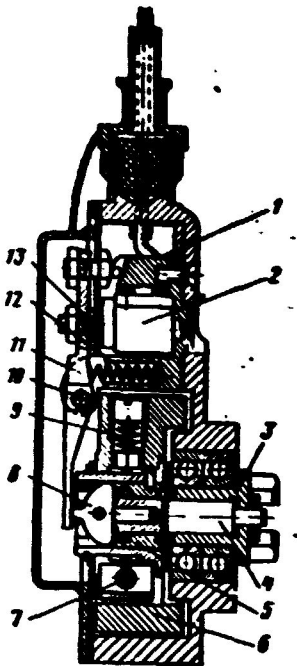


Figure 9.2. Construction of electroinertial controller.

1- stop; 2- limit switch; 3- spider; 4- shaft; 5- sleeve; 6- flywheel; 7- spring loaded clutch; 8- plunger; 9- spring; 10- shaft; 11- lever; 12- spring; 13- bolt.

flywheel 6. The spring loaded clutch 7 couples the flywheel 6 with the sleeve 5 and acts as a ratchet. In the absence of skidding, the flywheel 6 rotates synchronously with the wheel with rpm equal to

$$n_{f1} = i n_w,$$

where  $i$  is the gear ratio from the wheel to the controller.

The flywheel kinetic energy

$$K_w = \frac{J_{f1} \omega_{f1}^2}{2}, \quad (9.14)$$

where  $J_{f1}$  is the flywheel moment of inertia and  $\omega_{f1} = (\pi n_w / 30) i$  is the flywheel angular velocity.

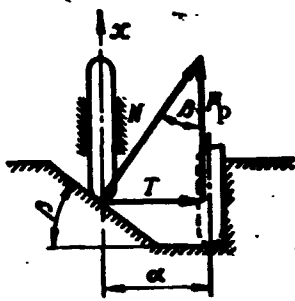


Figure 9.3. Activation mechanism force diagram.

As the wheel begins skidding, the rpm of the shaft 4, rigidly coupled with the wheel, decreases sharply. As a result of inertia, the flywheel and attached sleeve 5 lead the shaft and create an angular error of magnitude  $\alpha$  (Figure 9.3). The sleeve 5, having a threaded surface at the point of contact with the plunger 8, causes axial plunger

displacement whose magnitude is proportional to the helix rise angle  $\beta$  and the angle  $\alpha$ . The plunger 8 displaces the lever 11 which, as it rotates on the shaft 10, actuates the limit switch 2 by the head of the bolt 13 and applies an electrical pulse to the electromagnetic brake release valve.

After actuation, the lever reaches the stop 1 and holds the limit switch closed until either the skid terminates and the angular error disappears, or the flywheel loses all its kinetic energy because of friction as it rotates on the sleeve 5. After this, the spring 12 returns the lever 11 and plunger 8 to the original position and electrical signal transmission terminates. /133

Analysis of the electroinertial controller reduces to determining its basic design parameters — flywheel moment of inertia and friction clutch torque — from the initial data: the theoretical deceleration at which limit switch actuation should occur and the force necessary for switch actuation.

The plunger force required for switch actuation is

$$P_p = i_l P_1,$$

where  $P_1$  is the force required to activate the switch and compress the return spring;  $i_l$  is the lever gear ratio.

From examination of the force diagram (see Figure 9.3) without account for friction

$$P_p = T \operatorname{tg}(90^\circ - \beta),$$

where  $T$  is the component of the normal pressure  $N$  of the plunger 8 on the helical surface of the sleeve 5.

With account for friction, the plunger force will be:

$$P_p = T \operatorname{tg}(90^\circ - \beta - \rho). \quad (9.15)$$

where  $\rho$  is the friction angle with the sleeve sliding relative to the plunger.

The force component

$$T_{\max} = \frac{M_\phi}{r},$$

where  $M_\phi$  is the friction moment on the sleeve as the flywheel slides over it (friction clutch moment);  $r$  is the force radius of action.

For a given design deceleration

$$T = \frac{J_{f1}}{r} \epsilon_{dd} \quad (9.16)$$

where  $\epsilon_{dd}$  is the design angular deceleration at actuation.

Substituting the force component (9.16) into (9.15), we obtain

$$P_p = \frac{J_{f1}}{r} \operatorname{tg}(90^\circ - \beta - \rho) \epsilon_{dd}$$

or

$$i_\omega \cdot P_1 = \frac{J_{f1}}{r} \operatorname{tg}(90^\circ - \beta - \rho) \epsilon_{dd}, \quad (9.17)$$

hence

/134

$$J_{fl} = \frac{i_l P_l r}{\operatorname{tg}(90^\circ - \beta - \rho) \epsilon_{dd}} \quad (9.18)$$

The angle  $\beta$  is selected from constructional considerations (usually  $\beta = 25^\circ$ ) and the angle  $\rho$  is determined by the plunger and sleeve material. The friction clutch moment  $M_\phi$  must ensure positive limit switch actuation. We take

$$M_\phi = k J_{fl} \epsilon_{dd}$$

where  $k = 1.5 - 2.5$  is the safety factor. The pulse duration:

$$\tau = \frac{J_{fl}(\omega_0 - \omega)}{M_\phi}.$$

where  $\omega_0$  is the flywheel angular velocity at the instant the wheel starts skidding; and  $\omega$  is the flywheel angular velocity at the instant the wheel stops skidding.

In this case, the maximal pulse duration will be, when  $\omega_0 = \omega_{\max}$ , and  $\omega = 0$ , then

$$\tau_{\max} = \frac{J_{fl} \omega_{\max}}{k J_{fl} \epsilon_{dd}} = \frac{\pi n_{\max}}{30 k \epsilon_{dd}} \quad (9.19)$$

The electroinertial controller response speed is characterized by the time for the flywheel to rotate relative to the sleeve through the angle necessary for switch actuation. The controller response speed increases with reduction of the flywheel rotation angle.

An example of a direct acting controller is the Maxaret unit made by Dunlop, which is widely used on certain passenger airplanes in Western Europe.

A schematic of the controller is shown in Figure 9.4. As the airplane travels over the runway, the roller 1 with rubber rim rotates in the ball bearings 4 because of direct contact with the wheel rim 9. The flywheel 2 linked with the roller 1 by three-coil cylindrical spring 3 rotates together with the roller. In the

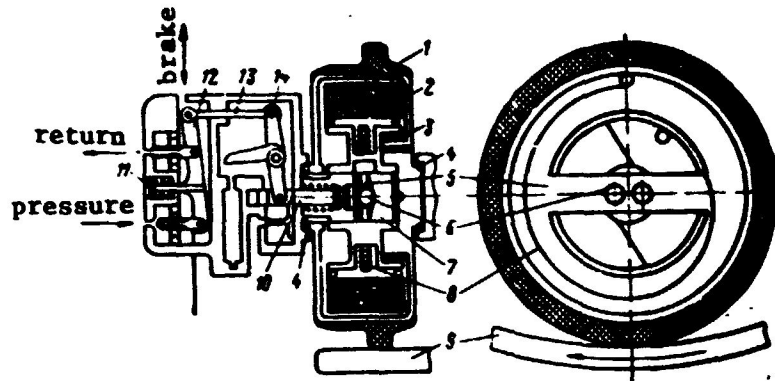


Figure 9.4. Maxaret direct acting antiskid controller.

1- roller; 2- flywheel; 3- spring loaded clutch; 4- ball bearing; 5- plate; 6- balls; 7- sleeve; 8- spiral spring; 9- wheel rim; 10- plunger; 11- spring; 12- arm; 13- link; 14- lever.

absence of skidding, the controller roller and flywheel rotate synchronously with the wheel. When a skid develops, the flywheel begins to lead the roller, rotating through a definite angle and thereby winding up the spiral spring 8. The spiral spring rotation angle and torsional force are proportional to the roller deceleration. As the flywheel rotates, the balls 6, retained in the plate 5, begin to displace among the sloping surfaces of the sleeve 7, coupled with the roller. As the balls displace along the sleeve ramps, they also displace axially, which shifts the plunger 10 to the left. As the plunger displaces, it rotates the lever 14 which is connected by the link 13 with the valve mechanism arm 12. In the absence of skidding, the outlet valve, connected with the return line, is closed, while the inlet valve is open and pressure from the brake reduction valve passes freely into the brake. If the wheel skids, the inlet valve closes and the outlet valve opens, connecting the brake system with the return line. The flow sections of the inlet and outlet valves are made small in order to avoid abrupt pressure change in the brake.

/135

The construction of the lever mechanism is such that the outlet valve opening depends on the wheel angular deceleration. If there is a large deceleration, the outlet valve has a large displacement, which is accomplished by additional displacement of the spring loaded support 11. When skidding stops, the flywheel is returned



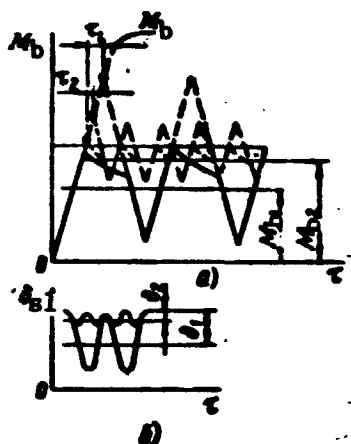


Figure 9.6. Variation of braking moment  $M_b$  (a) and relative slip  $\delta_{sl}$  (b) during operation of systems with different response speed.

and increase of the deceleration  $\epsilon_s$ . The angular velocity  $\omega_w$  decreases sharply. At point 2, the braking moment begins to decrease and, therefore, the difference moment  $-\Delta M$  decreases in absolute magnitude, altering the nature of the wheel angular velocity decrease (segment 2 — 3). As soon as the traction moment becomes larger than the braking moment (to the right of point 3), the wheel begins to speed up under the action of the moment difference  $+\Delta M$ . Electrical pulse output stops as soon as

the angular error in the controller sensing mechanism disappears (point 4). However, because of the system lag, the braking moment continues to decrease for some time  $\tau_2$  and then again increases to the original value. This figure reflects the pattern of the processes taking place in the case of a single system actuation. If the skidding regime continues for a long time, the system will operate continuously during the braking process, repeating the cycle described above with a frequency on the order of 5 — 10 Hz. The response speed of the entire system determines, to a considerable degree, the braking effectiveness. Figure 9.6 shows the braking moment variation for operation of systems with different response speed:  $\tau_1$  is the time lag of the first system;  $\tau_2$  is the time lag of the second system;  $\delta_{sl}$  is the relative sliding. /137

The time lag  $\tau_2$  is shorter than  $\tau_1$ . We see from comparison of the curves that reduction of the system lag leads to increase of the triggering frequency and reduction of the  $M_b$  oscillation amplitude, which increases the average braking moment  $M_b$  and reduces the relative sliding  $\delta_{sl}$ .

The overall time lag  $\tau$  is made up of the controller time lag  $\tau_1$ , actuator time lag  $\tau_2$ , and time lag  $\tau_3$  of the system itself, i.e.,

$$\tau = \tau_1 + \tau_2 + \tau_3$$

These time lags for existing systems are approximately  $\tau_1 \approx 0.01 - 0.02$  sec,  $\tau_2 \approx 0.02 - 0.04$  sec, and  $\tau_3 \approx 0.02 - 0.04$  sec.

Accordingly, the overall time lag is in the range  $\tau = 0.05 - 0.10$  sec. With this value of  $\tau$ , the braking moment oscillation amplitude can amount to 20 — 40%.

A no less important factor influencing braking effectiveness is controller sensitivity, by which we mean the magnitude of the deceleration  $\epsilon_s$  necessary for controller triggering and transmission of the brake release pulse to the actuating mechanism. The influence of controller sensitivity on the oscillation amplitude is seen in Figure 9.5. When the controller transmits a brake release pulse with the regulation  $\epsilon_s$  (point 1), the pulse transmission lag is  $\tau_3$ , while for the regulation  $\epsilon'_s$ , the lag is  $\tau_4$  (point 5). Here we have  $\epsilon_s < \epsilon'_s$  and  $\tau_3 < \tau_4$ .

While the lag  $\tau_3$  (together with the lag  $\tau_1$ ) determines  $\Delta M_1$ , the lag  $\tau_4$  (also together with  $\tau_1$ ) determines  $\Delta M_1'$ , and  $\Delta M_1 < \Delta M_1'$ .

The quantity  $\epsilon_s$  is found from the formula

$$\epsilon_s = i k \epsilon_w,$$

where  $i$  is the gear ratio from the wheel to the controller shaft;  $k$  is the safety factor; and  $\epsilon_w$  is the wheel deceleration which occurs when braking without skidding with maximal possible braking moment.

Operating experience shows that controller sensitivity with  $k < 1.5$  may lead to reduction of braking effectiveness because of false triggerings, while the sensitivity with  $k > 3$  increases tire wear without significant braking effectiveness improvement. The /138  
characteristic  $M_b = f(\tau)$  — the dependence of  $M_b$  on brake application and release time — is very important for system operating effectiveness. If, after brake release valve actuation,  $M_b$  decreases more slowly than  $M_{tr}$ , the wheel brake may not be fully released when the pickup pulse terminates. In this case,  $M_b$  increases to the original value and the wheel will be completely locked up. In designing automatic braking systems, we must try to ensure that the maximal brake release pulse hold time is 1.5 — 2 times longer than the time for  $M_b$  to decrease from its maximal value to zero. However, excessive steepness of the  $M_b = f(\tau)$  curve reduces the braking diagram fullness.

The sensitivity or the minimal angular deceleration ( $\epsilon_{s \min}$ ) at which the controller should not actuate is determined by the maximal linear airplane deceleration, which occurs with realization of the limiting traction coefficient.

From the specified airplane linear deceleration, we can find the controller shaft deceleration using the formula

$$\epsilon_{s \min} = ik \frac{a_{s \max}}{r_d},$$

where  $r_d$  is the dynamic wheel rolling radius.

Since

$$a_{s \max} = g\mu_{sl},$$

we obtain

$$\epsilon_{s \min} = ik \frac{1}{r_d} g\mu_{sl}.$$

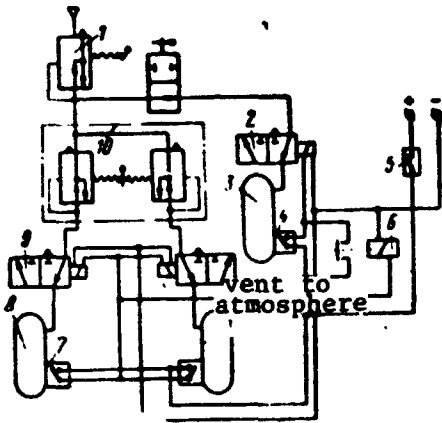


Figure 9.7. Single signal system with electroinertial controller.

1- reduction valve; 2, 9- electromagnetic valves; 3- nose wheel; 4, 7- electroinertial controllers; 5- manual switch; 6- relay coil; 8- main wheel; 10- differential.

### 3. Brake Systems and Antiskid Systems

Antiskid systems may be either single signal or two-signal. Most airplanes use single signal systems, in which an electroinertial controller reacts only to wheel angular deceleration. Two-signal systems, in which the controller reacts not only to wheel angular deceleration (first signal) but also to the angular velocity (second signal) have recently been introduced on some airplanes.

The electromagnetic valve receives the second brake release

signal when the electrical pulse from the first signal terminates. Use of the two-signal system improves braking safety, particularly at the first instant after touchdown, when the airplane wheels do not have adequate traction with the runway.

Figure 9.7 shows a single signal system with electroinertial controller for a light airplane with pneumatic tricycle gear braking system. Compressed air enters the brake line from the pressure bottle through the reduction valve 1, then passes through the electromagnetic valve 2 to the nose wheel brake 3 and through the differential 10 and valves 9 to the main wheel brakes 8. The electrical power for the automatic antiskid system is turned on and off by the manual switch 5. The wheel braking force is regulated by varying the brake pressure by displacing the rod of the valve 1. Braking of the right or left wheel, required for airplane control on the ground when taxiing with turns, or to prevent turns when taxiing in a straight line, is accomplished by the differential 10, whose lever is linked with the rudder pedals. Each wheel is equipped with an electroinertial controller 7 to prevent skidding. If one main wheel

/139

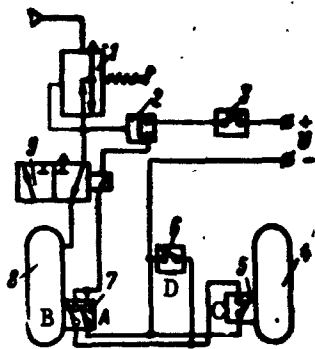


Figure 9.8. Two-signal antiskid system.

1- valves; 2, 3- switches; 4- unbraked wheel; 5- centrifugal controller; 6- switch; 7- controller; 8- main wheel; 9- valve.

starts skidding, the controller 7 of this wheel sends an electrical pulse to both main wheel 8 brake release valves 9 and to the winding of relay 6. Actuation of relay 6 sends an electrical pulse to the nose wheel valve 2. Thus, the brakes of all three wheels are released simultaneously. If the nose wheel 3 starts to skid, its controller 4 sends a signal only to the nose wheel valve 2. This wheel brake release sequence ensures the required airplane stability during landing rollout.

Figure 9.8 shows the two-signal antiskid system of an airplane with bicycle landing gear. The main wheel 8 is braked, the front wheel 4 is not braked. Compressed air flows from the bottle through the valve 1 into the main wheel brake line. On the main wheel 8 there is mounted the controller 7, having the contacts A of the single signal electroinertial controller which reacts to wheel deceleration and the contacts B of the centrifugal controller which actuates at a given wheel angular velocity. The contacts C of the centrifugal controller 5 mounted on the unbraked wheel 4 close and open at a set front wheel angular velocity. The electrical circuit: (+), switches 3 and 2, valve 9, contacts A, and (-) is the channel for transmission of the first signal of the single signal system and the circuit: (+), switches 3 and 2, valve 9, contacts B, C, D, and (-) is the channel for transmission of the second signal. In flight, when the front gear shock strut is not compressed, the contacts D of switch 6 are closed, and when the airplane is on the ground and the shock strut is compressed, these contacts are open. /140

The system operates as follows. Initially, the manual switch 3 is closed, contacts B are closed, and contacts A, C, and D are open. The electromagnetic valve 9 is de-energized and the pressure from the reduction valve 1 can enter the brakes freely. When the nose gear shock strut extends, the contacts D close and the second signal circuit is ready for operation. Prior to landing, pressure is created in the system by displacing the rod of the reduction valve 1. Then the pneumatic switch 2 closes the second signal circuit: (+), contacts B and D, (-) through the electromagnet winding of valve 9, as a result of which the pressure does not enter the brakes. After touchdown, as soon as the main wheel spins up to the set angular velocity, contacts B open, valve 9 opens, and air under pressure enters the brakes. After nose wheel spinup, contacts C close and contacts D open after nose wheel shock strut compression. If the wheel 8 starts to skid, the sensor reacting to deceleration (contacts A) triggers first and the system operates as a conventional one-signal system. If the airplane balloons or the wheel 8 enters a protracted skid, after 1.5 to 2 seconds, the first signal pulse from the controller 7 terminates, contacts A open, and the wheel begins to slow down, but does not come to a complete stop, since as soon as the wheel slows down to a set rpm, contacts B close and the wheel 8 will be unbraked by the second-signal channel. The system operates as a two-signal system to a speed of 50 — 70 km/hr. At speeds below 50 km/hr, contacts C of controller 5 open, contacts B of controller 7 close without energizing the valve 9, and the system operates as a single signal system.

Considering that the aerodynamic characteristics of some airplanes are such that the load on the wheels increases gradually during the landing rollout, programmed increase of the braking pressure as a function of airplane speed becomes necessary. This is achieved by using special electrical remote control systems, one of which is shown in Figure 9.9. This system with programmed step by step remote regulation of the pressure in the brakes was developed for an airplane having bicycle gear and braked front wheels.

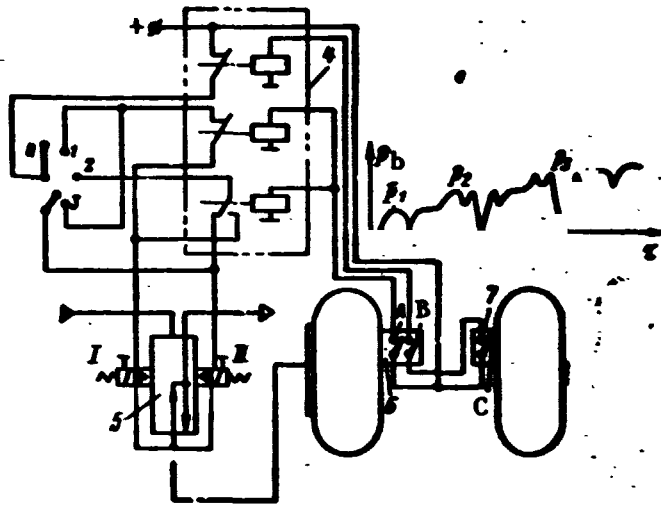


Figure 9.9. Brake system with programmed multistep brake pressure regulation.

1, 2, 3- switch positions; 4- relay; 5- electrohydraulic reducer; 6, 7- controllers.

The system operates as follows. As the airplane speed decreases during braking, the pilot places the manual switch in turn in the positions 1, 2, and 3. With the aid of relay 4, the electromagnetic reducer creates brake pressure:  $p_1$  — magnetic I is energized,  $p_2$  — magnet II is energized, and then  $p_3$  — both magnets are energized. When the switch is placed in the zero position, there is no brake pressure, since, in this case, both magnets are de-energized. Multistage pressure activation makes it possible to obtain, in each stage, a braking moment which is part of the maximal value. Since it is not possible in practice to maintain the skid-free braking relation  $M_b < M_{tr}$  throughout the landing roll when using multistep regulation, the antiskid system first-signal controller 6 will trigger (contacts A close) from time to time. In this case, relay 4 de-energizes either magnet I or magnet II and the pressure decreases from  $p_3$  to  $p_2$ , or from  $p_2$  to  $p_1$ , i.e., to the preceding value. However, if the skid continues with this brake pressure reduction, the second-signal controller 6 triggers and contacts B close, de-energizing both magnets, and the brake pressure drops to zero.

/142

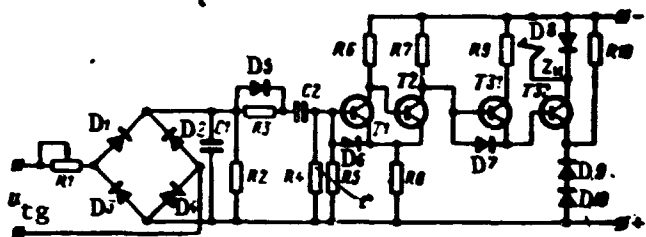


Figure 9.10. Electronic antiskid controller.

Figure 9.10 shows a single-signal electronic antiskid controller using semiconductor elements. The controller consists of identical amplifier transformer channels, the number of which corresponds to the number of tachogenerators installed on the braked wheels. The controller consists of an input circuit and a power amplifier. The input circuit has a bridge rectifier system (diodes  $D_1$  —  $D_4$ ), a capacitor  $C_1$  which smooths the rectified voltage pulsation, a differentiation loop ( $C_2R_2R_3$  —  $D_5D_6R_{in}$ ), and a variable resistor  $R_1$  for sensitivity regulation. The three-stage power amplifier is a noncontact semiconductor relay ( $T_1$ ,  $T_2$ ) which controls the output stage ( $T_{31}$ ,  $T_{32}$ ), whose load is the electromagnetic brake release valve winding. All four amplifier transistors operate in the switching mode. The resistor  $R_{10}$  and diodes  $D_7$ ,  $D_9$ , and  $D_{10}$  are used to block the composite power triode ( $T_{31}$ ,  $T_{32}$ ). Controller regulation stability with temperature variation is achieved by using deep feedback in the semiconductor relays and temperature-dependent biasing.

In the case of skid-free braking, the transistor  $T_1$  is saturated, while the transistor  $T_2$  and the composite output triode ( $T_{31}$ ,  $T_{32}$ ) are in the cutoff state; therefore, the electromagnetic valve winding is de-energized (in view of its smallness, the reverse collector current of transistor  $T_{32}$  is neglected) and pressure is supplied to the brake.

When a skid develops, the wheel angular velocity and the tachogenerator voltage decrease. This causes discharge of the capacitor  $C_2$ , whose discharge current creates on the semiconductor relay input resistance a voltage proportional to wheel angular deceleration

$$U_{in} = I_d R_{in}, \quad I_d R_{in} = -C_2 \frac{dU_{C2}}{d\tau};$$

$$\frac{dU_{C2}}{d\tau} = k_1 \frac{d\omega_w}{d\tau} = k_1 \epsilon_w;$$

$$U_{in} = -k_2 \epsilon_w,$$

where  $U_{in}$  is the relay input voltage;  $I_d$  is the discharge current of capacitor  $C_2$ ;  $R_{in}$  is the semiconductor relay input resistance;  $U_{C2}$  is the voltage on the plates of capacitor  $C_2$ ;  $\omega_w$  is the wheel angular velocity;  $\epsilon_w$  is the wheel angular deceleration; and  $k_1$  and  $k_2$  are proportionality coefficients.

The relay input voltage causes avalanche-like reversal (release) of the semiconductor relay circuit: the transistor T2 transitions to the cutoff regime and the transistor T1 and the composite output triode (T31, T32) transition to the saturation regime. As a result, current appears in the electromagnetic valve winding and the brake is released. If the wheel speed increases, the tachgenerator voltage increases, discharge of capacitor  $C_2$  terminates, reversal of the relay amplifier takes place, and air under pressure is supplied to the brake. However, if after brake release, the wheel continues to lose rpm, the electromagnetic valve will remain energized for some time, until the negative potential created on the base of transistor T1 by the discharge current of the capacitor  $C_2$  decreases to a value at which noncontact relay "triggering" and output triode transition to the cutoff regime takes place, which leads to wheel braking. This time is determined by the time constant of the capacitor  $C_2$  discharge circuit and by the initial voltage on this capacitor.

Figure 9.11 shows a remote control electrohydraulic system with electrical antiskid controller. The system consists of the pressure controller 2, electroblock 15, electrohydraulic valve 3, brake release valve 13, and the antiskid system generator 12. The pressure controller 2 is mounted in the cockpit. It is a transformer

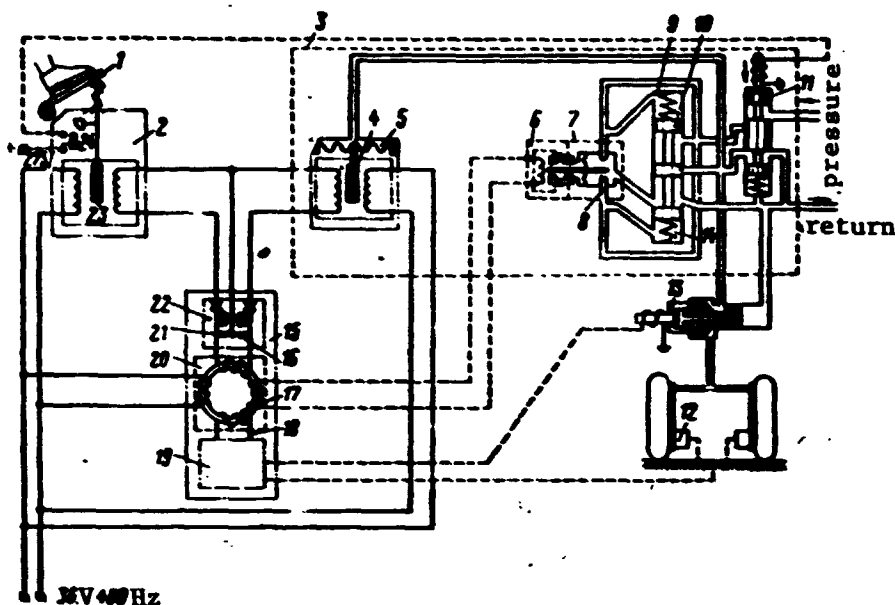


Figure 9.11. Electrohydraulic remote control system.

1- pedal; 2- pressure controller; 3- electrohydraulic valve; 4- core; 5- feedback sensor; 6- electromechanical transformer; 7- nozzle flapper unit; 8- nozzle; 9- controlling chamber; 10- working spool; 11- electrovalve; 12- antiskid system generator; 13- brake release valve; 14- controlling chamber; 15- electroblock; 16- resistance; 17- output winding; 18- magnetic amplifier winding; 19- antiskid system electronics; 20- magnetic amplifier; 21- resistance; 22- feedforward and feedback elements; 23- pressure controller core; 24- switch.

with variable transformation ratio (depending on brake pedal travel) and secondary electric switch.

The electroblock 15 consists of three elements: feedforward and feedback electrical system 22, magnetic amplifier 20, and antiskid system electronics 19.

The electrohydraulic reduction valve 3 is located near the brakes, as a rule, in the gear well. The electrohydraulic valve consists of the electromechanical transformer 6, nozzle flapper unit 7 — which controls the working spool 10, electrovalve 11 which blocks the hydraulic pressure in order to eliminate fluid flow through the nozzles and connects the brake with the return line when the brake pedal 1 is not depressed, and also the feedback sensor 5

/144

in the reduced pressure line. The brake release valve 13 is installed in the gear well and releases the pressure from the brakes during antiskid system operation. The antiskid system generator 12 is mounted on the wheel brake and is a DC or AC generator which puts out a voltage proportional to wheel rpm. The system is supplied 36 V 400 Hz AC and 27 V DC.

When the pedal 1 is depressed, the switch 24 closes, the electrovalve 11 supplies hydraulic fluid to the nozzles 8, and the control chambers 9 and 14 of the spool 10. If the currents (in opposite directions) in the resistances 16 and 21 are equal, the potential difference across the magnetic amplifier output winding 17 is equal to zero. The flapper is in the center position, the pressures on the ends of the spool 10 are equal, and fluid does not enter the brakes. /145

With further movement of the pedal and displacement of the core 23, the pressure controller 2 changes its transformation ratio, as a result of which the equilibrium of the currents flowing through the resistances 16 and 21 is disrupted and an error current proportional to the difference of the controller 2 and feedback sensor 5 signals appears in the output winding 17. The error current is amplified by the magnetic amplifier 20. The amplified signal is applied to the winding of transformer 6. The flapper displaces and the pressure increases in chamber 9 and decreases in chamber 14. Under the influence of the pressures in chambers 9 and 14, the spool 10 displaces, connecting the brake line with the hydraulic system. The reduced pressure displaces the core 4 of the feedback sensor 5, thus changing the sensor transformation ratio. Equilibrium of the currents in the resistances 16 and 21 is re-established, the error current disappears, the flapper returns to the original position, equalizing the pressures in chambers 9 and 14. The spool 10 returns to the original position. Thus, a pressure proportional to pressure controller rod displacement is established in the brake line.

When the pedal 1 is released, the process described above is repeated with the difference that current flows through the winding of transformer 6 in the opposite direction and the flapper displaces in the other direction from the neutral position. The reduced pressure will decrease.

If the wheel skids more than the set amount, the signal of the generator 12 is transformed in the braking controller 19 into a control signal which is applied to the brake release valve 13. At the same time, the brake release signal is applied to a corrector, from which it enters the magnetic amplifier winding 18. The signal from the corrector acts on the magnetic amplifier output current, reducing the brake pressure. With the next actuation of the controller, there is another reduction of the brake pressure, and so on, until the optimal pressure is established in the system. If the wheel traction with the ground increases and the controller stops triggering, the pressure increases smoothly to the magnitude commanded by the pilot.

The systems described above are not designed to maintain the braking regime in the limiting traction coefficient zone. These are relay type systems with actuating valve operating on the OPEN-CLOSED principle. Oscillations of the brake pressure and braking moment about the average value are characteristic for such systems when operating in the skid regime. Such systems have a quite definite percentage of loss, which, in the final analysis, leads to some increase of the airplane braking distance. The losses can be reduced by decreasing the pressure oscillation in the brakes by throttling the brake fluid or air entry and discharge or by increasing the system actuation frequency in the skid regime by increasing its response speed. However, experience has shown that even the fastest acting existing system with direct acting antiskid controller is not free of this drawback. /146

One possible solution of the problem of further braking effectiveness increase is the braking system of the type used in the RS-70 airplane. The computer of this system (Figure 9.12) receives a strain gauge signal proportional to the braking moment  $M_b$



to the right. The increase of the moment will cause reduction of  $dM_b/d\delta$  to zero. In this case, the control signal decreases and causes the spool to shift to the left. With a zero value of  $dM_b/d\delta$ , the spool will be in the neutral position, the brake chamber is isolated and is not connected with either the reduction valve or the return line. The valve 6 is a hydraulic amplifier with pressure feedback of the nozzle flapper type. The flapper is controlled by an electromechanical transformer. The transformer armature rotation angle  $\alpha$  is directly proportional to the controlling current  $I_c = \pm dM_b/d\delta$ .

Consequently, for  $dM_b/d\delta = 0$ ,  $\alpha = 0$  and the spool is in the center position; for  $+(dM_b/d\delta)_{\max}$ , the armature has the maximal deflection angle  $+\alpha_{\max}$ , corresponding to the extreme right-hand spool position. For  $-(dM_b/d\delta)$ , the armature rotation angle is  $-\alpha$ , which shifts the spool to the left and opens the brake chamber to the return line. This correction system makes it possible to maintain the brake pressure in the zone  $dM_b/d\delta = 0$ , which corresponds to the limiting traction coefficient zone.

Since the limit traction coefficient corresponds to a definite relative sliding zone, it is possible to create systems of quite high effectiveness, based on maintaining the braking regime in a given sliding zone. Such systems are simpler, although they are less effective than the systems which maintain the braking regime in the limit traction coefficient zone. An example of such a system is that shown in Figure 9.13. This system maintains a specified relative sliding magnitude. This system also provides for the possibility of altering the relative slip magnitude using manual control or a programmer. The system consists of several identical autonomous systems, each of which controls the braking of one wheel or a pair of wheels operating under the same conditions. The asynchronous tachgenerator  $\delta$ , which measures the braked wheel angular velocity  $\omega_w$ , serves as the sensor for each autonomous system. A

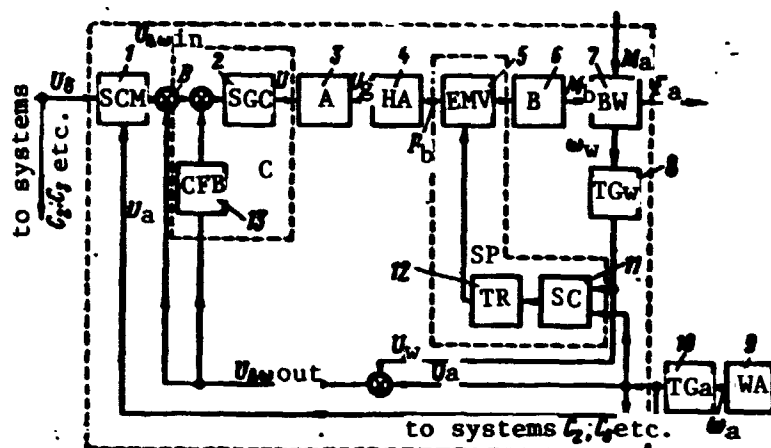


Figure 9.13. Automatic braking system with optimal regulation.

1- semiconductor multiplier; 2- semiconductor corrector; 3- amplifier; 4- hydraulic amplifier; 5- electromagnetic valve; 6- brake; 7- braked wheel; 8- tachgenerator; 9- unbraked wheel; 10- tachgenerator; 11- skid computer; 12- resistor relay; 13- correcting feedback unit.

similar tachgenerator 10, but only one for all the autonomous systems, measures the rotation rate  $\omega_a$  of the unbraked airplane wheel 9.

The multiplier 1 multiplies the input voltage  $U_\delta$  by the voltage  $U_a$ , proportional to the unbraked wheel rotational speed. At the same time, it is a programmer which provides a specified nonlinear law of  $U_{\Delta\omega_{in}}$  variation as a function of unbraked wheel velocity. The system corrector C consists of a series corrector 2 and a feedback corrector 13. The transistorized amplifier 3 applies the voltage  $U_g$  to the input winding of the hydraulic amplifier 4, which creates the pressure  $p_b$  in the wheel brakes. The skid protector SP consists of a skid computer 11, transistorized relay 12, and electromagnetic valve 5.

The system operates as follows. After the airplane wheels contact the runway surface and spin up, the system is activated by application of the voltage  $U_\delta$ , proportional to the specified skid magnitude  $\delta_s$ . At every instant of time, the voltage at the

output of the multiplier programmer 1 is proportional to the difference of the rotation rates of the unbraked and braked wheels, corresponding to the specified skid. Since the primary factor influencing the position of the extremum of the relation  $\mu_{s1}(\delta)$  is airplane speed, it is possible to find the law of  $U_{\Delta\omega_{in}}$  variation as a function of the velocity  $\omega_a$ , which ensures operation of the braking wheel with nearly optimal skidding. Reproduction of this law is achieved by selecting the phase shift between the voltage  $U_a$  and the reference voltage of the multiplier 1.

At the summation point B, the voltage  $U_{\Delta\omega_{in}}$  is compared with the voltage  $U_{\Delta\omega_{out}}$ , which is proportional to the actual velocity difference  $\Delta\omega_{out} = \omega_a - \omega_w$  at a given moment of time. In the steady state operating regime, the voltage at the input of the hydraulic amplifier 4 and, consequently, the braking moment  $M_b$  are proportional to the difference

$$U = U_{\Delta\omega_{in}} - U_{\Delta\omega_{out}}$$

or

$$U = k\omega_a(\delta_s - \delta_{out}),$$

where  $k$  is a coefficient of proportionality.

The amplifier gain is selected so that the difference between the specified and actual values of the relative skid does not exceed the allowable value

$$\delta_s - \delta_{out} \leq \Delta\delta_a.$$

In this case, the braking moment is sufficient to ensure the required skid value (with error  $\pm\Delta\delta_a$ ).

If the magnitude of the braked wheel skid deviates from  $\delta_s$ , the voltage  $U$  and braking moment  $M_b$  vary so as to return the skid to the required value.

Let us assume that, because of traction coefficient reduction wheel-ground (encountering wet ground), the rotational speed  $\omega_w$  begins to decrease (relative skid increases). Reduction of  $\omega_w$  leads to increase of the voltage  $U_{\Delta\omega_{out}}$ , reduction of the voltage  $U$  and, consequently, reduction of the braking moment, which causes wheel spinup to the previous speed. In this case, the relative skid will approach the required value.

The skid protector SP prevents the possibility of braked wheel skidding in the case of failure or malfunction of the primary system circuit elements. The skid computer 11 of the protector, constructed using two transistors similarly to the multiplier 1, determines the instantaneous value of the skid  $\delta_{out}$ . If the magnitude of the latter for any reason exceeds the specified critical value  $\delta_w$ , the protective unit activates the electromagnetic valve 5 and reduces the brake pressure. The wheel begins to increase its rotational speed and, as soon as the magnitude of the skid becomes less than  $\delta_w$ , the electromagnetic valve supplies pressure from the electroreduction valve to the brake.

/150

Of the systems examined above, those which provide optimal or nearly optimal braking are most effective. However, they are quite complex and this leads to limited use of such systems, particularly for light airplanes. In certain cases, effectiveness can be improved by the use of simple additional devices in the conventional systems.

Figure 9.14 shows an antiskid control system with programmed braking moment regulation. The system operates as follows. During braking, the pilot creates pressure in the wheel brake with the aid

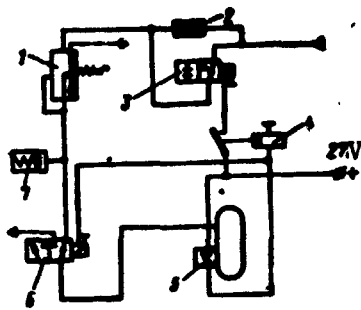


Figure 9.14. Antiskid control system with programmed braking moment regulation.

1- reduction valve; 2- restrictor; 3, 6- electromagnetic valves; 4- relay; 5- electroinertial sensor; 7- makeup chamber.

there is no skidding and the electromagnetic valve 3 is open, such a system operates as a conventional system. If the wheel starts to skid, an electrical signal from the inertial sensor 5 is fed to the electromagnetic valve 6 and through relay 4 to the electromagnetic valve 3. The valve 6 connects the wheel brake with the return line and the valve 3 blocks the line supplying the valve 1. The pressure in the brakes decreases. After skidding is eliminated, the brake release signal is no longer applied and the brake is again connected with the valve 1. As a result of regulation of the spring of the makeup chamber 7, the pressure in the brakes increases rapidly to a value somewhat less than that at which skidding occurred. Further /151 increase of the pressure to a value near the maximal will take place smoothly because of the presence of the restrictor 2 and the lag in the relay 4.

This system makes it possible to reduce the braking moment oscillation amplitude with simultaneous reduction of the number of antiskid system controller actuations.

Another system version which increases braking effectiveness is that shown in Figure 9.15 and is widely used on light airplanes. The system operates as follows. When the signal coming from the electroinertial controller 1 is of shorter duration than the

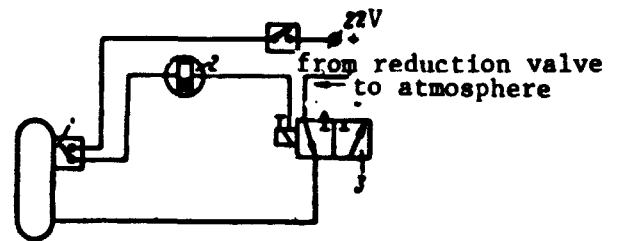


Figure 9.15. Antiskid system for light airplanes.

1- electroinertial controller; 2- electrical filter; 3- electromagnetic valve.

of the valve 1. The fluid flows to the brake practically without resistance through the electromagnetic valves 3 and 6. When

specified value, it does not pass through the filter 2 and brake release does not take place. Nor does tire scuffing occur, since, during this time, only angular deformation of the tire takes place. However, if the sensor signal is sufficiently long, it passes through the electrical filter 2 to the electromagnetic valve 3, which then releases the wheel brake.

This circuit makes it possible to filter out all the false signals which may be caused by irregularities of the airdrome surface, landing gear kinematics, and other factors.

## CHAPTER 10

### BRAKE SYSTEM COMPONENT DESIGN

/152

#### 1. Pneumatic Brake System Components

The following basic components are used in the direct acting pneumatic brake system: reduction valve, differential, electro-magnetic brake release valve, shuttle valve, and others.

##### Reduction Valve

The pneumatic reduction valve is the unit which primarily determines brake system effectiveness. The valve must have:

- linear reduced pressure dependence on plunger travel;
- maximal sensitivity with respect to plunger travel;
- immunity to vibration;
- hermeticity;
- response speed.

The valve operates as follows (Figure 10.1). During braking, the pilot displaces the plunger 1 by a lever. The spring 2 deforms, transmits the force to the piston 3, and displaces it. The piston, in turn, after taking up the clearance  $a$ , displaces the outlet valve 4 and, through a special needle, opens the inlet valve 5. Air from

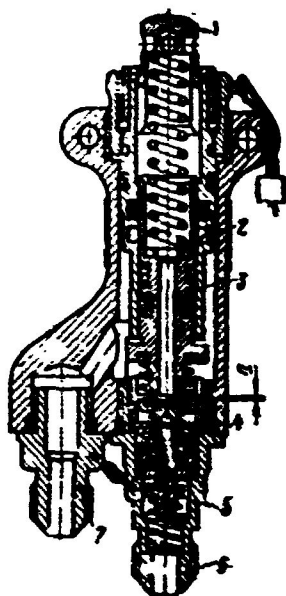


Figure 10.1. Pneumatic reduction valve.

1- plunger; 2- spring; 3- piston; 4- outlet valve; 5- inlet valve; 6, 7- fittings.

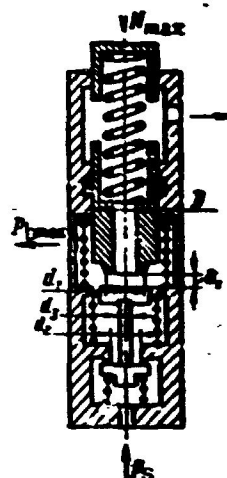


Figure 10.2. Schematic of pneumatic reduction valve.

the high pressure system (usually from a bottle) flows into the brake system through the fitting 6, open inlet valve 5, and the fitting 7.

The reduced pressure created in the brake system acts on the effective area of the piston 3, compresses the spring 2, and balances the load applied to the plunger 1, as a result of which the piston moves upward and the inlet valve closes.

In the equilibrium piston, the valves 5 and 4 are closed.

With reduction of the force on the plunger, the equilibrium is disrupted, the differential force moves the piston 3 upward, and the outlet valve 4 bottoms on the nut and opens. The excess pressure (with account for the new load on the plunger 1) is bled to the atmosphere.

*Static analysis of pneumatic reduction valve.* The basic data for the analysis are the following quantities (Figure 10.2):

/153



we have

$$d_1 = \sqrt{\frac{4F_1}{\pi}}; \quad \delta_1 = \frac{d_1}{4}; \quad d_2 = \sqrt{\frac{4F_2}{\pi} + d_1^2} \quad (10.3)$$

( $d_3$  is selected directly in the design).

The inlet and outlet passage flow areas must be at least three times the valve areas  $F_1$  and  $F_2$ .

The spring pretensions are selected with account for the constructional characteristics and may vary over fairly large ranges

$$\Pi_1 = (2 - 5) \text{ kG};$$

$$\Pi_2 = \Pi_3 = (0.5 - 1.5) \text{ kG}.$$

After selecting  $\Pi_1$ ,  $\Pi_2$ , and  $\Pi_3$ , we determine the maximal plunger travel  $Y_{\max}$ , which must not exceed the specified magnitude.

Since the value dead zone must not exceed 25% of the total travel, we have  $\delta_{\max} = 0.25 Y_{\max}$ :

$$\delta_{\max} = \delta_1 + \frac{\Pi_1 + \Pi_2 + \Pi_3 + p_s \frac{\pi d_2^2}{4} + T_p}{c_{rs}}$$

where  $c_{rs}$  is the reduction spring stiffness. But since

$$c_{rs} = \frac{N_{\max}}{Y_{\max}},$$

then

$$\delta_{\max} = \delta_1 + \frac{Y_{\max}}{N_{\max}} \left( \Sigma \Pi + p_s \frac{\pi d_2^2}{4} + T_p \right)$$

or

$$0.25 Y_{\max} = \delta_1 + \frac{Y_{\max}}{N_{\max}} \left( \Sigma \Pi + p_s \frac{\pi d_2^2}{4} + T_p \right),$$

hence,

$$Y_{\max} = \frac{\delta_1}{0.25 - \frac{\Sigma \Pi + p_s \frac{\pi d_2^2}{4} + T_p}{N_{\max}}}$$

It is obvious that, for normal valve operation, it is necessary that

$$N_{\max} > 4 \left( \Sigma \Pi + p_s \frac{\pi d_2^2}{4} + T_p \right). \quad (10.4)$$

The effective piston area is found from the formula

$$F_p = \frac{N_{\max} - T_p - \Sigma \Pi}{p_{b \max}},$$

where

$$\Sigma \Pi = \Pi_1 + \Pi_2 + \Pi_3 \quad (10.5)$$

#### Differential

Differentials are used in tricycle landing gear brake systems to permit braking of the left and right gear wheels with different braking moments, which is necessary in order to perform turns while taxiing.

The differential is a dual reduction valve which makes it possible to reduce the pressure in the wheels of one gear leg while maintaining the pressure in the wheels of the other leg. The construction of the most widely used differential is shown in Figure 10.3.

/156

The pistons 3 move freely in the sleeves 2 which are stationary in the differential body 6. The outlet valve 1 is spring loaded against the piston seat. The pressure supplied to fitting A passes freely to the brakes through the fitting B with the pistons tight

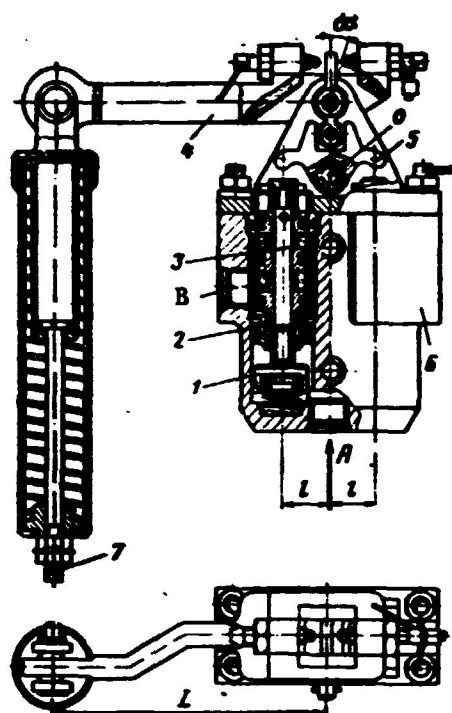


Figure 10.3. Brake system differential.

1- outlet valve; 2- sleeve; 3- piston; 4- lever; 5- rocker arm; 6- differential body; 7- spring loaded coupling rod.

3 moves up, the valve 1 is forced against the seat of the sleeve 2 and isolates the left brake chamber from the brake line. The piston 3 moves away from the valve 1 and the pressure in the brake decreases until equilibrium of the forces acting on the spring loaded coupling rod 7 is reached.

The differential dimensions are determined by static analysis. The data necessary for the calculation are the following:

$p_{b \max}$  is the maximal brake pressure;  $N_{\max}$  is the maximal spring loaded coupling force;  $X_{\max}$  is the maximal spring loaded coupling rod deflection; and  $\tau$  is the minimal time for brake release through the differential.

against the rocker arm 5. In the neutral position of the lever 4 and the spring-loaded coupling rod 7, the pressure flows freely to the brakes of both wheels.

When the spring-loaded coupling rod 7 moves up or down, the lever 4 deflects through some angle  $\alpha$  at which no change of the brake pressure takes place. This angle determines the dead zone  $\delta$ . Further up or down deflection of the rod 7 causes the appearance of an additional moment on the rocker arm 5 relative to the axis of rotation 0. In this case, the brake pressure changes because of the fact that with rotation of the rocker arm 5 in the clockwise direction, the left piston

The outlet flow area when releasing the brakes through the differential is found from (10.2) and (10.3).

For rod deflection (down, for example) by the distance  $X$ , we have

$$iLc_c X = p_1 F_p l - p_2 F_p l \quad (10.6)$$

or

$$iLc_c X = F_p l (p_1 - p_2), \quad (10.7)$$

where  $L$  and  $l$  are the unit linear dimensions (arms);  $F_p$  is the piston area;  $p_1$  and  $p_2$  are the pressures in the left and right brakes;  $c_c$  is the spring loaded coupling rod stiffness; and  $i$  is the gear ratio. We see from (10.7) that

$$\Delta p = kX,$$

where

$$\Delta p = p_1 - p_2$$

$$k = \frac{iLc_c}{F_p l}, \quad c_c = \frac{N_{\max}}{X_{\max}}$$

Thus, the pressure differential in the brakes is proportional to the rod displacement.

For full rod deflection

$$\Delta p_{\max} = kX_{\max}. \quad (10.8)$$

#### Electromagnetic Brake Release Valve

The electromagnetic valve reduces the brake pressure when the wheel starts skidding. Various valve constructions are used, but the servo-action valve (Figure 10.4) is most common.

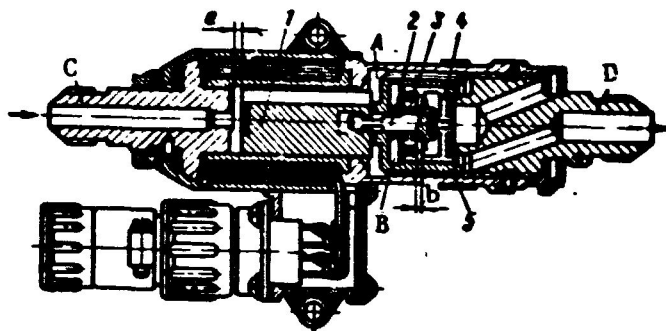


Figure 10.4. Electromagnetic brake release valve.  
1- armature; 2, 4- valves; 3- spring; 5- guide.

In the absence of wheel skidding, the valve connects the brake chamber with the reduced brake pressure line. The air flows freely from the reduction valve to the brake through fitting C, slots in the armature 1, guide 5, and fitting D. In this case, the pressure in the chamber B is equal to the pressure in chamber A and the main valve 4 is forced against the seat of fitting D by the spring 3 of the control valve 2 and by the air pressure.

When an electrical pulse for brake release is transmitted, as the wheels start skidding, the electromagnet displaces the armature 1, which, after traveling the distance  $a$ , closes the inlet valve and blocks air entry into the brakes. At the same time, the armature 1 displaces the valve 2 to the left, isolates chamber B from chamber A, and connects chamber B with the atmosphere (valve 2 displaces along the guide 5 with small clearance). As a result of the resulting pressure differential, the valve 4 will shift to the left and connect the brake chamber with the atmosphere.

/158

All the electromagnetic valve flow areas are calculated using the formulas obtained above to ensure minimal losses as the air flows through the valve, after which a static analysis is made of the electromagnet and servovalve spring forces.

## Shuttle Valve

The shuttle valve is used to supply a user service from two systems. Usually, the valve spring holds the shuttle in the position in which the brakes are connected to the primary system. In case of primary system failure, the pilot activates the emergency system and the shuttle valve is displaced by the pressure in the emergency system, thus switching the brake line from the primary to the emergency system.

## 2. Hydraulic Brake System Components

The following basic components are used in the direct acting hydraulic brake systems: main system reduction valve, emergency system reduction valve, hydraulic fuse, shuttle valve, and electromagnetic brake release valve.

### Main Brake System Reduction Valve

The reduction valve is the primary component which determines the reliability and effectiveness of the system as a whole. Therefore, the valve must be sufficiently sensitive, vibration resistant, and reliable in operation, and have a nearly linear static characteristic.

/159

Both direct acting and servo-action brake reduction valves may be encountered in component design practice.

The direct acting valve shown in Figure 10.5 is most widely used at the present time.

The valve operates as follows. As the pilot depresses the brake pedal, the cup 1 displaces and, in turn, through the spring 2, displaces the plunger 3 with the outlet valve 5. The outlet valve spring 4 is thus compressed. The outlet valve 5 travels 2 — 2.5 mm, displaces the sleeve 6 and, as it reaches the spool 7, isolates the

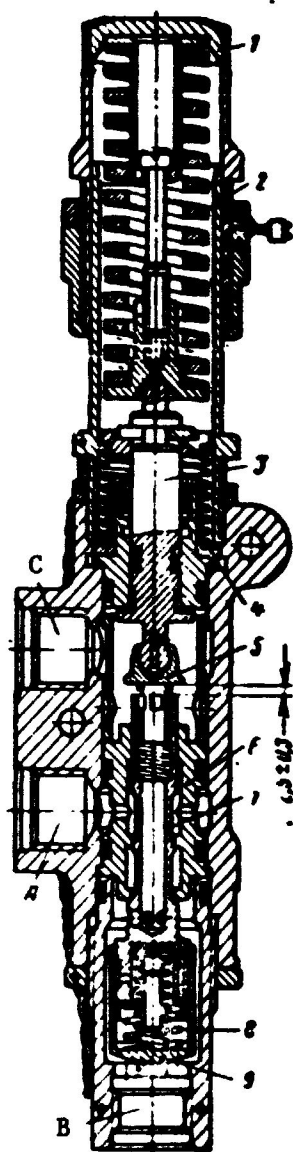


Figure 10.5. Direct acting hydraulic reduction valve.

1- cup; 2- spring; 3- plunger; 4- outlet valve spring; 5- outlet valve; 6- sleeve; 7- spool; 8- spring; 9- damper cup.

reducing the brake system pressure. A one-way damper is installed on the spool 7 to improve valve dynamic stability. In addition, fluid entry at the beginning of spool 7 travel is accomplished through specially profiled slots, also provision is made for throttling the working fluid at the beginning of outlet valve travel by introducing a special sleeve 6 located in the spool 7.

brake system from the return line, connected with fitting C. With further pedal movement, the spool 7 displaces along with the inlet valve, made in the form of a cone on the spool. The fluid enters the brake system from the high pressure line through fitting A, inlet valve, and fitting B.

Upon termination of further movement of the cup 1, the brake system pressure will increase until the fluid pressure force on the valve 5 compresses the spring 2 and the spool 7, under the influence of the spring 8, bottoms on the sleeve and cuts off fluid entry into the brake system. Upon pressure reduction, the spring 2 again displaces the spool 7 and a quite definite pressure corresponding to the position of the cup 1 will be maintained in the system.

With reverse movement of the cup 1, the outlet valve 5 opens and fluid will flow from the brake system into the return line through the fitting C,

/160

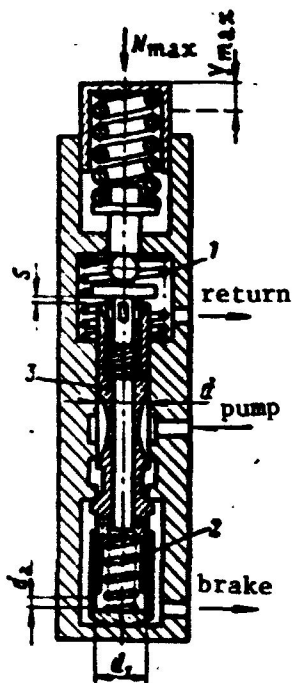


Figure 10.6. Idealization of hydraulic reduction valve.

The flow section areas of the spool 7 and the outlet valve and also the nature of the variation of these areas as a function of travel must be calculated and selected for each system separately.

Sensitivity and linearity of the valve static characteristic requires the use of high accuracy and also high surface finish of the detail parts, particularly the slide valve pair.

*Static valve analysis.* The basic design data are:  $p_s$  is the system pressure;  $p_{b \max}$  is the maximal brake pressure;

$\Delta p_{1 \max}$  is the maximal valve resistance with average fluid flowrate during brake application;  $\Delta p_{2 \max}$  is the maximal valve resistance with average fluid flowrate during brake release;  $Q_1$  is the average fluid flowrate during brake application;  $Q_2$  is the average fluid flowrate during brake release;  $N_{\max}$  is the maximal force on the valve stem;  $Y_{\max}$  is the maximal plunger travel;  $Y'_{\max}$  is the maximal valve plunger dead zone; and  $\Delta Y_{\max}$  is the maximal plunger travel insensitivity.

An idealized hydraulic reduction valve schematic is shown in Figure 10.6.

The equation of spool equilibrium with account for the friction and spring pretension forces has the form:

$$N_{\max} = p_{b \max} \frac{\pi d^2}{4} + P_1 + P_2 + T_{1 \max} + T_{2 \max}. \quad (10.9)$$

where  $P_1$  is the pretension force of spring 1;  $p_2$  is the pretension force of spring 2;  $T_{1 \max}$  is the maximal friction force of slide valve pair 3;  $T_{2 \max}$  is the maximal friction force of outlet valve unit;  $d$  is the slid valve pair diameter;  $d_1$  is the damper diameter; and  $d_2$  is the damping orifice diameter. /161

The following condition must be satisfied for quick return of the spool to the initial position

$$\left. \begin{aligned} P_2 &= (2-3)T_{1 \max}; \\ P_1 &= (1.5-2)T_{2 \max}. \end{aligned} \right\} \quad (10.10)$$

The friction force can be calculated from the formula:

$$T_1 = k \frac{\Delta p}{2} l d, \quad (10.11)$$

where  $T_1$  is the friction force;  $k$  is the coefficient of slide valve pair friction, equal to 0.04 — 0.06;  $\Delta p$  is the pressure differential; and  $l$  is the length of lapped part of slide valve pair.

The friction force  $T_2$  is determined basically by seal friction and may be taken as 1.5 — 2 kG.

Substituting the values of  $P_1$ ,  $P_2$ ,  $T_1$ , and  $T_2$  into (10.9) and replacing variables, we obtain

$$ad^2 + bd - c = 0, \quad (10.12)$$

where

$$a = p_b \max \frac{\pi}{4}.$$

Thus

$$\begin{aligned} b &= (3-4)k \frac{\Delta p}{2} l, \\ c &= -N_{\max} + (2.5 \div 3)T_{2 \max}; \end{aligned}$$

then

$$d = \frac{\sqrt{b^2 + 4ac} - b}{2a}.$$

The reduction spring stiffness:

$$c_{rs} = \frac{N_{max}}{Y_{max}}. \quad (10.13)$$

From the known stiffness and load values, we find the reduction spring dimensions.

The maximal spool flow section inlet ( $F_{1 \max}$ ) and outlet ( $F_{2 \max}$ ) areas are determined on the basis of the acceptable resistance for the average fluid flowrate during brake application and release. /162

The average fluid flowrate during brake application can be determined with account for the allowable brake application time (no more than 1.5 seconds) from the empirical formula:

$$Q_{L \ 1} = 75 V_{max} \text{ liters/minute}, \quad (10.14)$$

where  $V_{max}$  is the maximal fluid volume in liters required by the wheel brakes during a single brake application.

The maximal spool inlet flow section area

$$F_{1 \max} = \frac{Q_{L \ 1}}{0.663 \sqrt{k_1 \cdot p_s}} \text{ mm}^2, \quad (10.15)$$

where  $k_1 = 0.15 - 0.25$  is a coefficient accounting for the fluid pressure losses in the slide valve pair ports.

The average fluid flowrate during brake release is usually equal to the average flowrate during brake application, i.e.,

$$Q_{L \ 2} = Q_{L \ 1}.$$

The maximal spool outlet flow section area

$$F_{2 \max} = \frac{Q_{L2}}{0.663 \sqrt{k_2 \cdot p_s}} \text{ mm}^2 \quad (10.16)$$

where  $k_2 = 0.05 - 0.15$  is a coefficient accounting for the pressure losses during brake release.

The valve spool travel is taken in the limits of  $0.1 - 0.15$  of the plunger travel

$$X_{\max} = (0.1 \div 0.15) Y_{\max}. \quad (10.17)$$

The valve dead zone  $Y'$  is determined by the travel and the spring pretension forces  $P_1$  and  $P_2$ , where

$$Y'_{\max} \leq 0.25 Y_{\max} \quad (10.18)$$

or

$$0.25 Y_{\max} \leq S + \frac{P_1 + P_2}{c_{rs}}. \quad (10.19)$$

In order to reduce the valve dead zone, the pretension of the spring 2 is selected so as to eliminate the influence of springs 4 and 8 (see Figure 10.5).

The valve travel insensitivity is found from the formula

$$\Delta Y_{\max} = \frac{T_{\max}}{c_{rs}}, \quad (10.20)$$

where  $\Delta Y_{\max}$  is the maximal insensitivity;  $T_{\max}$  is the maximal overall friction force of all the valve moving elements; and  $c_{rs}$  is the reduction spring stiffness.

/163

*Valve dynamic analysis.* The most important valve characteristic is its dynamic stability. The primary cause of instability is the presence of hydrodynamic forces acting on the spool 3 during brake application or release. Loss of valve stability causes fluid flow from the high pressure chamber into the return and pressure pulsation, which may lead to failure of the valve, tubing, and other brake system components.

Stability analysis of the reduction valve can be reduced to stability analysis of the "valve brake" system and determination of the initial slide valve characteristics and valve damper characteristics.

For the analysis, we formulate the system of equations consisting of the flowrate equation and the regulator equation.

*Flowrate equation.* The instantaneous fluid flowrate through the slide valve during brake application (or release) can be expressed by the formula

$$Q_{L1} = AF_1(x)\sqrt{\Delta p}, \quad (10.21)$$

where

$$A = k_f \sqrt{\frac{2g}{\gamma}},$$

$k_f$  is the flowrate coefficient;  $\gamma$  is the specific weight of the fluid;  $\Delta p$  is the pressure differential in the valve (across the spool);  $F_1$  is the valve inlet flow section area; and  $x$  is the spool displacement coordinate.

For a short time interval, we take  $\Delta p = \text{const}$ , then

$$Q_{L1} = B_1 F_1(x), \quad (10.22)$$

where

$$B_1 = A\sqrt{\Delta p}.$$

Taking the function  $F_1(x)$  to be linear, we obtain

$$F_1(x) = kx,$$

where  $k = \tan \alpha$  is the spool travel characteristic. Then the flowrate equation takes the form:

$$\begin{aligned} Q_{L1} &= k_1 x, \\ k_1 &= B_1 k. \end{aligned} \quad (10.23)$$

For symmetric spool inflow and outflow characteristics, we have /164

$$Q_{L1} = Q_{L2} = k_1 x. \quad (10.24)$$

The pressure variation in the system for the flowrate  $Q_{L1}$  is defined by the equation

$$Q_{L1} = c_s \frac{dp}{d\tau}, \quad (10.25)$$

where  $c_s$  is the system stiffness coefficient;  $dp/d\tau$  is the rate of pressure change in the system

$$c_s = F_l l_l \left( \frac{d_l}{\delta_l E} + \frac{1}{E_1} \right) + \frac{V_s}{E_1}; \quad (10.26)$$

where  $F_l$  is the line area;  $l_l$  is the line length;  $d_l$  is the line diameter;  $\delta_l$  is the line wall thickness;  $E_1$  is the elastic modulus of the working fluid;  $E$  is the elastic modulus of the line material; and  $V_s$  is the overall volume of the line and brake.

From (10.24) and (10.25), we have

$$c_s \frac{dp}{d\tau} = k_1 x. \quad (10.27)$$

This is the controlled object (brake) equation.

C-3

*Regulator equation.* In order to formulate the spool equation of motion, we examine the forces acting on it.

In the transient regime, the following forces act on the spool.

Spool inertia force:

$$P_1 = -m \frac{d^2 X}{dt^2} \quad (10.28)$$

where  $m$  is the equivalent mass.

Viscous friction force

$$P_2 = -h \frac{dX}{dt} \quad (10.29)$$

where  $h$  is the spool damping coefficient (determined experimentally).

Reduction spring force

$$P_3 = c_1(Y - X) \quad (10.30)$$

Return spring force

$$P_4 = -c_2 X, \quad (10.31)$$

where  $c_2$  is the equivalent stiffness.

/165

Fluid pressure force on the valve

$$P_5 = F_v p, \quad (10.32)$$

where  $F_v$  is the valve area;  $p$  is the fluid pressure in the brake.

Hydrodynamic (reactive) force

$$P_6 = -c_3 X, \quad (10.33)$$

where

$$c_3 = 2k_f k \Delta p \cos \theta, \quad (10.34)$$

and  $k_f$  is the flowrate coefficient;  $k$  is the spool travel characteristic;  $\Delta p$  is the pressure differential across the spool;  $\theta = 69^\circ$  is the reactive force direction angle  $69^\circ$ .

Without account for the friction forces, the spool equation of motion takes the form

$$c_1 \dot{Y} = m \ddot{X} + h \dot{X} + (c_1 + c_2 + c_3) X + F_v p \quad (10.35)$$

or

$$m \ddot{X} + h \dot{X} + (c_1 + c_2 + c_3) X = - F_v p + c_1 \dot{Y}. \quad (10.36)$$

We introduce the notations

$$\left. \begin{aligned} T^2 &= \frac{m}{c_1 + c_2 + c_3}; \quad T_1 = \frac{h}{c_1 + c_2 + c_3}; \\ c &= \frac{c_1}{c_1 + c_2 + c_3}; \quad k_{\text{reg}} = \frac{F_v}{c_1 + c_2 + c_3}; \end{aligned} \right\} \quad (10.37)$$

and obtain

$$T^2 \ddot{X} + T_1 \dot{X} + X = - k_{\text{reg}} p + c \dot{Y}, \quad (10.38)$$

where  $T_1$  and  $T$  are time constants, and  $k_{\text{reg}}$  is the regulator coefficient.

*System equation.* The system equation is formulated on the basis of the regulator and flowrate equations:

$$\left. \begin{aligned} c_s \frac{dp}{dt} &= k_s X; \\ T^2 \frac{d^2 X}{dt^2} + T_1 \frac{dX}{dt} + X &= - k_{\text{reg}} p + c \dot{Y}. \end{aligned} \right\} \quad (10.39)$$

Converting to the operator form, we have

$$\left. \begin{aligned} k_s \lambda p &= X; \\ (T^2 \lambda^2 + T_1 \lambda + 1) X &= - k_{\text{reg}} p + c \dot{Y}. \end{aligned} \right\} \quad (10.40)$$

where

$$k_2 = \frac{c_2}{k_1}; \quad \lambda = \frac{d}{dt}$$

Excluding X from (10.40), we obtain

/166

$$k_2 \lambda (T^2 \lambda^2 + T_1 \lambda + 1) p + k_{reg} p = cY; \quad (10.41)$$

$$p[k_2 \lambda (T^2 \lambda^2 + T_1 \lambda + 1) + k_{reg}] = cY. \quad (10.42)$$

The characteristic equation will have the form

$$k_2 T^2 \lambda^3 + k_2 T_1 \lambda^2 + k_2 \lambda + k_{reg} = 0 \quad (10.43)$$

The system stability conditions are

$$\left. \begin{aligned} k_2 T^2 > 0; \quad k_2 T_1 > 0; \quad k_2 > 0; \quad k_{reg} > 0; \\ k_2 T_1 > k_{reg} T^2; \quad k_{reg} < \frac{k_2 T_1}{T^2}. \end{aligned} \right\} \quad (10.44)$$

The Vyshnegradskiy criteria are convenient for determining the form of the transient process in the present case.

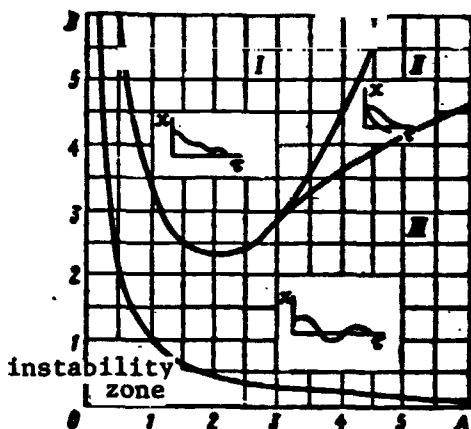


Figure 10.7. System stability diagram.

we change the damping coefficient and the valve characteristic (making the curve flatter, in this case  $k = \tan \alpha$  decreases), then a new analysis is made.

The diagram (Figure 10.7) shows, in the coordinates,

$$A = \frac{k_2 T_1}{\sqrt{k_2 T^2} k_{reg}}; \quad B = \frac{k_2}{\sqrt{k_2 T^2} k_{reg}^2} \quad (10.45)$$

the zones I — III in which spool operation is stable. The spool travel characteristic as a function of time is shown in each zone.

If the system is found to be unstable in the analysis,

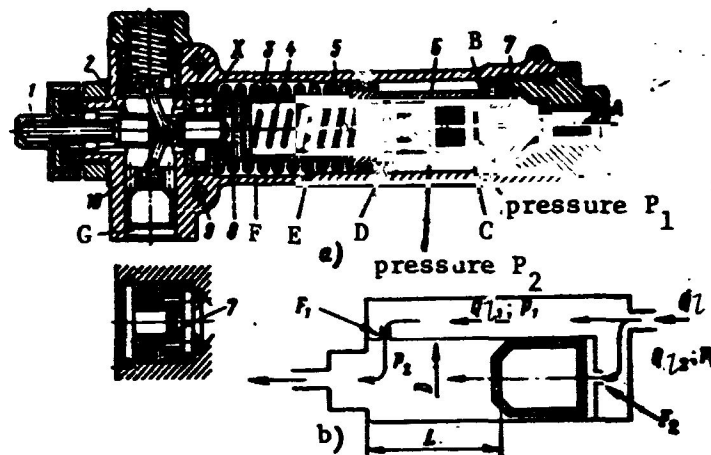


Figure 10.8. Hydraulic fuse construction.

1- rod; 2- shuttle valve; 3- sleeve; 4- spring; 5, 6- valves; 7- restrictor; 8- spring; 9- seat; 10- lever.

#### Emergency System Reduction Valve

/167

The construction of the emergency braking system reduction valve is the same as that of the main system reduction valve. Usually the emergency valve plunger has shorter travel. The valves for braking of both bogies are combined into a single housing in order to simplify installation. The valve analysis procedure is the same.

#### Hydraulic Fuse

The hydraulic fuse or flow limiter is a hydraulic component which passes a definite amount of fluid, after which it blocks off the line. It finds wide application in aircraft hydraulic systems as one of the most important protective components.

The hydraulic fuse works as follows. Fluid from the line downstream of the reduction valve enters fitting A and then chamber C and simultaneously flows through the fuse restrictor into chamber B under the fuse cutoff valve 6 (Figure 10.8). The primary fluid flow passes through the ports D, forces the valve 5 to the extreme left position, and after passing through the ports E enters the chamber F, then flows through the annular port of the seat 9 into

the line through the outlet fitting G. At the same time, the other (signal) part of the flow passes through the restrictor 7 and displaces the valve 6 to the extreme left position. The ports D will now be blocked and the primary fluid flow terminates.

The hydraulic fuse is designed so that, during normal operation, /168 the valve 6 will not travel all the way to the stop during the time of fluid flow. As soon as the braking operation is performed and fluid flow in the line terminates, the valves 6 and 5 again take the initial position under the influence of the spring 4.

If a line breaks or a brake fails downstream of the hydraulic fuse, the valve 6 reaches the seat in the sleeve 3 and blocks the line.

The pressure differential acting on the entire area of the sleeve 3 displaces it to the left by the distance X, compressing the spring 8. In this case, the shuttle valve 2 closes. The toggle lever 10 holds the valve in the closed position after pressure reduction in the brake line. This is necessary to avoid fluid loss during further braking. In this case, the valve is returned to the initial position manually by means of the rod 1.

*Hydraulic fuse analysis.* The basic data are:  $Q_L$  is the nominal fluid flowrate in the system;  $Q_{L \min}$  is the minimal fluid flowrate in the system;  $\Delta p$  is the pressure losses in the hydraulic fuse; and  $V_{mv}$  is the metering volume.

The basic hydraulic fuse geometric dimensions are determined by calculation: flow section area  $F_1$  in the ports D through which the primary flow passes, flow section area  $F_2$  through which the signal flow passes, valve diameter D, and travel L of the valve 2.

The overall fluid flowrate through the hydraulic fuse is made of the fluid flowrate  $Q_{L1}$  through section  $F_1$  and the flowrate  $Q_{L2}$  through section  $F_2$ :

$$Q_L = Q_{L1} + Q_{L2}, \quad (10.46)$$

but

$$Q_{L1} = AF_1 \sqrt{\Delta p}; \quad Q_{L2} = AF_2 \sqrt{\Delta p}.$$

Then

$$Q_L = AF_1 \sqrt{\Delta p} + AF_2 \sqrt{\Delta p} = A(F_1 + F_2) \sqrt{\Delta p} = AF_0 \sqrt{\Delta p}.$$

Hence

$$F_0 = \frac{Q_L}{A \sqrt{\Delta p}},$$

where

$$F_0 = F_1 + F_2; \quad \Delta p = p_1 - p_2.$$

For constant differential  $\Delta p$  during the time  $\Delta \tau$ , the amount of fluid passing through the hydraulic fuse is

$$V_{mv} = V_1 + V_2, \quad (10.47)$$

where

$$V_1 = Q_{L1} \Delta \tau, \quad (10.48)$$

$$V_2 = Q_{L2} \Delta \tau, \quad (10.48)$$

$$V_{mv} = Q_L \Delta \tau.$$

Then

$$\Delta \tau = \frac{V_{mv}}{Q_L} = \frac{V_1}{Q_{L1}} = \frac{V_2}{Q_{L2}}, \quad (10.49)$$

whence

$$\frac{V_{mv}}{Q_L} = \frac{V_1}{Q_{L2}}; \quad \frac{Q_{L2}}{Q_L} = \frac{V_2}{V_{mv}}; \quad \frac{F_2}{F_0} = \frac{V_2}{V_{mv}};$$

but

$$F_2 = F_0 \frac{V_2}{V_{mv}} = A \frac{Q_L}{\sqrt{p_1 - p_2}} \cdot \frac{V_2}{V_{mv}}. \quad (10.50)$$

We introduce the relation

$$V_2 = k V_{mv} \quad (10.51)$$

From design experience, we take  $k = (0.012 - 0.018)$  for fuses with  $V_{mv} = 200 - 1000 \text{ cm}^3$ . Then

$$V_{mv} = 200 - 1000 \text{ cm}^3.$$

$$V_2 = \frac{\pi D^2}{4} L$$

and taking  $L = k_1 D$ , where  $k_1 = 1.2 - 1.5$ , we obtain

$$D = \sqrt[3]{\frac{4}{k_1 \pi} V_2}$$

or

$$D = \sqrt[3]{\frac{4kV_{mv}}{k_1 \pi}}. \quad (10.52)$$

The section area  $F_1$  is found as the difference

$$F_1 = F_0 - F_2. \quad (10.53)$$

For precise operation of the fuse, it is necessary that the minimal actuating force acting on the valve be at least twice the friction force, i.e.,

$$N_{min} > 2T, \quad (10.54)$$

where

$$N_{min} = \frac{\pi D^2}{4} \Delta p_{min} = \frac{\pi D^2}{4} \left( \frac{Q_{L \min}}{Q_L} \right)^2 \Delta p; \quad (10.55)$$

$$T = f \frac{1}{2} \Delta p_{\text{max}} DL \quad (10.56)$$

for

$$f = 0.1 \div 0.08.$$

### Shuttle Valve

/170

Shuttle valves are used in brake systems to switch the brake supply from the primary system to the emergency system and back. The basic requirements imposed on shuttle valves are reliability, hermeticity, and absence of cross flow from system to system during switching.

Valve design reduces basically to calculation of the flow areas and spring forces. The valve resistance should not exceed 2 — 3% of the maximal braking pressure for the average flowrate  $Q_{L \text{ av}}$ . The calculation is made by the usual formulas for determining local resistances

$$F_v = \frac{Q_{L \text{ av}}}{0.663 \sqrt{\Delta p}},$$

where  $F_v$  is the valve port area in  $\text{mm}^2$ ;  $Q_{L \text{ av}}$  is the average flowrate in liters per minute; and  $\Delta p$  is the pressure drop in the valve in  $\text{kg/cm}^2$ .

The shuttle switching pressure is taken in the range of 2 — 4% of the maximal braking pressure.

### Electromagnetic Brake Release Valve

The construction of the electromagnetic brake release valve is similar to that of the conventional two-position electromagnetic valve. An important specific requirement on the brake release valve is minimal actuating time (no more than 0.03 seconds). Valve design

reduces to calculating the flow section areas and the spring and electromagnet forces. The flow section areas are calculated by the usual formulas for local resistances.

### 3. Remote Control Brake System Components

The functional diagrams and analysis of the remote control system reduction valves do not differ from those described above; however, these systems impose some specific requirements on the component configurations and construction.

#### Pneumatic Reduction Valve with Pneumatic Control

The controlling pressure is supplied to the valve fitting A (Figure 10.9) from the conventional reduction valve located in the cockpit. The pressure force is transmitted through the sylphon 1 to the piston 2 and then to the system of outlet 3 and inlet 4 valves. Pressure from the supply line is supplied through fitting B and reduced pressure is transmitted to the brake system through fitting C. The chamber beneath the bellows is open to the atmosphere through fitting D. The reduced pressure acting on the piston 2 balances the force from the controlling pressure action on the sylphon effective area.

/171

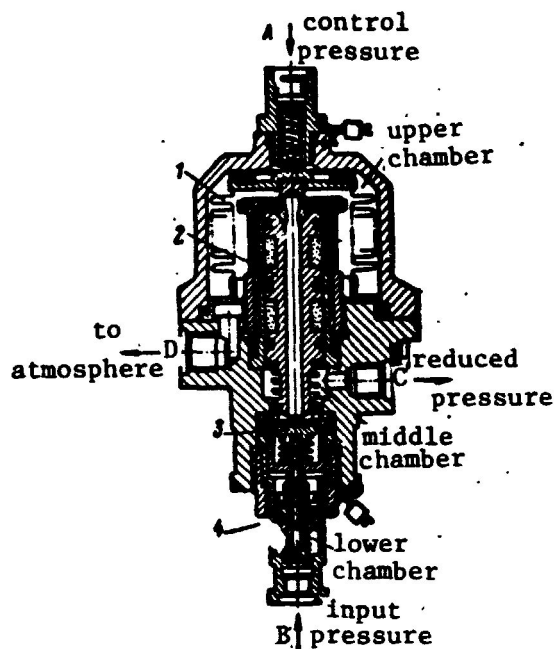


Figure 10.9. Pneumatic reduction valve with remote control:  
1- sylphon; 2- piston; 3- outlet valve; 4- inlet valve.

Without account for the friction force, spring stiffness, and sylphon hysteresis, we can write the relation:

$$p_b F_p = p_c F_{sy} \quad (10.57)$$

or

$$p_b = p_c (F_{sy} / F_p), \quad (10.58)$$

where  $p_c$  is the controlling pressure;  $p_b$  is the brake system pressure;  $F_{sy}$  is the effective sylphon area;  $F_p = (\pi/4)(D^2 - d^2)$  is the effective piston area;  $D$  is the piston diameter; and  $d$  is the outlet valve seat diameter. /172



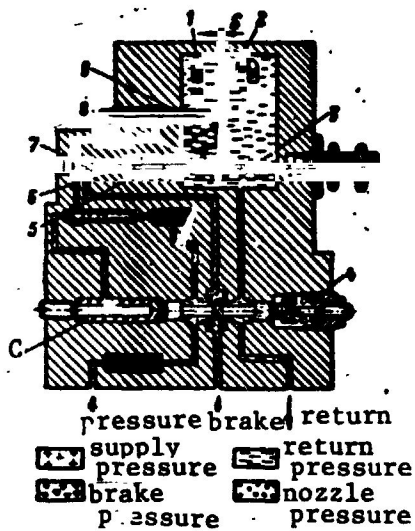


Figure 10.11. Valve with continuous reduced pressure regulation.

1- electromechanical transformer;  
2- flapper; 3, 4, 5, 8- springs;  
6- piston; 7- cylinder; 9- nozzle.

The electrohydraulic reduction valve shown in Figure 10.10 is more advanced. The valve is a pressure reducer with hydraulic drive which is controlled by an electrical bridge circuit whose resistances are the control potentiometer (CP) and feedback potentiometer (FBP). In the bridge diagonal, there is connected the coil of the polarized relay (PR), which sends signals to the electromagnets EMI and EMII of the slide valve which controls the hydraulic actuator piston. The electromagnet EMIII is provided for brake release if the electrical circuit power supply fails; if EMIII releases, the hydraulic

actuator piston chamber is connected to the return line.

Just as the conventional direct acting reduction valve, the valve described here has some irregularity of the output pressure dependence on brake pedal travel. This irregularity is determined by the insensitivity of the regulator itself and also by the insensitivity of the polarized relay PR which controls the electromagnets EMI and EMII.

/173

#### Valve with Continuous Reduced Pressure Regulation

The improvement in brake systems with the objective of automating the process of brake pressure regulation as a function of wheel traction force with the runway has led to the necessity for creating a valve which provides continuous regulation of the output pressure and has high operating speed. Such valves can be constructed only with the use of a signal transformer and a device of the "nozzle flapper" type.

One version of this valve type, shown in Figure 10.11, makes it possible to obtain reduced brake pressure which depends on the magnitude of the current applied to the transformer and has high response speed; however, it requires supply voltage stabilization. When the controlling current is applied to the electromechanical transformer 1, an electromagnetic moment is created which displaces the flapper 2 toward the nozzle 9, reducing the gap S. With reduction of the gap S, the fluid pressure in the nozzle and in the spool chamber C increases. Under the influence of this pressure, the spool overcomes the force of the spring 4 and shifts to the right, connecting the "pressure" chamber with the "brake" chamber. As the pressure in the "brake" chamber increases, the pressure in the cylinder 7 increases and the piston 6 moves to the right, reducing the force in the tension spring 8. Under the influence of the difference of the spring 3 and 8 forces, the flapper moves away from the nozzle. With increase of the gap S, the fluid pressure in the nozzle and in the spool chamber C decreases. Under the influence of the spring, the spool shifts to the left, and when the flapper reaches the neutral position, blocks the "brake" chamber. A pressure proportional to the controlling current is established in the "brake" chamber. With reduction of the controlling current, the electromagnetic moment acting on the flapper decreases, the gap S increases, and the fluid pressure in the nozzle and in the spool chamber C decreases. The spool moves to the left and connects the "brake" chamber with the return line. The pressure in the "brake" chamber and in the cylinder 7 decreases. Under the influence of the spring 5, the piston 6 moves to the left and stretches the spring 8. Under the influence of the difference of the forces of the springs 8 and 3, the flapper moves toward the nozzle, and the fluid pressure in the nozzle and in the spool chamber C increases. The spool moves to the right and isolates the "brake" chamber from the return line. A pressure proportional to the given controlling current is established in the "brake" chamber.

## CHAPTER 11

### AIRCRAFT BRAKE COOLING AND TIRE PRESSURE REGULATION SYSTEMS

#### 1. Brake and Wheel Cooling Techniques

/175

One of the basic characteristics of the aircraft wheel brake is its energy absorption capacity. Usually, the brake is designed to absorb the energy during a single landing. In this case, the temperature of the wheel and brake parts must not exceed a limiting value determined by the wheel drum and tire material strength. Usually the temperature at the point of tire contact with the wheel does not exceed 125° C.

However, in the case of long taxi distances with heavy braking or when making landings with short time intervals between them, overheating and failure of the tires, brakes, and wheels may take place.

The tires are the most vulnerable wheel system component; therefore, various measures are taken to avoid overheating them. Increase of the brake mass reduces its specific characteristics and natural cooling becomes slower, which reduces airplane mobility.

Natural cooling depends significantly on wheel and brake construction. Fast cooling requires free flow of cold air to the brake stack. Sealing of the wheels, installations of mud protection panels, and also compact configuration of the wheel components

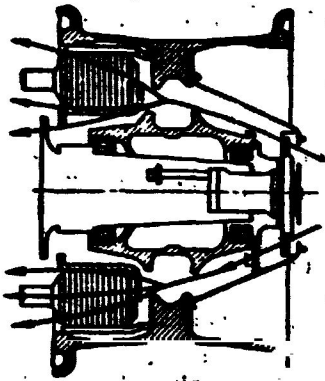


Figure 11.1. Boeing 727 braked wheel with air fan.

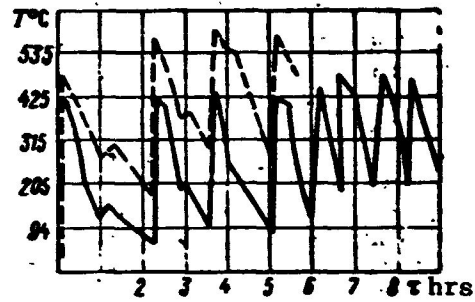


Figure 11.2. Temperature variation of air-cooled brake when performing sequential landings.

degrade the natural cooling conditions. For most unsealed wheels, the natural cooling time varies in the 1.5 — 2 hour range; with the installation of mud protection panels, the time is in the 2.5 — 3 hour range; and for the completely sealed wheels — in the 3 — 4 hour range.

The use of air fans to accelerate brake and wheel cooling has recently been initiated.

Figure 11.1 shows a Boeing 727 braked wheel equipped with an air fan. The fan is driven by an electric motor located in the wheel axle. The cool air is drawn from outside by the fan, flows through the annular gap between the brake and the wheel drum, and also between the individual brake components and the axle. The air flow creates a sort of curtain between the brake and the wheel drum, protecting the tire against overheating.

Figure 11.2 shows the Boeing 727 brake temperature variation when performing scheduled flights of short duration. The solid line shows the temperature variation when using the cooling system and the dashed line is without the cooling system. We see from the figure that eight landings were made in the course of nine hours. In every landing, the mass average disc temperature of the brake with operating cooling system did not exceed 450° C, and the fan caused more rapid brake disc temperature reduction after braking.

/176

During the first four flights (with the fan operating in flight), the brake temperature decreased markedly and prior to landing was about 94° C. During the remaining flights (shorter duration flights), the brake disc temperature decreased to 205° C. In the absence of the cooling system, there was gradual heat accumulation, which led to increase of the brake temperature after each landing. When performing the fourth landing, the brake (and, consequently, wheel drum) temperature reached the critical value, the fusible plug melted, and tire pressure was lost.

Air cooling systems have recently become very widely used in civil aviation airplanes. However, use of the cooling system with a fan built into the axle is possible only if there is adequate space in both the wheel axle and the wheel itself. Mobile ground-based cooling systems are used when the wheel is small and it is not possible to install a fan. /177

The air cooling system with a fan cannot provide any practical brake energy absorption capacity increase, since the fan cannot provide any practical reduction of the heat sink temperature during the braking process, which only lasts 15 — 20 seconds. Only liquid cooling systems can increase the brake energy absorption capacity and also reduce the wheel temperature regime. All the various cooling schemes and their hardware implementations can be divided into two groups.

The first group includes the liquid cooling schemes in which the heat released during braking warms a coolant which circulates continuously in the cooling system (Figure 11.3). The warmed coolant is cooled in a special cooler 2 and again enters the brake. Such systems are closed with forced coolant circulation provided by the pump 1. Design-wise, this scheme is most simply realized for the expander tube brakes, since the heat sink (brake lining) is mounted rigidly on the wheel. /178

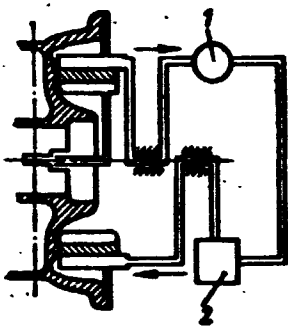


Figure 11.3. Schematic of forced brake cooling system using circulating coolant.

1- pump; 2- cooler.

However, we note that, because of their considerable weight, systems of this kind cannot improve brake specific energy absorption capacity. Therefore, they are used only as systems which reduce the temperature regime of the wheel and its elements in order to increase airplane utilization.

The second group includes the liquid cooling systems in which cooling of the brake and the wheel elements is accomplished by vaporizing the cooling liquid supplied to the brake. The liquid may be supplied either in the dispersed state or in the form of a solid jet. Water or a mixture of water and alcohol is most often used as the cooling liquid. The advantage of such systems is the possibility of increasing the brake energy absorption capacity by vaporizing the water (or other cooling liquid), which absorbs a considerable amount of heat.

However, it is impossible in practice to create conditions with brake cooling rate equal to the rate of heat release. Therefore, the existing vaporizing type liquid cooling systems remove from the brake only part of the heat (20 — 30%). However, even in this case, a gain is obtained in both brake weight and size.

An evaporative type disc brake cooling system is shown in Figure 11.4. During airplane landing at the moment of brake application, the pilot depresses the brake reduction valve 6 and actuates the electrical switch 7 which energizes the relay 4 which then applies electrical pulses of definite duration to the valve 2. At the moment of actuation of the valve 2, water under pressure flows from the tank 3 through the valve 2 into the spray manifold 1. Air under the same pressure enters the spray manifold along with the water. As the water leaves the spray manifold orifice, it is atomized by the air. As the water strikes the friction surface, it

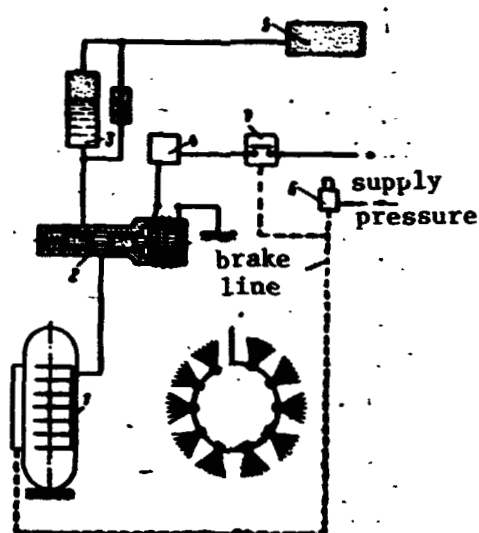


Figure 11.4. Vaporizing type cooling system for disc brake.

1- spray manifold; 2- electro-magnetic valve; 3- tank; 4- pulsed relay; 5- pneumatic accumulator; 6- reduction valve; 7- electrical switch.

transforms into steam and cools the brake and the wheel drum. Such systems have made it possible to increase the brake energy absorption capacity by 15 — 20% without increasing brake size and weight, reduce wheel temperatures, and permit successive takeoffs and landings with very small time intervals between landings when using heavy braking. Figure 11.5 shows the brake element and wheel temperature variation with and without the cooling system. The solid lines show the uncooled brake and the dashed lines — the brake with the liquid cooling system.

This cooling system can be installed on any disc brake without significant modification of the latter.

When designing liquid cooled brakes, it is necessary to consider that the brake must withstand one-time absorption of all the kinetic /179 energy in case of cooling system failure.

The weight of the brake heat absorbing elements is determined on the basis of the emergency braking condition (case of cooling system failure). In this case, the heat sink bulk temperature can be taken equal to  $\approx 800^\circ \text{C}$ .

Let us calculate the basic parameters for an example case. We find the heat absorber weight from the emergency braking condition

$$G_{ha} = \frac{A_b}{ac_p(t_{max} - t_1)},$$

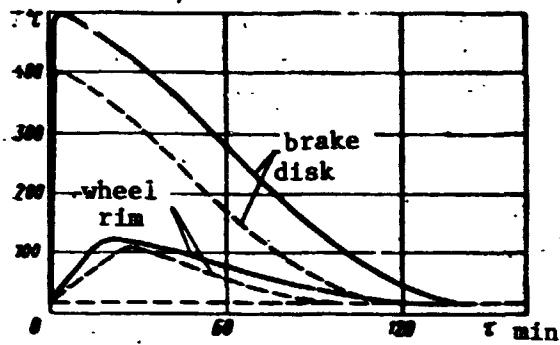


Figure 11.5. Brake element and wheel temperature variation after braking.

where  $A_b$  is the total kinetic energy absorbed by the brake during emergency braking;  $a$  is the mechanical equivalent of heat;  $c_p$  is the mean specific heat of the heat absorber materials;  $t_{\max}$  is the maximal mass average heat absorber temperature; and  $t_i$  is the initial heat absorber temperature.

We take  $t_{\max} - t_i = 800^\circ \text{C}$ .

Specifying the heat absorber temperature during braking with the cooling system operating, we find the energy going to heat the heat absorber

$$A_b = ac_p G_{ha} (t_w - t_i),$$

where  $G_{ha}$  is the heat absorber weight, found from the emergency braking condition; and  $t_w$  is the heat absorber working temperature equal to  $350 - 450^\circ \text{C}$  (we take  $t_w - t_i = 400^\circ \text{C}$ ). Then we find the part of the energy which, after being transformed into heat, goes to vaporize the cooling liquid

/180

$$A''_b = A_b - A_b$$

where  $A'_b$  is the energy going to heat the heat absorber with the cooling system working.

Knowing  $A''_b$  and the total heat of vaporization of the cooling liquid, we find the amount of cooling liquid in the ideal case (i.e., with 100% vaporization)

$$G_{\text{cool}} = \frac{A''_b}{aI_{\text{cool}}},$$

where  $I_{\text{cool}}$  is the total heat of vaporization.

Under actual conditions,

$$G_{\text{cool}}^a = \alpha \frac{A_b''}{a I_{\text{cool}}},$$

where  $\alpha$  is a coefficient accounting for incomplete liquid vaporizability ( $\alpha = 1.3 - 1.5$ ).

After determining the amount of cooling liquid required for brake cooling under actual conditions and knowing the braking time, we calculate the cooling liquid weight flowrate

$$G = \frac{G_{\text{cool}}^a}{\tau},$$

where  $\tau$  is the braking time.

Then, depending on the brake design, we determine the most rational places for installation of the nozzles which spray the cooling liquid. After determining the nozzle location and number, we calculate the flow area

$$f_{\phi} = \frac{Q_{\text{cool}}}{n A \sqrt{\Delta p}},$$

where  $f_{\phi}$  is the flow section area of a single nozzle;  $n$  is the number of nozzles;  $A$  is the effective flowrate coefficient for cooling liquid (or mixture) discharge; and  $\Delta p$  is the pressure differential across the nozzles.

## 2. Tire Pressure Regulation Systems

The need to operate airplanes on airfields with different soil strengths has led to the necessity for using tire pressure regulation systems. These systems, which vary the tire pressure within definite /181 limits, increase the area of wheel contact with the ground and reduce the specific pressure on the ground. As a rule, the pressure regulation systems are remotely controlled from the cockpit.

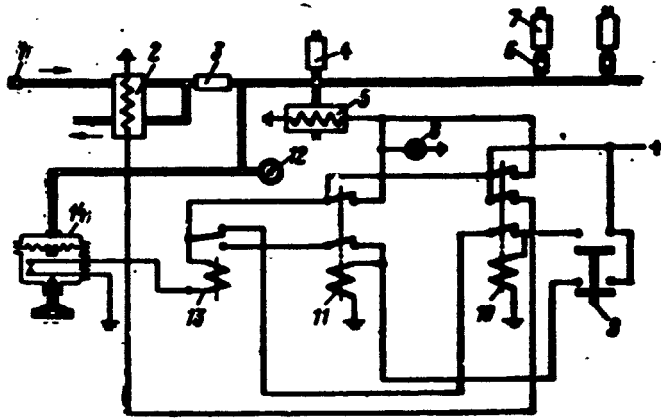


Figure 11.6. Tire pressure regulation system.

1- fitting; 2- electromagnetic valve; 3- restrictor; 4- safety valve; 5- electromagnetic valve; 6- gland; 7- transfer valve; 8- signal lamp; 9- on-off button; 10, 11, 13- relays; 12- pressure gage; 14- pressure controller.

Let us examine the tire pressure regulation system of a particular airplane (Figure 11.6). The system consists of air lines connecting the engine compressors with the tires and several components. Air is bled from the compressor through the fitting 1 and, after passing through a heat exchanger and moisture absorber, enters the electromagnetic valve 2. When the valve opens, the air enters the main line, passes through the restrictor 3, and then enters the tire through the rotating glands 6 and the transfer valves 7, located directly on the wheels. When the transfer valve 7 opens, the tire is filled with air or air is bled from the tire, depending on the air pressure in the main line. The transfer valve 7 is constructed so that it opens when the supply pressure rises above  $2 \text{ kg/cm}^2$ , connecting the tire with the pressure regulation system line. The valve closes when the pressure in the line is  $2 \text{ kg/cm}^2$  or less. The lines running to the electromagnetic valve 5, pressure controller 14, and pressure gage 12 are connected with the main line.

The system is controlled from the cockpit, where the pressure selector 14, pressure gauge 12, signal lamp 8, and system on-off button 9 are located on the pilot's console. The relays 10, 11, and 13 in the electrical remote control system to provide automatic valve actuation. The safety valve 4 is installed to protect the lines and components against overpressure.

The system operates as follows. In the de-energized state, the electromagnetic valve 2 connects the main air line through the restrictor 3 with the atmosphere and blocks air flow from the pressure sources. In the de-energized state, the electromagnetic valve 5 also connects the main air line with the atmosphere. In order to increase the pressure in the tires, the knob of the pressure selector 14 is rotated to set the selector pointer opposite the required pressure on the instrument scale. In this case, the selector contacts are open. Activation of the system is accomplished by briefly depressing the start button 9, which supplies current to the windings of relays 10 and 11. The relay 10 remains energized after pressure is released from the button 9, since the winding circuit of relay 10 is closed by the contacts of relay 13. Relay 10 energizes the electromagnetic valves 2 and 5, and at the same time, the signal lamp 8 illuminates indicating that the system is operating. Valve 5 blocks venting of the air into the atmosphere and valve 2 at the same time connects the main air line with the pressure source. Air begins to flow through the restrictor 3 to the transfer valve 7. When the pressure reaches  $2 \text{ kg/cm}^2$ , the transfer valves open and connect the tires with the main air line. With further increase of the pressure in the system, the tires fill with air. Filling of the tires can be monitored on the pressure gauge 12.

When the pressure in the tires reaches the value established by the pressure selector 14, the selector contacts close and relay 13 actuates. This opens the winding circuit of relay 10 and resets the relay contacts and, therefore, valves 2 and 5 to the original position. The signal lamp goes out, valve 2 prevents air entry into the system, and valve 5 dumps the air from the main line into the atmosphere. In this case, the pressure in the system is less than  $2 \text{ kg/cm}^2$  and the transfer valves 7 close. The air in the tires will be isolated from the main air line.

In order to reduce tire pressure, the knob of the selector 14 is rotated to set the pointer opposite the required scale division. The system is activated by depressing the start button 9.

Let us examine the two pressure reduction stages. The first stage is with the start button depressed, relays 10 and 11 have actuated and have applied current to the electromagnetic valves 2 and 5. In this case, the previously examined filling process repeats. The pressure in the main air line increases and, upon reaching  $2 \text{ kg/cm}^2$ , opens all the transfer valves 7. When the line pressure reaches the tire pressure, the contacts of selector 14 close and relay 13 actuates. The second stage is with the start button released, the contacts of relay 10 have returned to the original position but relay 11 remains actuated. The valve 2, controlled by relay 10, is de-energized and returns to the original position, blocking air flow into the system and connecting the system to the atmosphere through the restrictor 3. In both the first and second stages, the valve 5 and the signal lamp remain energized and, consequently, air is not vented from the air line into the atmosphere. A pressure equal to the pressure in the tires is established in the line between the restrictor 3 and the transfer valves 7. This pressure is above  $2 \text{ kg/cm}^2$ , and, therefore, all the transfer valves 7 remain open. The tire pressure decreases, since air is vented into the atmosphere through the restrictor 3 and valve 2. The pressure reduction process terminates when the pressure selected by the selector 14 is established in the system. At this moment, the selector contacts open, the winding of relay 11 is de-energized, and the contacts of relay 13 open the supply circuit of relay 11. Relay 11 de-energizes the valve 5 and the latter dumps the air into the atmosphere. The pressure in the main air line falls below  $2 \text{ kg/cm}^2$  and all the transfer valves 7 close, isolating the tires from the regulation system. The signal lamp goes out. /183

This is an electrical remote control system. It is used on heavy airplanes with low tire pressure which do not require pressure correction as a function of speed. Since the tire speed characteristic depends on tire pressure, pressure reduction below a definite level may lead to tread separation and tire failure during takeoff. In this case, the pressure regulation system with correction based on speed may provide both improved airplane flotation over the ground and retention of the required tire speed characteristics.

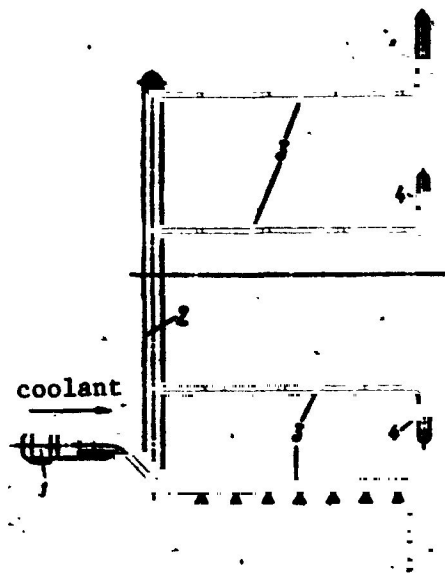


Figure 11.7. Spray manifold of liquid cooling system.  
1- fitting; 2- line; 3- tubes;  
4- vertical tubing extensions.

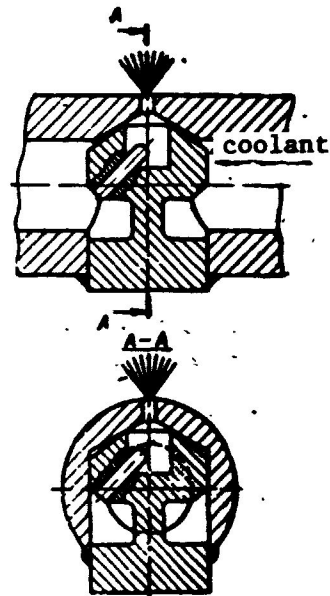


Figure 11.8. Liquid cooling system spray nozzle.

### 3. Liquid Cooling and Tire Pressure Regulation System Components

The spray manifold (Figure 11.7) is the main component of the vaporizing type cooling system and determines, to a considerable degree, the effectiveness of the entire system. The manifold consists of an annular line 2 with fitting 1 for connection to the cooling system. Tubes 3 of smaller diameter branch off from the annular line in the axial direction and are arranged in the brake housing slots. Each tube 3 terminates in a vertical extension 4 which is attached by a spring to the brake housing support flange. The vertical extensions are located between the sectors, which are riveted to the supporting flange. The tubes 3 and the vertical extensions 4 have calibrated orifices. These orifices are positioned so that the sprayed liquid impacts directly on the friction surface. In some designs, the liquid is sprayed using special nozzles. The construction of one such nozzle is shown in Figure 11.8.

/184

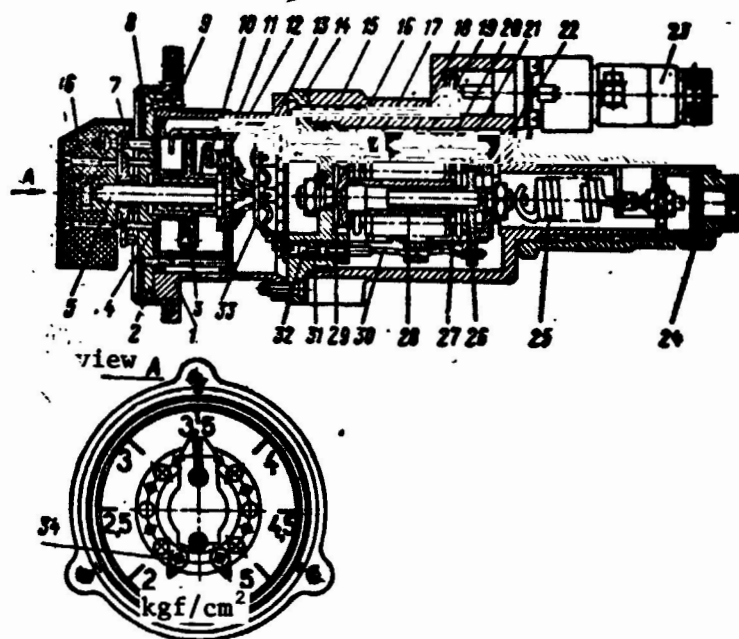


Figure 11.9. Tire pressure regulation system pressure selector.

1- housing; 2- flange; 3- sleeve; 4- spring; 5- shaft; 6- knob and pointer; 7- detent pin; 8- scale; 9- spacer; 10, 11, 17, 18- contacts; 12, 13, 16, 30, 33- wires; 14- flange; 15- housing; 19- ring; 20- spring; 21- cup; 22- contactor; 23- electrical connector; 24- filter; 25- spring; 26- piston rod; 27- sylphon; 28- guide; 29- sylphon unit; 31- feedthrough; 32- electrical lead.

We shall examine some characteristics of the tire pressure regulation system components. The pressure selector is a manually controlled pressure relay. The operating pressure is selected by setting the pointer opposite the corresponding selector scale division. The operating pressure ranges from 2 to 5 kG/cm<sup>2</sup>. The operating pressure is independent of the ambient pressure, since a sylphon with evacuated inner chamber is used as the sensing element.

The unit operates as follows (Figure 11.9): with increase of the pressure supplied to the unit, the sensitive element (sylphon) 27 contracts and displaces the contactor 22 coupled with the sylphon. /185 In this process, the contacts 18 close sequentially with the stationary contacts 17, whose positions are set so that closure of each of the seven contact pairs (contact 18 and the stationary contact 17) takes place at a definite pressure (from 2 to 5 kG/cm<sup>2</sup> at 0.5 kG/cm<sup>2</sup>

intervals). Closure of each contact pair does not prevent closure of the next pair. After closure of each contact pair, the contactor 22 continues to displace, compressing the springs 20 of the previously closed contacts 18. As the pressure supplied to the unit decreases the contactor 22 displaces to the original position under the influence of the spring 25 and the elasticity of the syphon 27, which leads to opening of the contact pairs.

In order to set the required operating pressure, the pointer 6 is rotated to the left, the detent pin 7 withdraws from the hole in flange 2, and the pointer 6 is set opposite the division of the scale 8 corresponding to the required operating pressure. The pointer 6 is held in this position by the detent pin 7, which drops into the corresponding hole in the flange 2 under the influence of the spring 4.

As the pointer 6 is rotated to the required position, the teeth of the shaft 5, which are in the grooves of the sleeve 3, shift the sleeve and attached contact 10 to a position in which the contact 10 closes with contact 11, connected by the wire 16 with the contact 17, which is set to the operating pressure corresponding to the position of the pointer 6. The lead of the electrical connector 23, connected by the wire 13 with the movable contact 10, is now connected to contact 17, which is set to the operating pressure corresponding to the position of the pointer 6. The lead of the electrical plug 23 is connected by the wire 33 with the contacts 18. Closure of the electrical circuit of the electrical connector leads with increase of the pressure supplied to the unit and opening of the circuit with reduction of the pressure takes place at pressures corresponding to the position of the pointer 6. /186

The transfer valve is installed right at the wheel and is connected by tubing with the tire and the air supply line. The valve makes it possible to automatically increase or decrease the pressure in the tire in the range from 2 to 6 kG/cm<sup>2</sup>. In the absence of pressure in the supply line, the transfer valve maintains the pressure in the tire. A schematic of the valve operation is shown

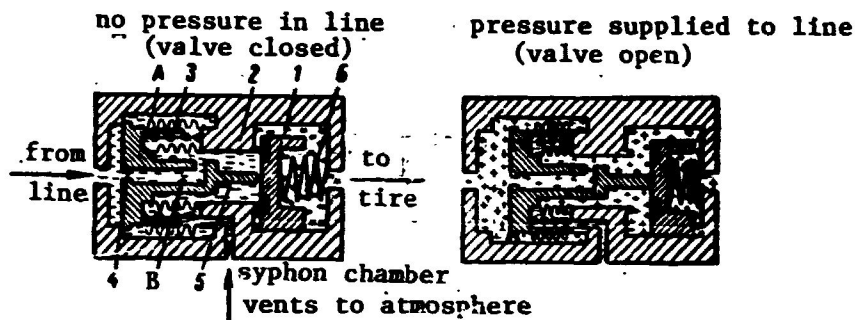


Figure 11.10. Operation of transfer valve.

1- valve; 2- housing; 3, 6- springs; 4- restrictor; 5- plunger.

in Figure 11.10. Crosses indicate supplied pressure chambers, dashes indicate atmospheric pressure chambers, and stars indicate pressure in a closed chamber. In the initial position without pressure in the line, the valve 1 is seated on the housing 2 by the spring 6 and by the air pressure in the tire. With increase of the line pressure to  $1.5 - 2 \text{ kg/cm}^2$ , the syphon unit A displaces and forces the valve 1 from the seat 2, thus connecting the tire chamber with the air line through passage B in the plunger 5. At a pressure less than  $1.5 \text{ kg/cm}^2$ , the spring 3 returns the syphon unit A to the original position and the valve 1 under the action of the spring 6 and the tire pressure is forced against the seat 2.

/187

The opening pressure of the valve 1 is practically independent of the tire pressure, since the working area of the valve 1 is considerably less than the difference of the effective areas of the large and small sylphons. In the chamber B of the plunger 5, there is the restrictor 4, which creates a pressure differential which aids the spring 3 in returning the syphon unit rapidly to the original position if there is an abrupt drop of the pressure from the line. This valve construction prevents any loss of tire pressure. The inner chamber between the sylphons is vented to the atmosphere.

## CHAPTER 12

### STAND TESTS OF AIRPLANE LANDING GEAR AND BRAKE SYSTEMS

#### 1. Landing Gear Shock Absorber Tests

/188

We noted previously that wheel and tire service life and reliability depend, to a considerable degree, on the effectiveness of the landing gear shock absorbing system. If the gear shock absorber does not absorb all the design airplane impact energy during landing, the remaining part goes into the tire and may cause unacceptable tire deformation. Operating experience has shown that a properly designed landing gear shock absorber ensures reliable wheel and brake operation.

Shock strut testing is conducted on an impact testing machine. The shock strut is mounted on the tester housing and is released together with the housing and a weight of definite magnitude. By varying the weight of the housing and ballast and its free-fall height, we can vary the magnitude of the vertical load acting on the wheels at the instant of contact as a function of shock strut travel and released load center of gravity displacement. The drop process is recorded on an oscillograph. The resulting oscillograms are used to plot curves of the load  $P$  on the shock strut and wheels as a function of dropped load center of gravity displacement  $h$  and shock strut travel  $\delta_{ss}$  for absorption by the shock strut of the design, maximal, and ultimate works (Figures 12.1 and 12.2). The

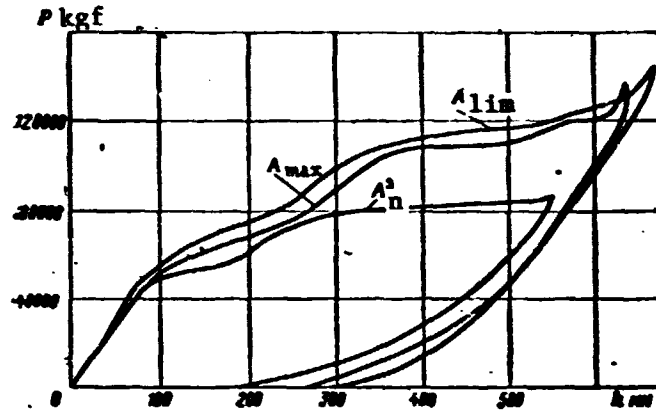


Figure 12.1. Vertical force  $P$  versus dropped load center of gravity displacement  $h$ .

resulting loads on the wheels should not exceed the specified and design values. If the measured loads are excessive, the shock strut basic parameters (charging pressure or needle flow area) are changed and the tests are repeated.

In addition to the dynamic characteristics obtained by dropping the shock strut, we also study the shock strut static characteristics, for example, the shock strut force dependence on its travel. As a rule, these characteristics are recorded for various shock strut charging pressures. In certain cases, the gear drop tests are made with the wheels spun up to speed in order to obtain more precise results.

Oscillations (shimmy) of the swivelling part of the gear strut have considerable influence on the operation of wheels installed on the nose gear. Both the wheel and brake elements and the strut as a whole can fail in the presence of these oscillations. During such strut oscillations, the airplane directional stability decreases markedly. The nose gear is subjected to special tests to evaluate the stability margin against shimmy. The technique for conducting these tests is as follows. The strut with wheel mounted on it is installed in a special adapter on the drop test machine housing. The test machine drum is accelerated to the required speed, after which the housing is lowered so that the tire has the specified deflection. After the wheel comes up to speed, the swiveling part

/189

/190

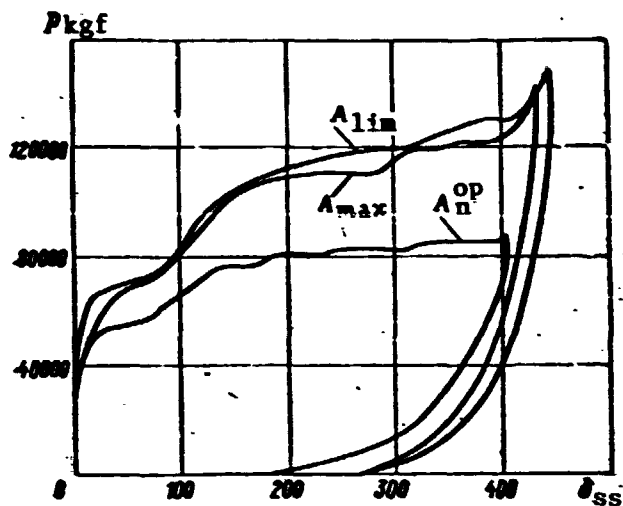


Figure 12.2. Vertical load  $P$  versus shock strut travel  $\delta_{ss}$ .

of the strut, together with the wheel, are turned through a definite angle (usually  $8 - 10^\circ$ ) by a special attachment, after which the attachment used to rotate the strut is disconnected abruptly. The traction force of the wheel with the drum will tend to return the wheel and swiveling part of the strut to the neutral position. If there is adequate damping of the swiveling part of the nose gear strut, it, together with the wheel, returns to the neutral position

after completing some number of oscillations. If damping is inadequate, the oscillations may become undamped and the amplitude may even increase. The tests are conducted with various drum speeds and various loads on the wheel. If necessary, the damper system is corrected by selection of the throttling elements.

## 2. Basic Wheel Tests

*Wheel tests for static strength.* Testing of the wheel under radial loading is conducted on a special press (Figure 12.3) with the tire load and deflection recorded by a special recorder. During this testing, the tire is filled with water. The pressure in the tire must not exceed the operating pressure in the course of the tests; this is ensured by the use of pneumohydraulic compensators. The load is increased smoothly until failure of the wheel or its individual components. The wheel is considered to pass the radial loading test if the radial load at failure is equal to or greater than the design failure load.

/191

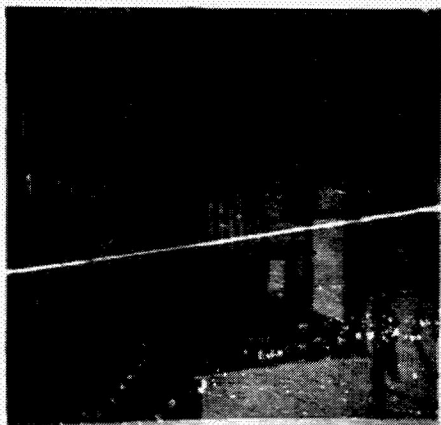


Figure 12.3. Press for aircraft tire static tests.

Wheel testing under internal pressure is conducted in a special armored room. The tire is filled with water, after which the pressure is increased using a hand pump until the wheel fails.

The wheel is considered to pass the test if

$$p_f/p_0 \geq n,$$

where  $p_f$  is the pressure at which wheel failure occurs;  $p_0$  is the operational tire pressure; and  $n$  is the safety factor.

Wheel testing under the action of maximum braking moment is conducted on a special inertial test stand. The wheel with tire installed is mounted on the test stand pressure plate and brought against the drum which is rotating at a speed of 3 — 5 m/sec. With tire deflection equal to  $\delta_{st}$  and the maximum possible operational load, a braking moment equal to the design or ultimate value is created. The wheel and tire are considered to pass the test if failure does not occur.

*Wheel fatigue strength tests* are conducted on special stands to wheel failure. The facility is equipped with strong armor protection to avoid the consequences associated with tire bursting under pressure at failure. Such a stand, but with the armor protection removed, is shown in Figure 12.4. The stand has two axles. The distance between the axles can be varied, depending on the sizes of the tires being tested. One of the wheels is rotated by an electric motor. After the wheels are mounted in the fixture, the distance between their axles is established so that the tire deflection of each wheel will be the same as under the static load  $P_{st\ ldg}$  or  $P_{st\ to}$ . In this case, each wheel is subjected to a radial load equal to the takeoff or landing load. The wheel rotational speed

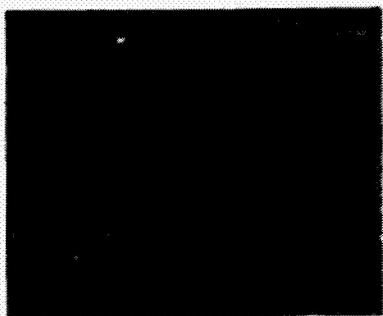


Figure 12.4. Setup for wheel fatigue strength testing (armor protection removed).

(rolling speed) during the tests is taken equal to

$$v_{\text{rot}} = \frac{v_{\text{to}} + v_{\text{ldg}}}{m},$$

where  $v_{\text{to}}$  is the takeoff speed;  $v_{\text{ldg}}$  is the landing speed; and  $m$  is an empirical coefficient.

Since the tires heat up in the rolling process, they must be continually cooled by water circulating in the test setup. The loads (takeoff or landing) are alternated after definite intervals.

The minimal number of wheels of a single lot subjected to the tests is three. However, this number may be increased, depending on several factors. The wheel initial service life is found from the formula

/192

$$N_i = \frac{L_{\text{av}}}{l_{\text{ldg}} + l_{\text{to}} + l_{\text{tax}}} \cdot \frac{1}{\eta},$$

where  $N_i$  is the initial wheel service life, expressed in number of takeoffs and landings;  $L_{\text{av}}$  is the average test wheel running distance prior to failure in km [ $L_{\text{av}} = (L_1 + L_2 + \dots + L_n)/n$ ];  $L_1, L_2, \dots, L_n$  are the total running distances of each wheel prior to failure;  $n$  is the number of wheels tested;  $l_{\text{ldg}}, l_{\text{to}},$  and  $l_{\text{tax}}$  are the specified wheel landing rollout, takeoff roll, and taxiing distances per takeoff and landing; and  $\eta$  is the reliability factor (its value is selected as a function of the number of wheels tested).

### 3. Brake Tests

The basic braking characteristics of the brake and its temperature regime are checked in the normal operating regime on the inertial stand. The stand drum with masses attached to it is accelerated to a definite speed, after which the electric motor is disconnected and the wheel, mounted on the stand pressure plate, is forced against the drum with radial load equal to  $P_{st\ ldg}$ , after which the brake is applied and braking takes place until the stand drum comes to a complete stop. The braking process is recorded by an oscillograph or a manometric recorder. The recorded braking moment diagrams are used to evaluate the brake characteristics, and the temperature curve is used to evaluate its thermal regime. The primary criteria which determine brake effectiveness are:  $M_{b\ min}$  is the minimal braking moment;  $M_{b\ max}$  is the maximal braking moment; and  $M_{b\ av}$  is the average braking moment.

The average braking moment can be found from the formula:

$$M_{b\ av} = \frac{A_b r_d}{L_{st}},$$

where  $A_b$  is the energy absorbed by the brake;  $r_d$  is the dynamic wheel rolling radius; and  $L_{st}$  is the running distance (on the stand). /193

Brake service life tests are also conducted on the inertial stand in the operational regime. The brake and wheel must withstand the required number of brakings while retaining the braking characteristics. The friction element wear rate and service life are determined in the service life tests.

### 4. Wheel and Brake Test Equipment

The wheel and brake loading conditions during operation determine the complexity of the test equipment required for wheel and brake development and inspection tests in the development and production process. As a rule, the factories or firms which



Figure 12.5. Laboratory for testing aircraft wheels and brakes.

fabricate aircraft wheel. have special laboratories. Figure 12.5 shows the test laboratory of one foreign firm. This laboratory is divided into individual sections. The instrumentation and operators are located in section I; the test stands are in section II, the power supply is in section III, and the stockroom is in section IV. The inertial stand A with two pressure plates for wheel and brake testing and the setup C for wheel fatigue strength testing are located in section II. The motor-generator DC power supply is located in section III. In modern test laboratories, the room in which wheels and brakes are tested on inertial stands is separate from the control room, is sound-proofed, and has good exhaust ventilation. The test result recording equipment is automatic.

/194

Figure 1.6 shows an inertial stand of the Paur firm, which makes it possible to test wheels and tires with some angle in relation to the drum in order to simulate side loads. The stand drum circumferential speed reaches 500 km/hr.



Figure 12.6. Inertial stand.

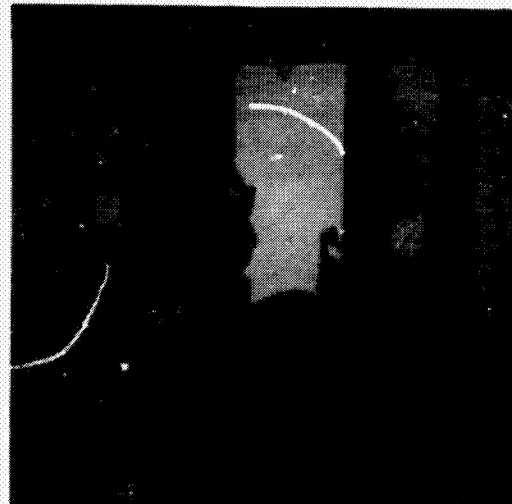


Figure 12.7. Fixture for tire impact tests.

The increasing requirements have led to the creation of equipment which makes it possible to simulate high temperature operating conditions. An example of such a setup is the Dunlop Aviation stand, equipped with a chamber for preheating the wheels. Forcing of the wheel against the stand flywheel is accomplished by a system following a specified program. The stand electric motor power is about 400 hp and the drum circumferential speed is about 320 km/hr.

A special high temperature chamber completely surrounding the test wheel is used to heat the wheel. Heating is accomplished by hot air obtained from a special heating facility.

*Tire test setup.* As a rule, tire testing is conducted on the same inertial stands, impact testers, and presses on which the wheels are tested. However, special facilities have recently appeared because of the increasing tire requirements. One such facility (Figure 12.7) is the Dunlop tester for tire impact testing, which makes it possible to simulate the most severe conditions to which tires are subjected under actual conditions. The energy required for failure of one ply of the tire carcass is determined on the tester. For this purpose, the tester drop housing with ballast of definite weight is equipped with cones of different shape and height.

/195

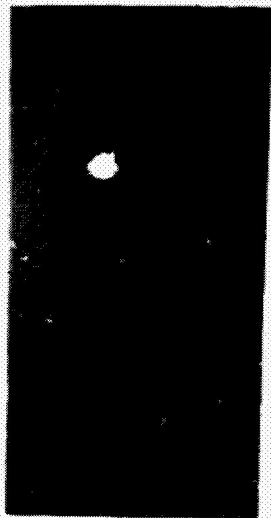


Figure 12.8. Stand for testing electroinertial sensors and direct acting controllers.

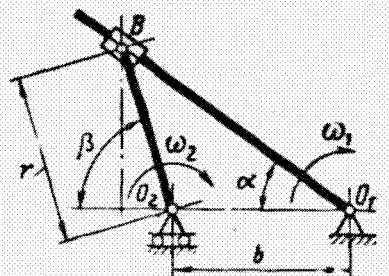


Figure 12.9. Stand kinematics.

By varying the drop height and weight, we can determine tire resistance to impact loads.

Special bogies on which the wheel with the test tire is mounted are used to test tires for resistance to punctures and cuts. The bogie is loaded with ballast of given weight and is rolled over a concrete track on which various sorts of articles (bolts, nuts, etc.) are spread. The tire resistance to mechanical damage is evaluated on the basis of cut size and depth.

##### 5. Stand Check of Inertial Sensors and Antiskid Controllers

Verification of antiskid system electroinertial sensor direct acting antiskid controller operating conditions is carried out on a special stand (Figure 12.8). This stand permits checking all the basic characteristics (sensitivity, pulse duration, etc.) under both laboratory and field conditions. The stand is equipped with a crank and rod mechanism for determining sensor sensitivity. The driving member of this mechanism is a sliding block which rotates uniformly about the axis  $O_1$  (Figure 12.9) with the constant angular velocity

$$\omega_1 = \frac{\pi n_1}{30},$$

where  $n_1$  is the sliding block rpm.

Along the sliding block slot travels the slider B, with which there is connected the crank  $O_2B$  which rotates about its axis  $O_2$ . The distance  $b$  between the sliding block and crank rotation axes is regulated by parallel shift of the shaft crank axis relative to the stationary sliding block axis. With increase of the distance between the sliding block and crank rotation axes to the magnitude  $b$  and with constant sliding block angular velocity, the crank shaft will have a variable angular velocity  $\omega_2$ . Its angular acceleration will change sign once per sliding block revolution. The sensor closes and opens the electrical circuit during one crank revolution.

The magnitude of the angular acceleration with which the crank shaft will rotate is found from the relation

$$\omega_2 = \omega_1 a \frac{\sin \beta (1 + 2a \cos \beta + a^2) (1 - a^2)}{(1 + a \cos \beta)^3},$$

/197

$a = b/r$ ;  $b$  is the distance (spacing) between the sliding block and crank centers of rotation; and  $r$  is the crank radius.

The sensor is attached to the stand sleeve for testing. We rotate the slide block mechanism handle to alter the distance  $b$  between the centers  $O_1$  and  $O_2$  (see Figure 12.9). The displacement is measured using a vernier. At a definite head displacement the sensor begins to generate single pulses. This instant is characterized as the sensor sensitivity threshold. Stable clear-cut sensor pulses appear with further slid block mechanism head displacement. The difference in magnitude between the clear-cut and initial pulses characterizes the stability of the mechanism.

In order to check the brake release pulse duration, the speed reducer handle is placed in the high speed position; the slide block is released from the flywheel and the handle is used to set zero head displacement between the centers  $O_1O_2$ . Then the motor is again energized at the required rpm. After 3 — 5 seconds, when

the sensor flywheel has the required speed, the sensor shaft is disconnected from the speed reducer and braked sharply. At this instant, the sensor generates an electrical signal. The time in the course of which the signal is maintained is recorded by an electrical stop watch. The technique for checking direct acting antiskid controllers does not differ from the technique for checking the inertial electromechanical sensors with the exception that the test stand must be equipped with a pneumatic or hydraulic system.

## 6. Brake and Antiskid System Stand Tests

Stand tests of the brake and antiskid systems are conducted in order to check functioning of both the entire system and its individual components. For correct evaluation of system functioning, its plumbing lines must have length and diameter close to those used aboard the airplane. During the tests, the system is connected either to the brakes or to special mockups whose stiffness and volume characteristics are as close as possible to those of the actual brake. In order to obtain more accurate test results, the hydraulic fluid pressure should be the same as that used on the airplane. As a rule, stand tests of the entire system are conducted with ambient temperature close to standard. However, each system component is further subjected to all the required tests throughout the operating temperature range. /198

During the system stand tests, we check system functioning, nature of brake pressure variation with linear input signal variation, values of the basic parameters (brake pressure, control current, brake pedal travel, etc.), and system response speed (brake application and release times).

After checking the brake system, the antiskid system controller functioning and effectiveness is checked. As a rule, this check is made on an inertial stand. Testing of the antiskid system controller on the stand is made in two regimes: skidding and nonskidding. The tests begin in the nonskidding regime. For this, the wheel, mounted on the stand pressure plate, is brought against the drum which is already up to speed. The rotating drum mass must be selected so as

to complete the braking process in the course of the specified time. Then the wheel is forced against the drum and loaded by a radial load equal to the static load. After this braking pressure is applied to the brake and braking takes place. Triggering of the antiskid system controller should not take place in this regime.

In the skidding regime tests, the wheel, just as in the first case, is forced against the spinning drum, but in this case, the tire deflection should be 25% of the total deflection (so that the traction moment will be definitely less than the maximal braking moment). After pressure is applied to the brake, a braking regime is established in which the braking moment will be greater than the traction moment. The wheel begins to skid, but the antiskid system controller must eliminate the skid from the moment of braking initiation down to a speed of 20 — 30 km/hr. The braking time  $\tau_1$  in the skidding regime (with tire deflection equal to 0.25% of the total deflection) should not exceed  $4\tau$  (where  $\tau$  is the braking time with complete tire deflection).

Modeling principles have been used more and more recently in brake system testing and development.

Figure 12.10 shows the block diagram of a stand which makes it possible to check airplane antiskid system functioning. The stand operation is based on using electrical and physical analogs of the real processes taking place during system testing. The primary parameters which determine the braking process under actual conditions (energy absorbed by the wheel brake, braking moment, traction moment, wheel moment of inertia, angular velocities and accelerations, and certain others) are modeled on the stand by mechanical analogs. The variable quantities which determine the braking moment are simulated by electrical voltages and the automatic operations on these quantities are performed by mathematical modeling methods. /199



The stand operates as follows. A sensor which converts the system pressure into an electrical signal is connected to wheel brake line. The airplane system inertial sensor is taken from the wheel and its gearing is meshed with the wheel simulator gearing. The electrical connection of the sensor with the airplane system is retained. Then the motor accelerates the flywheel to the speed specified by the test program and is then switched off. The control voltage  $U_{M_{tr}}$ , proportional to the magnitude of the traction moment ( $M_{tr}$ ), is applied to the traction clutch. The wheel simulator begins to rotate at a definite speed and drives the inertial sensor gearing. The process corresponds to unbraked airplane landing rollout.

The operator creates the braking pressure  $P_b$ , with increase of which there appears a voltage  $U_{M_b}$  in the braking clutch control channel, simulating the braking moment  $M_b$ . If the voltage  $U_{M_b} < U_{M_{tr}}$ , the brake clutch operates in the slip regime — the process corresponding to braked rollout without skidding takes place. However, if  $U_{M_b} > U_{M_{tr}}$ , the wheel simulator begins to lose speed and transitions to skidding. The automatic brake release sensor coupled with the wheel simulator also loses speed and when the deceleration reaches the design value, closes the braking system electrovalve circuit and the pressure is released from the brake. With pressure decrease, the current to the braking clutch decreases correspondingly. The wheel simulator speeds up, the airplane system allows the working pressure to flow to the brake, etc. The rollout process with automatic controller triggering takes place. After the stored energy is dissipated, the flywheel comes to a stop and the process terminates.

The total number of flywheel revolutions during landing rollout (to the adopted scale) corresponds to the number of revolutions of the ideal airplane wheel rolling without skidding and is proportional to the braking distance. The process time is equal to the airplane landing rollout time.

## CHAPTER 13

### WHEEL AND BRAKE SYSTEM FLIGHT TESTS

#### 1. General Information

/201

Flight tests verify and confirm the suitability of wheels and brake systems for operation on the airplane. The tests include:

- determination of landing rollout distance and braking effectiveness;
- determination of optimal brake pressure;
- evaluation of antiskid system operation under various climatic conditions and with different runway surfaces;
- determination of wheel and brake temperatures during normal operating conditions and in the emergency regimes;
- determination of brake friction element service life;
- evaluation of auxiliary system (cooling system, tire pressure regulation system, etc.) operation.

As a rule, the tests are conducted under various climatic conditions. In order that the test results be objective, the following basic parameters characterizing braking system operation should be recorded during the tests:

- brake pressure;
- braked and unbraked wheel rpm;
- current pulses from the antiskid system controller;
- temperatures of the basic wheel and brake elements;
- braking moment or braking force in the gear drag links;
- load factor acting along the wheel axis.

These parameters are recorded using standard instrumentation. Multichannel oscillographs of the K20-21 type are used for recording. Membrane type sensors are used to record brake pressure. Wheel speed recording is accomplished using a pulse type sensor consisting of a coil mounted on the brake cylinder block and a permanent magnet installed on the wheel drum. As the magnet passes the coil, an electrical pulse appears in the latter and is recorded by the oscillograph. Wheel rotation speed can also be recorded using a photocell. In this case, one half of the tire is painted white and the other half is left black. The photocell reacts to the tire color change and generates a pulse which is recorded by the oscillograph. Recording of the antiskid system operating pulses is accomplished by connecting a pulse sensor in parallel with the electromagnetic brake release valve. Portable contact pyrometers are used to record wheel and brake element temperatures. If continuous recording of the brake temperature variation as a function of time is required, chromel-kopel thermocouples are installed at certain brake points (in the block, discs, and brake housing) and are connected through an amplifier with the oscillograph. Recording of the braking moment or force is accomplished by strain gages bonded in a definite pattern on the brake housing or drag rod. In those cases, when it is necessary to evaluate the load factors acting along the wheel axle, vibration apparatus of the VI6-MA type with DU-5 acceleration sensor installed on the brake housing is used. /202

Oscillograph paper speed of at least 50 mm/sec is recommended in order to obtain high quality recording. After installing all the required monitoring and recording equipment, the airplane on which the flight tests are to be made is first subjected to ground tests.

## 2. Ground Tests

During the ground tests, a preliminary check is made of functioning of the wheels, brakes, and brake systems as a whole. The ground tests start with performing several taxi runs at low speed using light braking (for the minimal necessary brake wear-in). After the taxi runs are completed, an evaluation is made of the static braking moment with the engines running. This check is made on a dry runway at maximal airplane takeoff weight. With the design brake pressure, the moment must be such that the wheels do not turn and hold the airplane securely with the engines operating. Airplane movement with the wheels braked indicates that the thrust force exceeds the wheel traction force with the runway. In this case, increase of the brake pressure will not have any effect, and the noted characteristic is pointed out in the airplane flight operating instructions. However, if, as the engine thrust increases, the wheels rotate, indicating inadequate braking moment, increase of the brake pressure can hold the airplane in position with the design thrust. After the brake pressure required to hold the airplane in position has been determined and recorded, we turn to evaluation of the optimal operational pressure in the brake system, since increase of the kinetic energy spectrum of the modern airplanes has led to the necessity for different pressures in the brakes for the takeoff and operational regimes (for braking during landing rollout). /203

For preliminary evaluation of design pressure correspondence to the operational pressure, three to five high speed taxi runs are made on a dry runway with acceleration of the airplane to  $(0.7 - 0.8)v_{to}$  and subsequent heavy braking. The resulting records are analyzed. Figure 13.1 shows recordings of two airplane rollouts with different operational brake pressures. In Figure 13.1a we see clearly the frequent antiskid system controller triggerings, while in Figure 13.1b, the controller triggerings are infrequent. Frequent controller triggerings indicate that the braking moment exceeds the traction moment. As a rule, reduction of the brake pressure reduces the number of controller triggerings, increases

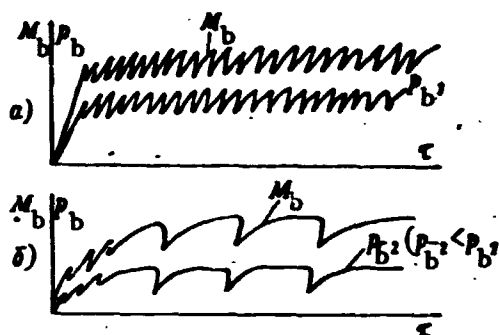


Figure 13.1. Oscillograms of brake moment  $M_b$  with brake pressure  $P_b$  variation during ground testing of the airplane brake system.

braking effectiveness, and reduces the level of the dynamic loads acting on the gear components. After determining the optimal brake pressure, two or three more high speed taxi runs are made, accelerating the airplane to  $0.7 - 0.8 v_{to}$  with subsequent heavy braking in order to determine the braking distance, which can be found from the formula

$$L_{bd} = 2\pi r_d N,$$

where  $r_d$  is the dynamic wheel rolling radius; and  $N$  is the number of wheel revolutions from braking initiation until stopping.

If the braking distance meets the requirement and the wheel and brake temperatures do not exceed the allowable value, the flight tests are started. Exceeding the temperature regime indicates the necessity for introducing limitations, for example, on the speed at which braking is initiated. /204

### 3. Flight Tests

Flight tests include landings at normal and maximal landing weight, at normal and maximal landing speed, and landings with short time intervals between them. The tests must also include verification of brake system functioning in case of rejected takeoff with the airplane at maximum takeoff weight. At least 25 — 30 landings must be made in order to obtain reliable results.

In conducting the tests, the landings must be made using the technique approved for the given airplane with recording of the parameters indicated above. For evaluation of braking system effectiveness, the landings must be made on a dry runway, while for

evaluating antiskid system reliability, they must be made on a wet runway. In the first case, the pilot must use maximal brake pressure. If, in this case, the number of antiskid system triggerings during braking does not exceed 10 — 15, we can consider that the brake pressure has been established quite close to its optimal value. A large number of antiskid system sensor triggerings indicates insufficient wheel traction moment with the runway or excessive sensor sensitivity. Triggering of the system in the first half of the landing rollout indicates insufficient traction because of the presence of high wing lift force. In this case, the wing mechanization which reduces lift force during rollout must be improved in order to increase braking effectiveness. If it is not possible to reduce the lift force influence, gradual increase of the brake pressure in the first half of the rollout and increase of the pressure to the maximal value only in the second half of the rollout should be recommended.

During the flight tests, the temperature must be checked after each landing at the critical wheel and brake locations. When measuring the temperature, we must bear in mind that the maximal temperature on the wheel drum (at the point of wheel contact with the tire) occurs 20 — 25 minutes after termination of braking. If the wheel drum temperature exceeds the allowable value, the drum must be cooled with water to avoid tire failure or explosion. The braking moment created by the brake must not have large oscillations relative to the average value and must not have sharp overshoots. Large braking moment variations or overshoots indicate either abnormal brake operation or abnormal system operation.

/205

Considering that, in most cases, the brake thermal regime is calculated on the basis of the brake absorbing the energy of a single landing and that a definite time for brake cooling is required before the subsequent braking, the performance of landings with short time intervals between them may cause overheating of both the brake and the wheel and tire. In this case, the allowable number of landings and the conditions under which they are made must be determined during the flight tests. For example, closed pattern

flights with the gear down may reduce the temperature regime and increase the allowable number of landings.

As a rule, the rejected takeoff regime is an emergency condition, in which the brake must absorb two to three times more energy than during normal operation. Overheating of the wheels, brakes, and tires is unavoidable in this regime. Subsequent failure of individual structural elements is also possible. Therefore, during the flight tests, the rejected takeoff regime is performed at the very end of the tests with observance of special safety measures. In these tests, the temperature measurements must be made remotely only, and if, the critical temperatures are reached, it is recommended that immediate cooling of the wheels and tires with water be carried out to prevent an explosion.

During the tests, the wheels, brakes, and other brake system elements must be subjected to periodic inspection to evaluate their technical status. If it is necessary, during the flight tests, to evaluate the magnitude of the brake friction element wear, the number of landings with heavy braking must be increased by a factor of two or three, since it is impossible to evaluate the degree of wear after 25 — 30 landings when using wear resistant friction materials.

## CHAPTER 14

### BASIC RULES FOR TECHNICAL OPERATION OF BRAKES, WHEELS, AND TIRES

#### 1. Rules for Brake, Wheel, and Tire Use

/206

Braking after touchdown requires special attention and skill on the part of the pilot. Numerous studies and observations show that braking effectiveness may be different on the same airplane under the same landing conditions for different pilots. If we consider that braking duration after touchdown is 15 — 20 seconds, it becomes clear that the smallest delay in initiating braking or lack of skill in using the brakes may increase braking distance considerably. Even with the most advanced brakes, it is difficult to achieve good results if the touchdown is rough. Therefore, the touchdown must be smooth in order to obtain the minimal landing rollout braking distance. After touchdown, there should be some time interval delay in order that the airplane acquire directional stability, and only after this should braking be initiated. Depending on the airplane aerodynamic characteristics, upon landing, it may immediately "squat" to the ground. In this case, the lift force decreases sharply, the wheels acquire sufficient traction with the runway, and the pilot can, in the course of two or three seconds, create the maximal braking moment, which makes it possible to obtain minimal rollout distance.

If the lift force decreases gradually after touchdown, it is recommended that maximal brake pressure not be used in the first half of the rollout, since, in this case, the braking moment will not be fully realized because of inadequate traction with the runway. Only after the wheels acquire sufficient traction with the runway can the brake pressure be increased to its maximal value. As a rule, this takes place in the second half of the rollout.

In spite of the fact that all modern airplanes are equipped with antiskid systems which eliminate skidding, it is still not recommended that the wheel approach the skid regime. Periodic brake application and release by the antiskid system causes impulsive loading of the brakes and gear elements, which reduces their service life. /207

If the airplane has a tendency to veer during rollout, this is easily eliminated by varying the brake pressure in the corresponding brakes. After bringing the airplane to a stop and taxiing to the parking area, the brake pressure should be released, since, in this case, the brakes cool faster and, in addition, the probability of brake seal overheating decreases. Greater care should be used when taxiing on a wet runway, since, in this case, the wheel may start to skid and the braking controller, if installed, may be inoperative at low speed and the airplane may lose directional stability. Brake functioning and effectiveness must be checked every time prior to takeoff. As a rule, the brakes should be able to hold the airplane in position with the engines operating at takeoff power.

When new brakes are installed on an airplane, it is recommended that they first be checked and broken in using light braking and only then should normal use of the brakes be initiated. Usually three such break-in brake applications is sufficient. We must bear in mind that improper treatment of the brakes may lead to shortening of their service life, failures, and even aircraft accidents. In order to avoid premature wear and obtain maximal effect from the brakes, it is recommended that taxiing not be done with partly braked wheels, particularly in order to maintain constant taxiing

speed when the airplane engine has high idle thrust. Only in case of extreme necessity should so-called "pulsed braking" be used, i.e., periodic brake application and release. Smooth braking should be used when turning and changing heading. When making tight turns, it is recommended that the airplane not be turned around one wheel (or bogie), since this leads to overloading of the gear leg, the wheel, and particularly the tire, which, in this case, may be torn from the wheel rim. A tight turn should always be made with the airplane moving forward. To prevent reduction of brake effectiveness, the brake friction elements must be protected against contact with oil and lubricants. When disconnecting the hydraulic line from the brake, care must be taken to avoid hydraulic fluid getting in the brake, since, in addition to reduction of effectiveness, this may lead to ignition of the brake during the next brake application.

Proper tire operation increases their service life and reliability considerably. One of the basic parameters determining tire effectiveness is their working pressure, which must be checked continually, and the airplane should not be released for flight with /208 excessively high or low pressure. If the pressure is low, the tire may turn on the rim during landing or fail during takeoff. In addition, with insufficient pressure, the tire wears out rapidly during taxi because of the large deformations.

In hot weather or in case of several short flights, there is some tire pressure increase caused by heating of the air, but this increase is usually no more than  $0.5 \text{ kgf/cm}^2$ . In this case, it is not recommended that the pressure be bled down to the normal value in the heated tire, since the pressure would then be too low when the tire cooled.

In order to avoid premature tire failure, they should be protected against contact with oil, lubricant, or fuel, since this softens the rubber. If the airplane is parked for an extended period, it is recommended that the tires be covered to protect the rubber from aging under the influence of sunlight, and also, the tires should be unloaded by placing the airplane on jacks. The

runup area and the entire runway strip should be carefully cleared of stones, glass, and other objects which damage tires. This is particularly important when operating airplanes with high pressure tires (10 — 13 kgf/cm<sup>2</sup>).

## 2. Installation of Assembled Wheel on Airplane Landing Gear

When installing braked wheels on the gear strut, the brake is first installed on the strut axle flange. As a rule, brakes are right hand and left hand rotation, depending on the direction of wheel rotation. The direction of rotation is indicated by an arrow stamped on some part of the brake. The brake is installed (Figure 14.1) so that its housing A fits tightly to the strut flange B without any tilt, and so that the shoulder of the axle or the spacer sleeve, which must be perfectly concentric to the axle seating surfaces, be a sliding or light press fit into the central hole of the housing. This ensures brake centering relative to the axle. Attachment of the brakes by bolts alone to the gear strut flange is not permitted, since any possible eccentricity in the brake installation or installation of the brake with misalignment leads to abnormal brake operation.

In order to prevent any possible brake misalignment, the end face of the flange which the brake housing joins must be absolutely perpendicular to the axle. Experience shows that the axial wobble of the flange face surface at the attach bolt hole radius should not exceed 0.5 mm.

In the shoe or expander tube brakes, the generator of the cylindrical shoe friction surface must be parallel to the axle, which /209 is ensured by machining the friction lining surface at the manufacturer's plant.

In the mounted brake, the location of the openings for verifying and adjusting the clearances and the brake pressure input fitting location should be convenient. These detail parts should not be located in a region blocked by the gear strut or fork, since access

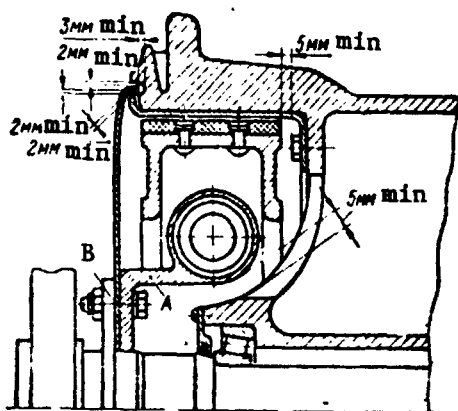


Figure 14.1. Brake installation on gear strut and minimal allowable clearances between individual brake and wheel components.

to them will be difficult in this case. For convenience in releasing air from the brake chambers or the hydraulic brake cylinders when filling the system with fluid, it is recommended that the drain plugs be located at the top.

The brake, installed on the axle observing these rules, is bolted to the gear strut flange and the bolts are tightened uniformly and saftied securely.

Figure 14.2 shows the installation of a dual brake wheel with expander tubebrakes installed on the gear axle.

Prior to installing the wheel on the strut axle, dust and moisture are removed from the brake friction elements. If oil accidentally gets on the shoes, they are washed with pure gasoline and then dried with a dry clean rag. Prior to assembly, the bearings are packed with grease. In order to avoid grease leakage onto the brakes when they are heated, the bearings should be lubricated so that the labyrinths between the rollers and the race are just filled.

Grease of the NK-50 type can be used when operating wheels at ambient air temperatures above freezing and also at temperatures down to  $-20^{\circ}\text{C}$ ; with ambient air temperature below  $-20^{\circ}\text{C}$ , a mixture of 50% NK-50 and 50% TsIATIM-201 by weight should be used. The use of other greases is not recommended. /210

After this preparation, the wheel is slid onto the axle, the grease seals and conical sleeve are installed, after which the bearings are tightened using a special nut. If the wheel does not have a spacer sleeve, the wheel should be rotated manually as the nut is tightened with simultaneous tightening of the nut until wheel dragging is elt. This indicates the absence of axial clearance in

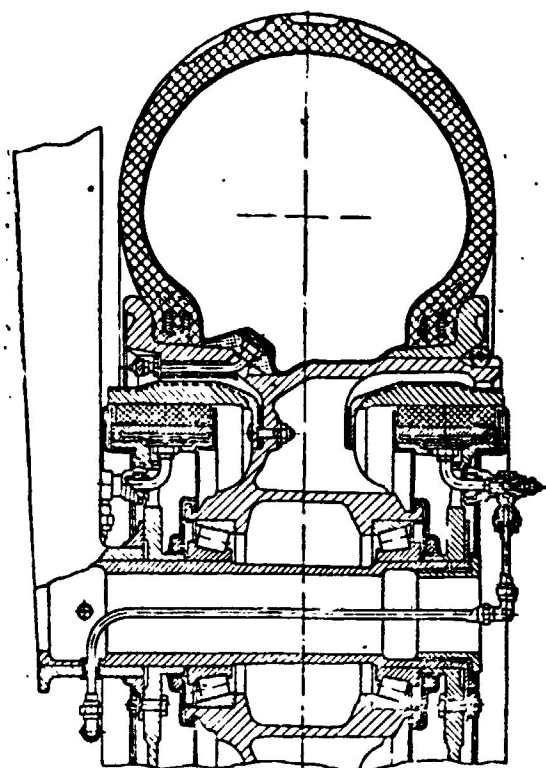


Figure 14.2. Installation of wheel with dual expander tube brakes on cantilever gear.

the roller bearings. Further tightening of the bearings at the expense of elastic deformations of the wheel and axle details is forbidden. After this, the nut should be unscrewed by the following amounts to ensure normal operational clearance in the bearings (in order to compensate for the difference of the wheel hub and axle elongations as the wheel and brake heat up):

— for wheel sizes up to 900 mm — by one eighth of a turn for thread pitch 1.5 mm and by one tenth of a turn for thread pitch 2 mm; /211

— for wheel sizes from 900 to 1200 mm, by one fifth of

a turn for thread pitch 1.5 mm and by one sixth of a turn for thread pitch 2 mm;

— for wheel sizes 1200 mm and larger, by one quarter of a turn for thread pitch 2 mm.

After establishing the operational clearance, the wheel should turn freely by hand without any perceptible axial play. The retention nut is saftied in this position.

When installing a wheel equipped with antiskid system controller, particular attention must be paid to proper meshing in the gearing between the wheel and the controller. The wheel must be rotated slightly in order to facilitate assembly. If the controller mounting is such that its installation and removal after installing the wheel on the axle are possible, it should be installed only after installing

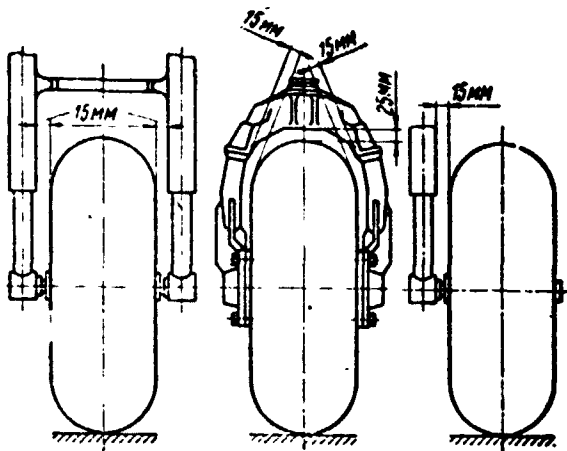


Figure 14.3. Minimal allowable clearances between wheel and gear structure.

the wheel. When installing the controller, the wheel should be rotated slightly on the axle to facilitate meshing of the gearing.

After mounting the wheel on the axle, the tire pressure should be checked, and the clearances between the wheel, tire, and strut should also be checked (Figure 14.3). Not only is contact not allowed, small clearances between the tire and any part of the strut are not

permitted. We must also remember that, during operation, the tire dimensions increase by about 4% in diameter and by 2 — 3% in width. Therefore, if the clearances between the new tire and any part of the landing gear are small, they may disappear during operation, which leads to failure of the tire and the landing gear structure.

/212

### 3. Inspections

Periodic inspections are made to prevent problems and identify and eliminate various malfunctions. The inspection timing is established for each airplane type individually. The first wheel and brake inspection should be made after 100 — 150 landings, combining this inspection with airplane inspections. As a rule, inspections for the modern wheel with disc brake include the following: wheel disassembly and external inspection, brake inspection, and disassembly and reassembly if necessary.

In order to inspect the wheel, it is necessary to remove it from the axle and, without taking the brake from the gear, make an external inspection of the wheel and brake. Prior to the inspection, the inside of the wheel and brake should be carefully cleaned to remove the wear products, blowing them out with compressed air. When

inspecting the wheel, particular attention should be paid to the condition of the grease seals and roller bearings. The grease seals (felt, rubber, or labyrinth) should not have any traces of damage or excessive wear, and the roller bearings should not have any damage to the separators or the inner or outer races. Lubrication of the bearings must be within the specification limits.

If grease seal or bearing damage is found, they must be replaced with new parts, and if the lubrication is not adequate, it must be replenished. There must not be any damage to the inner chamber of the drum, antiskid controller gearing, or bearing spacer sleeve.

When inspecting the tire, attention must be paid to its proper assembly on the wheel drum. Shifting of the tire relative to the drum is now allowable. If the rubber signal layer (usually red) on the tread surface or fabric is showing, the tire is not suitable for further use and must be replaced with a new tire.

During external inspection of the brake, the tightness of its sealing elements must be checked. This requires several operating pressure application and release cycles. If the pressure in the brake does not decrease in the course of 5 -- 10 minutes, the brake seals are considered to be tight. If leaks through the sealing elements are found, the brake is disassembled and the seals are replaced with new ones. When pressure is applied to the disc brake, /213 the pressure disc must compress the entire brake stack, and when the pressure is released, they must return to the original position. In this case, the clearance between the pressure disc and the brake packet must be no less than 2 — 3 mm. Misalignment of the pressure disc by more than 1.5 mm is not allowed. If there is misalignment or if there is no clearance between the pressure disc and the packet in the released condition, a check should be made of the operation of the brake release components. The bimetallic or cermet discs, coupled with the brake housing by their tenons, must displace freely in the axial direction. Failure of the tenons to mesh with the brake housing is not allowable. Local crushing no more than 0.3 mm deep

is allowable at the point of tenon contact with the brake housing slot. Crushing of the tenon in the same limits is also allowable. If any malfunctions or damage of the individual brake elements are found, they must be demounted and taken apart. When performing inspections and when mounting the wheel after replacing the tire, a very careful check must be made of the proper installation and tightening of the roller bearings, since improper tensioning can cause bearing and wheel failure.

#### 4. Tire Installation and Removal

Since the wheels are subjected to preservation treatment at the manufacturer's plant, they must be depreserved prior to installing the tire. The shipping plugs are removed from the wheel hub, the inner roller bearing races and also the spacing sleeve are removed. The bearings are washed with clean gasoline and dried. The wheel rim and inner part of the hub must be carefully wiped and the cloth cover and paper in which the tire is packed at the factory must be removed. In order to avoid contamination of the wheel parts, tube, or inside of the tire, assembly is performed on clean and dry decking, plywood, or canvas. The following are required for assembly of tires with an inner tube:

- special fixture or tool for mounting the tire — a wooden mallet, metal pry bars, and tire irons;
- set of wrenches (for tightening valve nuts and the through-bolts on split wheels);
- talc for dusting the inner tube and inner surface of the tire;
- pressure gauge for measuring the pressure (with scale divisions no more than  $0.5 \text{ kgf/cm}^2$ ) and with special adapters.

If the tire has been used previously, it must be carefully inspected prior to mounting on the wheel, on both the outside and inside after removing all sand and dirt from the tire. After this check, the inner tube and the inner surface of the tire are dusted

/214

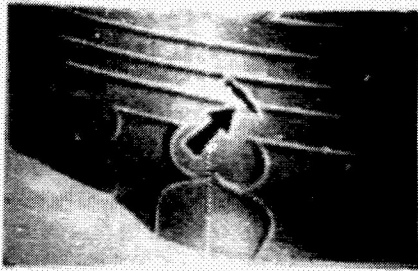


Figure 14.4. Mechanical damage.



Figure 14.5. Tearing of tire casing inner layers.

with talc, after which the inner tube is placed in the tire. The inserted inner tube is inflated slightly with air to straighten out any folds which may have formed.

Tires having mechanical damage such as tears, punctures, and cuts (Figure 14.4), tearing of tire casing inner layers (Figure 14.5), sidewall abrasion with cord showing, bulging in any part of the tire, which is sometimes detected only at the working pressure, and cracks or separation of the longitudinal and transverse tread joints to 2 mm deep are not suitable for mounting.

Separation of the tread joints differs from the usual cracks in that the cracks which form as a result of natural rubber aging from the action of solar rays, moisture, wind, etc., develop in any direction, forming a network on the surface of the tire. The tread joint, however, separates in quite definite directions. The first two tire defects form suddenly during operation, while the others develop slowly as a result of gradual tire failure.

/215

Not suitable for mounting are inner tubes having cracks in the inner tube wall which can be detected when stretching the tube by hand, mechanical damage such as tears (Figure 14.6), punctures, abrasions, deformed valve body, leaks at the point where the valve body attaches to the core, loosening of the rubber-metal valve flange edge, longitudinal and transverse folds in the tube body, cracks in the rubber sleeve of the rubber-metal valve.

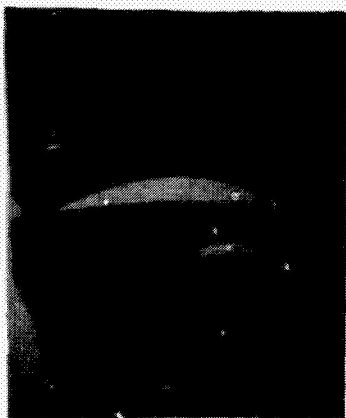


Figure 14.6. Inner tube mechanical damages.

Depending on wheel construction, tire mounting and demounting may differ somewhat; therefore, in the following, we examine tire mounting for the three most widely used wheel constructions.

*Mounting tire with inner tube on wheel with removable flange. The wheel is placed on clean decking with removable*

flange up (Figure 14.7), the lock pin 1 is removed, and the removable flange 3 is slid down along the drum 4. Then the locking half rings 2 with keys or pins are removed from the groove and the removable flange is taken from the drum. If the removable flange is a tight

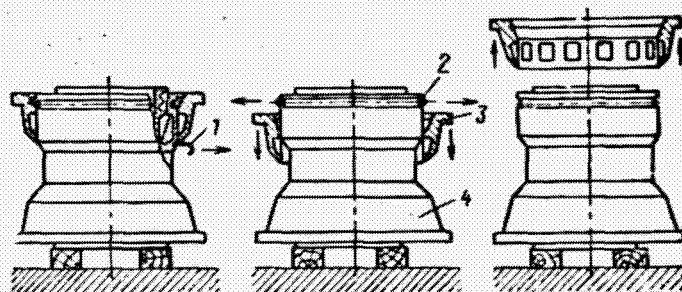


Figure 14.7. Tire mounting on one piece wheel.  
1- lock pin; 2- half ring; 3- split flange; 4- drum.

fit, it can be removed by light wooden mallet blows or using a special tire puller. Then the tire with inner tube inside and slightly inflated is placed on the drum, aligning the valve position with the red mark on the tire. The inner tube valve is directed into its hole in the rim, the washer is slipped on and the nut is screwed on, attaching the metal valve tightly to the drum.

On most wheels, rubber pads are placed under the inner tube valve head to protect the inner tube against tearing under the act of internal pressure in the valve region. In this case, care must be taken to ensure proper installation of the valve pad during

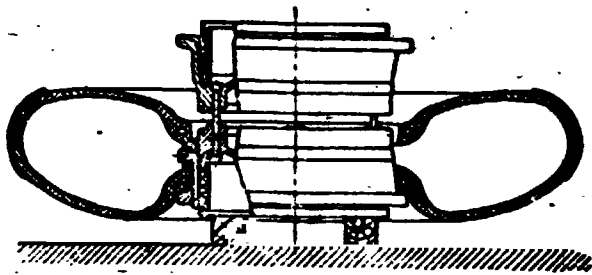


Figure 14.8. Mounting tire on split wheel.

tire bead along the entire circumference. Then the removable flange is placed on the drum and forced down on the drum, flattening out the tire until it becomes possible to install the flange lock (locking half rings with keys or pins) in its place. After this, the removable flange is pulled up by increasing the pressure in the tube.

If the removable flange consists of two half flanges, the tire bead is forced toward the nonremovable drum flange until it is possible to install the half flanges freely on the drum rim. In this case, the protruding parts of the keys must enter the mating half flange recesses. Tires having balance marks (red circle in the lower part of the sidewall) must be installed on the rim so that the red circle is aligned with the inner tube valve.

*Mounting tire with inner tube on split wheel.* When mounting a tire on a split wheel (Figure 14.8), we first separate the wheel halves and remove the tiebolts. The tire with inner tube inside is slipped on the half wheel rim so that the inner tube valve enters the hole in the rim. It is recommended that two diametrically opposed tiebolts be placed in the second half wheel so that the protruding bolt ends enter the corresponding tiebolt holes in the first half wheel, after which, they are joined. The first two bolts are initially screwed in and tightened with a normal wrench, then the remaining bolts are tightened in a crisscross pattern. Excessive, inadequate, or nonuniform tightening can lead to bolt failure during operation.

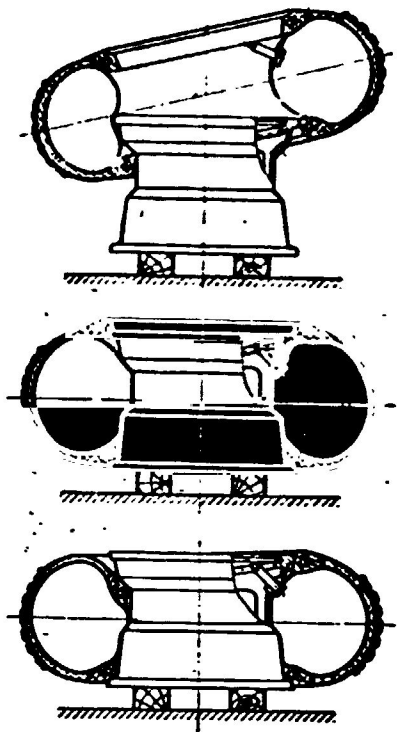


Figure 14.9. Mounting tire on wheel with nonremovable flange.

*Mounting tire with inner tube on wheel with integral flange.* The wheel is placed on wooden blocks so that the wide rim collar is down and the narrow collar is up (Figure 14.9). The /218 tire with inner tube inside and slightly inflated is placed on the wheel so that the inner tube valve is opposite the hole in the wheel rim. The tire bead is guided onto the wheel with the aid of a tire iron. The inner tube valve is directed into the rim hole, the inner tube folds are straightened out, and the other tire bead is guided onto the wheel rim with the aid of tire irons. The second bead should be started from a spot

opposite the valve, and then gradually around the entire circumference so that pinching of the inner tube does not take place.

After mounting the tire, it is inflated by compressed air from a ground servicing bottle, which should be equipped with a pressure gauge and reducing valve. Inflating the tire without a pressure gauge and reducing valve is not permitted. The compressed air used to inflate the tire must be clean and have moisture content within the specifications.

Since all tire casings are made with stretch fit over the seating diameter, the installation of the casing beads on the drum shoulder with a stretch fit is accomplished by internal air pressure. The use of any lubricant to facilitate seating on the rim is absolutely forbidden. There should not be any clearance between the wheel flange and tire bead in a tire which is correctly mounted and inflated to the working pressure.

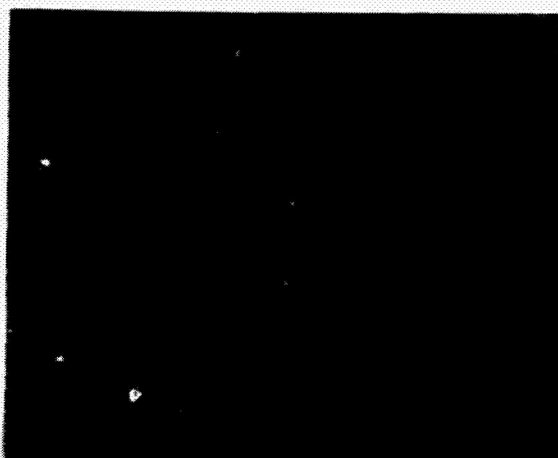


Figure 14.10. Demounting tire using mechanical puller.

In order to demount a tire with inner tube from a wheel, it is necessary to remove the grease seals, inner bearing rings, spacer sleeve, unscrew the valve core, and let the air out of the inner tube. The operations should be performed on a clean surface without permitting contamination of the wheel detail parts. Special pullers, one of which is shown in Figure 14.10, should be used to facilitate tire removal.

The puller sleeves 20 and axle 13 are inserted into the wheel bearings in order to ensure normal puller operation (Figure 14.11). Then the wheel is placed on the ground and the frame 2 is slipped over the protruding end of the shaft (Figure 14.10). The shaft 13 is pulled upward and locked by the pin 1. With the aid of the crews 9, the loading screws 4 are adjusted so that the distance between the anvils 10 and the wheel flange is 2 — 5 mm. After installing the puller on the wheel, the tire is demounted. By turning the loading screws 4 with the wrench 3, we force the tire bead from the wheel flange. When the loading screw anvil 10 loosens the tire bead, the pad 14 is placed along the anvil in the gap between the wheel flange and tire and the pad is forced as far as possible under the wheel flange. Then the loading screws are unscrewed and the frame is turned so that the anvils lie on the middle of the pads and the anvil notches coincide with the pad notches, then the tire bead is again forced down, now through the pads. By shifting the pads sequentially and forcing them down with the loading screws, the tire bead is displaced.

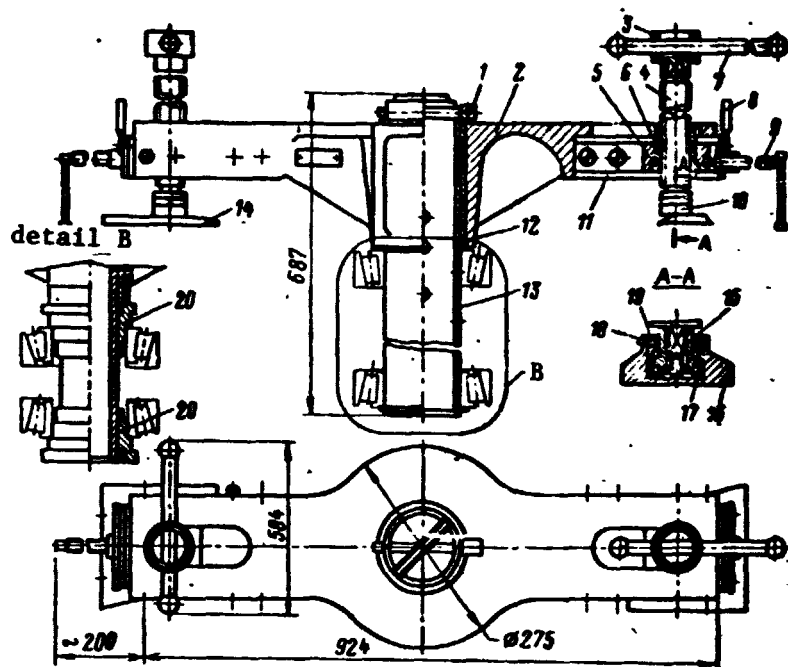


Figure 14.11. Mechanical tire puller.

1- pin; 2- frame; 3- wrench; 4- loading screw; 5- block; 6- nut; 7, 8- handles; 9- screw; 10- anvil; 11- guide; 12- sleeve; 13- axle; 14- pad; 15- stub shaft; 16- anvil body; 17- bearing; 18- set screw; 19- nut; 20- sleeve.

When demounting a tire which has bonded itself securely to the wheel flanges, it is necessary to unscrew the loading screw part way and increase the number of resettings of the puller on the wheel to avoid excessive pad misalignment and large tire bead deflection, which can lead to bead damage. The removal of the tire bead from the removable wheel flange is performed similarly to the procedure described above. In order to prevent dropping of the removable wheel flange along with the tire, it is recommended that the removable flange be tilted on the drum by one-sided pressure on the tire by a single loading screw. After removing the removable flange, the tire is easily removed from the drum. /219

In the absence of a puller, the tire can be removed from the wheel manually with the aid of a pry bar and tire iron.

In the wintertime, tire mounting and demounting should be performed in a room with the air temperature above freezing. When it is necessary to perform tire mounting and demounting at temperatures below freezing, special care should be taken to protect the inner tube from damage because of its increased stiffness.

/220

Mounting and demounting of tubeless tires does not differ fundamentally from mounting and demounting of tires with an inner tube. One characteristic feature of the mounting process is the necessity for faster inflation of the tire with air, which is achieved by removing the core from the valve prior to beginning inflation. With the valve core removed, the tire is rapidly inflated with air, and at a pressure of 2 — 3 kgf/cm<sup>2</sup>, partial seating of the tire beads on the profiled part of the drum takes place, creating a tight seal. After this, the valve core is screwed in and the tire is inflated with air to the operating pressure.

## REFERENCES

1. Bashta, T. M. Samoletnyye gidravlicheskiye privody i agregaty (Airplane Hydraulic Drives and Components). Moscow, Oborongiz Press, 1951.
2. Bel'skiy, V. L., et al. Konstruktsiya letatel'nykh apparatov (Flight Vehicle Design). Moscow, Oborongiz Press, 1963.
3. Belyayev, N. M. Soprotivleniye materialov (Resistance of Materials). Moscow, Gostekhteorizdat Press, 1958.
4. Voronov, A. A. Elementy teorii avtomaticheskogo regulirovaniya (Fundamentals of Automatic Regulation Theory). Moscow, Oborongiz Press, 1954.
5. Yeger, S. M. Proyektirovaniye passazhirskikh reaktivnykh samoletov (Design of Jet Passenger Airplanes). Moscow, Mashinostroyeniye Press, 1964.
6. Zaytsev, A. M., and R. V. Korostashevskiy. Aviatsionnyye podshipniki (Aircraft Bearings). Moscow, Oborongiz Press, 1963.
7. Kragel'skiy, I. V., and I. E. Vinogradova. Koeffitsienty treniya (Friction Coefficients). Moscow, Mashgiz, 1962.
8. Povysheniye effektivnosti tormoznykh ustroystv (Improving Brake System Effectiveness) (collection of articles). Moscow, Press of the Academy of Sciences of the USSR, 1959.
9. Treniye i iznos v mashinakh (Friction and Wear in Machines) (collection of articles). Moscow, Press of the Academy of Sciences of the USSR, No. 12, 1958.
10. Kharkevich, A. A. Avtokolebaniya (Self-Oscillations). Moscow, Gostekhteorizdat Press, 1954.

11. Khol'zunov, A. G. Osnovy rascheta pnevmaticheskikh privodov (Fundamentals of Pneumatic Drive Design). Moscow, Mashgiz Press, 1959.
12. Chupilko, G. Ye. Samoletnyye tormoznyye ustroystva (Airplane Brakes). Moscow, Oborongiz Press, 1940.
13. Chichinadze, A. V. Raschet i issledovaniye vneshnego treniya pri tormozhenii (Calculation and Analysis of External Friction During Braking). Moscow, Nauka Press, 1967.
14. Sheynin, V. M. Vesovaya i transportnaya effektivnost passazhirskikh samoletov (Weight and Transport Effectiveness of Passenger Airplanes). Oborongiz Press, 1962.
15. Shul'zhenko, M. N., and A. S. Mostovoy. Kurs konstruktsii samoletov (Airplane Design). Mashinostroyeniye Press, Moscow, 1971.
16. Author's Certificate No. 247793, 1969. Official Bulletin of the Committee on Inventions and Discoveries of the Council of Ministers of the USSR, No. 22, 1969.
17. Author's Certificate No. 168134, 1964. Official Bulletin of the Committee on Inventions and Discoveries of the Council of Ministers of the USSR, No. 3, 1965.
18. Author's Certificate No. 145140, 1960. Official Bulletin of the Committee on Inventions and Discoveries of the Council of Ministers of the USSR, No. 4, 1962.
19. Author's Certificate No. 201077, 1967. Official Bulletin of the Committee on Inventions and Discoveries of the Council of Ministers of the USSR, No. 17, 1967.
20. Author's Certificate No. 199680, 1967. Official Bulletin of the Committee on Inventions and Discoveries of the Council of Ministers of the USSR, No. 15, 1967.
21. Author's Certificate No. 234062, 1968. Official Bulletin of the Committee on Inventions and Discoveries of the Council of Ministers of the USSR, No. 3, 1969.
22. Author's Certificate No. 171702, 1963. Official Bulletin of the Committee on Inventions and Discoveries of the Council of Ministers of the USSR, No. 11, 1965.
23. Antiskid Device Perma Research and Development. Journal of the RAS, Vol. 71, No. 633, 1963.
24. Automatic Adjustment Device for a Brake. Automobile Engineer, Vol. 56, No. 1, 1966.

25. McBee, L. S. Effective Braking — A Key to Air Transportation Progress. SAE preprints, No. 376, 1969.
26. Collins, R. L., and R. I. Brack. Experimental Determination of Tire Parameters for Aircraft Landing Gear Shimmy Stability Studies. ATAA Paper No. 68-311. AIAA/ASME, 9<sup>th</sup> Structures, Structural Dynamics, and Materials Conference, Palm Springs, California, April 1 — 3, 1968.
27. Conway, H. G. Landing Gear Design. London, 1958.
28. Davis, J. E., and R. C. Curry. The Cost of Landing an Airplane. SAE Journal, Vol. 71, No. 12, 1963.
29. Dunlop's New High Speed Aircraft Tire Test Installation. Intervia Air Letters, No. 6473, 1968.
30. Liquid Cooled Brakes. Airlift, Vol. 24, No. 18, 1961.
31. Magnesium-Lithium Alloys Combine Lightness and Stiffness. Materials in Design Engineering, Vol. 62, No. 5, 1965.
32. Moneher, F. L., and L. D. Taylor. Design Trends and Developments. Machine Design, Vol. 34, 1962, p. 166.
33. New Airplane Developments of the Messier Firm. Luftfahrt-zubehoer, No. 1, 1966.
34. Notes on the Messier Material Technique, 1968.
35. Wheels and Brakes. Luftfahrzubehoer, No. 1, 1966.
36. Ring Disc, New Approach to Aircraft Brake Design. American Aviation, Vol. 27, No. 10, 1964.
37. Schulze, K. H., and L. Beckman. The Adhesiveness of Wet Road Covers at Various Velocities. ATZ, No. 7, 1963, p. 65.
38. USAF Performs Tests on XB-70 Brakes. Aviation Week and Space Technology, Vol. 78, No. 1, 1963.
39. Forced Air Cooling for Brakes. Luftfahrtzubehoer, No. 1, 1966.

Translated for National Aeronautics and Space Administration under contract No. NASW-2483 by SCITRAN, P. O. Box 5456, Santa Barbara, California, 93108.